UNIVERSITÉ DU LUXEMBOURG

PhD-STM-2023-069
The Faculty of Science, Technology and Medicine

DISSERTATION

Defence held on 18/07/2023 in Esch-sur-Alzette, Luxembourg

to obtain the degree of

DOCTEUR DE L'UNIVERSITÉ DU LUXEMBOURG EN BIOLOGIE

by

Marion Melanie SENGUPTA
Born on 19th October 1988 in Dresden (Germany)

CHARACTERIZING THE ROLE OF *ADAM17* IN NEURONAL DEVELOPMENT IN THE CONTEXT OF ALZHEIMER'S DISEASE

Dissertation defence committee

Dr Alexander SKUPIN, dissertation supervisor
Professor, Université du Luxembourg

Dr Anne GRÜNEWALD, Chair
Professor, Université du Luxembourg

Dr Jochen SCHNEIDER, Vice-Chair
Professor, Université du Luxembourg

Dr Anindita BASU
Professor, University of Chicago

Dr Natalia KONONENKO
Professor, University Hospital Cologne
Principal Investigator, University of Cologne

Dissertation

Presented on 18/07/2023 in Esch-sur-Alzette Luxembourg
to obtain the degree of

DOCTEUR DE L'UNIVERSITÉ DU LUXEMBOURG EN BIOLOGIE

by Melanie Sengupta
Born on 19 October 1988 in Dresden (Germany)

Dissertation defence committee

Dr Anne GRÜNEWALD, Chair
Professor, Université du Luxembourg

Dr Jochen SCHNEIDER, Vice-Chair
Professor, Université du Luxembourg

Dr Alexander SKUPIN, Dissertation supervisor
Professor, Université du Luxembourg

Dr Anindita BASU
Professor, University of Chicago

Dr Natalia KONONENKO
Professor, University Hospital Cologne
Principal Investigator, University of Cologne

AFFIDAVIT

I hereby confirm that the PhD thesis entitled “Characterisation of *ADAM17* in Alzheimer’s disease by analysis of early neuronal differentiation” has been written independently and without any other sources than cited.

Melanie Sengupta

Luxembourg, 09. June 2023

ACKNOWLEDGEMENTS

I want to express my sincere thanks to everyone supporting my scientific growth during the PhD work.

First of all, I want to express my sincere gratitude to my supervisor Prof Dr Alexander Skupin, for the opportunity to work on this project and allowing me to fulfill my dream of conducting PhD studies. Thank you for the continuous help, patience, scientific discussion, and financial support.

My sincere thanks go to the members of my CET Committee, Prof Dr Anne Grünewald and Prof Dr Lasse Sinkkonen for critical evaluation of my project and the supporting feedback you provided during the years.

I want to thank Prof Dr Anindita Basu, Prof Dr Natalia Kononenko, and Prof Dr Jochen Schneider for agreeing to become members of the PhD committee and reviewing my PhD thesis.

I appreciate the contributors to my project for their work, time, and repetitive explanations. Dr Javier Jarazo who supported me with advice and practical support. Dr Kamil Grzyb for the single cell experiments and motivational backup. Dr Corrado Ameli for the help with data analysis and coding. Lena Schaack for the (!) Western blot, and Marc Warmoes for conducting the metabolomic experiments. Thanks to Kyriakis Barmpa for her patient and practical advice.

My sincere gratitude to Olga and Cri, for getting me started and helping me to go through, motivate me and for everything else. Without both of you, I would never be in the position in which I am currently.

I am happy that I could be a part of ICS. Thank you for the support and friendship, for hands-on support and the steady supply of (Belgian) chocolate. Thanks to Thais for reviewing my thesis manuscript.

A big thank you to my family: I appreciate that both of you were always there for me and kept yourself busy to allow me some free time in lab. Thanks to my parents, my brother and my in-laws, for being there for me, Anupam and Zieshan, and for your understanding when I could not be available for you.

Finally, I want to thank everyone who made me smile during this long journey.

SUMMARY

Owing the growing elderly population, the incidence of neurodegenerative diseases of ageing is steadily increasing during the last decades. These diseases are often complex and multi-factorial with overlapping symptoms and pathophysiological markers. Alzheimer's disease is the most common form of dementia and is characterized by intracellular tau accumulations and extracellular amyloid plaques. Although some genes have been identified as causal in some patients, the majority of cases occur sporadic and disease onset remains unexplained. Recent research has linked a heterozygous, single nucleotide variant in *ADAM17* (SNV rs142946965) to the onset of a mendelian form of AD, but the mechanistic link between the mutation and AD is not yet understood. The recent development in induced pluripotent stem cells technology allow for examination of the effects of genetic variants in a personalized manner. In this study, a stable iPSC line was generated using a fluorescence based CRISPR/Cas gene editing approach. To investigate the effect of the *ADAM17* SNV rs142946965 mutation on early neuronal development, the generated clones were used for induction of differentiation into basal forebrain cholinergic neurons and midbrain dopaminergic neurons, respectively. Neuronal differentiation was followed up by deep phenotyping including single-cell transcriptomics and metabolomics at early developmental stages.

Five genes were found to be differentially expressed at all timepoints during basal forebrain cholinergic neuron differentiation between mutant and control and could be linked to impairments in neuronal development. Metabolomic analysis also revealed perturbance of AD-relevant pathways, indicating the importance of ADAM17 in neuronal development and disease development. Overall, this study employed state-of-the-art CRISPR/Cas9 gene editing and multi-omics technologies to investigate the impact of ADAM17 on early neuronal development.

TABLE OF CONTENTS

TABLE OF FIGURES

TABLE OF TABLES

ABBREVIATIONS

ABCA7	ATP Binding Cassette Subfamily A Member 7
AChE	Acetylcholine esterase
AD	Alzheimer's disease
ADAM	A Disintegrin And Metalloproteinase
ADAM17	ADAM metallopeptidase domain 17 (gene)
ADAM17	A Disintegrin And Metalloproteinase domain-containing protein 17 (protein)
AGC	Automated Gain control
AICD	APP intracellular domain
APOE	Apolipoprotein E
APP	Amyloid precursor protein
α-syn	Alpha-synuclein
Aβ	Amyloid-ß peptides
BACE1	β-APP-cleaving enzyme-1
BBB	Blood-brain barrier
BDNF	Brain-derived neurotrophic factor
BEX3	Brain expressed X-linked 3
BFCN	Basal forebrain cholinergic neurons
BIN1	Bridging integrator 1
BTE	Base-to-be-edited
CANDIS	Conserved ADAM seventeeN Dynamic Interaction Sequence
CD2AP	CD2-associated protein
CLU	Clusterin
CR1	Complement C3b/C4b receptor 1
CSF	Cerebrospinal fluid
ctr	Isogenic control
CX3CL1	Fractaline
dcSAM	Decarboxylated s-adenoyslmethionine
DEG	Differentially expressed gene
DLB	Dementia with Lewy bodies
EGFR	Epidermal growth factor receptor
EOAD	Early onset Alzheimer' disease
fAD	Familial AD
FDR	False discovery rate
FTD	Frontotemporal dementia
GWAS	Genome-wide association study
HILIC	Hydrophilic Interaction Liquid Chromatography
HD	Huntington’s disease
ICMS	Ion Chromatography – Mass spectrometry
IGF1	Insulin-like growth factor 1
IGFPB5	Insulin-like growth factor binding protein 5

IL-1β	Interleukin 1 beta
IL-6	Interleukin 6
iPSC	Induced pluripotent stem cell
iRhom1	Inactive rhomboid protein 1
iRhom2	Inactive rhomboid protein 2
LHA	Left homology arm
LOAD	Late onset Alzheimer' disease
LTP	Long term potentiation
MAT1	S-adenosylmethionine synthase
MCI	mild cognitive impairment
NADE	Nerve growth factor receptor-associated protein 1
mDA	Midbrain dopaminergic neurons
NDA	Neurodegenerative diseases of ageing
NFT	Neurofibrillary tangles
NGFR	Neurotrophic receptor tyrosine kinases
NMDA	N-methyl D-aspartate
Notch1	Neurogenic locus notch homolog protein 1
NTRK	High affinity nerve growth factor receptor
ODC	ornithine decarboxylase
Padj	Adjusted p-values
PAM	Protospacer adjacent motif
PD	Parkinson’s disease
PICALM	Phosphatidylinositol Binding Clathrin Assembly Protein
PLCG2	Phospholipase C gamma 2
PSEN1	Presenilin 1
PSEN2	Presenilin 2
RHA	Right homology arm
ROS	Reactive oxygen species
SAM	S-adenoyslmethionine
SAT1	diamine acetyltransferase 1
sc-RNAseq	Single-cell RNA-sequencing
sgRNA	Single-strand guide RNA
SIX3	SIX homeobox 3
SIX6	SIX homeobox 6
SMS	Spermine synthase
SMOX	Spermine oxidase
SNP	Single nucleotide polymorphism
SNV	Single nucleotide variant
SORL1	Sortilin Related Receptor 1
SRM	Spermidine synthase
SR medium	Serum replacement medium
STAG2	STAG2 cohesin complex component
TCEAL9	Transcription elongation factor A like 9

TNFα	Tumor necrosis factor alpha
TNR1A	Tumor necrosis factor receptor superfamily member 1A
TNR1B	Tumor necrosis factor receptor superfamily member 1B
TREM2	Triggering Receptor Expressed On Myeloid Cells 2
UMAP	Uniform manifold approximation
VKI primers	Primers to validate knock-in
WGS	Whole genome sequencing
XIST	X inactive specific transcript

CONTRIBUTIONS BY OTHERS

Following people contributed to the work presented:

Dr Javier JARAZO provided a MATLAB code to help with the fluorescence guided picking of the clones and helped with the configuration of the FACS gates for colony purification (Section 3.2.3, page - 43 -).

Lena SCHAACK from the Medical Translational Research group (LCSB) performed the Western blot analysis of the iPSC lines: WTSIi010-A, R215I, PB005.1, clone 1 and clone 2 (Section 3.6, page - 52 -).

The single-cell experiments (DROP-seq and 10x Genomics) and subsequent Illumina sequencing was carried by Dr Kamil GRZYB and Dr Rashi HALDER from the LCSB single-cell platform (Section 3.7, page - 53 -).

Dr Marc WARMOES (LCSB metabolomics platform) performed the analysis of the metabolome for the differentiation experiments (Section 3.8.1, page - 56 -).

Dr Corrado AMELI accomplished the computational data analysis of the single-cell RNA -sequencing and metabolomic data (Section 3.7.1.3, page - 55 -; and Section 3.8.2, page - 58 -).

The proteomics analysis was performed by the Proteomics of Cellular Signaling group of Luxembourg Institute of Health under supervision of Prof. Gunnar DITTMAR (Section 3.9, page - 58 -).

1 Introduction

As the population continues to age, there has been a steady increase in age-related diseases. In particular, the incidence of neurodegenerative diseases has been on the rise with only limited treatment options available. To address this challenge, a multi-facet approach is necessary to better understand underlying disease mechanisms and factors that contribute to disease progression including environmental, genetic, and personal risk factors. Current approaches rely on biomarker identification and integration of clinical data with *in vitro* and *in vivo* models. Recent technological advancements have made it possible to investigate transcriptomic, epigenetic, metabolomic, and proteomic changes often at single-cell level. In this respect, the presented thesis contributes to these approaches in the framework of Alzheimer's disease (AD) by investigating *ADAM17* (ADAM metallopeptidase domain 17) as a relevant candidate gene by a multiscale analysis. *ADAM17* has recently been associated with AD and has a wide range of substrates that could impact disease onset and progression, albeit details on potential mechanisms are not understood at present. The Introduction will provide an overview on neurodegenerative diseases and specifically AD as well as an introduction to the ADAM17 shedding protease. Subsequently the Aims of the thesis are described in Chapter 2 and Methods, Results and Discussion are presented in Chapters 3-5 before the Conclusion and Outlook in Chapter 6.

1.1 Neurodegenerative diseases of ageing

Neurodegenerative diseases of ageing (NDA) are marked by gradual neuron loss that results in impairments of central nervous system functioning, leading to a progressive cognitive and functional decline of the patients (Culig, Chu and Bohr, 2022). Well known examples are AD, Parkinson's disease (PD), Huntington's disease (HD), dementia with Lewy bodies (DLB) and Frontotemporal dementia (FTD). Most important risk factor is age. As the average lifespan is rising worldwide, so is the incidence of NDA, which are a major social and medical burden. At the moment, no cure for these detrimental conditions is available. Approved medications merely alter the immediate symptoms. The cognitive decline has a major impact on morbidity and mortality in the aged population (Murdaca *et al.*, 2022). Typically, NDA have a long prodromal phase marked by steadily aggravation of pathological changes in the absence of clinical symptoms. The clinical

picture of NDA picture is divers, including cognitive, neuropsychiatric, and motor symptoms, which often overlap. Even within one NDA patients show a wide variety of phenotypes, which might even change during disease development (Menéndez-González, 2023). Neuropsychological test batteries often do not mirror disease progression (Jónsdóttir, Harrison and Hannesdóttir, 2023), additionally complicating diagnosis. Often, established biomarkers are not available. Current classification of NDA is based on clinical symptoms or molecular hallmarks.

1.1.1 Common pathways in neurodegenerative diseases of ageing (NDA)

Scientific consensus recognizes NDA as proteinopathies: one or more proteins are accumulating and thereby triggering a disease or significantly contributing towards it (Menéndez-González, 2023; Wilson *et al.*, 2023). The pathogenic protein varies between the diseases, and the affected brain regions and neuronal subtypes differ (Fu, Hardy and Duff, 2018). These varieties explain the difference in clinical symptoms and pathophysiological hallmarks (Wilson *et al.*, 2023). Examples are such as amyloid β (Aβ) and hyperphosphorylated tau in AD, alpha-synuclein (α-syn) in PD and DLB, and Huntingtin in HD. FTD can be associated with deposition of tau, TDP-43 (TAR DNA-binding protein 43) or so called FET-proteins (Boeve *et al.*, 2022). Commonly, the accumulating protein or its precursors are encoded by disease-associated genes. Increased synthesis, occurrence of structurally abnormal forms or decreased degradation, alone or in combination, are the triggers leading to protein accumulation. Apart from that, the approach to NDA as pure proteinopathies is self-limiting. While some protein accumulations might be the defining symptom for one disease, the same proteinopathies could occur in another NDA. α-syn, a hallmark of PD and DLB, aggregates are found in a large population of AD patients (Marsh and Blurton-Jones, 2012). Conversely, some patients with DLB, and to a lesser extent patients with PD related dementia show Aβ pathology (Lim *et al.*, 2019). Tauopathies, diseases with tau deposition, include, among many others progressive supranuclear palsy (a subform of PD), AD and some forms of FTD (Bidesi *et al.*, 2021; Zhang *et al.*, 2022). The occurrence of several proteins misfolding could be partly explained by cross-seeding, a phenomenon where misfolded proteins affect one another's seeding. In the context of NDA, it has been documented for Aβ/tau, Aβ/α-syn, and tau/α-syn (Gadhave *et al.*, 2020). Cross-seeding significantly influences the propagation of various protein aggregates and can be an important driver for disease progression (Westermark and Westermark, 2013; Subedi *et al.*, 2022; Ge *et al.*, 2023).

Besides the before mentioned protein accumulation, NDA share other common pathological hallmarks, which are more or less pronounced in the individual disease. NDA often show synaptic

and neuronal network dysfunction, alterations of the endo-lysosomal network, perturbed energy metabolism, DNA and RNA defects, and inflammation (Fu, Hardy and Duff, 2018; Knupp *et al.*, 2020; Wilson *et al.*, 2023). Alterations in these pathological characteristics develop before the onset of clinical symptom. Their steady but subtle decline often hinders a timely diagnosis.

Synaptic dysfunction and thus altered neuronal circuitry with neuronal hyperexcitability plays a key role in the development of NDD (Wilson *et al.*, 2023). Synaptic loss can be found before the onset of clinical symptoms in dementia. BDNF (Brain derived neurotrophic factor) is a crucial neurotrophin for synaptic plasticity, neurogenesis, and long-term potentiation (LTP). Impairments in BDNF signalling and decreased BDNF levels in AD patient's brain, same effects have been found in PD and HD. BDNF has been suggested as a therapeutic target for this diseases (Colucci-D'Amato, Speranza and Volpicelli, 2020).

Alterations in the **endosomal-lysosomal network** are common in NDA, too. The endosome is important to remove proteins from the cell membrane and guide them to either recycling or destruction. Alterations in this pathway are associated with neuroinflammation and synaptic dysfunction (Vagnozzi and Praticò, 2019). The endo-lysosomal trafficking and protein degradation are processes that are directly impacted by the products of several genetic risk factors, including *APOE*, *PINK1*, *LRRK2*, and *HTT* (Wilson *et al.*, 2023).

Impairments in glycolysis, mitochondrial metabolism and lipid metabolism alter **the energy flux** in all neural cell types and are a common hallmark of NDA. Changes in the glucose supply and energy production can lead to immense detrimental effects. The brain has a high energy demand, to keep ion-gradients upright and recycle vesicles. Insufficient glucose supply can result in hyperexcitability, and functional impairment of neuronal networks (Oyarzabal and Marin-Valencia, 2019; Cunnane *et al.*, 2020). Neurons remain almost exclusively on oxidative phosphorylation, which is accompanied by the production of reactive oxygen species (ROS). ROS directly damages proteins, DNA, and lipids, and thereby undermines their functionality. It has been suggested that a decline of the reserve respiratory capacity is associated with the incidence of a range of neurodegenerative diseases and ageing (Aldana *et al.*, 2017).

Changes in **DNA and RNA expression** are associated with NDA. ROS can induce DNA damage and single strand breaks. Persistent DNA damage induces apoptosis in neurons. Furthermore, mRNA axonal transport, local protein generation at synapses is commonly impaired (Wilson *et al.*, 2023). Apart from that, epigenetic changes, such as a higher methylation level, are associated with NDA (Saul and Kosinsky, 2021).

Exacerbated **inflammation** is a common hallmark of NDA. Microglia are activated by disease associated protein aggregates and trigger an immune response. This does not only result in the partial degradation of cellular debris, but a prolonged immune response also induces apoptosis in neurons. A general upregulation of genes involved in the innate immune system is associated with ageing (Perry and Holmes, 2014). Immunosenescence is a common hallmark of NDA, described by the low-level release of inflammatory cytokines, as well as an overall decrease of the immune response (Tansey *et al.*, 2022). The continued exposure to pro-inflammatory cytokines or misfolded proteins can prime microglia. This process leaves the microglia more susceptible to a secondary inflammatory stimulus on which it will react with an exaggerated response compared to stimulus-naïve microglia. Primed microglia show an increased expression of cytokines (Perry and Holmes, 2014). The priming and the following inflammatory reaction give raise to exacerbated tissue damage in an AD mouse model (Lopez-Rodriguez et al., 2021), but it has been described for other NDA as well (Tansey *et al.*, 2022; Wilson *et al.*, 2023). The immune response itself uses a considerable amount of energy (Wang, Luan and Medzhitov, 2019) and contributes to the imbalance in energy metabolism.

1.1.2 Models to investigate neurodegenerative diseases of ageing (NDA)

Research of neurodegenerative disease employs brain imaging studies, *post mortem* brain investigation and relies on animal and cellular models for exploration and validation of molecular pathways. *Post mortem* examinations are important for assessing pathological changes and estimating disease progression. However, they usually examine only a small area of interest, neglecting changes of disease progression in rate and severity between different regions (Harris *et al.*, 2020).

Animal models are established to elucidate enzymatic pathways. Animals should ideally present a similar phenotype and similar pathomechanisms as humans, which is not always the case. For example, wide-spread neuronal loss in the cortex and hippocampus is not yet reproduced in AD animal models (Esquerda-Canals *et al.*, 2017; Sims, Hill and Williams, 2020). Enzymes might have different functions in animals compared to humans and gene expression can differ between the species (Szabo *et al.*, 2022; Yvanka de Soysa *et al.*, 2022). In the context of neurodegenerative disease, animal models can only represent familial forms, not the much more frequent sporadic type. Notably, rodents do not develop AD naturally and require genetic manipulation to induce relevant molecular and cognitive changes (Sims, Hill and Williams, 2020; Ferrer, 2023). Gene knock-out might be fatal for the animals. Our current understanding of AD as

a multifactorial disease implies that multiple such modifications of the rodents are necessary to generate a precise model, which artificializes the model. However, animal models provide insight into the key altered pathways. In addition to several transgenic mouse models, *Drosophila melanogaster* or *Caenorhabditis elegans* are frequently employed to observe conserved neurobiology pathways (Caldwell, Willicott and Caldwell, 2020; Ye *et al.*, 2023).

Cellular models are beneficial, and the majority of them are less ethically problematic. Immortalized cells have been developed to investigate specific diseases. However, different cell types and different maintenance protocols can produce contradictory outcomes (Foster *et al.*, 2019). In recent years, a technique to generate human induced pluripotent stem cells (iPSC) have been developed. They are a vital approach to personalized medicine (Delenclos *et al.*, 2019; Frederiksen *et al.*, 2021). CRISPR/Cas genetic editing allows the introduction or correction of genetic mutations, opening new ways to investigate disease causing mutations. Isogenic controls can be generated, enabling exploration of the impact of a specific gene more precisely. Differentiation of subtype specific neurons is often possible. In recent years, cellular models which are comprised of different cell types have been developed. Current cellular 3D models are useful to study disease kinetics and relationships between different cell types. 3D cellular models of AD are able to generate neurofibrillary tangles (NFT) and Aβ plaques, 2D models not (Slanzi *et al.*, 2020). Recently a 3D model of AD, mimicking the Blood-brain barrier (BBB) and the inflammatory response to a certain degree, was developed (Shin et al., 2019). Drawbacks of iPSC models include that previously obtained cell ageing is at least partly reversed during reprogramming and neurons differentiated from iPSC cannot yet reproduce the physiological alterations due to ageing. Reprogramming might also induce other epigenetic changes (Kim *et al.*, 2010; Miller *et al.*, 2013).

Taken together, pathohistological hallmarks of NDA are similar to those of physiological ageing, they are frequently aggravated. This includes especially immunosenescence and alterations in energy metabolism. Different disease models have been developed, which are getting more fine-tuned over the years. Each experimental method has its own advantages and drawbacks and should be selected based on the hypothesis.

1.2 Alzheimer's disease: a general overview

Alzheimer's disease is a complex disease, with different pathological characteristics and highly individual symptom development, characterized by progressive neurodegeneration. The interplay

of genetic and environmental factors, impacting disease risk, age at onset and progression, define AD as complex disease (Loy *et al.*, 2014; Sims, Hill and Williams, 2020).

This Section provides an overview of the prevalence and symptoms of AD, followed by a presentation of the underlying pathology. Thereafter, underlying genetic risk factors will be outlined. Finally, pathomechanistic theories aiming to explain of AD onset and progression will be introduced.

A comprehensive and exhaustive discussion would go beyond the scope of project, hence the details presented are focusing on the relevant and most consensual theories.

1.2.1 Definition and prevalence, symptoms of Alzheimer's disease

AD is the most common cause of dementia, a symptom of progressive neurodegeneration. Between 60 and 80 % of the estimated 55 million dementia cases are attributed to AD (Alzheimer's association, 2022; WHO, 2022). The incidence of AD is predicted to increase due to the ageing of the population (WHO, 2022). Neuropathologically, AD is defined by the occurrence of Aβ plaques and neurofibrillary tangles. Aβ plaques are extracellular spheroid-like lesions with agglomerated amyloid β peptide, surrounded by abnormal axonal endings (Calabrò *et al.*, 2021). NFT are aggregates of paired helical filaments consisting of hyperphosphorylated tau protein. Other pathological hallmarks include energetic hypometabolism (Rabinovici, 2019), altered oxidative stress response, and inflammatory changes (Yang *et al.*, 2022). The pathophysiology will be detailed below in Section 1.2.2.

The most important clinical symptoms are deficits in intellectual functions and cognitive abilities (Naj *et al.*, 2017). Memory loss, language difficulty, and behavioural abnormalities are among the early symptoms. Individuals in the later stages show problems in movements, such as walking and swallowing. The varied character of the symptoms, along with the insidious disease progression, renders accurate diagnosis difficult. While biomarkers for Aβ peptides and hyperphosphorylated tau exist, they are not as sensitive as *post mortem* tissue examination. Current clinical diagnostic is either expansive or invasive and might not be widely available (Jack *et al.*, 2018; Khan, Barve and Kumar, 2020). To address this challenge several studies are aiming for a better definition of the disease and to define biomarkers for the which can be used in clinical and research context. The most prominent initiative in this regard is the "National Institute on Aging—Alzheimer's Association Research Framework", which was last updated in 2018 (Jack *et al.*, 2018).

Disease cases are categorized into two distinct groups, namely, early onset (EOAD) and late onset (LOAD). Patients with an early onset account for approximately 10 % of all AD cases (Cacace, Sleegers and Van Broeckhoven, 2016). They start showing symptoms at age < 65 years, and often present other symptoms than dementia and memory loss at time of the first diagnosis (Barnes *et al.*, 2015). These “atypical” symptoms include troubles in visual-spatial orientation, language difficulties, executive and behavioural abnormalities, and motor dysfunction (Graff-Radford *et al.*, 2021). LOAD represents the majority of AD patients. The heritability for these cases has been estimated to 60-80 % (Gatz *et al.*, 2006). Disease onset and progression of LOAD was proposed to origin from polygenic effects. Environmental effects are equally important for disease onset, which could explain individuals reaching a high age without cognitive decline despite possessing multiple risk factors (Cahill, Chandola and Hager, 2022; Gómez-Isla and Frosch, 2022). At a late stage of the disease, the pathologic states of LOAD and EOAD patients are nearly indistinguishable, so that they can only be classified by their age of onset (Cacace, Sleegers and Van Broeckhoven, 2016).

Among multiple risk factors for AD, age and genetic background have the strongest evidence. Multiple modifiable risk factors have been associated with AD: stronger formal education, mentally stimulating activity and physical activity throughout life, and high socio-economic status are associated with a decreased risk of AD. Other treatable or modifiable factors, which are known to increase the risk of AD include midlife obesity, hypertension, hypercholesterinaemia, *diabetes mellitus*, smoking habits and exposure to pesticides (Norton *et al.*, 2014; Hendrie *et al.*, 2018; Armstrong, 2019; Edwards III *et al.*, 2019; Alzheimer’s association, 2022).

Currently, most of the AD patients are women. Thus, it was estimated that women have a higher risk to develop AD then men (20 % vs. 10 % at age 45, respectively). However, other studies attributing for environmental factors and cardiovascular mortality, do not find any influence of the gender on disease risk (Ruitenberg *et al.*, 2001; Gatz *et al.*, 2006; Shaw *et al.*, 2021). An explanation for this observation might be the increased risk of death before the age of 65 years due to cardiovascular disease for men compared to women. As the cardiovascular health protects against AD, studies investigating the risk for women to get AD at an age > 65 years might be biased.

Additionally, a family history of AD represents an important risk factor. People with first grade relative affected by AD have a higher risk to develop the disease (Loy *et al.*, 2014). In this respect, it is important to discriminate between family history and genetic background. Family history includes not only genetic background, but common habits and eating preferences. Indeed, only few families show a mendelian form of AD (Loy *et al.*, 2014).

A genetic risk factor for developing AD is *Apolipoprotein E* (*APOE*), estimated to account for 20 % of the AD attributable risk, which is similar to those identified for major genes in other Mendelian diseases (Dourlen *et al.*, 2019). Three different alleles of *APOE* (ε2, ε3, ε4) are expressed in the human population. Disease risk is increased in carriers of ε4 up to 12%, and decreased in carriers of ε2 to 0.5%, respectively to the most common form ε3 (Loy *et al.*, 2014). A minority of the human population hast one or more ε2 alleles (22 % of African Americans, 13 % of European Americans and 5 % of Japanese ethnicity). One or more ε4 allele is more common (33 %, 24 %, and 10 %, respectively). The ε3/ ε3 phenotype is the most common across ethnicities, ranging from 45 %, 63 %, to 86 % respectively (Nishimura *et al.*, 2017; Rajan *et al.*, 2017) The ε2 phenotype can significantly increase the age of disease onset in EOAD (Cacace, Sleegers and Van Broeckhoven, 2016). APOE has been linked to AD progression via multiple pathways, such as the facilitation of Aβ plaque formation, the disruption of the BBB, alterations in the endo-lysosomal pathway, neuroinflammation and AD related changes to the lipid metabolism. Mechanistic background on the action of APOE and additional genetic risk factors will be outlined in Section 1.2.3.

Therapeutic intervention, although only symptomatic, is available for AD patients. Approaches to reduce behavioural symptoms of AD, such as sleep disturbances, wandering and aggression, include psychological treatment and music-based therapies (Alzheimer's association, 2022). Symptomatic drug-based therapy options are available for AD patients. This includes the acetylcholine esterase (AChE) inhibitors rivastigmine, galantamine and donepezil. They prolong and intensify the neurotransmitter acetylcholine signal and thereby slow down the progression of neurological symptoms (Hampel, Hardy, *et al.*, 2021; Tatulian, 2022). Recent studies suggest a potential disease-modifying effect of donepezil, by substantially reducing rate of degeneration in the hippocampus, cortex, and basal forebrain volume (Cavedo *et al.*, 2016, 2017). Memantine, an inhibitor of the N-methyl D-aspartate (NMDA) receptor, impedes neurotoxicity derived from uncontrolled glutamate signalling (Tatulian, 2022), altering clinical symptoms but not curing the underlying pathology. Aβ plaque is a major pathohistological hallmark, removal of Aβ was proposed as a therapeutic target. While most BACE1 (β-APP-cleaving enzyme-1) inhibitors and anti-Aβ antibodies failed in clinical trials, the anti-Aβ antibody aducanumab was approved by the United States Food and Drug Administration for patients suffering mild cognitive impairment or mild dementia due to AD in 2021. This decision is highly controversial, as aducanumab showed beneficial effects for only a small subgroup of patients, accompanied by the risk of severe side effects (Harris *et al.*, 2020; Hollmann, 2022).

Another potential target is the alteration of the inflammatory response in AD. Clinical and animal studies investigate the employment of immunosuppressive agents, flavonoids, antioxidants, and supplement of essential vitamins and/ or minerals. Lifestyle changes, such as calorie restriction and endurance exercise, are suggested to prevent or ameliorate symptoms (Onyango *et al.*, 2021; Alzheimer's association, 2022). More recent approaches suggest the use of gene therapy. Potential strategies include i) inducing regeneration of neurons by delivery of nerve growth factors, or ii) cell replacement therapy with gene corrected, autologous cells (Khan, Barve and Kumar, 2020; Frederiksen *et al.*, 2021).

The repetitive failure of potential AD therapies in clinical studies (Wang, 2014; Sun *et al.*, 2021) raises doubts, whether we tackle the right therapeutic targets. The failure of clinical trials could have several reasons, such as inappropriate patient inclusion scheme, various states of disease progression, substantial neuronal loss and histological changes during the prodromal phase, administered dose of the therapeutic and appropriate outcome measurement (Tatulian, 2022). While further trials in reducing the Aβ burden of the brain are valid, a focus on primary and secondary prevention trials (Barnes and Yaffe, 2011; Norton *et al.*, 2014), or intervention on other pathologic pathways than Aβ removal, might be likewise beneficial for patients and caretakers.

To summarize, our understanding of the underlying cause for the disease onset and factors enhancing disease progression are still limited. The difficulties to diagnose AD *ante mortem*, and the complex interplay of genetic and environmental risk factors make it difficult to investigate disease mechanisms. To date, several theories on the causes of AD have been proposed, the most important ones will be briefly outlined in Section 1.2.4.

1.2.2 Pathohistological findings

AD has a long pre-clinical phase, defined as an extended period with measurable physiological changes in the absence of symptoms. This prodromal progression can proceed diagnosis up to 5 -10 years (Buchhave et al., 2012; Gordon et al., 2018). Pathophysiological changes do not only include formation of Aβ plaques and NFT, but many other molecular, cellular, and histological alterations.

Aβ is often hypothesized to be the starting point of the AD neuropathological cascade (Selkoe and Hardy, 2016; Hanseeuw *et al.*, 2019). The plaques develop first in the basal, temporal, and orbitofrontal cortex of the brain, and later progress to involve the neocortex and all areas of the isocortex (Braak and Braak, 1991; McGirr, Venegas and Swaminathan, 2020). Notably, the Aβ abundance does not correlate very well with cognitive decline (Selkoe and Hardy, 2016). Aβ

aggregation is proposed as an upstream pathophysiological event that may trigger or facilitate downstream alterations in tau processing, such as tau-mediated toxicity and formation of NFT (Busche and Hyman, 2020; He *et al.*, 2018). *In vivo* experiments indicated a positive correlation of tau production rate and amyloid burden, where Aβ exposure is increasing the concentration of tau in the cerebrospinal fluid (Sato *et al.*, 2018).

Amyloid β is a product of the amyloid precursor protein (APP), which is widely abundant in neurons, especially at the synaptic end feet (Hampel, Hardy, *et al.*, 2021). Previous work revealed that APP might be physiologically involved in neurogenesis, participating in LTP and neurite growth via calcium release regulated pathways (Morley *et al.*, 2019). Emerging evidence suggests that APP is required pre- and postsynaptic for functional synaptic development (Dourlen *et al.*, 2019). While both Aβ and APP have physiological functions, aberrant APP degradation contributes to amyloid aggregation and extracellular plaque development.

The most inquired degradation pathways, namely the amyloidogenic and the non-amyloidogenic pathway, are illustrated in Figure 1.1. They produce several species with their own distinct intrinsic properties and putative functions (Hampel, Hardy, *et al.*, 2021). The cleavage of APP by an α-secretase result in a soluble APP fragment (sAPPα) and the C83 fragment. While sAPPα is released in the extracellular space, C83 is cleaved by a γ-secretase into P3 and the APP intracellular domain (AICD). AICD has been shown to regulate apoptosis and gene expression in the nucleus (Bukhari *et al.*, 2017). In contrast to the products of the amyloidogenic pathway, none of these products is known to facilitate Aβ plaque formation.

Different members of the ADAM (A Disintegrin And Metalloproteinase) family, namely ADAM9, ADAM10, and ADAM17, have been proposed in the function of the α-secretase. Additional evidence hints towards ADAM10, which has been found to be essential for APP shedding in mouse brain and was proven to be active in human neurons (Kuhn *et al.*, 2010; Suh *et al.*, 2013). The γ-secretase is a complex of different proteins; the catalytic element consists of PSEN1 (Presenilin 1) and PSEN2 (Presenilin 2) (Hampel, Hardy, *et al.*, 2021). Mutations in the genes involved in this cascade have been found detrimental to AD progression.

Cleavage of APP via BACE1 initiates the amyloidogenic pathway. The cleavage takes place after endocytosis of both, APP and BACE1, in early endosomes (Gao *et al.*, 2021). APP is cleaved at another position resulting in another soluble APP fragment (sAPPβ) and the intramembrane C99 terminus. This C99 terminus is further cleaved by γ-secretase releasing Aβ monomers and the AICD into the cell plasma (LaFerla, Green and Oddo, 2007; Hampel, Hardy, *et al.*, 2021) The γ-secretase may cleave APP at different positions, resulting in Aβ species with varying lengths and aggregation characteristics. The high ratio of two such Aβ peptides, Aβ42 and Aβ40, is

utilized as a surrogate measure suggesting a larger tendency for agglomeration and hence a higher neurotoxic potential the higher the ratio.

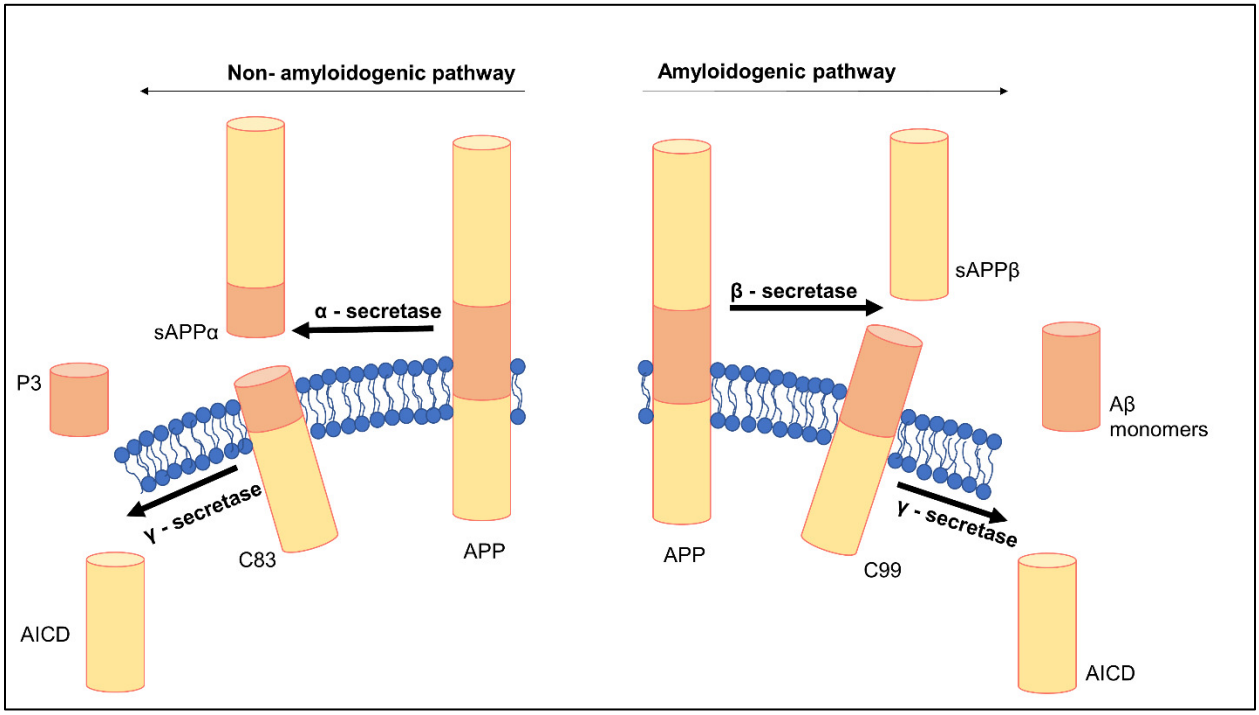

Figure 1.1 Cleavage of Amyloid precursor protein (APP) via Non-Amyloidogenic or Amyloidogenic pathway. The location of APP plays a crucial role. At the plasma membrane, it is preferentially cleaved by an α-secretase; at the endosomal membrane it is preferentially processed by the β-secretase. The γ-secretase acts on the transmembrane part of the APP protein.

Aβ peptides tend spontaneously to oligomerize, further agglomerate to protofibrils and eventually form dense, insoluble fibrils called plaques. All states are highly flexible and interchangeable (Hampel, Hardy, *et al.*, 2021; Buell, 2022). Although it was observed in overexpression studies, there seems to be no competition on APP cleavage between the α- and the β-secretase in physiological conditions. Reasons could be that the APP concentration is not rate limiting or that both reactions occur in different cellular locations (Kuhn *et al.*, 2010).

Prodromal AD brains demonstrate a significantly reduced hippocampal neurogenesis of AD patients compared to healthy persons (Moreno-Jiménez *et al.*, 2019). Hippocampal atrophy has further been reported as one of the initial signs of AD (Dourlen *et al.*, 2019). Interestingly, the grey matter volume of the cholinergic basal forebrain is proposed as a better predictor of the cognitive decline than the hippocampal volume (Brueggen *et al.*, 2015). While the basal forebrain volume physiologically declines with age, this decline was exacerbated in pre-clinical state of AD (Pini *et*

al., 2016). Loss of cholinergic neurons of the basal forebrain parallel cognitive decline (Bissonnette *et al.*, 2011), their loss initiates the impairments of short-term memory recall.

Another early event in AD is synaptic loss, which has been identified as the driving force towards impairments in memory and spatial learning (Xie *et al.*, 2017). Impairments of synaptic mitochondria function is another important change in prodromal AD (Cai and Tammineni, 2017). Mitochondria are the main producer of ATP in brain cells and their presence in synaptic terminals is critical for neurons since ATP is vital to maintaining synaptic function. Synaptic mitochondria appear to be more susceptible to soluble forms of Aβ, resulting in decreased respiration, elevated production of ROS, and compromised Ca^{2+} buffer capacity (Flannery and Trushina, 2019). The induced oxidative stress, another manifestation in early AD, causes damage of mitochondrial DNA and induction of apoptosis (Guo *et al.*, 2020). The high vulnerability of synaptic mitochondria to soluble Aβ species (Cai and Tammineni, 2017), could explain synaptic loss (Ribarič, 2023) and glucose hypometabolism (Swerdlow, 2018), which were both observed in prodromal AD. Additionally, mitochondrial axonal transport has been found to be impaired in AD neurons early on, so that the damaged synaptic mitochondria could not be replaced (Flannery and Trushina, 2019).

Neuroinflammation is another prodromal sign of AD. While the innate immune system shows a higher initial activity in older individuals, its activity is further boosted in AD early on (Sala Frigerio *et al.*, 2019). The prolonged neuroinflammation substantially elevates the secretion of pro-inflammatory cytokines such as TNFα (tumor necrosis factor alpha), IL-1β (interleukin 1 beta) and IL-6 (interleukin 6), with harmful effects. The permeability of the BBB increases, mitochondrial and oxidative stress worsens, leading to a vicious cycle by further activating the microglial response (Calabrò *et al.*, 2021). Microglia activation does not only affect the surrounding tissue, it also effects organization of long-distance neuronal networks (Tondo *et al.*, 2020). In the case of AD, reactive microglia can be detected in prodromal stages in human and even before the aggregation of Aβ plaques in a mouse model (Qian, Shen, and Wang, 2016; Yang *et al.*, 2020). The etiology of neuroinflammation and inflammaging has been outlined in the previous Subsection (Section 1.1, Neurodegenerative diseases of ageing).

1.2.3 Genetic risk factors

AD, as a complex disease, can be caused by genetic and environmental factors, both individually and in combination. Dourlen *et al.*, 2019, argues that the vast majority of the AD pathophysiological pathways are driven by or include genetic determinants. The observation that some families have a larger proportion of AD patients indicates a genetic component of the disease. This familial AD (fAD) form has been estimated to account for 15-25 % of all AD cases and occur mostly at an early age at onset (D'Argenio and Sarnataro, 2020). In particular, approximately 5 % of AD cases follow an autosomal-dominant inheritance pattern. No genetic mutation has been identified to be causative to LOAD; instead, most cases are probably caused by mutations in one or several susceptibility loci accompanied by environmental factors (Bekris *et al.*, 2010).

The first genetic risk factor associated with AD was *APOE* in 1993. Its effect on EOAD and LOAD is outlined in Section 1.2.1 above. The advent of genome-wide association studies (GWAS) allowed the identification of rare single nucleotide variants (SNV) linked to LOAD. Approximately 95 genes have been associated with LOAD in the last two decades (Kamboh, 2022).

1.2.3.1 Genome - wide association studies (GWAS)

In GWAS, entire genomes of patient and control cohorts are compared, in order to find single nucleotide polymorphisms (SNP), which could explain pathological changes. This method allows the detection of rarer risk genes with a small effect size. The detected SNP may be directly causative in case it is located in coding exons or regulatory elements. However, in the majority of cases variants are located in non-coding regions of the genome and cannot be directly linked to a gene or an alteration in protein structure or function (Farh *et al.*, 2015; Ata *et al.*, 2021). In these cases, usually the nearest gene is associated to the loci, which might not be the case. Many of the trait-associated variants of small effect size are non-coding, and many of them are concentrated in regulatory regions (Maurano *et al.*, 2012; Farh *et al.*, 2015). In the context of AD many potential SNP were excluded from further analysis as they might not be linked to existing disease-evolving theories or they are not expressed in the relevant tissue or cell type (Bien *et al.*, 2019).

To reach statistical significance, large sample sizes are needed. While the first GWAS in AD context included approximately 15'000 participants (Harold *et al.*, 2009; Lambert *et al.*, 2009), number of participants increased over time. Several data sets have been joined in recent years to enhance sample size and detect rare SNP. To adjust for difficulties in definition of case and

control samples, genome-wide association study by proxy (GWAX) were developed. This type of study separates not only trait affected subjects, but also relatives of the affected and un-affected individuals. This method allows for stronger statistical power, while being logistically more viable than gathering conventional examples (Liu, Erlich and Pickrell, 2017; Kamboh, 2022).

Novel approaches to identify rare variants and provide new molecular mechanistic insights for AD include further increase of the data set, and use of up-to-date sequencing techniques, such as whole-exome microarray, whole-exome sequencing, and whole-genome sequencing (WGS). Correction for phenotypes such as age-of-onset, ethnic background, or biomarker expression, promises detection of additional genetic polymorphisms (Naj *et al.*, 2017; Bien *et al.*, 2019; Veitch *et al.*, 2019).

Discovery of additional new susceptibility loci for AD will most likely not only help to unravel the complex disease mechanisms, but it has the potential to identify new genetic markers to refine the different genetic signatures of clinical AD (Cacace, Sleegers and Van Broeckhoven, 2016). According to current estimates, rare genetic variants associated with LOAD could account for 13-16 % of the genetic susceptibility of AD (Ridge *et al.*, 2016; THE BRAINSTORM CONSORTIUM *et al.*, 2018). It has been suggested that the combination of multiple genes might explain a major part of the heritability (Cruchaga *et al.*, 2012). Confirmation of susceptibility loci in animal or cell model experiments to define underlying pathways are necessary; albeit one-third of suspected risk genes do not have mouse orthologs (Abubakar *et al.*, 2022).

1.2.3.2 Genetic risk variants associated with Early-onset Alzheimer´s disease

EOAD is an almost entirely genetically determined disease with a heritability ranging between 92-100 % (Wingo *et al.*, 2012). High-penetrance mutations in the genes *APP*, *PSEN1,* and *PSEN2* explain about 10-15 % of the cases, leaving most of the autosomal dominant inheritance cases of EOAD unexplained (Cacace, Sleegers and Van Broeckhoven, 2016; Ayodele *et al.*, 2021). The transcripts of these mutations alter the way APP is processed towards the amyloidogenic pathway and eventually increase the amount of Aβ formed.

Mutations in *APP* follow mostly an autosomal-dominant inheritance pattern and have been estimated to account for up to 16 % of all cases of autosomal-dominant AD (D'Argenio and Sarnataro, 2020). However, variants with a recessive pattern of inheritance have been found (Tomiyama *et al.*, 2008; Xia *et al.*, 2021). Mechanistically, changes in APP have been postulated to not only accelerate BACE1-mediated shedding, but also to modify the aggregation characteristics of the resultant Aβ peptide and hence exacerbate neurotoxicity (Götz *et al.*, 2019).

Interestingly, a protective variant of APP has been found (Jonsson *et al.*, 2012). Finally, triplication of APP in some patients with Down syndrome renders them to develop AD symptoms at an early age (Sawa *et al.*, 2022).

Within the γ-secretase complex, *PSEN1* and *PSEN2* are the main contributors towards the enzymatic cleavage of APP. Mutations in these genes are expected to enhance the amyloidogenic pathway and/or shift the Aβ42/Aβ40 ratio towards a more aggregating state. *PSEN1* is the most common gene related to familial AD, with more than 200 pathogenic mutations associated. A haplotype of different SNP in carriers of a *PSEN1* mutation has been found to increase the age at onset by 10 years. Interestingly, no mutation in *BACE1* has been identified causal to fAD.

In recent years, case-control studies suggested *SORL1* (*Sortilin Related Receptor 1*) as an additional genetic risk factor for both, EOAD and LOAD (Alvarez-Mora *et al.*, 2022). These rare, non-mendelian *SORL1* variants are expected to raise the risk of EOAD by up to 5 times (Nicolas *et al.*, 2016). SORL1, participates in APP trafficking from and to the trans-Golgi network. Its loss-of-function might lead to an increased release of APP from the Golgi to the plasma membrane and decreased retrieval of APP from the endosomes towards degradation in the lysosome, leaving more substrate for the amyloidogenic pathway. As SORL1 directs retrograde transport of the neurotrophins BDNF and GDNF (Glial cell line-derived neurotrophic factor), it might further be linked to synaptic pruning (Glerup *et al.*, 2013; Rohe *et al.*, 2013). Additionally, SORL1 has been found to target already produced Aβ peptides for lysosomal degradation (Campion, Charbonnier and Nicolas, 2019; Ayodele *et al.*, 2021). A recent study found increased APP concentration in early endosomes in human iPSC derived neurons lacking *SORL1* expression. These cells showed a higher Aβ burden which was reversible by BACE1 inhibition (Knupp *et al.*, 2020).

Taken together, genetic risk factors for EOAD are very well established and linked to pathological mechanisms, they only explain a minor part of the familial EOAD cases.

1.2.3.3 Genetic risk variants for Late-onset Alzheimer's disease

The picture for LOAD is dramatically different, as the majority of cases develop sporadic (Valdes *et al.*, 2022). However, a high heritability has been estimated, which might be explained by a polygenic model. This implies combination of multiple alleles of weak genetic effects and low genetic penetrance to increase AD risk (Medway and Morgan, 2014; Naj et al., 2017).

To date, approximately 95 risk loci have been identified with LOAD. During subsequential analysis of the gene function and the function of their products, they seem to converge into a few pathways,

which reflect the existing theories of AD progression. These pathways include: APP processing, endocytosis, lipid metabolism, involvement of the immune system, tau pathology and BBB integrity (Dourlen *et al.*, 2019; Bellenguez, Grenier-Boley and Lambert, 2020; Hampel, Hardy, *et al.*, 2021). An illustration is provided in Figure 1.2. In the following, the validated risk loci will be briefly introduced.

The Aβ cascade theory places the pathological **accumulation of Aβ** as the trigger for AD onset and starting point for all other pathological events. The concentration of hazardous Aβ species rises as a result of altered or enhanced cleavage of APP via the amyloidogenic pathway.
As stated before, mutation or overexpression of *APP*, *PSEN1*, and *PSEN2* may be causal to AD. Furthermore, loss-of-function mutations in *ADAM10* and *ADAM17* can lead to a decreased non-amyloidogenic pathway, leaving more APP to be processed via the alternative amyloidogenic pathway (Kamboh, 2022). *APOE* has been found to influence APP transcription, with APOE ε4 showing the biggest stimulating effect (Huang *et al.*, 2017).
The trafficking of APP and BACE1 is another way to influence APP processing. Genetic risk variants associated with altered APP trafficking in AD are: *SORL1* (outlined in the previous Section), *BIN1* (*Bridging integrator 1*), *CD2AP* (*CD2-associated protein*), and *ABCA7* (*ATP Binding Cassette Subfamily A Member 7*) (Satoh *et al.*, 2015; Szabo *et al.*, 2022). The *BIN1* transcript plays a key role in the sorting of BACE1 into early endosomes. This is supported by increasing evidence linking *BIN1* downregulation to BACE1 accumulation in early endosomes and increased Aβ generation (Miyagawa *et al.*, 2016; Ubelmann *et al.*, 2017). Similarly, CD2AP and ABCA7 transport APP towards the early endosomes, alteration in their activity can enrich endosomes with APP and guide it towards amyloidogenic processing (Satoh *et al.*, 2015; Ubelmann *et al.*, 2017).

The gene products of *PICALM* (*Phosphatidylinositol Binding Clathrin Assembly Protein*), *SORL1*, *BIN1*, and *CD2AP* have been linked to the **endo-lysosomal network in AD** (Dourlen *et al.*, 2019; Szabo *et al.*, 2022). Endosomal/lysosomal abnormalities are an early symptom of prodromal AD (Aikawa *et al.*, 2019). The above-mentioned trafficking of APP and BACE1 is the most crucial aspect of endosome involvement in AD. Apart from this, cell-to-cell communication might be mediated by exosome release. To demonstrate, *BIN1* downregulation in forebrain neurons led to transcriptomic changes in microglia, which might have been mediated via the endosome-exosome pathway (McAvoy *et al.*, 2019; Szabo *et al.*, 2022). PICALM is a known mediator of trafficking between endosomes and the trans-Golgi network. In a *post mortem* brain study, *PICALM* expression was altered in AD brains and localized in NFT, which further strengthens the

association of *PICALM* to AD (Ando *et al.*, 2013; Szabo *et al.*, 2022). One study linked APOE ε4 reduced endocytosis of astrocytes to PICALM. However, the exact mechanism remains unclear (Narayan *et al.*, 2020; Szabo *et al.*, 2022).

Several genes, among them *CLU* (*Clusterin*), *APOE*, *TREM2* (*Triggering Receptor Expressed On Myeloid Cells 2*), and *ABCA7* have been linked to **lipid metabolism**. CLU has been found to bind to Aβ oligomers and fibrils and promote their endocytosis by astrocytes and microglia (Foster *et al.*, 2019). TREM2 is a microglial receptor, necessary for the endocytosis of apolipoproteins, such as CLU and APOE. Aβ uptake via TREM2 has been found to be increased, when Aβ was bound to CLU or APOE (Yeh *et al.*, 2016). ABCA7 shuttles toxic lipids out of astrocytes and neurons, an impairment in this function could lead to cell death (Dib, Pahnke and Gosselet, 2021).

Approximately half of all confirmed GWAS risk variants are associated with the **immune system**. Among them, *ADAM17*, *ABCA7*, *APOE*, *CLU, CR1* (*Complement C3b/C4b receptor 1*), *PLCG2* (*phospholipase C gamma 2*) and *TREM2* were validated by recent GWAS studies. Importantly, *TREM2, CR1,* and *PLCG2*, are strongly expressed in microglia, indicating a role for the innate immune system in the pathogenesis of AD (Medway and Morgan, 2014; Kamboh, 2022; Lichtenthaler, Tschirner and Steiner, 2022).

TREM2 is a membrane-bound receptor of microglia, binding cellular lipids which were released from cellular damage of surrounding tissue (Efthymiou and Goate, 2017). It is substantial to the microglial phagocytosis of Aβ and enhances the production of anti-inflammatory cytokines. TREM2 overexpression in a mouse model resulted in reduced Aβ plaque load, neuroinflammation, synapse loss and memory impairments (Selkoe and Hardy, 2016). TREM2 has a protective impact in the early and middle stages of AD, but it becomes deleterious in the late stages by activating the adaptive immune system (Jay *et al.*, 2017).

As mentioned before, Aβ phagocytosis microglia via TREM2 is facilitated by CLU and APOE (Yeh *et al.*, 2016). Apart from that, APOE can alter AD progression in via TREM2 dependent pathways (Yang *et al.*, 2020). *CR1* is expressed in microglia. Two SNP associated with increased risk in AD are associated with decreased *CR1* expression in brain tissue. Thus, it seems obvious, that these *CR1* variants are less capable of mediating the microglial activity, including immune activation and synaptic pruning (Efthymiou and Goate, 2017). Finally, *ABCA7* haplodeficiency has been shown to trigger an insufficient microglial response in a mouse model (Aikawa *et al.*, 2019).

The substantial portion of AD risk genes involved in immune system pathways underline the importance of the immune system in AD. Aberrant function of the immune system was, among others, suggested as a starting point of AD pathology.

The gene transcripts of *BIN1*, *PICALM*, *ABCA7*, *SORL1* and *APOE* have been associated with **tau pathology.** BIN1 might not only be involved in cell-to-cell spreading of prion-like tau aggregates, but also mediate tau-induced toxicity (Sartori *et al.*, 2019; Gao *et al.*, 2021). PICALM has been found to bind tau, and it is speculated it might promote tau fibrillisation (Ando *et al.*, 2013).

An epigenetic study associated altered DNA methylation and higher expression of *SORL1*, *BIN1* and *ABCA7* to higher NFT density (Yu *et al.*, 2015). They also observed higher tau tangle density correlated with higher expression levels of *SORL1* and *ABCA7*. However, we still do not understand, how the mechanistic interaction on either gene or protein level could look like. AD patients carrying two *APOE ε4* alleles show a higher tau burden compared to patients with only one or none *APOE ε4*. This observation was replicated in studies employing iPSC derived neurons. An effect of the APOE ε4 on tau hyperphosphorylation compared to APOE ε3 was measurable, however, the expression of *APOE* was not altered. This finding suggests an isoform-specific effect, however, the underlying mechanism is still unclear (Wadhwani *et al.*, 2019; Yamazaki *et al.*, 2019).

The **BBB** is a thin layer of endothelial cells surrounded by astrocytes, which regulates the exchange of goods and metabolites from blood to CSF (cerebrospinal fluid) and *vice versa*. Thereby it influences the neuronal environment, which homeostasis is important for neuronal and synaptic function. Imaging studies find impairment of BBB integrity in prodromal AD (Montagne, Zhao and Zlokovic, 2017). Polymorphisms in *APOE*, *PICALM*, *CD2AP*, and *CLU* have been associated with altered BBB integrity in AD. APOE, CLU, and PICALM participate in the transcytotic trafficking of Aβ in endothelial cells from the abluminal side toward the vesicular side. Again, the efficiency of this transport is dependent on the APOE isoform, with APOE ε4 being the least efficient one (Huang *et al.*, 2020). CD2AP is highly enriched in cerebrovascular endothelial cells and CD2AP deficiency has been shown to lead to disruption of the BBB in a mouse model (Cochran *et al.*, 2015). However, exact molecular mechanisms of the transport of Aβ through the BBB are not yet completely understood.

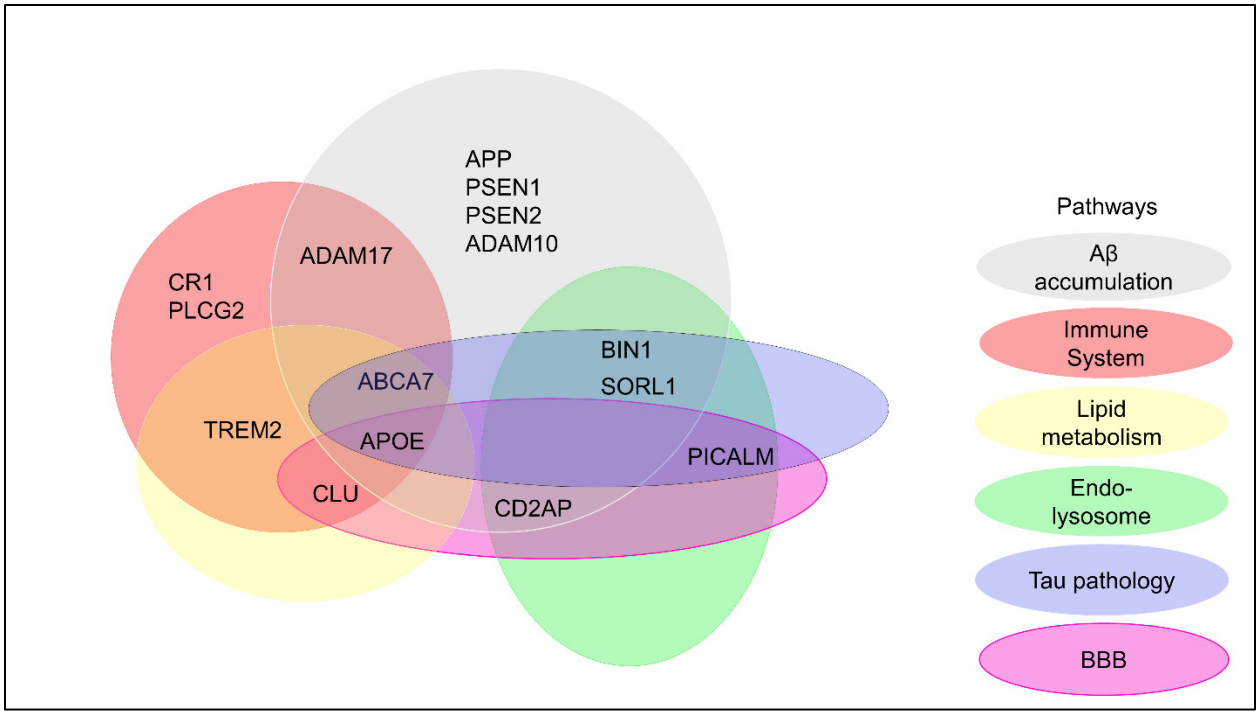

Figure 1.2 Genetic risk factors for AD converge into different pathways. This figure illustrates how this "post GWAS analysis" adds to the complexity of the mechanistic understanding.

Other pathways suggested by analysis of GWAS data include mitochondrial cascade, gene expression regulation, and synaptic plasticity (Dourlen *et al.*, 2019; Hoogmartens, Cacace and Van Broeckhoven, 2021). It needs to be understood that genetic mutations, have a minimal influence on the overall AD prevalence, as they are either rare or introduce a small risk (Calabrò *et al.*, 2021). Notably, for some loci protective variants have been found (Sims, Hill and Williams, 2020).

1.2.4 Overview of mechanistic theories

The molecular mechanisms behind disease development and progression remain unknown despite intensive investigation over the last decades. The scientific community has advanced several theories on the underlying cause of the neurodegeneration. These theories are supported by scientific data, yet they frequently overlap. Below, the most consensual theories will be discussed.

1.2.4.1 Amyloid cascade hypothesis

The amyloid cascade hypothesis postulates that Aβ plaque aggregation is the main driver of AD progression. Amyloid plaques have long been recognized as a pathohistological hallmark, and as such, they have been proposed as the disease's etiological agent and key feature. The fact that

Aβ accumulates in AD brains over time and seems to precede other pathological events, suggested that it might be the triggering factor. Furthermore, genetic polymorphisms causing Aβ plaques were found to cause EOAD, initiating studies on the potential cause of Aβ accumulation and it´s detrimental effects on the patients' health (Hampel, Hardy, *et al.*, 2021). Recently, several genetic risk loci have been associated with Aβ related pathways, including APP processing, Aβ trafficking and degradation (Lambert *et al.*, 2013; Kunkle *et al.*, 2019; Kamboh, 2022).

Aβ monomers participate in cytoprotective pathways, intracellular signalling, and synaptic function. Released monomers at the synaptic cleft have a critical role in sustaining neuronal bioenergetic levels essential for proper synaptic activity (Giuffrida *et al.*, 2015; Chen and Mobley, 2019).

While Aβ monomers show neuroprotective qualities, Aβ oligomers, protofibrils and Aβ plaques have detrimental effects on the functions of several brain cell types, including neurons, astrocytes, and microglia. Aβ oligomers obtained intracellularly from APP-expressing cultured cell lines, disrupt hippocampal LTP in brain slices and *in vivo*, impair memory of complex learned behaviour in rats, and decrease dendritic spine density in hippocampal slice cultures (Mucke and Selkoe, 2012). Similar results were reproduced with extracts from human *post mortem* brain containing naturally secreted human Aβ, which additionally proved Aβ oligomers to facilitate long-term depression (LTD) (Shankar *et al.*, 2008). Furthermore, oligomeric Aβ can disrupt intracellular calcium balance, thereby inducing mitochondria dysfunction, and trigger the production of ROS (Guo *et al.*, 2020). They have been shown to induce inflammatory response (Forloni and Balducci, 2018). Experimental models of ageing and AD indicate that Aβ-mediated molecular pathways are linked to lipid homeostasis and angiogenesis (Hampel, Hardy, *et al.*, 2021). Alterations in BDNF signalling, driven by Aβ oligomers, may impair hippocampus neurogenesis and adult synaptic plasticity (Zimbone *et al.*, 2018). However, Aβ oligomers at low concentration could support synaptic transmission (Mucke and Selkoe, 2012).

Synthetic Aβ protofibrils, a precursor to thicker and more regular fibrils, can induce neurotoxic effects (Mucke and Selkoe, 2012). Concentration of Aβ protofibrils in the brain, but not of total Aβ, correlated with spatial learning impairment in mice (Lord *et al.*, 2009). It was shown that Aβ protofibrillar species impair cognitive and behavioural functions and inhibit LTP-mediated synaptic plasticity in rodent hippocampus. Furthermore, Aβ protofibrils have been linked to inflammatory responses in AD brain (O'Nuallain *et al.*, 2010; Hampel, Hardy, *et al.*, 2021; Tsoi *et al.*, 2023).

Aβ fibrils and plaques are the insoluble forms of the Aβ aggregates and can be found in regions with increased synaptic loss in AD brain. They are associated with inflammatory response,

synaptic dysfunction, decreased spine density and neuronal loss in in AD animal models and in AD patients (McGirr, Venegas and Swaminathan, 2020; Hampel, Hardy, *et al.*, 2021). Synthetic amyloid fibrils have been found to induce cell death in cultured neuron cells (Guo *et al.*, 2011).
To conclude, most amyloid species show neurotoxic effects. The current focus of the amyloid cascade hypothesis lies on the soluble forms of Aβ, which are suspected to be more dangerous compared to the insoluble ones (Ricciarelli and Fedele, 2017). Their abundance correlates better with dementia stage of the AD patients compared to amyloid plaque burden (Shankar *et al.*, 2008).

The amyloid cascade hypothesis remains the most accepted theory on AD pathologic mechanisms, however, some researchers raise doubts. This concern is based on several observations, among them the claim that, while Aβ oligomers show neurotoxic effects *in vitro*, these effects could not yet be replicated *in vivo* (Ricciarelli and Fedele, 2017). Furthermore, there is no evidence that the formation of Aβ is causally linked to LOAD (Medway and Morgan, 2014), even though susceptibility genetic polymorphisms connected to Aβ biosynthesis and metabolism have been found recently. Recent literature suggests a beneficial effect of elevated Aβ concentration in AD patients (Imbimbo *et al.*, 2022). Despite intensive research since the postulation of the amyloid cascade hypothesis it was not yet undoubtedly verified or mechanistically resolved.

1.2.4.2 Inflammatory cascade hypothesis

This hypothesis places altered immune response as the initial event in AD progression, inducing all other pathological changes and Aβ plaque formation. AD shows cytopathology in different cell types, not only neurons, but also microglia and astrocytes, which are enriched for AD risk genes (Harris *et al.*, 2020). Different cells of the immune system, such as microglia, astrocytes, macrophages, and oligodendrocytes are substantial to disease onset and progression, individually and synergistically (Heneka *et al.*, 2015; Skaper *et al.*, 2018).

Microglia are the resident immune cells of the brain and part of the innate immune response. In physiological conditions they scan their local environment through brief contact with the surrounding cells by changing the shape of their filipodia (Wake *et al.*, 2009). Thereby, they mediate synaptic pruning (Paolicelli *et al.*, 2011), and stimulate neuronal growth via the release of growth factors such as IGF1 (insulin-like growth factor 1) and BDNF. Additionally, they phagocytose cellular debris and dying cells (Lenz and Nelson, 2018). Activation of microglia happens through different stimuli, such as mitochondrial DNA, loss of inhibitory neuronal ligands,

or excess cellular debris and misfolded proteins. This activation leads to transcriptomic changes, leading to release of pro-inflammatory and anti-inflammatory cytokines, upregulation of surface antigens and enhanced proliferation (Perry and Holmes, 2014). Indeed, microglial proliferation correlates with AD progression in humans and mouse models (Hou *et al.*, 2022).

The anti-inflammatory properties of microglia (such as tissue repair) and pro-inflammatory functions (such as the clearance of cellular debris) must be tightly balanced. A disruption of equilibrium might result in chronic inflammation, which in turn damages the tissue (Rea *et al.*, 2018; Murdaca *et al.*, 2022). This is detrimental to the central nervous system, as the brain has limited capacity for regeneration (Perry and Holmes, 2014). Activated microglia can contribute to the removal of synapses via phagocytosis or release of synaptotoxic cytokines (Wang *et al.*, 2015; Xie *et al.*, 2017; Murdaca *et al.*, 2022). The release of cytokines prompts and aggravates the seeding of protein aggregates, such as Aβ plaque and NFT (Heneka *et al.*, 2015; Wang *et al.*, 2015). Interestingly, with increasing age microglia tend to be constantly activated and release the pro-inflammatory cytokines TNFα, IL-1β and IL-6. This might explain why LOAD patients show low-grade activation of the innate immune system before the accumulation of Aβ plaque (Yang *et al.*, 2020). During AD progression, activated microglia are surrounding Aβ plaques and neurons containing NFT (Serrano-Pozo *et al.*, 2011; Fixemer *et al.*, 2022). This is not surprising, as microglia contributes to Aβ clearance by phagocytosis (Efthymiou and Goate, 2017) and thereby limit plaque growth. However, a study of cortical brain samples of AD patients revealed that microglia surrounding the plaques show signs of impaired Aβ uptake (Onyango *et al.*, 2021). Microglia can phagocytose and, thus, reduce the abundance of Aβ species, but also contribute to Aβ aggregation and excessive neuro-inflammation (Lichtenthaler, Tschirner and Steiner, 2022).

Taken together, scientific evidence suggests that microglia play a vital role in AD pathogenesis and not only react in a physiological manner to neurodegeneration.

Apart from microglia, astrocytes are substantial to the onset and development of AD (Acosta, Anderson and Anderson, 2017). The physiological functions of astrocytes include trophic support of neurons and regulation of synaptic pruning (Durkee and Araque, 2019; Preman *et al.*, 2021). Similar to microglia, astrocytes can be both, neuroprotective (reducing inflammation and stimulating repair), and neurotoxic (promoting inflammation and potential neurodegeneration), depending on their activation (Onyango *et al.*, 2021; Preman *et al.*, 2021). Reactive astrogliosis, the increased astrocyte proliferation, is a prominent hallmark in preclinical AD and suspected to precede the Aβ agglomeration (Preman *et al.*, 2021). It might be triggered by Aβ oligomers or hyperphosphorylated tau, though not by Aβ plaque (Schöll *et al.*, 2015).

Reactive astrocytes contribute to the clearance of Aβ deposits by release of different factors, including APOE (Arranz and De Strooper, 2019). Phagocytosis of Aβ has been observed in studies of rodents and *post mortem* human brain (Gomez-Arboledas *et al.*, 2018; Hampel, Hardy, *et al.*, 2021). Reactive astrocytes secret pro-inflammatory cytokines, and thereby intensify the neuroinflammatory response (Van Eldik *et al.*, 2016; Hampel, Hardy, *et al.*, 2021). Additionally, astrocytes are a major component of the BBB. The breakdown of which is an important pathophysiological hallmark of AD and contributes further to inflammation and neurodegeneration (Sweeney, Sagare and Zlokovic, 2018; Arranz and De Strooper, 2019).

As outlined in the previous Section 1.2.3 (Genetic risk factors), various genetic risk factors have been established for AD. In fact, more than half of these risk genes are involved in the innate immune system and physiological microglia function (Onyango *et al.*, 2021), among them *APOE*, *TREM2*, *BIN1*, *CD33*, and *PICALM* (Sala Frigerio *et al.*, 2019). This underlines the key role of the immune system in the pathogenesis of AD.

The evident genetic and functional contribution of the immune system towards AD strongly suggests an active role of the innate immune system in the disease progression (Shi and Holtzman, 2018). However, the microglial reaction in AD are also appearing during normal ageing, albeit slower and quantitatively more limited (Sala Frigerio *et al.*, 2019).

1.2.4.3 Cholinergic hypothesis

The finding that acetylcholine signalling is impaired in AD led to the idea that AD pathology could be based on this neurotransmitter. This is supported by the discovery of severely degenerated cortical cholinergic axons in AD brains.

The cholinergic neurons of the basal forebrain (BFCN), mainly located in the Nucleus basalis Meynert, constitute the most important cholinergic input of the brain. Axons of Nucleus basalis Meynert neurons project into the cerebral cortex and the hippocampus, providing the only cholinergic input to these regions. Cholinergic neurotransmission is required for cognitive functions, such as sleep, memory, attention, and motivation. The eponymous neurotransmitter acetylcholine, affects neuronal excitability, regulates circuits dynamics and participates in synaptic plasticity (Goard and Dan, 2009; Harris *et al.*, 2020). While the loss of BFCN is part of physiological ageing, the atrophy is exacerbated in AD and correlates with the cognitive functions of the patients (Mesulam *et al.*, 2004). A selective loss of BFCN is observed in the prodromal

phase of AD progression, potentially preceding the spread of Aβ plaques in this area (Hall *et al.*, 2008; Giacobini, Cuello and Fisher, 2022).

BFCN are determined by the expression of the NGFR (nerve growth factor receptor) and NTRK1/2 and 3 (neurotrophic receptor tyrosine kinases) in addition to their cholinergic identity. These neurotrophin receptors play a vital role in neuronal development regulation. The NGFR has the ability to bind mature neurotrophins (BDNF, NGF and Neurotrophin-3 and -4) and their respective premature pro-forms. Depending on the ligand, NGFR recruits different receptors. Binding of pro-NGF and recruitment of sortilin activates downstream apoptotic pathways. In contrast, binding of BDNF or NGF and recruitment of NTRK receptors promotes cell survival, differentiation, and synaptic plasticity (Meeker and Williams, 2015). Pre-synaptic binding of mature NGF initiates as signalling cascade stimulating acetylcholine release from the synapses (Abubakar *et al.*, 2022). Interestingly, NGFR shows an approximately 5x higher affinity to the premature compared to the mature neurotrophins (Lee *et al.*, 2001). Cleavage of NGFR by ADAM17 shows different neuroprotective properties, which will be elucidated in Section 1.3.4.

In AD brains, an impairment of NGF maturation renders neurons to an excess of pro-NGF with potential detrimental effects. This defect in maturation can be triggered by Aβ or neuroinflammation but other potential triggers, *e.g.* ROS, have not yet been investigated (Hampel *et al.*, 2018). The high levels of pro-NGF leads to an imbalance in NGF signalling towards the apoptotic effects (Yao *et al.*, 2015). This imbalance is aggravated by loss of NTRK1 receptor, which would otherwise promote neuronal cell survival via mature NGF binding. The decline of expression of NTRK1 has been associated to the cognitive deterioration of AD patients, NGFR expression has not (Ginsberg *et al.*, 2006). Additionally, Aβ peptides have been shown to activate NTRK and stimulate Aβ endocytosis (Ovsepian *et al.*, 2014; Boskovic *et al.*, 2019). The application of mature NGF has been proposed as a new therapeutic approach in AD. While promising, delivery of exogenous NGF into the basal forebrain remains challenging (Giacobini, Cuello and Fisher, 2022).

The reasons behind the selective loss of BFCN in the Nucleus Basalis Meynert are still have not yet been elucidated. Other cholinergic neurons, particularly those in the hypothalamus and thalamic nuclei, are generally unaffected (Hampel *et al.*, 2018). Mammalian forebrain cholinergic neurons have been characterised among the largest and most complex neurons (Wu, Williams and Nathans, 2014) These characteristics leave BFCN especially vulnerable to changes in the environment. Notably, the basal forebrain exhibits diminished Aβ plaque formation as compared to the cortex, but shows high load of intracellular plaque, potentially disrupting intracellular

signalling (Baker-Nigh *et al.*, 2015). This might be explained by the previously mentioned Aβ uptake via NGFR (Ovsepian *et al.*, 2014). Apart from AD, other dementias, such as DLB and PD, show BFCN depletion and hence a lack of cholinergic signalling (Fu, Hardy and Duff, 2018; Boskovic *et al.*, 2019; Bidesi *et al.*, 2021).

This cholinergic hypothesis of AD is different, in the sense that, it does not try to explain the onset of AD, but the progression of some of the symptoms. Depletion of cholinergic signalling, triggered by the atrophy of BFCN, is clearly linked to cognitive decline, including loss of memory, sleep disturbances and changes in behaviour. However, it is unlikely that this lack of cholinergic signalling triggers Aβ pathology and neuroinflammation.

1.2.4.4 Mitochondrial cascade hypothesis

Due to the increasing evidence of a strong impairment of mitochondrial function in prodromal AD, a “mitochondrial cascade hypothesis” has been proposed as a supplement to the previously established amyloid cascade hypothesis in 2004. It accounts for mitochondrial dysfunction, namely decreased mitochondrial oxidative phosphorylation, increased rate of anaerobic glycolysis, and high rates of mitochondrial ROS production, as a primary event. These impairments will lead eventually in direct or indirect fashion to the sporadic, late-onset form of AD (Swerdlow and Khan, 2004). To acknowledge the fact that Aβ can cause mitochondrial dysfunction (Wang *et al.*, 2008; Cenini *et al.*, 2016), genetic as well as early-onset forms are not implemented in this theory. Aβ impairs mitochondrial respiratory activity and increases the mitochondrial permeability transition pore. Additionally, Aβ and hyperphosphorylated tau impair mitochondrial axonal transport (Bull *et al.*, 2012; Fang *et al.*, 2019; Du *et al.*, 2010), a process necessary for the energy balance of neurons. Mitochondrial alterations were observed close to amyloid plaques in an AD mouse model (Xie *et al.*, 2013).

Independently from Aβ plaques, previous studies revealed impairment of several important mitochondrial functions in AD patients. During the preclinical stages of AD diverse mitochondrial functions have been found to be compromised, eventually leading to a lack in ATP production, which is characterizes both sporadic and familial AD (Kerr *et al.*, 2017). As the activity of respiratory chain complexes is decreasing, the membrane potential is diminished and hence the ATP production lessens. Other crucial functions of mitochondria, namely the Ca^{2+} buffering (Butterfield and Halliwell, 2019), are also compromised. Astrocytes close to Aβ depositions in AD show aberrant calcium dynamics, which could impair synaptic plasticity and trigger pro-inflammatory astrogliosis (Verkhratsky *et al.*, 2017; Preman *et al.*, 2021).

Impaired mitochondrial fission and fusion actively drives AD pathology (Cenini and Voos, 2019). This might further deepen the mitochondrial bioenergetic deficit through perturbation of the complex assembly for the electron chain formation (Liu *et al.*, 2011), or increase production of ROS (Yu, Robotham and Yoon, 2006). Higher ROS generation leads to a higher rate of mitochondrial DNA mutation, thereby impacting renewal of mitochondrial genes.
In vivo positron emission tomography studies assess not only the metabolism, but also the activation state of microglia in the brains of AD patients. Tondo and colleagues found significant microglial activation in EOAD, which co-localized with hypometabolism in AD relevant regions (Tondo *et al.*, 2020).

While mitochondria abnormalities are detectable early in prodromal AD, it remains unclear whether they are causal or caused by other underlying impairments. For example, while the release of mitochondrial DNA, or per-oxidized lipids can trigger an inflammatory response, a prolonged inflammatory response could also lead to failure of glycolysis and oxidative phosphorylation (Joshi *et al.*, 2019). To date, the initial event in AD pathophysiology is not elucidated.

1.2.4.5 Alzheimer's disease as "type 3 diabetes"

The term "type 3 diabetes" suggests a causal role of cerebral insulin resistance to AD, suggesting it triggers Aβ deposition, mitochondrial dysfunction and increased inflammatory response.

The fact that diabetes mellitus type 2 is a risk factor for AD (García-Casares *et al.*, 2014; Edwards III *et al.*, 2019) and cerebellar hypometabolism is preceding AD onset, led researchers to investigate whether impaired insulin signalling is causal to AD. Insulin is involved in the regulation of cell growth, apoptosis, autophagy, protein synthesis in the brain (Gabbouj *et al.*, 2019), downstream effects improve and synaptic plasticity and cognitive processes in physiological conditions (Griffith *et al.*, 2018). *In vitro* experiments suggested Aβ oligomers as a competitive inhibitor of the insulin receptor (Xie *et al.*, 2002), eventually increasing insulin concentration in the brain microenvironment. Downstream signalling pathways are compromised, leading to impairments regulation of synaptic activity (Van Der Heide *et al.*, 2005; Ghasemi *et al.*, 2013). Additionally, increased levels of insulin in the brain promote inflammation via TNFα signalling pathways (Fishel *et al.*, 2005). High insulin levels lead to enhanced tau phosphorylation via insulin related pathways, usually regulating tau expression and phosphorylation (Schubert *et al.*, 2004; Bian *et al.*, 2016). Tau can also induce inflammasome activation in the brain, which may further

contribute to increased ROS concentration and impaired insulin signalling (Kulas, Weigel and Ferris, 2020). Apart from this, insulin is involved in the modulation of neurotransmitter channel activity, brain cholesterol synthesis, and mitochondrial function (Abolhassani *et al.*, 2017). Taken together, altered insulin signalling further increases Aβ concentration and exacerbates hyperphosphorylation of tau in a vicious cycle (Calabrò *et al.*, 2021). Aβ oligomers can induce insulin resistance via inflammatory pathways (Lourenco *et al.*, 2013).

The evident insulin resistance (Talbot *et al.*, 2012) in the brain led de la Monte and Wands to propose the term “type 3 diabetes” in 2008 (de la Monte and Wands, 2008). However, the exact mechanism of brain insulin resistance in AD remains unclear (Biessels and Despa, 2018; Gabbouj *et al.*, 2019). Late-life obesity and *diabetes mellitus* can induce a low-grade inflammatory response, which could prime the microglia (Perry and Holmes, 2014).

Recent evidence suggests that Aβ plaques start to accumulate approximately 20-25 years before an estimated age of onset, followed by metabolic changes 15-17 years before the age of onset. Significant cortical thinning and neuronal functioning decline was detected not earlier than 5 years before the age of onset (Gordon *et al.*, 2018; McDade *et al.*, 2018). These results indicate that neuronal hypometabolism could be triggered by the earlier Aβ plaque formation and not *vice versa*.

Several pathways have been hypothesized to be causal to AD and trigger the different observed pathologies. The main important of them were outlined above. However, it is still unclear which events are the initial triggers and which are subsequent events. The fact, that several proposed mechanisms partially overlap, hinders the untangling of disease-causing factors. Both, mitochondria and microglia, can be made responsible for the early loss of synapses. Furthermore, while one hypothesis might adequately explain some forms of the disease, such as fAD, it does not capture aspects and underlying complex mechanisms of other forms, for example sporadic LOAD cases.

1.3 ADAM17

ADAM17 (Disintegrin and metalloproteinase domain-containing protein 17) is a member of the ADAM family. This family of membrane standing sheddases is essential for cell-cell adhesion and cellular communication. The most researched catalytic active members of this family are ADAM17 and its closest homologue ADAM10. ADAM17 is widely expressed in several organs and in the majority of brain regions in humans. The expression pattern of *ADAM17* changes during human lifetime, which emphasizes its pivotal role in all stages of life (Gadhave *et al.*, 2020; Calligaris *et al.*, 2021). A SNV in *ADAM17* had been recently associated with AD (Hartl *et al.*, 2018).
This section describes first the structure and regulation of ADAM17 and will subsequently introduce different targets of ADAM17. Finally, the role of ADAM17 in neurodegenerative disease will be discussed.

1.3.1 ADAM17 protein structure

ADAM17 has a complex structure of several domains, which are illustrated in Figure 1.3. The catalytic **metalloprotease domain** harbours the catalytic center, which is highly conserved across multiple species. It ligates Zinc, which enables the shedding of the target proteins (Qian, Shen and Wang, 2016).
The **pro-domain** at the N-terminus of the enzyme acts as a self-inhibitor. It is progressively cleaved by the protease furin during maturation and trafficking of ADAM17 from the Golgi-network to the cell membrane (Lambrecht, Vanderkerken and Hammad, 2018). As a first step, pro-ADAM17 is cleaved at a motif located position 56-58, inducing a conformational change which allows further cleavage at position 211–214. This cleavage sequence is necessary for proper maturation. If the cleavage at position 211–214 occurs first, the pro-domain remains attached to the catalytic metalloprotease domain, forming an inactive tightly bound binary complex (Wong *et al.*, 2015). Recent evidence underlines the necessity of the pro-domain during activation, protein trafficking and proteolysis. Investigation of a cellular model carrying a specific mutation in the pro-domain had a severe impact on ADAM17 activity, suggesting a chaperone function of the pro-domain (Pavlenko *et al.*, 2019). However, the molecular mechanisms of the interaction of the pro-domain with the catalytic domain remain elusive.

The **disintegrin domain** is able to bind different cell adhesion proteins, thereby playing an integral role in cell-cell-adhesion, cell proliferation and migration (Yang *et al.*, 2021).

The **membrane proximal domain** contains the highly conserved ADAM17 stalk region **CANDIS** (Conserved ADAM seventeeN Dynamic Interaction Sequence). A conformational change in both regions was suggested to bring ADAM17 catalytic domain closer to its targets (Düsterhöft *et al.*, 2015; Sommer *et al.*, 2016), thereby enabling shedding activity. CANDIS was also reported to bind ADAM17 targets directly (Düsterhöft *et al.*, 2015).

The other regions of ADAM17, the **transmembrane domain** and the **cytoplasmic tail**, have mainly regulatory functions (Calligaris *et al.*, 2021).

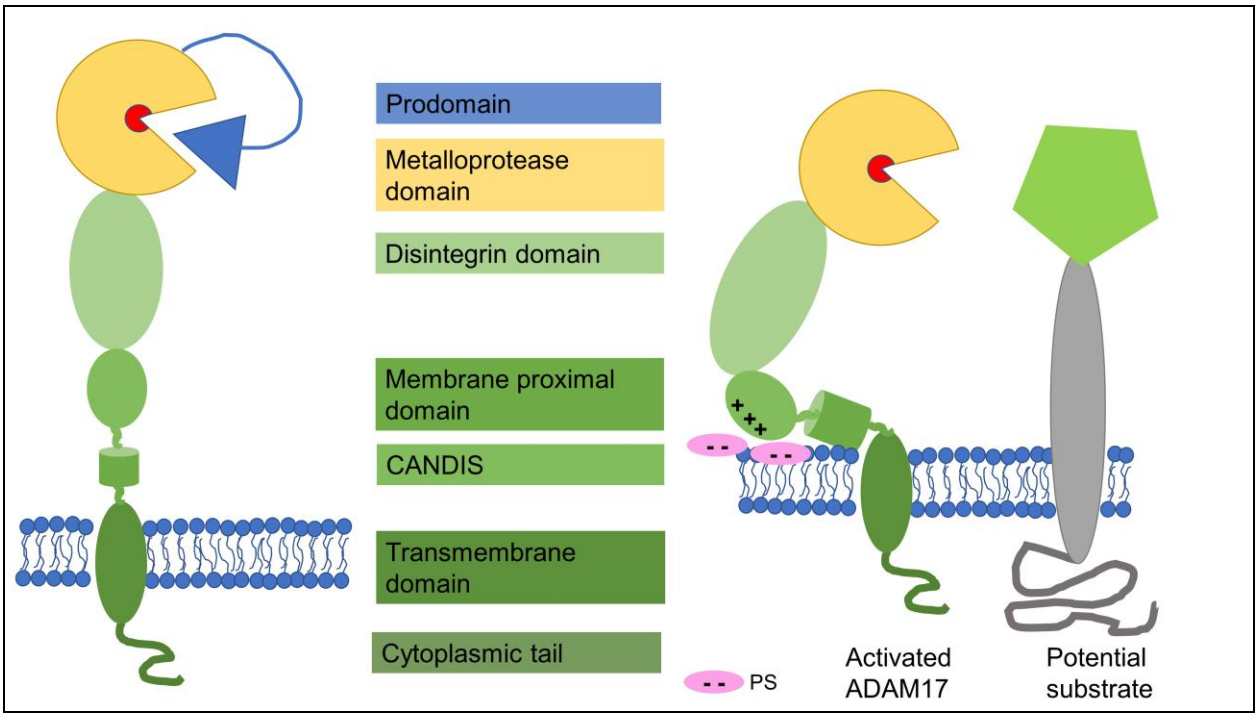

Figure 1.3 ADAM17 structure and activation. Negatively charged phosphatidylserine (PS) attracts residues of ADAM17's membrane proximal domain. The induced conformational change brings the catalytic center (in red) in close proximity to the cleavage side of the substrate.

1.3.2 Regulation of ADAM17 activity

ADAM17 has multiple different targets involved in cell-to-cell communication and cell-fate. As it is expressed ubiquitously, tight regulation is needed to prevent hyperactive shedding. Major regulatory steps are the cleavage of the inhibitory pro-domain, trafficking through the trans-Golgi network, plasma membrane composition and internalization for degradation.

In the last years iRhom1 (Inactive rhomboid protein 1) and iRhom2 (Inactive rhomboid protein 2) emerged as essential regulators of ADAM17 activity (Calligaris *et al.*, 2021). iRhoms bind to

ADAM17 pro-form in the ER and stimulate trafficking towards the plasma membrane via the trans-Golgi network. Even after the enzymatic cleavage of the inhibitory pro-domain, iRhoms remains attached. This interaction is critical because it inhibits ADAM17 catalytic activity before reaching the plasma membrane. Additionally, the pro-domain and the membrane-proximal domain were found to be essential in ADAM17 trafficking and protein maturation (Pavlenko *et al.*, 2019).
Once at the plasma membrane binding of iRhom2 prevents degradation of ADAM17 into the lysosome. Upon intracellular signalling, possibly after phosphorylation of the cytoplasmic tail of iRhom, 14-3-3 protein binds to iRhom, triggering a conformational change. This releases ADAM17 from the iRhom binding, enabling its activity (Christova *et al.*, 2013; Künzel *et al.*, 2018). Both iRhoms mediate ADAM17 activation, however, they are expressed in different cell types and appear to have slightly different activation mechanisms, indicating they are not redundant (Christova *et al.*, 2013; Calligaris *et al.*, 2021). This might also explain how iRhoms mediate ADAM17 substrate specificity (Maretzky *et al.*, 2013).

Phosphorylation of the cytoplasmic tail of ADAM17 was shown to stimulate the protein in response to shedding stimulants. As the removal of the entire cytoplasmic domain did not alter activation, the effect of the phosphorylation is still unclear (Cavadas *et al.*, 2017; Schumacher and Rose-John, 2022).

Finally, the local composition of the plasma membrane influences ADAM17 activity, both cholesterol and phosphatidylserine have been reported to alter ADAM17 shedding (Düsterhöft *et al.*, 2015; Sommer *et al.*, 2016).

1.3.3 ADAM17 substrates

More than 80 different targets of ADAM17 have been discovered to date (Yang *et al.*, 2021). These substrates are involved in processes like cell-to-cell communication, cell proliferation and differentiation and cell adhesion and cellular transport. Cleavage by ADAM17 is irreversible, which does not only imply down-regulation of receptors, but also formation of soluble ectodomains capable of participating in paracrine or autocrine signalling pathways (Düsterhöft *et al.*, 2015).

ADAM17 was discovered as the TNFα shedding enzyme. In recent years, many other ADAM17 substrates have been identified, which participate in the inflammatory response. This includes TREM-2, IL-6, and CX3CL1 (fractaline), which are associated with neuroinflammation.

Other important substrates of ADAM17 are ligands of the EGFR (Epidermal growth factor receptor) signalling pathway. EGFR is widely expressed in the developing brain and linked to

neuronal proliferation, differentiation, and survival. EGFR expression is reduced in the adult brain, but upon re-expression during neuroinflammation it can diminish myelination of neurons by oligodendrocytes or induce the release of pro-inflammatory cytokines by microglia. Both responses cause substantial neuronal damage (Mitchell, Luwor and Burgess, 2018; Jayaswamy *et al.*, 2023). Impairment on the EGFR pathways cause perinatal death to *ADAM17* knock-out mice. These animals are born with open eyes, and show severe skin barrier defects, heart deformations and defective lungs (Maretzky *et al.*, 2013). Both *ADAM17* and *EGFR* are genetic risk factors for Parkinson's disease (Zunke and Rose-John, 2017).

Apart from these substrates, Notch1 (Notch receptor 1) and its ligands (*e.g.,* Protein jagged-1 and -2) are targets of ADAM17 shedding (Saad, Rose-John and Jenkins, 2019). Notch signalling is involved in neural development and function, angiogenesis, and maintenance of neuronal stem cells (Kapoor and Nation, 2021). Neuronal activity controls Notch signalling, which conversely can modify neuronal function by affecting synaptic plasticity and neuronal morphology (Salazar, Yang and Yamamoto, 2020). Alterations in Notch signalling have been associated with different neurodegenerative diseases, such as AD, PD, and HD. Exact mechanisms are still unclear, but the influence of Notch on angiogenesis could explain the cerebrovascular lesions detectable in prodromal AD brains. Given that *PSEN1* mutations associated with AD are targets of y-secretase, Notch signalling may be impacted. Notch1 was found to interact directly with APP and localize with NFT (Brai, Alina Raio and Alberi, 2016; Kapoor and Nation, 2021), highlighting its influence on AD progression. Albeit alterations in Notch signalling alone might not be sufficient to provoke neurodegeneration, they are likely to modulate disease progression. As the effects of Notch signalling are highly dependent on species and developmental stage, different experiments often reach opposite conclusions, hindering our way towards a mechanistic understanding of Notch signalling (Salazar, Yang and Yamamoto, 2020).

Furthermore, ADAM17 sheds several cell adhesion molecules, thereby inhibiting cell attachment one another and anchoring in the cellular matrix. Additionally, cellular communication and sensation are affected, as are cell migration and sorting mechanisms all of which have a significant influence on cell development, tissue homeostasis, and inflammation (Bajanca *et al.*, 2015; Calligaris *et al.*, 2021).

Taken together, ADAM17 substrates play important functions in cell fate, immune response, and cell adhesion reactions (Saad, Rose-John and Jenkins, 2019; Calligaris *et al.*, 2021). They are important for a manifold of different pathways, as logical consequence dysregulation of ADAM17 activity has detrimental impact on different tissues. In fact, ADAM17 has been associated with

different diseases, such as several types of cancer, acute lung infections, myocarditis, rheumatoid arthritis, and neurodegenerative diseases. The following section explains several targets of ADAM17 which are relevant for AD and PD.

1.3.4 ADAM17 in neurodegeneration

It is not unexpected that ADAM proteases are associated with neurodegenerative diseases given their essential role for the growth and control of the central nervous system, particularly axonal growth and myelination (Yang *et al.*, 2021).

Neurons expressing *ADAM17* are often co-localized with Aβ plaques in brains of AD patients, indicating that ADAM17 might be involved in AD pathogenesis. Additionally, higher ADAM17 activity was detected in both CSF and plasma of AD patients (Qian, Shen and Wang, 2016; Yang *et al.*, 2021). Different substrates of ADAM17 are involved in AD pathogenesis, some are even risk factors themselves. Hence, it not surprising that two genetic polymorphisms in *ADAM17* have been associated with AD (Hartl *et al.*, 2018; Bellenguez *et al.*, 2022).

One of them, a single rare nonsynonymous variant (SNV rs142946965) was suggested causal to LOAD in a WGS study in a Spanish family (Hartl *et al.*, 2018). Analysis of sequences from international gene banks verified the absence of the SNV in controls and additional 5 heterozygous carriers were identified. The implied mutation at position 215 from arginine to isoleucine (R215I) is critical, as it is introducing a change in polarity of the sequence in close proximity of the cutting side for furin to remove the inhibitory pro-domain. SNV rs142946965 impairs activation of ADAM17 by unsuccessful removal of the inhibitory pro-domain in a cell model (Hartl *et al.*, 2018), resulting in a loss-of-function variant. This result goes hand-in-hand with the recent finding of another SNV (rs72777026) in a non-coding locus on *ADAM17*, associated to LOAD in a large GWAX by (Bellenguez *et al.*, 2022). In this analysis, *ADAM17* showed up in all of the ten topmost GO analysis terms.

ADAM17 activity is clearly linked to the amyloid cascade hypothesis. Despite ADAM10 being the physiological α-shedding enzyme of APP, ADAM17 can cleave APP upon stimulation, a process known as controlled shedding. Physiological stimuli include IL-1β, EGF (epidermal growth factor), and insulin (Qian, Shen and Wang, 2016). Furthermore, ADAM17 inhibits APP expression by a yet unknown mechanism. Interestingly, the rs142946965 variant did not alter APP gene expression (Hartl *et al.*, 2018). Apart from this, Aβ has been found to directly downregulate ADAM17 expression in mouse models (Yao *et al.*, 2015).

Additional to the involvement in APP shedding, ADAM17 is involved in neuroinflammation. Of note, it is constitutively expressed in microglia (Qian, Shen and Wang, 2016), and so are some of its targets. ADAM17 is a major contributor to the TNFα signalling cascade, as it not only sheds membrane-standing TNFα to soluble TNFα, but both of its receptors TNF-R1 (Tumor necrosis factor receptor superfamily member 1A) and TNF-R2 (Tumor necrosis factor receptor superfamily member 1B). ADAM17 has a major regulatory role in this case. TNF-R2 has a higher affinity to transmembrane TNFα and is predominantly linked to neuroprotective pathways. Soluble TNFα binds preferentially to TNF-R1, initiating pro-inflammatory signalling pathways (Calligaris *et al.*, 2021; Yang *et al.*, 2021). An inhibition of ADAM17 shedding activity may reduce inflammatory processes. Thus, ADAM17 downregulation has been suggested as therapeutic target for inflammatory disease, such as rheumatoid arthritis, psoriasis, and atherosclerosis (Gooz, 2010; Calligaris *et al.*, 2021).

A similar “switch” function for ADAM17 is relevant in the IL-6R (IL-6 receptor) signalling. Binding of IL-6 to its membrane standing receptor induces an anti-inflammatory and proliferative response. IL-6R, shed by ADAM17, can still bind IL-6 and stimulate the so-called trans-signalling pathway. The IL-6/IL-6R complex has the ability to bind the second receptor IL-6RB (Interleukin-6 receptor subunit beta), resulting in a robust pro-inflammatory response (Rose-John, 2020). Additionally, IL-6 mediated neuroinflammation is detrimental to adult neurogenesis and hence contributes to AD progression (Kim, Rhee and Paik, 2014). Inhibition of IL-6R receptor shedding by downregulation of ADAM17 might be beneficial against an overshooting neuroinflammation.

In addition, CX3CL1 shedding by ADAM17 influences microglia activity and neuroinflammation. Overexpression of the soluble CX3CL1, the molecule produced by ADAM17 shedding, had no impact on Aβ accumulation but attenuated tau pathology. Mice lacking CX3CL1 receptor were more susceptible to neuron loss in models of PD and Amyotrophic lateral sclerosis. Taken together, increased CX3CL1 signalling was advantageous in AD and PD mouse models, while the precise mechanism is unknown (Finneran and Nash, 2019; de Queiroz, Lakkappa and Lazartigues, 2020).

TREM2 can be shed by ADAM17 into a soluble TREM2 (sTREM2) and a membrane-retained C-terminal fragment (Schlepckow *et al.*, 2017; Calligaris *et al.*, 2021). Genetic variants of TREM2 are known to alter the shedding efficiency of the TREM2 enzyme by ADAM17 (Lambrecht, Vanderkerken and Hammad, 2018). Elevated sTREM2 is correlated with hyperphosphorylated tau and Aβ (Henjum *et al.*, 2018). As TREM itself, sTREM2 exerts neuroprotective or neurodegenerative functions. It stimulates the innate immune system and guides microglia

towards Aβ fibrils and abnormal neurons to facilitate phagocytosis. TREM2 and sTREM2 both concentrate next to Aβ plaques, hindering it from spreading into the surrounding healthy tissue. Apart from that, sTREM2 plays a key role in tau phosphorylation, thereby exaggerating neurodegeneration. sTREM2 is associated with transport and metabolism of Aβ and tau (Yang *et al.*, 2020).

Finally, the cleavage of NGFR by ADAM17 triggers a switch in the effects of the receptor. Aβ and pro-NGF can bind NGFR and induce an apoptotic response. This signalling pathway is suppressed by NGFR shedding. On top of this, the soluble NGFR ectodomain acts neuroprotective against Aβ, by suppressing BACE1 expression as well as Aβ-induced neurotoxicity, overexpression, and aggregation. While the cleavage of NGFR is reduced in AD, increase of the concentration of the soluble ectodomain can protect against neurodegeneration in AD animal models (Yao *et al.*, 2015; Conroy and Coulson, 2022).

Taken together, ADAM17 has several different substrates which are associated with AD. Two mutations of the *ADAM17* gene have been associated with AD onset. At least one of them, potentially impedes the maturation of the enzyme. The ramifications of this are still unknown. ADAM17 has multiple targets associated with AD, reduced cleavage might affect disease progression in a variety of ways.

2 AIMS OF THE THESIS

As outlined in the introduction above, age-related neurodegenerative diseases are complex disorders where multiple environmental and genetic risk factors contribute to disease onset and progression. However, the detailed pathological mechanisms underlying these diseases are still not entirely clear for many diseases. Particularly, AD as the most common neurodegenerative disease exhibits a broad spectrum of clinical symptoms and potential disease mechanisms where the interplay of different genetic risk factors can lead to distinct phenotypes. This thesis focuses on the *ADAM17* gene which has been recently associated with AD, but the underlying disease mechanism in terms of genetic interactions and molecular establishment of the disease phenotype remains elusive. To address this challenge, the project considers the AD-related rs142946965 polymorphism on the *ADAM17* gene and investigates its role in neuronal development and homeostasis by combining an isogenic iPSC approach with a molecular multiscale analysis.

The underlying hypothesis of this approach is that neurodegeneration induced by ADAM17 loss-of-function is mediated by impaired pathways which will be visible in neuronal development. While ADAM17 is involved in several clinical conditions, there is limited understanding of its impact on neurodegeneration in the context of AD and PD. To investigate the influence of ADAM17 in neuronal development a corresponding isogenic pair of iPSC consisting of a control line and a line carrying an AD-associated mutation was generated and subsequently differentiated into basal forebrain cholinergic neuronal precursors and early midbrain dopaminergic neurons. Investigation of the differentiation dynamics by deep phenotyping at different timepoints along the differentiation allows for insights in neuronal homeostasis. For identification of impaired pathways, the differentiation was characterized by multiscale analysis including single-cell RNA-sequencing and metabolomics. Hence, the thesis has the specific aims for:

1. Generation of a stable iPSC line carrying the *ADAM17* rs142946965 mutation

The mechanistic etiopathology and the underlying molecular cause of AD associated with *ADAM17* is not well understood beyond its general involvement in the main pathological hallmarks, namely, the amyloid cascade and neuroinflammation. The loss-of-function mutation rs142946965 on *ADAM17* gene has been associated with AD. To explore the molecular pathways, iPSC are state-of-the-art disease models. However, an iPSC model of the heterozygous SNV rs142946965 on the *ADAM17* gene is not available. As a first step of my work,

I established a stable iPSC line by CRISPR/Cas9. This approach is described in the Results Section 4.1 with corresponding Methods detailed in Section 3.2.

2. Characterization of ADAM17 phenotype in early differentiation

To explore common traits implied by the SNV mutation in *ADAM17* on early neurogenesis, iPSC were differentiated into disease relevant neurons precursors: a) basal forebrain cholinergic neurons and b) midbrain dopaminergic neurons. Thorough investigation of single cell RNA expression and the metabolome during the development of both cell types on a temporal scale, revealed insight into *ADAM17* impact on neuronal development. This approach is described in the Results Section 4.2 with corresponding Methods detailed in Sections 3.3.-3.9.

The insights gained from this research may contribute towards developing targeted therapies for individuals with AD and potentially also patients with PD in the future.

3 MATERIALS AND METHODS

This chapter explains experimental steps conducted during the PhD project. First, a summary of all reagents, special materials and devices is provided in Table 3.1. Section 3.2 (Method for generation of *ADAM17* clone) outlines the workflow to generate a stable iPSC cell line harbouring the heterozygous SNV rs142946965 in *ADAM17*. Thereafter, Section 3.3 (Cell Culture) explains iPSC handling and differentiation protocols. Starting from Section 3.4, the following sections contain the analytical steps of the differentiated cells, which include qPCR, immunocytochemistry, Western blot, single-cell RNA-sequencing (sc-RNAseq), metabolomics, and proteomics.

3.1 Reagents, Materials, and Devices

Reagent	Catalogue number	Manufacturer
Reagents used to generate the clones		
Ampicillin	A9518	Sigma-Aldrich
Bacto Agar	DIFC214010	VWR
Bovine serum albumin	A3059	Sigma-Aldrich
D-(+)- glucose solution (45 %)	G8769	Sigma-Aldrich
DPBS, no calcium, no magnesium	14190-094	Thermo Fisher Scientific
FastDigest BpiI	FD1014	Thermo Fisher Scientific
HapI	R0105S	New England Biolabs
LB Broth (Miller)	244610	VWR
NEBuilder HiFi DNA Assembly Cloning Kit	E5520S	New England Biolabs
OneShot TOP 10 chemically competent *E. coli*	C4040-03	Thermo Fisher Scientific
P3 Primary Cell 4D-Nucleofector™ X Kit L	V4XP-3024	Lonza
Puromycin	15653	PeproTech
pX330-U6-Chimeric_BB-CBh-hSpCas9	42230	Addgene
QIAGEN Plasmid Maxi Kit	12165	QIAGEN
QIAGEN Plasmid Mini Kit	12123	QIAGEN
QIAquick PCR purification kit	28104	QIAGEN
QuickExtract DNA Extraction Solution	QE9050	Epicentre
Shrimp Alkaline Phosphatase	M0371	New England Biolabs
SOC medium	15544034	Thermo Fisher Scientific
Stemfect RNA transfection kit	00-0069	Stemgent
SYTOX Blue Dead Cell Stain	S34857	Thermo Fisher Scientific
T4 DNA Ligase	M0202S	New England Biolabs
T4 Polynucleotide Kinase	M0201S	New England Biolabs
Reagents used for iPSC culture and differentiation		
2-mercaptoethanol	21985-023	Thermo Fisher Scientific
Ascorbic Acid	5088177	PeproTech
B-27 supplement	12587010	Thermo Fisher Scientific
BrainPhys neuronal medium	05790	STEMCELL Technologies
cAMP	D0627	Sigma-Aldrich

CHIR99021	72054	STEMCELL Technologies
CTS N-2 Supplement	A1370701	Thermo Fisher Scientific
DAPT	2634	R&D Systems
GelTrex, hESC qualified	A1413302	Thermo Fisher Scientific
GlutaMAX Supplement	35050061	Thermo Fisher Scientific
Human NGF Recombinant Protein	A42578	Thermo Fisher Scientific
Human Recombinant BDNF	78005.2	STEMCELL Technologies
Human Recombinant FGF-8B	78008.2	STEMCELL Technologies
Human Recombinant GDNF	78058.3	STEMCELL Technologies
Human Recombinant Shh	78065	STEMCELL Technologies
Human/Mouse Recombinant TGF-beta 3	78131	STEMCELL Technologies
Knock-out Serum Replacement	10828028	Thermo Fisher Scientific
KO-DMEM	10829018	Thermo Fisher Scientific
LDN193189	72147	STEMCELL Technologies
MEM Non-Essential Amino Acids Solution (100X)	11140035	Thermo Fisher Scientific
mTeSR PLUS kit	100-0276	STEMCELL Technologies
mTeSR1 Complete Kit	85850	STEMCELL Technologies
mTeSR1 Medium Without Select Factors	5896	STEMCELL Technologies
Neurobasal medium	21103049	Thermo Fisher Scientific
NeuroCult SM1 Neuronal Supplement	05711	STEMCELL Technologies
Penicillin-Streptomycin	15140122	Thermo Fisher Scientific
Purmorphamine	72204	STEMCELL Technologies
SAG	73412	STEMCELL Technologies
SB431542	72234	STEMCELL Technologies
StemPro Accutase	A11105-01	Thermo Fisher Scientific
Synth-a-Freeze Medium	A1371301	Thermo Fisher Scientific
TrypLE Select CTS	A12859-01	Thermo Fisher Scientific
UltraPure 0.5M EDTA, pH 8.0	15575-038	Thermo Fisher Scientific
Y-27632 (ROCK inhibitor)	Ab120129	Abcam
Other reagents used in this project		
4% Paraformaldehyde in PBS	J61899.AP	Alfa Aesar
Agarose	A9539	Sigma-Aldrich
bovine serum albumin	A3059	Sigma-Aldrich
D-(+)- glucose solution (45%)	G8769	Sigma-Aldrich
DAPI dihydrochloride	D9542	Sigma-Aldrich
DNeasy Blood & Tissue Kit	69504	QIAGEN
DPBS, no calcium, no magnesium	14190-094	Thermo Fisher Scientific
DreamTaq Green PCR Master Mix (2 X)	K1082	Thermo Fisher Scientific
Herculase Enhanced DNA Polymerase	600677	Agilent
MassRuler DNA Ladder Mix	SM0403	Thermo Fisher Scientific
MassRuler DNA Loading Dye (6 X)	R0621	Thermo Fisher Scientific
Maxima SYBR Green/ROX qPCR Master Mix	K0222	Thermo Fisher Scientific
PE Mouse Anti-Human CD271 Clone C40-1457 (RUO)	557196	BD Biosciences
RNeasy Plus Universal Kit Mini	73404	QIAGEN

Superscript III First-Strand Synthesis System for RT-PCR	18080051	Thermo Fisher Scientific
SYBR Safe DNA gel stain	S33102	Thermo Fisher Scientific
Taq DNA Polymerase	GC-002-1000	GeneCraft UK
Triton-X-100	T1565	Sigma-Aldrich
Material used in this project		
CellCarrier-96 ultra (microscopy plates)	6055300	Perkin Elmer
Falcon 5ml Round Bottom test tubes	352063	Corning
Nunc OmniTray	165218	Thermo Fisher Scientific
Nunclon Sphera 96U Bottom Plate (ULA coated)	174925	Thermo Fisher Scientific
Pre-separation filter (20µm)	130-101-812	Miltenyi Biotec

Table 3.1 List of reagents and materials used in this project.

To complete the experiments following devices were employed:

Microscopy: - Yokogawa CV8000 CellVoyager (FUJIFILM Wako)

- Leica TCS SP8 STED (LEICA)

- Nikon Eclipse Ti-E RCM

FACS: - BD MELODY cell sorter (Becton Dickinson)

- FACS AriaIII Flow cytometry cell sorter (Becton Dickinson)

Other: - Lightcycler 480II (Roche)

- 4D-Nucleofector X Unit (Lonza)

3.2 Method for generation of *ADAM17* clone

This section explains the techniques to generate a stable iPSC cell line harbouring the heterozygous single nonsynonymous variant rs142946965 [p.R215I] in *ADAM17*. A previously published procedure was adapted for this purpose (Jarazo, Qing and Schwamborn, 2019). The iPSC line WTSIi010-A (Depositor cell line name HPSI0314i-xugn_1; ECACC Catalogue No. 66540080) was employed in this section of the experiment. This cell line was obtained from the European Bank for induced pluripotent Stem Cells. Cells were donated by a male person aged between 65-69 years. Reprogramming was performed at the Wellcome Trust Sanger Institute (Great Britain).

The experimental procedure is divided in 3 steps: i) the *in silico* work to design the necessary DNA fragments; ii) the benchwork to generate the plasmids; and iii) the cell culture part including transfection and selection steps.

3.2.1 In silico work

The base-to-be-edited (BTE) is located at position 34'569 on the *ADAM17* gene (NC_000002.12:c9555830-9488486 Homo sapiens chromosome 2, GRCh38.p14 Primary Assembly). The nucleotide base guanine at this position needs to be mutated in a heterozygous manner to thymine (G>T). The single-strand guide RNA (sgRNA) for the CRISPR machinery was defined comparing results from CRISPOR (version 4.92; Concordet and Haeussler, 2018) and GPP sgRNA Designer (Doench *et al.*, 2016; Sanson *et al.*, 2018). In this experiment, 2 different sgRNA were tested. A TTAA box, necessary for transposase steps later in the protocol, was identified at position 34'518 (51 bp from the BTE), using http://resitefinder.appspot.com. Homology arms were designed to exclude repetitive elements, which were assessed using RepeatMasker (Smit, Hubley and Green, 2013). The BTE and protospacer adjunct motif (PAM) were edited on the right homology arm (RHA). All primers, the sgRNA template, and the homology arms were purchased from Eurogentec (Belgium), the complete sequence of the arms is listed in the Supplementary material. The sequence of the sgRNA and all primers used in this part of the project are listed in Table 3.2.

Name	Sequence 5' -> 3'
sgRNA	
sgRNA1_fwd	CACCGAATTTACACGTGTTCTTCAT
sgRNA1_rev	AAACATGAAGAACACGTGTAAATTC
sgRNA2_fwd	CACCGCACGTGTTCTTCATGGGATC
sgRNA2_rev	AAACGATCCCATGAAGAACACGTGC
Primers used for plasmid generation	
hU6	GAGGGCCTATTTCCCATGATTCC
L589_rev	CGCGCTAAAAACGGACTAGC
Primers used to check insertion of the homology arms into pDonor	
LHAF	AGCTTGGATCCCCTAGGTTGTTTCATCATGTTGGCCAGGCT
LHAR	CAGACTATCTTTCTAGGGTTAAATCAAAATTCACCAAAACAAGGAGTTTTATGG
RHAF	ATGATTATCTTTCTAGGGTTAATAGTGCATACAAATTCATATTAGAGCTTGT
RHAR	GCATACGCGTATACTAGGTTTCCACTTGACATGAAAGGGAAGGG

Primers used to validate the correct knock-in (VKI) into the genome (details see Figure 3.2)	
VKI 1	AACATGCCCGGCCAAAGA
VKI 2*	AGATGTCCTAAATGCACAGCG
VKI 3*	CGTCAATTTTACGCATGATTATCTTTAAC
VKI 4	CAGCAACCCTCCTTCTTTTGT
VKI 5*	GCTGCCTATCAGAAGGTGGTG
VKI 6*	GCAGCCACTGGTAACAGGAT
Primers used for sequencing (if not listed above)	
LHA_rev_seq *	AGATGTCCTAAATGCACAGCG
RHA_fwd_seq	GATATACAGACCGATAAAACACATGC
RHA_rev_seq	CAGGAAACAGCTATGAC
ADAM17_fwd	AAAGAGGCACTTGTCCTTGG
ADAM17_rev	GAGTATCTGGAACAGATCTGG

Table 3.2 Primers used for the generation of an ADAM17 clone. Primers with an asterisk (*) were designed by Jarazo, Qing and Schwamborn, 2019

3.2.2 Bench work: Cloning and plasmid generation

In total 3 different plasmids were prepared. A scheme of the plasmid layout is visualized in Figure 3.1.

3.2.2.1 Preparation p(GUIDE)

sgRNA forward and backward strand were annealed by incubation of 100 µM solutions in 1X T4 DNA Ligase Reaction Buffer (Thermo Fisher Scientific) starting at 95 °C for 5 min with decreasing temperature 5 °C/min until the temperature reached 25 °C. sgRNA was 5' phosphorylated by incubating at 37 °C for 30 min in T4 DNA Ligase Reaction Buffer with T4 Polynucleotide Kinase (NEB), with the same reagent 3' phosphoryl groups were removed for subsequent ligation.

The plasmid pL589, a modified version of the human codon-optimized SpCas encoding plasmid pX330-U6-Chimeric_BB-CBh-hSpCas9 (Addgene), was kindly provided by Dr Javier Jarazo (Cong *et al.*, 2013; Arias-Fuenzalida *et al.*, 2017). pL589 was used for the generation of the guide plasmid by initial digestion with FastDigest BpiI (Thermo Fisher Scientific) for 3 h at 37 °C. DNA was purified using QIAquick PCR purification kit (QIAGEN) as per protocol and eluted in 30 µl RNase-free water. Dephosphorylation was performed with Shrimp Alkaline Phosphatase (New England Biolabs) following the manufacturer's instructions. The ligation step was carried out with T4 DNA Ligase (New England Biolabs), 112 ng digested and de-phosphorylated pL589 and 2 µl annealed and phosphorylated sgRNA were incubated for 18 h at 16 °C, followed by 10 min at 37 °C in shaking condition (300 rpm). Thereafter, the ligase was heat inactivated at 65 °C for 10 min at 300 rpm.

OneShot TOP 10 chemically competent *E. coli* were transformed with the ligation product as per manufacturer´s protocol using 950 µl SOC medium (both Thermo Fisher Scientific). 450 µl of the transformation reaction was spread on Bacto agar (VWR) plates made from LB Broth (VWR) containing 100 µg/ml Ampicillin (Sigma-Aldrich). To confirm a successful transformation, colony PCR has been performed using the primers hU6 and L589_rev with Taq DNA Polymerase (GeneCraft UK), with the following cycling conditions: 95 °C 5 min, 38 x (95 °C 1 min, 59 °C 1 min, 72 °C 1 min), 72 °C 5 min. Sanger sequencing with the primer hU6 was performed at Microsynth Seqlab (Germany). Successfully cloned cells were incubated overnight in LB broth, supplemented with 100 µg/ml Ampicillin; plasmids were extracted with QIAGEN Plasmid Maxi Kit (QIAGEN)

3.2.2.2 Preparation p(DONOR)

The plasmids pDONOR-tagBFP-PSM-EGFP and pDONOR-tagBFP-PSM-dTOMATO were generously gifted by Dr Javier Jarazo. Plasmids were digested with HpaI (New England Biolabs) for 2 h at 37 °C. The digested plasmids, the left homology arm (LHA), and the RHA were purified with QIAquick PCR purification kit as per manufacturer´s protocol. DNA Assembly was performed using NEBuilder HiFi DNA Assembly Cloning Kit (New England Biolabs, generous gift from Kyriaki Barmpa) in the ratio 1:2:2 (vector: LHA: RHA) for 60 min at 50 °C. OneShot TOP 10 chemically competent *E. coli* (Thermo Fisher Scientific) were transformed with 2 µl pDonor. After overnight incubation at 37 °C, the plasmid was isolated with QIAGEN Plasmid Mini Kit (QIAGEN). PCR fragments were obtained using the primers LHA_fwd, LHA_rev, RHA_fwd, and RHA_rev with Taq DNA Polymerase (GeneCraft UK), with the following cycling conditions: 95 °C 5 min, 35 x (95 °C 1 min, 55 °C 1 min, 72 °C 1 min), 72 °C 5 min. Sanger sequencing was performed at Microsynth Seqlab (Germany) using the sequencing primers LHA_fwd, LHA_rev_seq, RHA_fwd_seq, and RHA_rev_seq. Successfully cloned cells were incubated overnight and plasmid was extracted with QIAGEN Plasmid Maxi Kit (QIAGEN) to yield a high concentration of DNA for the next steps.

DNA concentration of all plasmids (pGUIDE, pDONOR-tagBFP-PSM-EGFP-LHA-RHA; pDONOR-tagBFP-PSM-dTomato-LHA-RHA) were measured with Nanodrop 2000C (Thermo Scientific).

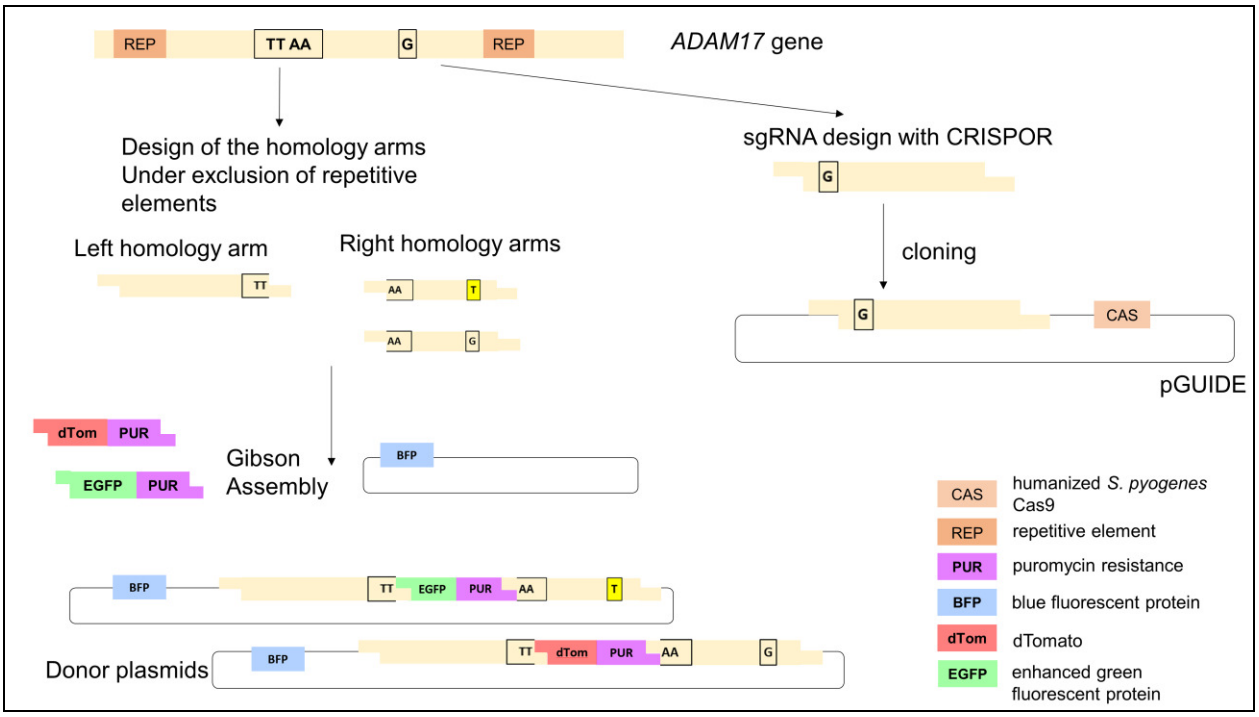

Figure 3.1 Overview of plasmid generation. The pGUIDE carries the sgRNA and a human codon - optimized SpCas9. The donor plasmids (pDONOR-tagBFP-PSM-EGFP-LHA-RHA and pDONOR-tagBFP-PSM-dTOMATO-LHA-RHA) carry the homology arms and the positive selection markers.

3.2.3 Cell culture: Nucleofection, selection, FACS, transposase, purification

For each nucleofection, one million cells were treated using a 4D-Nucleofector X Unit (Lonza) and the P3 Primary Cell 4D-Nucleofector X Kit L (Lonza). Latest two days after the last passage iPSC (cell line WTSIi010-A) were detached using StemPro Accutase (Thermo Fisher Scientific), neutralized with complete mTeSR1 medium (STEMCELL Technologies), and centrifuged at 200 x g for 3 min. After resuspension and counting, 1 million cells per reaction were spun down again (200 x g, 3 min), resuspended in 100 µl Nucleofector solution completed with 1.5 µg of each donor and 2.5 µg of sgRNA-Cas and transferred to an electroporation cuvette. Cells were electroporated with a CB150. Thereafter, transfected cells were washed out with mTeSR1 supplemented with 10 µM Y-27632 (ROCK inhibitor, Abcam) and plated into a GelTrex- coated Nunc OmniTray (both Thermo Fisher Scientific) 1-well plate. 50 % of the medium was changed after 24 h. After small colonies have formed, 0.1 µg/ml Puromycin (PeproTech) was added for selection. During the following days, puromycin concentration was raised stepwise to maximum 0.3 µg/ml for a maximum of 24 h per treatment. Medium was supplemented with 0.1 µg/ml Puromycin until the transposase reaction.

Approximately one week after electroporation, cells were ready for fluorescence guided picking. Cells were imaged with Yokogawa CV8000 CellVoyager (FUJIFILM Wako). The settings were as follows: excitation wavelength 405 nm, 445 nm, 488 nm, 561 nm and brightfield; Filter BP445/45, BP600/37, BP525/50; 4X magnification. Image analysis was performed using Matlab (MathWorks) with a code provided by Dr Javier Jarazo. Colonies having an EGFP+/dTomato+/BFP- or an EGFP+/dTomato-/BFP- fluorescence were gently detached with a pipette and plated individually on a 96-well plate. mTeSR1 Medium was supplemented with 10 µM ROCK inhibitor. After the colonies have expanded, they were split into four 96-wells, of which two were used later for DNA extraction with QuickExtract DNA Extraction Solution (Epicentre) as per manufacturer´s protocol.

To detect events of random integration, PCR was performed with DreamTaq Green PCR Master Mix (2X) (Thermo Fisher Scientific) with the VKI primers (see Table 3.2). The primer binding sites and intended targets are illustrated in Figure 3.2. Cycling conditions were 95 °C 5 min, 38 x (95 °C 30 s, 59.5 °C 30 s, 72 °C 1 min), 72 °C 5 min. For the reaction of the primers VKI 1 + VKI 4 cycling conditions had to be altered due to of the long product size: 95 °C 5 min, 38 x (95 °C 30 s, 59.5 °C 30 s, 68 °C 8 min), 68 °C 5 min. Clones not showing the desired products were discarded. As a next step to purify the clones, cells were sorted on FACS AriaIII Flow cytometry cell sorter (Becton Dickinson).

For FACS sorting, cells were dissociated for 5 minutes using StemPro Accutase and then centrifuged at 200 x g for 3 minutes. Cells were counted after being resuspended in FACS Buffer (2 % bovine serum albumin, 1 % Penicillin-Streptomycin, 30 µM ROCK inhibitor in DPBS). Doublets were removed by straining through a 20 µm pre-separation filter (Miltenyi Biotec) into Falcon 5 ml FACS test tubes (Corning). Cells were sorted on FACS AriaIII Flow cytometry cell sorter (Becton Dickinson), with an 85 µm nozzle and the 2.0 Neural density filter at 4 °C. After the last run, a sample of the sorted cell suspension was stained with SYTOX Blue Dead Cell Stain (Thermo Fisher Scientific), to estimate the percentage of debris, which might be interpreted as GFP+ cells. For the first run, cells were sorted using the “yield” mask, in the second run the “4-way purity” mask was used. After the dead-stained sample was 100 % GFP+/dTOMATO-/BFP-, the cells were further expanded to start the transposase reaction.

The transposase reaction is necessary to remove the positive selection markers. Transfection was performed on twice on consecutive days with the Stemfect RNA Transfection Kit (Stemgent) as per manufacturer´s protocol. In short, cells were plated at a density of 1 million/well in two 6-wells at the day before transfection. Cells were fed 1 h prior transfection. The transfection

reagent mixture (60 µl Stemfect Transfection buffer and 4.0 µl Stemfect RNA transfection reagent) and the mRNA mixture (60 µl Stemfect Transfection buffer and 1.0 µg RNA) were mixed equivoluminar, incubated for 15 min and added to the cells drop-wise. Successful transposase reaction was confirmed by imaging with Nikon Eclipse Ti-E RCM with brightfield and GFP channel (Excitation: 500 nm Emission: 520/10)

After expansion of the cell culture, FACS sorting for GFP-/dTOMATO-/BFP- cells was conducted as described before. This time, the sorting was repeated twice.

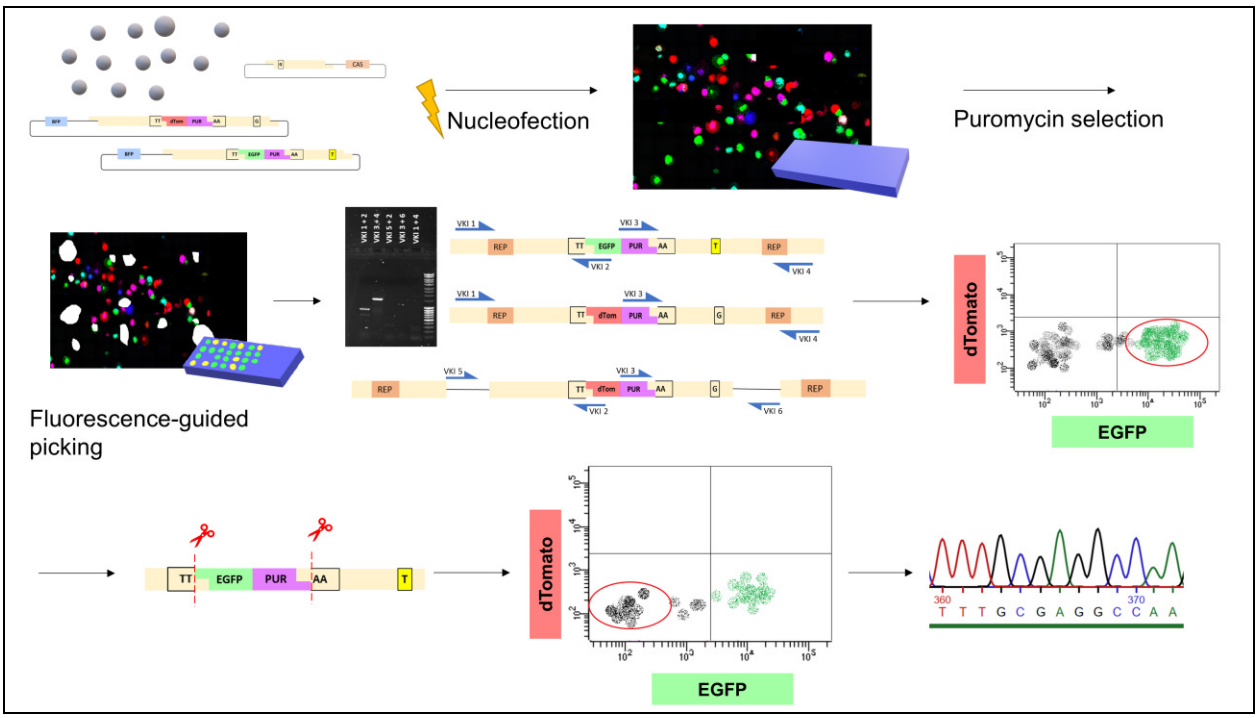

Figure 3.2 Schematic overview of the cell culture steps necessary for ADAM17 clone generation.

3.2.4 Assessment of quality: Sequencing and Karyotyping

3.2.4.1 Sequencing

DNA was extracted with DNeasy Blood & Tissue Kit (QIAGEN). The region of interest was amplified using Herculase II Fusion DNA Polymerase (Agilent) as per manufacturer´s recommendation with the following cycling parameters: 95 °C 2 min, 30 x (95 °C 20 s, 53 °C 20 s, 72 °C 3 min), 72 °C 3 min with the primers ADAM17_fwd and ADAM17_rev. Purity of the PCR product was verified with gel electrophoresis (3.5 % Agarose gel, 90 V, 90 min) (Agarose from Sigma-Aldrich) with SYBR Safe DNA gel stain (Thermo Fisher Scientific) against MassRuler DNA Ladder (Thermo Fisher Scientific). DNA was purified using QIAquick Purification Kit and sent for

Sanger sequencing to Microsynth Seqlab (Germany) with the primers ADAM17_fwd and ADAM17_rev. ApE version 3.1.3 (Davis and Jorgensen, 2022) was used to evaluate sequencing quality and for sequence alignment.

3.2.4.2 Karyotyping

Cells pellets were prepared using TrypLE Select CTS (Thermo Fisher Scientific) for 3 min. Thereafter, the medium was neutralized, and cell suspension was centrifuged at 300 x g for 3 min. Cells were counted after resuspension, and a cell suspension of minimum 2 million cells were spun down at 500 x g for 3 min. Supernatant was removed and cells were sent frozen to CUB Characterization Services from Life Technologies in Madison (WI, USA). Karyotype was analysed using KaryoStat+ Assay service provided by Thermo Fisher Scientific.

3.3 Cell Culture

In this section human iPSC lines will be described, and their maintenance will be outlined. Next, the differentiation into BFCN and mDA (midbrain dopaminergic neurons), respectively, will be explained.

3.3.1 Maintenance of iPSC (including description)

Three iPSC lines were used during this work. For the cell line WTSIi010-A a healthy male (65-69 y) donated cells, which were reprogrammed to iPSC by Wellcome Trust Sanger Institute. Human iPSC lines “PB005.1” (donor: Caucasian female 45 years of age) and “ADAM17 in/rep Cln 40.37.16 (w)” were supplied by the Gene Editing Facility at the Murdoch Children´s Research Institute (Australia) (Vlahos *et al.*, 2019). The heterozygous mutation (c.644G>T [p.R215I]) in *ADAM17* was introduced into iPSC line PB005.1 by the same institute, generating the cell line “ADAM17 in/rep Cln 40.37.16 (w)”, in the following referred to as R215I.

Human iPSC were cultured on GelTrex (Thermo Fisher Scientific) coated plates in complete mTeSR PLUS (STEMCELL Technologies) medium at 37 °C and 5 % CO_2. Medium was changed every second day if not stated otherwise. Cells were usually passaged with 0.5 mM EDTA (Thermo Fisher Scientific), 2 min incubation time at room temperature.

3.3.2 Differentiation into BFCN

The protocol to generate BFCN from iPSC was previously published by Ortiz-Virumbrales *et al.*, 2017, and is visualized in Figure 3.3. In short, cells were plated at a density of 600'000 cells per 6-well in complete mTeSR PLUS supplemented with 10 µM ROCK inhibitor. Medium was refreshed after 6 hours. After cells grew to confluency the next day, medium was replaced by mTeSR1 Medium Without Select Factors supplemented with 10 µM SB431542 and 250 nM LDN193189 (all STEMCELL Technologies). After 2 days medium was changed to mTeSR1 Medium Without Select Factors supplemented with 10 µM SB431542, 250 nM LDN193189, 500 nM SAG, and 2 µM Purmorphamine (all STEMCELL Technologies). Cells were fed until Day 8, after which medium was gradually changed to BrainPhys Neuronal Medium supplemented with 1X NeuroCult SM1 Neuronal Supplement (both STEMCELL Technologies). Medium was again changed at Day 11, when BrainPhys was supplemented with 1X NeuroCult SM1, 50 ng/ml NGF (Thermo Fisher Scientific), and 50 ng/ml BDNF (STEMCELL Technologies). Neural progenitors at Day 12 of differentiation were dissociated using StemPro Accutase supplemented with 10 µM ROCK inhibitor for 10 min. Cells were collected by centrifugation at 300 x g for 3 min. Thereafter, cells were resuspended in FACS Buffer (DPBS supplemented with 0.5 % bovine serum albumin, 500 U/ml Penicillin-Streptomycin, 2 mM EDTA, 20 mM Glucose (Sigma-Aldrich), 20 µM ROCK inhibitor) and counted. Cell suspension was centrifuged again, and the volume of medium was reduced before straining the suspension through a 20 µm pre-separation filter (Miltenyi Biotec) to yield a single cell suspension. After addition of the PE Mouse Anti-Human CD271 Clone C40-1457 RUO (BD Biosciences) in a ratio of 1 µl antibody per 1 million cells, the cell suspension was incubated for 20 min on ice in the dark. After the incubation time, cells were washed with FACS Buffer and strained again into Falcon 5 ml FACS test tubes (Corning). NGFR positive cells were purified in a BD MELODY cell sorter (Becton Dickinson), using the 100 µm nozzle and neutral density filter 2.0, and sorted into medium containing 20 µM ROCK inhibitor. After sorting, were seeded at a density of 80.000 cells per well in an ULA U-shaped Nunclon Sphera 96U-plate (Thermo Fisher Scientific), and spun down at 300 x g for 3 min. The medium was supplemented with 20 µM ROCK inhibitor that day. Next day, medium was diluted by replacing 100 µl medium per well with fresh medium. After that, 75 µl medium were refreshed every second day until day 20, when cells were split into monolayer. For this purpose, pellets were incubated in StemPro Accutase for 10 min, after neutralization the plate was spun down at 300 x g for 3 min. Cells were collected in medium supplemented with 20 µM ROCK inhibitor and after short pipetting pellets were distributed in GelTrex coated wells. 2-5 pellets were collected per 96 - well, medium was

again supplemented with 20 µM ROCK inhibitor. 75 µl medium/well were refreshed every second day until harvest at Day 39.

For metabolomics, qPCR, immunostaining, and single-cell RNA expression profiling, progenitor cells were harvested at Day 0, Day 8, and Day12.

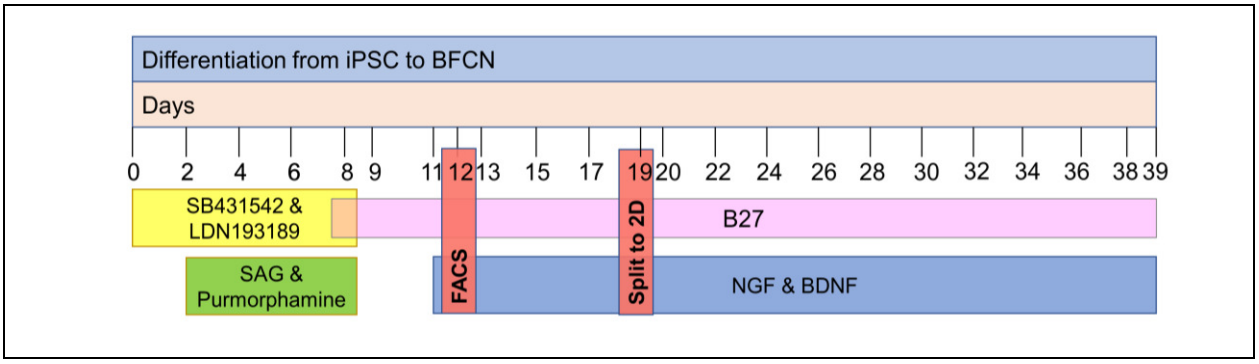

Figure 3.3 Schematic overview of the differentiation of iPSC to BFCN

3.3.3 Differentiation into midbrain dopaminergic neurons

The protocol to generate mDA from iPSC was significantly adapted from Kriks et al., 2011 (Kriks *et al.*, 2011; Tomishima, 2012; Novak *et al.*, 2022), visualized in Figure 3.4.

In short, cells were plated at a density of 1.4 x 10^6 cells per 12-well in mTeSR PLUS supplemented with 10 µM ROCK inhibitor. After 6 hours ROCK inhibitor was removed, and cells were allowed to recover for an additional 18 hours. Thereafter, cells were fed twice daily. The medium composition for each day can be found in Table 3.3. Three different media were used in this protocol. The first one is knockout serum replacement medium (SR medium), containing KO-DMEM, 15 % knockout serum replacement, 2 mM L-glutamine (GlutaMAX Supplement), 1X MEM Non-Essential Amino Acids Solution, and 10 µM 2-mercaptoethanol (all Thermo Fisher Scientific). The second one is N2 medium containing Neurobasal medium, 2 mM L-glutamine, 1 % Penicillin/Streptomycin, 1X CTS N-2 Supplement, 1X B-27 supplement (all Thermo Fisher Scientific). The last one, NB/B27 medium, contains Neurobasal medium, 1 % Penicillin-Streptomycin, 1X B-27 supplement. Differentiation was stopped at day 21 as the early differentiation was targeted with this approach.

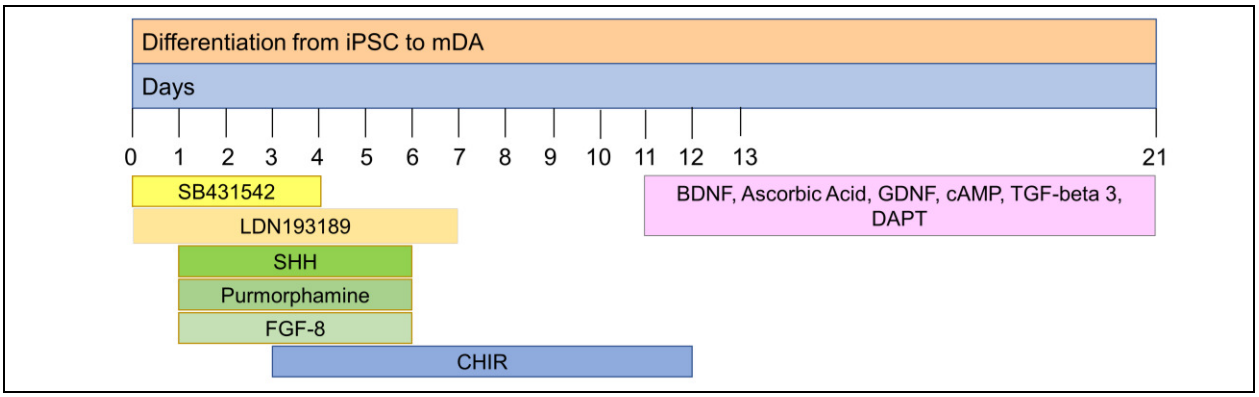

Figure 3.4 Schematic overview of the differentiation of iPSC to mDA

For qPCR, immunostaining, proteomics, and single-cell RNA expression profiling, progenitor cells were harvested at Day 0, Day 8, and Day 12, for metabolomics Day 0 and Day 8 were included.

Day of Differentiation	Base medium	Supplements
Day 0	SR medium	10 µM SB431542, 100 nM LDN193189
Day 1 / 2	SR medium	10 µM SB431542, 100 nM LDN193189, 100 ng/ml Shh, 2 µM Purmorphamine, 100 ng/ml FgF-8b
Day 3 / 4	SR medium	10 µM SB431542, 100 nM LDN193189, 100 ng/ml Shh, 2 µM Purmorphamine, 100 ng/ml FgF-8b, 3 µM CHIR
Day 5 / 6	75 % S medium, 25 % N2	100 nM LDN193189, 100 ng/ml Shh, 2 µM Purmorphamine, 100 ng/ml FgF-8b, 3 µM CHIR
Day 7/ 8	50 % SR medium, 50 % N2	100 nM LDN193189, 100 ng/ml Shh, 3 µM CHIR
Day 9 / 10	25 % SR medium, 75 % N2	100 nM LDN193189, 100 ng/ml Shh, 3 µM CHIR
Day 11 / 12	NB/B27	3 µM CHIR, 20 ng/ml BDNF, 0.2 mM Ascorbic Acid, 20 ng/ml GDNF, 1 mM cAMP, 1 ng/ml TGF-beta 3, 10 µM DAPT
Day 13 - 21	NB/B27	20 ng/ml BDNF, 0.2 mM Ascorbic Acid, 20 ng/ml GDNF, 1 mM cAMP, 1 ng/ml TGF-beta 3, 10 µM DAPT

Table 3.3 Medium composition for midbrain dopaminergic differentiation (Novak et al., 2022). For catalogue numbers please refer to Table 3.1.

3.4 qPCR

QPCR analysis was performed for 3 biological replicates. Total RNA was extracted from a cell pellet of a 12-well plate well using the RNeasy Plus Universal Kit Mini (QIAGEN), following the manufacturer instructions. 200-600 ng mRNA was employed to generate cDNA with Superscript

III First-Strand Synthesis System for RT-PCR (Thermo Fisher Scientific), using oligo(dT)20 as specified in the manufacturer`s protocol. Primers used for different reactions can be found in Table 3.4. All primers were synthesized by Eurogentec (Belgium).

Gene	forward primer	reverse primer	reference
Primers used for qPCR expression analysis of the BFCN differentiation			
NGFR	TGAGTGCTGCAAAGCCTGCAA	TCTCATCCTGGTAGTAGCCGT	Okumura *et al.*, 2003
PAX3	AGCCGCATCCTGAGAAGTAA	TTCTGCGCTGTTTCCTCTTT	Jiang *et al.*, 2009
B3GAT1	GCAAGAAGGGCTTCACTGAC	GCCCCCAGAATAGAAAGGAG	Jiang *et al.*, 2009
ACHE	GCTTCCTCCCCAAATTGCTCA	TGGAACTCGGCCTTCCACTG	Designed myself
MNX1	GCACCAGTTCAAGCTCAAC	GCTGCGTTTCCATTTCATCC	Ma *et al.*, 2020
NTRK1	GAGGTCTCTGTTCAGGTCAACGTCT	CTCAGTGAAGATGAAGCTGGTCT CATTGA	Bissonnette *et al.*, 2011
Primers used for qPCR expression analysis of the mDA differentiation			
OTX2	GAGGTGGCACTGAAAATCAAC	TCTTCTTTTTGGCAGGTCTCA	Novak *et al.*, 2022
EN1	CGTGGTCAAAACTGACTCGC	CGCTTGTCCTCCTTCTCGTT	Novak *et al.*, 2022
LMX1A	GCTCAGAGCAGTTCAGAGGG	CAAGCAGGAGTTTGCCCAAC	Novak *et al.*, 2022
FOXA2	ATTTTAAACTGCCATGCACTCG	ATGTTGCTCACGGAGGAGTAG	Novak *et al.*, 2022
TH	GGAAATTGAGAAGCTGTCCACG	GAATCTCAGGCTCCTCAGACAG	Novak *et al.*, 2022
KCNJ6	AGCTGCCCAAAGAGGAACTG	ACAGGTGTGAACCGGTAACC	Novak *et al.*, 2022
POU5F1	CTTGCTGCAGAAGTGGGTGGAGG AA	CTGCAGTGTGGGTTTCGGGCA	Tomizawa *et al.*, 2018
Primers used to compare BFCN and mDA differentiation stage			
MAP2	CCATCTTGGTGCCGAGTGA	GGAGTCGCAGGAGATTTTGG	Designed in house
TUBB3	GGAAGAGGGCGAGATGTACG	GGGTTTAGACACTGCTGGCT	Figiel-Dabrowska *et al.*, 2021
SOX1	GGAATGGGAGGACAGGATTT	ACTTTTATTTCTCGGCCCGT	Liu *et al.*, 2020
Primers for housekeeping genes			
GAPDH	CAGGGCTGCTTTTAACTCTGG	AAGTTGTCATGGATGACCTTGG	Crompton *et al.*, 2013
ACTB	CGAGGACTTTGATTGCACATTGTT	TGGGGTGGCTTTTAGGATGG	Smajić *et al.*, 2022

Table 3.4 Sequences of qPCR-primers. All primers are spanning an intron except LMX1A, SOX1, MAP2, TUBB3, and ACTB

qPCR was performed on a Lightcycler 480II (ROCHE) with Maxima SYBR Green/ROX qPCR Master Mix (Thermo Fisher Scientific) which was programmed as follows: initial denaturation at 95 °C for 10 min, followed by 45 cycles of 95 °C for 15 s, 59 °C for 30 s, and 72 °C for 60 s. To verify that only one PCR product is present a melting curve was performed with the following settings: heating to 95 °C for 5 s, 65 °C for 60 s, and heating to 97 °C with continuous acquisition every 5 °C. 3 biological replicates of each cell line were collected at each Differentiation Day 0, 8,

12 (for BFCN) and Day 0, 8, 21 (for mDA). The generated quantification cycle (Cq) values were standardized with GAPDH, a stable housekeeping gene for neuronal differentiation (Novak *et al.*, 2022). R was used for data analysis (version 4.0.2, R Core Team, 2022), employing packages dyplr, ggplot2, ggsignif, tidyverse, ggtext and patchwork (Wickham, 2016; Wickham *et al.*, 2019, 2023; Constantin and Patil, 2021; Pedersen, 2022; Wilke and Wiernik, 2022). Statistical analysis for the qPCR analysis was performed in R using Mann-Whitney-Wilcoxon U-test and Benjamini-Hochberg correction.

3.5 Immunocytochemistry

Cells designated for immunostaining were cultured on CellCarrier-96 ultra plates (Perkin Elmer). Cells were fixed in 4 % Paraformaldehyde in PBS (Alfa Aesar) for 10 min at room temperature. Wells were washed 3 times with DPBS and stored at 4 °C until the staining. Before the addition of the antibodies, cells were permeabilized with 0.1 % Triton X-100 (Sigma-Aldrich) for 20 min at room temperature and incubated in blocking solution, containing 2 % BSA (Sigma-Aldrich) in DPBS for 1 h at room temperature. Cells were incubated with a solution containing the primary antibody at 1:500 in blocking solution overnight at 4 °C. The reference for the antibodies can be found in Table 3.5 below.

The next day, cells were washed 3 times with DPBS before a solution of the secondary antibody was added. Dilution and references of the secondary antibody can be found in Table 3.5. After 1 h at room temperature, cells were washed with DPBS and incubated in a 1 ng/ml solution of DAPI dihydrochloride (Sigma-Aldrich) in blocking solution for additional 30 min at room temperature in the dark. Images were acquired with the Leica TCS SP8 STED (LEICA) with a 40x air objective of the LCSB imaging facility. Fiji software (Schindelin *et al.*, 2012) was used for image processing.

Target	Host	Catalogue #	Manufacturer	Dilution	Fluorochrome
Oct-3/4	mouse	sc5279	Santa Cruz Biotechnology	1:500	-
TRA-1-60	mouse	MAB4360	Merck Millipore	1:500	-
MAP-2	mouse	MAB3418	Merck Millipore	1:500	-
ChAT	rabbit	PA5-29653	Invitrogen	1:500	-
DAT (SLC6A3)	rabbit	PA1-4656	Invitrogen	1:500	-
TH	rabbit	AB152	Merck Millipore	1:500	-
Mouse IgG	donkey	715-605-150	Jackson immuno research	1:300	Alexa Fluor 647
Mouse IgG	donkey	A32773	Invitrogen	1:500	Alexa Fluor Plus 555

Rabbit IgG	Donkey	A32790	Invitrogen	1:500	Alexa Fluor Plus 488

Table 3.5 Primary and secondary antibodies used in this work.

3.6 Western blot

Western blot analysis was performed by Lena Schaack from the Medical Translational Research group (LCSB). 2 replicates of each WTSIi010-A, clone 1, clone 2, PB005.1 and R215I iPSC line were further characterized by Western blotting.

Cells were detached with Accutase, washed with PBS, and the cell pellet was resuspended in RIPA - buffer (89900, Thermo Fisher Scientific) supplemented with HALT protease inhibitor 1:1000 (1861281, Thermo Fisher Scientific). Samples were incubated in shaking conditions (1000 rpm) at 4 °C for 15 min. After centrifugation at 4 °C for 20 min at 21'600 x g, the supernatant was collected for measurement of protein content with Pierce BCA (23227, Thermo Fisher Scientific) as per manufacturer's instructions. Samples were diluted with RIPA buffer to achieve a concentration of 30 µg protein and loaded with a solution of Sample buffer (NUPAGE LDS Sample Buffer) and reducing agent (NUPAGE Sample reducing agent) into a 4-12 % NuPAGE gel (NP0323, Thermo Fisher Scientific). Precision Plus Protein Standards Kaleidoscope (161-0375) and Precision Plus Protein Standards Dual Color (161-0374) were used as protein ladders. The gel was run in a Western Blot XCell Surelock Western blot kit in 1X NUPAGE Running Buffer (NP0001, Thermo Fisher Scientific), with NUPAGE Antioxidant solution (NP0005, Thermo Fisher Scientific) for 5 min at 100 mV, thereafter at 150 mV for approximately 1 h. The gel was transferred onto a nitrocellulose membrane (LC2009, Thermo Fisher Scientific) with Transfer buffer (20 X NUPAGE Transfer Buffer, 100 ml methanol and 850 ml water) at 32 V for 1 h. Protein transfer was verified with Ponceau staining (P7170-1L). Unspecific binding was blocked for 1 h with 5 % milk or 5 % BSA, depending on the antibody. Membranes were then incubated with primary ADAM17 antibody overnight rotating at 4 ºC. For the full-length enzyme, ADAM17 rabbit antibody PA5-27395 (Thermo Fisher Scientific) was used in 1:500 dilution in 5% milk. For the pro-form ADAM17, antibody ADAM17 rabbit PA5-17079 was used in 1:1000 in 5 % BSA. Beta-Actin 40 kDa mouse was used as loading control in 1:5000 dilution (3700S, Cell Signal). Membranes were incubated for 30 min. Membranes were washed 3 times with Tris buffered saline (pH 7.6) supplemented with 1 % TWEEN (P7949-500ML). Anti-rabbit IgG (H+L) DyLight 800 4X PEG Conjugate (5151S) and anti-mouse IgG (H+L) DyLight 680 Conjugate were used as secondary antibodies, incubation in 1:5000 dilution for 30 min.

ODYSSEY LI-COR with the Image Studio Ver 5.2 software was used for the imaging of the membrane. Empiria (LI-COR) studio was used for analysis.

3.7 Single-cell RNA- sequencing

At the predefined days of the differentiation, cells were prepared for sc-RNAseq as per the following protocol: the wells were washed with DPBS and incubated with Accutase supplemented with 10 µl ROCK inhibitor until all cells were completely dissociated. Accutase was neutralized with buffer (0.04 % BSA in DPBS), and the suspension was centrifuged at 300 x g for 3 min at 4 °C. Cells were washed 2 times with the same buffer, subsequently strained through a 20 µm pre-separation filter (Miltenyi Biotec) and counted. Further steps were done by Dr Kamil Grzyb from the single-cell platform of the LCSB following the established workflows for 10x Genomics and Drop-seq (Dirkse *et al.*, 2019; Novak *et al.*, 2022).

During the BFCN differentiation samples were collected on Day 0, 8, and 12 and processed with 10x Genomics kit. During the mDA differentiation, samples were collected at Day 0, Day 8 and Day 21 and processed by Drop-seq (Macosko *et al.*, 2015).

3.7.1.1 10x Genomics

Single-cell RNA library preparation and sequencing was performed according to the manufacturer's protocol Chromium Next GEM Single Cell 3' Reagent Kits v3.1 User Guide, Rev D with the kits specified there. In brief, cell suspension was loaded with a targeted recovery rate of 7,000 cells per sample. Libraries quality was assessed using Bioanalyzer High Sensitivity DNA Chip (Agilent) and further sequenced on a 150 cycles High Output Kit using Illumina NextSeq 500 with targeted sequencing depth of 25,000 read pairs per nucleus. Raw FASTQ files were processed with the pipeline Drop-seq bioinformatics pipeline (Macosko *et al.*, 2015)

3.7.1.2 Drop-Seq

Microfluidic devices and silicon-based polymer-based Drop-seq chips were fabricated as previously published (Trapnell *et al.*, 2014; Macosko *et al.*, 2015). Single-cell RNA encapsulation was performed according to a previously published method (Sousa *et al.*, 2018). Synthesized barcoded beads (ChemGenes Corp., USA) were co-encapsulated with cells inside the droplets containing Drop-seq Lysis buffer using an optimal bead concentration of 180 beads/µl. Cellular mRNA was captured via barcoded oligo (dT) handles synthesized on the bead surface. The subsequent steps of droplet breakage, bead harvesting, reverse transcription and exonuclease treatment were conducted in accordance with the Drop-seq method. Purified Drop-seq cDNA

libraries were sequenced using Illumina NextSeq 500 with the recommended sequencing protocol except for 6 pM of custom primer (GCCTGTCCGCGGAAGCAGTGGTATCAACGCAGAGTAC) applied for priming of read 1. Paired-end sequencing was performed for the read 1 of 20 bases and for read 2 of 60 bases of the genes. Quality control of the sequencing libraries was performed with FASTQC codes (Wingett and Andrews, 2018). Finally, sequencing reads were converted into a digital gene expression matrix using the Drop-seq bioinformatics pipeline (Macosko *et al.*, 2015).

3.7.1.3 Single-cell RNA-sequencing data analysis

Data analysis was performed by Dr Corrado Ameli. The pipeline was written by using the Seurat v4 R package (Hao *et al.*, 2021). The identification of low-quality cells was performed separately for each dataset. For each cell, the percentage of mitochondrial and ribosomal expression over the total expression were calculated. Additionally, for each cell the number of non-zero genes (number of features) and the sum of the detected transcripts were calculated. Each metric was then normalized by centering the distribution via a robust calculation of the mode (Bickel, 2002). Quality control metrics distributions were then scaled by calculating the number of standard deviations away from the mean. Cells were then filtered by applying the following constraints:

- Percentage of mitochondrial RNA standardized < 1 (see Osorio and Cai, 2021 for why hard thresholding (e.g. 5 %) in human cells is not a correct approach)
- Number of transcripts detected standardized < 3
- Percentage of mitochondrial RNA > 0
- Percentage of ribosomal RNA > 0

Note that since the number of non-zero features correlates almost linearly with the number of transcripts per cells, the two quality control metrics can be used interchangeably. The quality control plots containing the raw measurements, the centered measurements, and the scaled measurements are shown in Supporting Figure 8.2.

Each dataset was then normalized individually by performing the canonical log normalization of the transcript concentration (see NormalizeData by Seurat R package). A batch correction was then performed to correct for the small differences present in sequencing depth amongst all datasets. To do so, we scaled the log distributions in such a way that each dataset has equal mean concentration. Such distributions were then multiplied by a constant factor (average log concentration of the dataset that had the greatest of such value). The normalization and batch correction plots are shown in Supporting Figure 8.3.

The individual datasets were then integrated by using SCTransform v2 by Seurat. Briefly, cells coming from the same condition at different days of the differentiation were merged and then integrated with the other condition. Note that the SC transform was performed on the raw counts prior to normalization and batch correction as suggested by the guidelines. The integrated dataset was then used to perform principal component analysis, uniform manifold approximation (UMAP) and clustering via shared nearest neighbour (see FindClusters function by Seurat). The resolution parameter that defines the coarseness of the clusters was set to 0.35.

In order to find the differentially expressed genes (DEGs), we used Wilcoxon ranked sum test, performed over the normalized and batch corrected dataset. Correction for multiple testing was automatically performed via the usage of the FindMarkers function by Seurat.

Functional profiling of DEGs was performed with G: Profiler (version e109_eg56_p17_1d3191d, Raudvere *et al.*, 2019).

3.8 Metabolomics

The metabolomic extraction and measurement was performed by Dr. Marc Warmoes of the Metabolomics platform at the LCSB. BFCN cells medium samples were collected at feeding time (t0), after 12 h, and after 24 h for differentiation Day 8, Day 12; for the Day 0 samples were collected at t0 and after 18 h. For mDA samples medium was collected at t0 and after 12 h. The analysis was performed for 3 biological replicates. The medium was analysed with Gas Chromatography - Mass Spectrometry (GCMS), performed as previous described (Modamio *et al.*, 2021). Cellular extracts were analysed with Ion Chromatography - Mass Spectrometry (ICMS) and Hydrophilic Interaction Liquid Chromatography (HILIC).

3.8.1 Metabolite extraction, ICMS, and HILIC experiments

For **metabolite extraction**, cells were first gently washed with 1 ml MilliQ water (Milli-Q Advantage A10). Thereafter, 560 µl pre-cooled (- 20 °C) extraction fluid (7:3 methanol/20 mM with internal standards) was added to the wells, cells were immediately scraped, and suspension was transferred to a tube prefilled with 200 µl chloroform placed on ice. Next, the extract was vortexed for 10 min at 4 °C using at maximum speed (Eppendorf Thermomixer C). Phase separation was initiated by adding 200 µl chloroform and 200 µl MilliQ water, followed by centrifugation at 21’000 x g for 5 min at 4 °C. For ICMS and HILIC analysis, 200 µl and 100 µl, respectively, supernatant were collected. The two polar extract aliquots were evaporated overnight at - 4 °C to

metabolite pellets using a refrigerated centrifugal vacuum concentrator (CentriVap 7310000, Labconco) and stored at - 80 °C until analysis.

For **the ICMS measurements**, polar extracts were analysed as previously described (Wang *et al.*, 2020) with the following adjustments. Dried polar metabolite pellets were reconstituted in MilliQ water and filtered using PHENEX-RC 4 mm syringe filters. Reconstitution volume was based on the cell number counted in a reference well (see Supporting Table 8.1).

The ICMS system consisted of a Dionex ICS-6000+ ion chromatograph with a QExactive high resolution mass spectrometer (both Thermo Fisher Scientific). The IC autosampler injected 20 µl reconstituted sample. The heated electrospray ionization settings were as follows: spray voltage 2'500 kV, auxiliary gas temperature 420 °C, sweep gas flow rate 0, auxiliary gas flow rate 15 units, and sheath gas flow rate 50 units. The settings for acquisition of MS1 data were m/z scan range 80-750, resolution 17.5 K, automatic gain control (AGC) target 1e6, and maximum injection time 100 ms. Data were acquired using two micro-scans. For the MS2 data acquisition, the following settings were used: resolution 17.5 K, AGC 2e5, maximum injection time 50 ms, loop count 2, isolation window 4.0 m/z, and collision energy 30 eV.

For the targeted HILIC-MS measurements, metabolite pellets were reconstituted in 50 % acetonitrile and analysed using a Themo UHPLC Vanquish UHPLC equipped with a quaternary pump and coupled to a Thermo Q Exactive HF mass-spectrometer. Reconstitution volume was based on the cell number counted in a reference well (see Supplementary Table 8.1) and injection volume was 5 µl. Metabolites were separated using a SeQuant ZIC pHILIC column (5 µm particles, 2.1 x 150 mm) coupled to a Orbitrap Exploris 240 mass-spectrometer. The column oven temperature was set at 45 °C and the autosampler was maintained cooled at 4 °C. Mobile phases, applied at a flow rate of 0.2 ml/min, consisted of MilliQ water with 20 mM ammonium carbonate in water pH 9.2 and 5 µM medronic acid (mobile phase A) and acetonitrile (mobile phase B). The gradient was minute 0, 80 % B; minute 18-19, 20 % B; after 20 min, 80% B; with an increase of the flow rate at 25.5 min to 0.4 ml/min. For the MS analysis, the following settings were used: sheath gas flow rate 35, auxiliary gas flow rate 7, sweep gas flow rate 0 (arbitrary units for all gas flow rates), auxiliary gas heater temperature 275 °C, ion transfer capillary temperature 400 °C, spray voltage 3 kV in both positive and negative mode, S-lens radio frequency 70. The MS1 scan parameters were as follows: AGC "Standard"; maximum injection time 100 ms; micro scans 1; resolution 60'000; scan range 75-1000 m/z. The MS2 scan parameters were set to AGC "Standard"; maximum injection time "Auto"; isolation window 0.4 m/z; collision energy 30 eV; resolution 30'000; loop count 3; dynamic exclusion time 3 s with exclusion after 1 acquisition.

Peak areas were integrated and exported to Microsoft Excel via the Thermo TraceFinder software (version 5.1), for both HILIC and ICMS. Metabolite identification confidence was level 1 (Schymanski *et al.*, 2014). Metabolites were verified by an in-house library of standards.

3.8.2 Data analysis for metabolomics data

Initially, Dr Corrado Ameli first performed hierarchical clustering to identify potential outliers. For both ICMS, HILIC and GC-MS no outlier was found. For calculating significant differences, we used unpaired t-test. The corresponding p-values were adjusted via Benjamini-Hochberg correction at each day of the differentiation.

Following Dr Ameli's analysis, over representation analysis for metabolic compounds in the SMPDB database differing significantly in abundance between R215I and control (adjusted p-value (padj) < 0.05; $Log_2FC > 0.25$) was performed with MetaboAnalyst version 5.0 (Xia and Wishart, 2011; Lu, Pang and Xia, 2023). Hypergeometric test was used for calculating significance, one-tailed p-values are proved correct for multiple testing.

3.9 Proteomics

The proteomics analysis was performed by the Proteomics of Cellular Signaling group of Luxembourg Institute of Health under supervision of Prof. Gunnar Dittmar. Three biological replicates of mDA neuronal precursor cells of Differentiation Day 0, Day 8, and Day 12 were analysed as per a previously published protocol (Novak et al., 2022). In short, washed cell pellets were lysed in 1 % sodium deoxycholate in 50 mM sodium bicarbonate pH8. Thereafter, samples were sonicated, kept on ice for 30 min and centrifuged at 4 °C for 30 min at 16'000 × g. Protein content of the supernatant was quantified with PierceTM BCA Protein Assay Kit (23225, Thermo Fisher Scientific). The extract volume containing 10 µg protein extract was first reduced with 10 mM Dithiothreitol for at 37 °C 45 min, then alkylated with 25 mM iodoacetamide for 30 min at room temperature in darkness after incubation for 15 min. For digestion, proteins were incubated in 0.2 µg of trypsin/Lys-C Mix (V507A, Promega) at 37 °C overnight. After acidification in 1% formic acid, samples were centrifuged at 12'000 × g for 10 min. Supernatants were desalted on Sep-Pak tC18 µElution Plates (186002318, Waters), dried by vacuum centrifugation, and reconstituted in 25 µl of 1 % Acetonitrile/0.05 % trifluoroacetic acid. Protein concentration was measured with Nanodrop 2000C (Thermo Scientific), and 200 ng of each sample was used for Liquid Chromatography - Mass Spectrometry (LC-MS). Therefore, a Dionex Ultimate 3000 RSLC chromatography system configured in column switching mode was set up. The loading phase

consisted of 0.05 % trifluoroacetic acid and 1 % acetonitrile in water, mobile phases comprised 0.1 % formic acid in water (mobile phase A) and 0.1 % formic acid in acetonitrile (mobile phase B). A Thermo pepmap100 C18 (3 µm particles, 75 µm × 2 cm) was used a loading column, the separation column was Thermo pepmap100 C18 (2 µm particles, 75 µm × 15 cm) analytical column (loading 5 µl min−1; analytical 300 µl min−1). A linear gradient ranging from 2 % B to 35 % B over 66 min was applied. Sample was sprayed with a Nanospray Flex ion source into Q Exactive-HF (both Thermo Scientific) operated in data-dependent acquisition mode. The MS1 scan parameters were as follows: AGC 3e6; resolution 60'000; scan at 200 m/z. For the MS2 scan, the top 12 most intense peptide fragments were detected at AGC 1e5, resolution 15,000 at 200 m/z with 20 s dynamic exclusion of already fragmented peptides.

The MaxQuant software package version 1.6.17.0 was used for analysis (Cox and Mann, 2008), with label-free quantification 2 and an FDR < 1 % for peptides and proteins. Andromeda search (Cox et al., 2011) was performed on a human Uniprot database (July 2018). Fixed modifications were carbamidomethylation and cysteine, variable modifications comprised oxidized methionine and acetylated N-termini, with a peptide tolerance of 20 ppm. The MaxLFQ algorithm (Cox et al., 2014), implemented in MaxQuant, with the match-between-runs feature, was employed for the normalisation.

4 Results

This Chapter presents the results generated during my PhD studies. This includes the generation of an *ADAM17* rs142946965 stable iPSC cell line (Aim I), followed up by the phenotypic characterization of the early neuronal development during BFCN and mDA differentiation of the ADAM17 clone (Aim II).

4.1 Generation of a stable iPSC cell line carrying rs142946965 in *ADAM17*

The recent development of iPSC technology allows for personalized investigation of diverse cellular phenotypes where potential disease-causing mutations can be studied in the context of the natural genetic background. In this study, iPSC technology was applied by introducing the AD-related rs142946965 polymorphism of *ADAM17* into a healthy control to investigate molecular impairment during neuronal development. A CRISPR/Cas approach for gene editing, followed by a FACS selection process, was used to select for a heterozygous mutation (Arias-Fuenzalida *et al.*, 2017; Jarazo, Qing and Schwamborn, 2019).

4.1.1 Design and cloning of the sgRNA into the guide plasmid

The BTE, located at position 34'569 on the *ADAM17* gene, is a guanine base which will be edited to a thymine base (G>T). CRISPOR (Concordet and Haeussler, 2018) and GPP sgRNA Designer (Doench *et al.*, 2016; Sanson *et al.*, 2018) results were combined to define the single-strand guide RNA (sgRNA) for the CRISPR machinery. Out of the top 10 predictions from each software, two sgRNA were chosen when they appeared in both programs and when they were in close proximity to the BTE. Location of the sgRNA on *ADAM17* is shown in Figure 4.1. Both sgRNA were separately cloned into the plasmid pL589, a modified version of the human codon-optimized SpCas encoding plasmid pX330-U6-Chimeric_BB-CBh-hSpCas9 (Addgene), generously provided by Dr Javier Jarazo (Cong *et al.*, 2013; Arias-Fuenzalida *et al.*, 2017). Sequencing confirmed successful cloning for 5 out of 5 sgRNA1-containing plasmids and 4 out of 5 sgRNA2-containing plasmids.

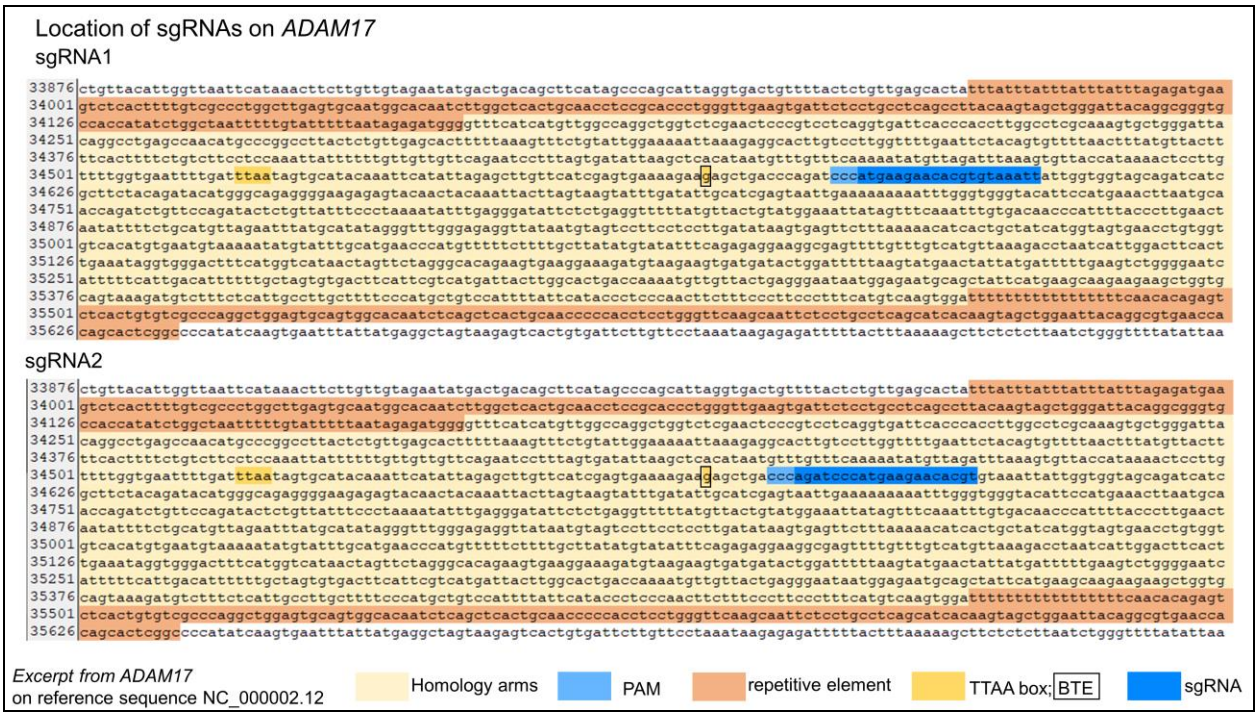

Figure 4.1 Illustration of the location of the TTAA box, the BTE, the sgRNA and the respective PAM. The BTE is in position 34'569; instead of the guanine base thymine will be introduced (G>T). ADAM17 *reference sequence NC_000002.12:c9555830-9488486, homo sapiens chromosome 2, GRCh38.p14 Primary Assembly. Image generated with APE version 3.1.3 (Davis and Jorgensen, 2022).*

4.1.2 Design and cloning of the homology arms into the donor plasmid

The homology arms serve as the elongation template for the DNA synthase to repair the double strand break introduced by the Cas enzyme. The region between the TTAA box and the adjunct repeating section makes up their sequence. The TTAA box, which will house the selection markers, is positioned 51 bp upstream the BTE. RepeatMasker (Smit, Hubley and Green, 2013) was used to identify the repetitive elements. A silent mutation at the PAM was introduced to avoid subsequent DNA double strand breaks after the mutation was inserted. Each PAM's 3'-cytosine will be replaced with a 3'-thymine. To achieve a heterozygous mutation, two different sets of homology arms were generated using Gibson Assembly. The LHA and the RHA without the mutations were cloned into a single plasmid carrying a dTomato selection marker (pDONOR-tagBFP-PSM-dTOMATO). The LHA and the RHA with the mutations on the BTE and PAM were cloned into a single plasmid carrying an EGFP selection marker (pDONOR-tagBFP-PSM-EGFP). Figure 3.1 depicts the structure of the donor plasmids. Sequencing verified successful cloning of all the donor plasmids (2 out of 5 for pDONOR-EGFP-sgNRA1; 3 out of 10 for pDONOR-dTOMATO-sgNRA1; 3 out of 10 for pDONOR-EGFP-sgNRA2 and 2 out of 5 for pDONOR-dTOMATO-sgNRA2).

4.1.3 iPSC nucleofection, selection and FACS sorting

The iPSC cell line WTSIi010-A was electroporated with the LONZA Nucleofector. In one experiment 5 nucleofections per sgRNA, each employing 1 million cells, were carried out. In total 50 nucleofections were performed during the project. Puromycin was employed to select for clones throughout the recovery of the cells. Approximately one week after the nucleofection cells were manually picked based on their fluorescence expression. In case colonies displayed yellow fluorescence, selection markers had been incorporated one in each allele. If the colonies show green fluorescence, EGFP was inserted into one or two alleles. On average, 10-30 colonies were picked per experiment.

After fluorescent-based picking, PCR was used to confirm the accurate insertion of the homology arms. The reaction of the primers VKI (validate the knock-in) 1 and VKI 2 confirms the right insertion of the LHA, whereas VKI 3 and VKI 4 reaction validates the correct insertion of the RHA. DNA amplification with the primers VKI 2 and VKI 5, or VKI 3 and VKI 6 respectively, is only possible if a part of the plasmid backbone was incorporated in the cell's genome. Colonies showing this amplification were discarded. Additionally, the reaction of the primers VKI 1 and VKI 4 validate the correct insertion of the entire homology arm region. In this selection process, most clones did not show the desired reactions, only 2 clones were selected for FACS purification. Both of these colonies showed green fluorescence.

Subsequently, FACS sorting was performed to purify the colonies. Two successive sorts were required for each clone to get a 100 % pure EGFP expressing clone (Figure 4.2). For the first sorting, the proportion of cells of interest was 52.2 % for clone 1 and 47.6 % for clone 2 for the first sorting, 92.4 % and 87.2 % respectively for the second sorting. After the second sorting, colonies for both clones consisted of 100 % of viable cells expressing EGFP. After FACS sorting of the clones, the positive selection markers were removed employing a transposase reaction. The transposase reaction was successful for approximately 3 % of cells of clone 1 and 6.9 % of cells of clone 2. See Figure 4.2 for illustration.

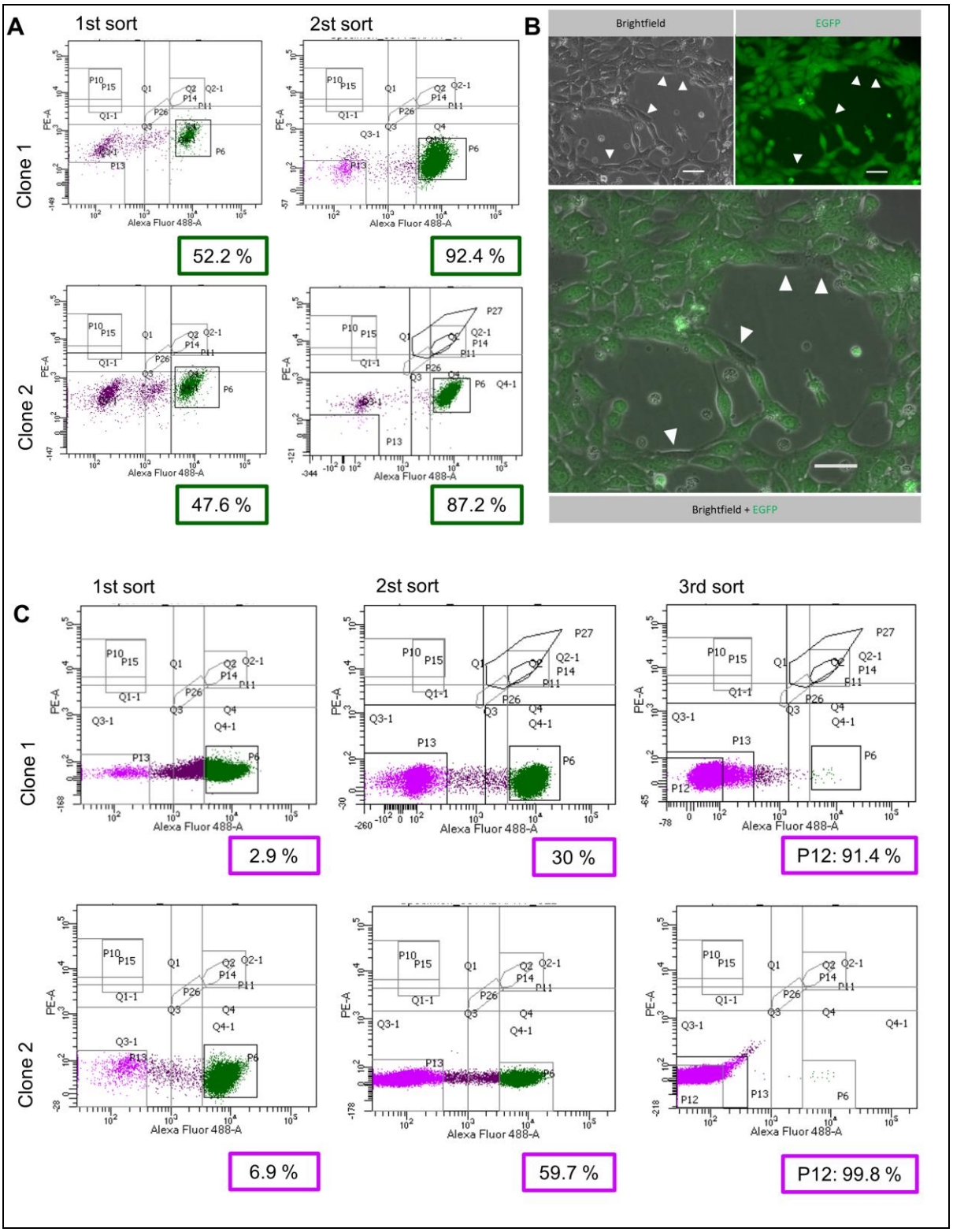

Figure 4.2 FACS assisted selection of the clones. ***(A)*** *After validating the correct knock-in of the selection markers two subsequent FACS sorting were performed to purify the colonies.* ***(B)*** *The transposase reaction was used to exclude the positive selection module from the genome. Successful reaction was verified with live cell imaging. White arrows point towards cells which lost the selection markers. Scale bar 50 µm* ***(C)*** *Final sorting for purification of the clone. After 3 subsequent sortings the colonies were 100 % pure.*

After the transposase reaction, FACS sorting was repeated. This time, the cells lacking fluorescence markers were purified. Colonies were enriched to 30 % non-fluorescent cells for clone 1 and 59.7 % for clone 2 during the first sort. Before the third sort, colonies consisted of approximately 91.4 % and 99.8 % cells of interest, respectively. After the third sort, colonies were 100 % free of fluorescence markers.

4.1.4 Sequencing and Karyotyping

Before DNA samples were sent for sequencing, the region of interest was amplified by PCR. Surprisingly, after gel electrophoresis the sample for clone 1 showed two bands. These different bands were separately purified and sequenced at Microsynth Seqlab (Germany). The sequencing results are displayed in Figure 4.3. The results of the karyotyping are shown in Supporting Figure 8.1.

Clone 1 did not show the correct mutation, however other mutations downstream of the BTE are detected. Among them, a big insertion of around 80 bp, explaining the second band on the gel. The karyotype of clone 1 was normal.

Clone 2 had the desired mutation. However, downstream of the BTE sequence alignment to the reference gene was not possible. This could indicate one or several insertions or deletions. The karyotype of clone 2 was abnormal, it showed an insertion of 1’683 bp at chromosome 20.

Due to the technical problems in generating the stable iPSC cell line, a complementary strategy was taken in the meantime by outsource the generation to the facility of the Murdoch Children’s Hospital (Australia).

4.1.5 Verification of Australian clones

The Murdoch Children´s Research Institute (Australia) prepared the *ADAM17* clone (R215I) from the isogenic control iPSC line PB005.1 (Vlahos *et al.*, 2019). The isogenic control allows to control the influence of genetic background on the experiments.

The mutation was verified by sequencing. In order to prevent re-cutting by the CRISPR/Cas9 complex and to correct for a 1 bp insertion several silent mutations were introduced by the facility. Sequence alignment is displayed in Figure 4.3. The karyotype of both cell lines is normal (Supporting Figure 8.1).

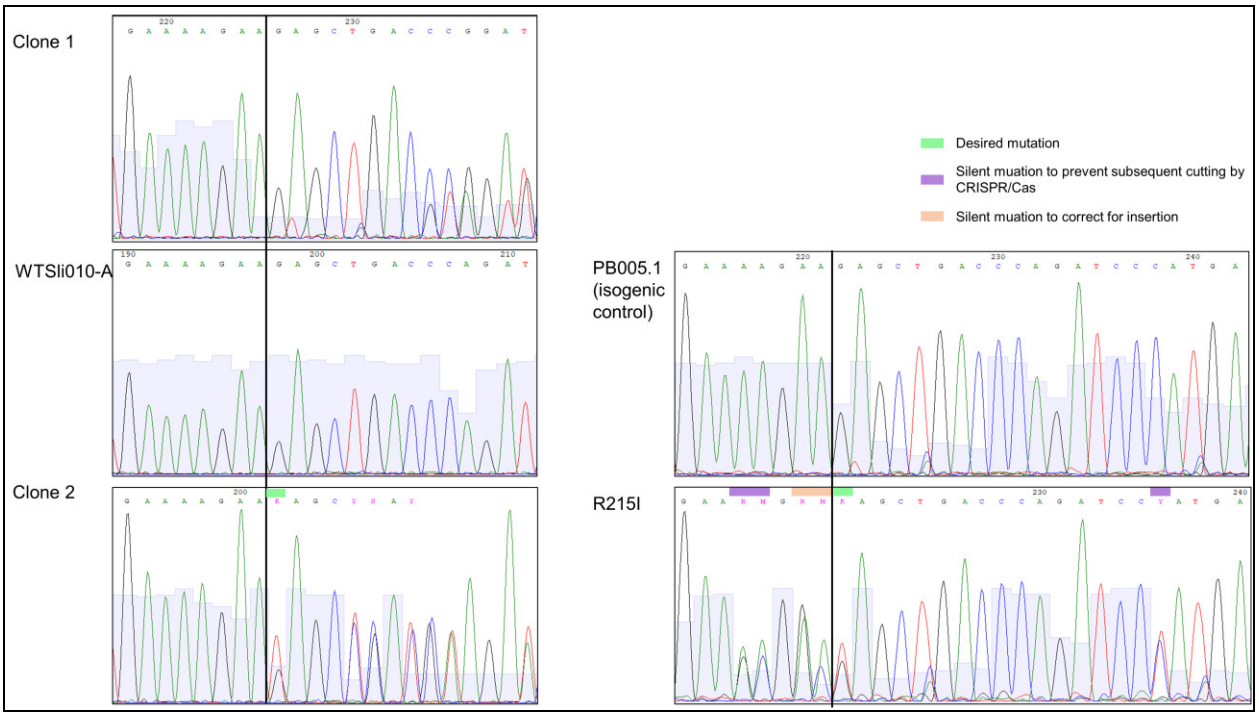

*Figure 4.3 Sequencing results of the clones generated during this project. Sequencing results of **(left)** the clones generated during this work and **(right)** the clone provided by the Murdoch' Children´s Research Institute (Australia) with their respective isogenic controls.*

4.1.6 Western Blot

Western blot for the clones generated in this project were performed by Lena Schaack (Medical Translational Research group, LCSB) to test whether the *ADAM17* rs142946965 mutation influences post-translational maturation of ADAM17. As the inserted mutation is close to the cleavage side of the inhibitory pro-domain and because it reduces the local charge, an altered cleavage pattern is highly suspected.

We used two different antibodies, one targeting the c-terminal end of the ADAM17 (amino acids 668-824), and one targeting the pro-domain (approximately binding at amino acid Val200). The antibody binding to the c-terminal end allows the approximate quantification of both, pro-ADAM17 and mature ADAM17 (mADAM17). As expected, two fragments are visible with this antibody in every cell line. The intensity of the mature form (size approximately 70 kDa) does not differ between the cell lines. The pro-form shows a striking difference. The clone 1 and clone 2 show reduced levels of pro-form (approx. 135 kDa) compared to their wildtype WTSIi010-A. The clone R215I, generated by the Murdoch Children´s Research Institute (Australia), does not show any difference in intensity for the pro-form compared to its isogenic control PB005.1 (Figure 4.4 A).

The picture is confirmed by the other antibody, targeting only the pro-form. The cell lines clone 1 and clone 2 show much less pro-ADAM17 compared to their wildtype control (WTSIi010-A). Again, R215I shows a similar band size as its isogenic control PB005.1 (Figure 4.4 B).

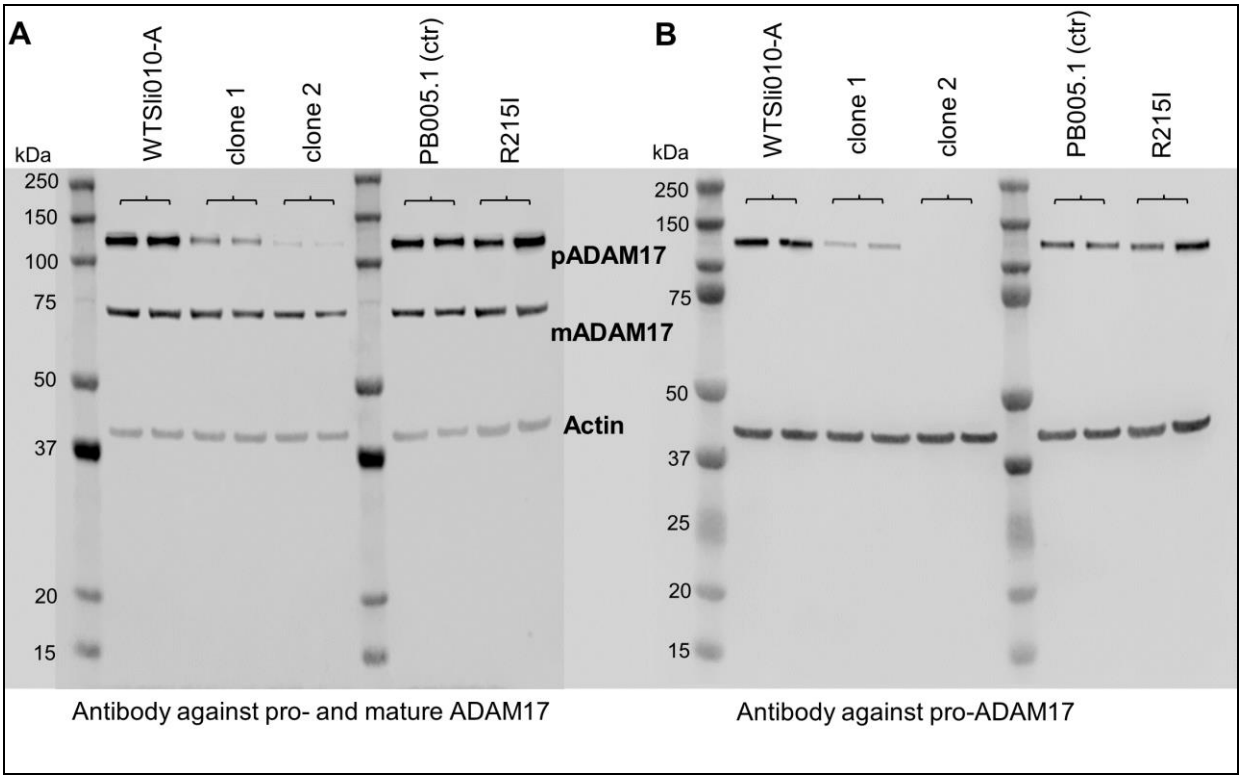

Figure 4.4 Western blot confirms changes in ADAM17 maturation. ***(A)*** *The antibody binding to the c-terminal end reveals no change in abundance of the mature ADAM17 form for any clone compared to their control. However, the clone 1 and clone 2 show less abundant pro-ADAM17.* ***(B)*** *The antibody binding only the pro-domain confirms this result* ***(right)****.*

4.2 ADAM17 in early neuronal development

To investigate the impact of an *ADAM17* mutation on early neuronal development, iPSC clones carrying the rs142946965 mutation, in the following referred to as “R215I” mutation, were differentiated into BFCN and mDA progenitors, respectively.

For these experiments, both the R215I iPSC line and its isogenic control PB005.1 (ctr) were differentiated simultaneously, and phenotypic characterization was carried out at different timepoints during the cell development. Each timepoint is an independent biological replicate, initiated at a different time and with cells of a different passage number.

4.2.1 Differentiation of BFCN

Following a previously described protocol (Ortiz-Virumbrales *et al.*, 2017), iPSC were differentiated into BFCN. This protocol includes FACS sorting of the progenitor cells at Differentiation Day 12, which is accompanied by substantial cell loss. For the purpose of this project to investigate neuronal differentiation dynamics, cells at the early timepoints of differentiation (Differentiation Day 0, Day 8, and Day 12) were analysed regarding their single-cell expression and metabolome.

4.2.1.1 Estimation of BFCN progenitors count using FACS

To estimate the share of neuronal progenitor cells investigated in the single-cell RNA sequencing and the metabolomic experiment, cells of a reference well were stained by NGFR antibodies conjugated to phycoerythrin and analysed with BD MELODY cell sorter (Becton Dickinson). An overview of the results is listed in Table 4.1. The gating strategy is illustrated in Figure 4.5.

	Day of Differentiation	% of PE- positive cells
Sorting for single cell		
R215I	12	21.5
ctr	12	7.24
R215I	8	21.5
ctr	8	24.9
Sorting for metabolomic experiment		
R215I	12	6.75
ctr	12	2.1

R215I	8	5.09
ctr	8	8.19

Table 4.1 Share of NGFR-positive cells in BFCN differentiation. Cells were stained with a NGRF-antibody linked to phycoerythrin.

For the sorting for the single-cell experiment, the NGFR antibody was diluted 1:10'000'000 instead of 1:1'000'000 for the control cells at Differentiation Day 12, which explains the low number of stained cells.

For the metabolomic experiments, cells were developing overall much slower than observed in previous experiments. For Differentiation Day 12 we would have expected > 10 % PE-positive cells, based on our experience with previous experiments, but the quantification showed only about half of positive cells.

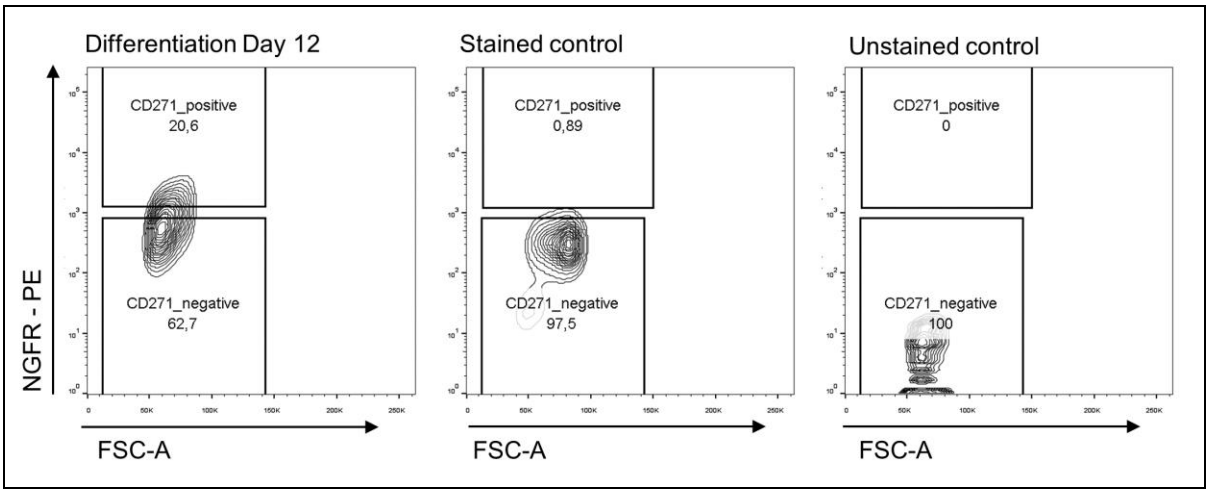

*Figure 4.5 Sorting strategy for identification of NGFR expressing cells. After identification of the single cells, the sorting gate **(left)** was defined based on exclusion of signals from NGFR-PE-stained iPSC **(middle)**, and an unstained sample of the differentiated cells **(right)**.*

4.2.1.2 Verification of BFCN progenitor phenotype by qPCR

As a first approach, qPCR was employed to verify cell differentiation into the desired phenotype. Among all of the markers tested, *NGFR* and *POU5F1* showed a reliable signal (see Figure 4.6). *POU5F1,* a marker for pluripotency, was expressed at Day 0 and dropped in expression the following days, as expected. Levels of *NGFR,* a marker for BFCN development and identity, are supposed to increase steadily during the differentiation. However, cells harvested at Differentiation Day 12 showed a substantial decrease of *NGFR* expression compared to Day 8,

indicating a slower development of the cells collected at Day 12. This is in accordance with the FACS data showed in Section 4.2.1.1.

ACHE and *NTRK1*, further markers of BFCN lineage, were not detected at any timepoint. This might be due to the fact that the cells have not yet formed a stable neuronal phenotype but are still developing. Absence of cholinergic motor neurons was validated with *MNX1*, which was not detectable at any timepoint.

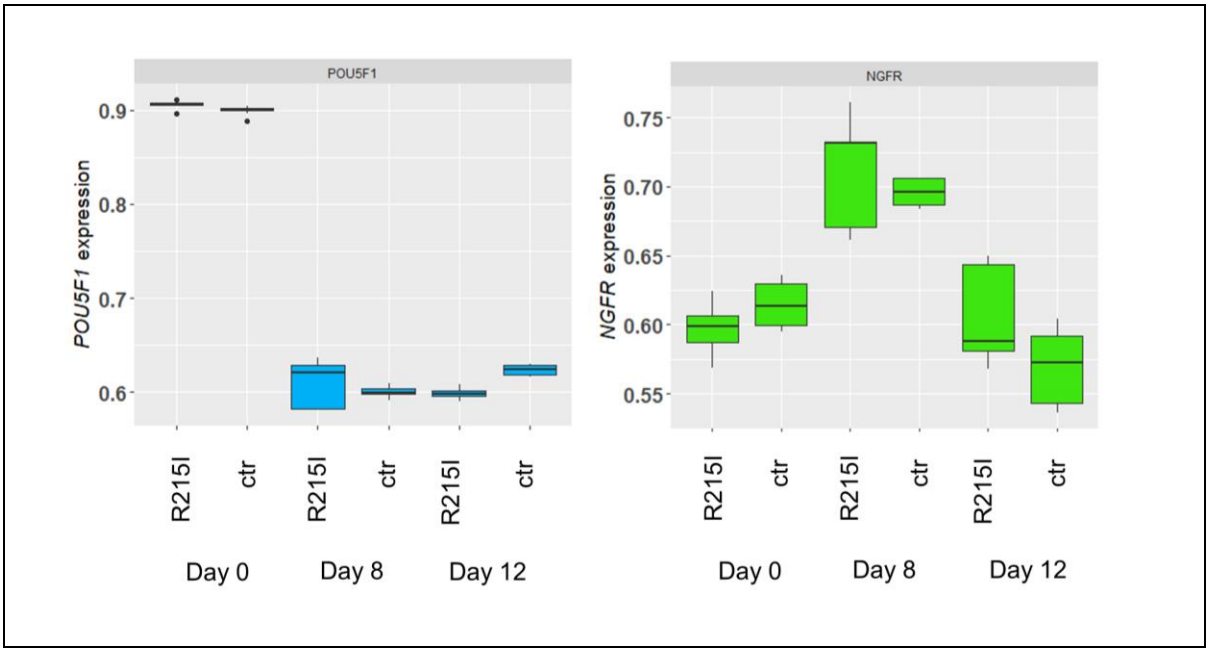

Figure 4.6 Verification of BFCN differentiation using qPCR. POU5F1 *levels decreased as expected* ***(left)****. The levels of* NGFR *are increasing from Day 0 to Day 8. The levels of cells at Day 12 are unexpected low* ***(right)****. Expression levels are quantified in relation to GAPDH. Three biological replicates were examined for each cell line. Data are presented as mean ± SD, no statistically significant changes were detected (Mann-Whitney-Wilcoxon U-test with Benjamini-Hochberg correction.)*

4.2.2 Differentiation of mDA

iPSC were differentiated into mDA following a previously published protocol (Novak *et al.*, 2022). To generate comparable datasets between development of the different neuron types, cells at Day 0, Day 8, and Day 21 were collected for analysis of regarding their single-cell expression, metabolome, and proteome.

4.2.2.1 Verification of mDA development progenitor phenotype

qPCR was employed to confirm differentiation of iPSC into the desired phenotype (Figure 4.7 A). As expected, the levels of the pluripotency marker *POU5F1* decreased during the differentiation. *TH*, a main marker for dopaminergic neurons, was detected via qPCR and immunostaining at

Day 21 (Figure 4.7 B). Midbrain specific markers *LMX1A* and *KCNJ6*, were measurable from Day 8 and Day 21, respectively. The expression levels of *OTX2*, a marker for midbrain neuronal progenitor cells, increased during the course of the differentiation. No differences between R215I and isogenic control were evident, except for *POU5F1.* Expression of *POU5F1* was detected at Day 21 for the mutant R215I, but not for the control cell line, suggesting an overall slower or less efficient differentiation of the mutant.

Another marker of pluripotency, TRA-1-60, was detected via immunocytochemistry at Day 0, but was not detected at subsequent timepoints of differentiation for any cell line. Neuronal differentiation was verified by detection of the neuronal marker MAP2. DAT, a marker for dopaminergic neuronal cells, was not stably detectable at Day 21. This is not surprising, as Day 21 is an early timepoint for mDA specific expression profiles.

Figure 4.7 provides a summary of the findings described in this Subsection.

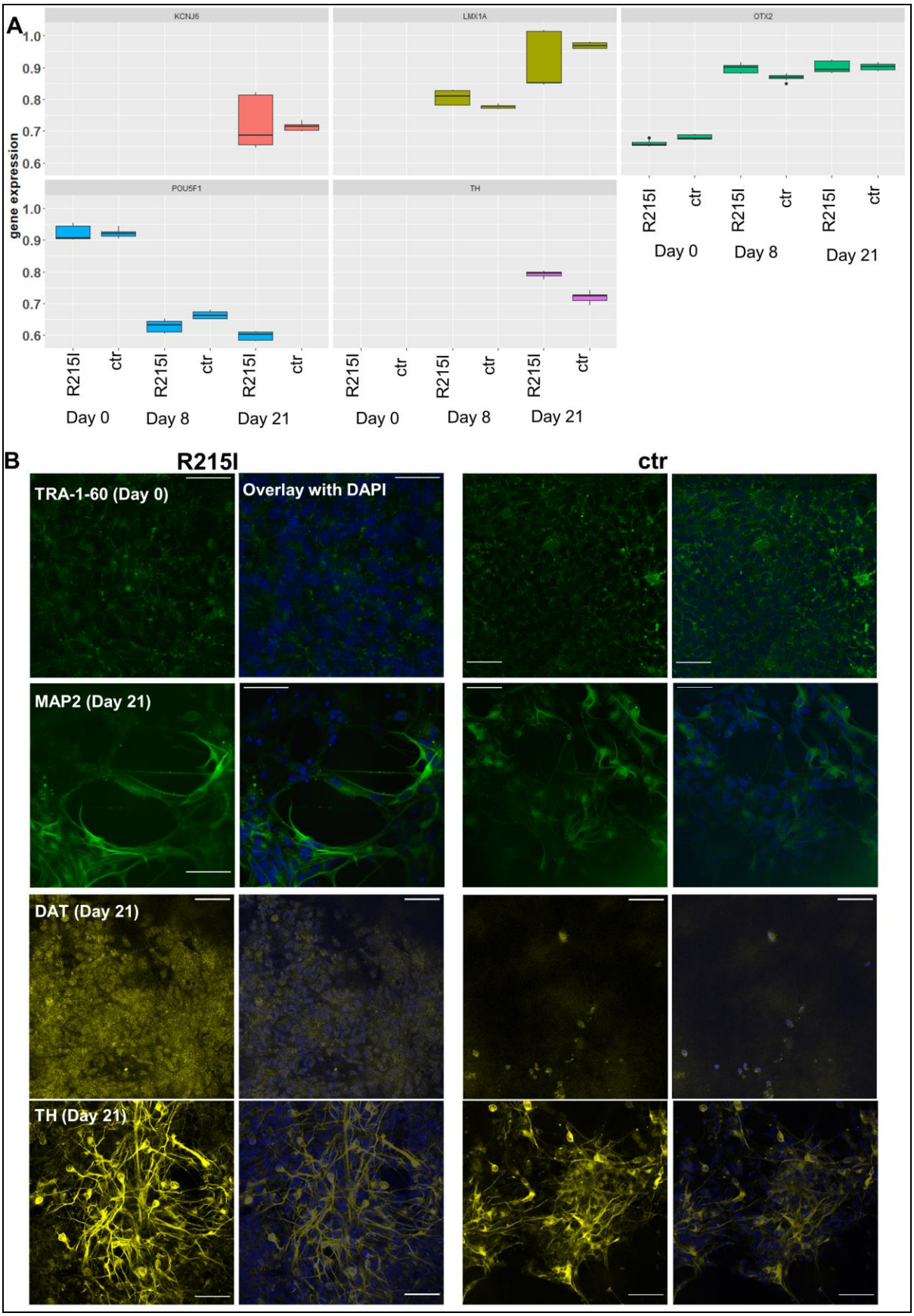
A
KCNJ6
LMX1A
OTX2
POU5F1
TH
gene expression
1.0
0.9
0.8
0.7
0.6
R215I
ctr
Day 0
Day 8
Day 21
B
R215I
ctr
TRA-1-60 (Day 0)
Overlay with DAPI
MAP2 (Day 21)
DAT (Day 21)
TH (Day 21)

Figure 4.7 Characterization of mDA differentiation. ***(A)*** *qPCR confirmed iPSC differentiation into desired phenotype.* POU5F1 *levels decreased as expected,* TH *was detected at Day 21,* LMX1A *and* KCNJ6 *were measurable at Day 8 and Day 21 respectively, and* OTX2 *increased during differentiation. R215I showed slower differentiation than control, with POU5F1 detected only in the mutant at Day 21. Expression levels are quantified in relation to GAPDH. Three biological replicates were examined for each cell line. Data are presented as mean ± SD. Using Mann-Whitney-Wilcoxon U-test with Benjamini-Hochberg correction following statistically significant changes were found: OTX2 R215I cell line p-value = 0.04194 (Day 0 – Day 8), p-value = 0.03059 (Day 0 – Day 21); OTX2 ctr cell line p-value = 0.003855 (Day 0 – Day 8), p-value = 0.03572 (Day 0 – Day 21)* ***(B)*** *Immunostaining confirmed expression of relevant markers. TRA-1-60 was detected at Day 0 but not during differentiation. Neuronal differentiation verified by MAP2, but DAT was ambiguous at Day 21, an early timepoint for dopaminergic neurons. Scale bar 50 µm.*

4.2.2.2 Comparison of neuronal development between the differentiation protocols

Neuronal progenitor marker qPCR was carried out to evaluate whether the timepoints selected are equivalent. *TUBB3, SOX1,* and *MAP2* expression is similar amongst various progenitor cells at the different timepoints. It should come as no surprise that *SOX1* and *TUBB3* expression levels vary between latest timepoints since the actual differentiation state will differ between several days of differentiation. Results are presented in Figure 4.8.

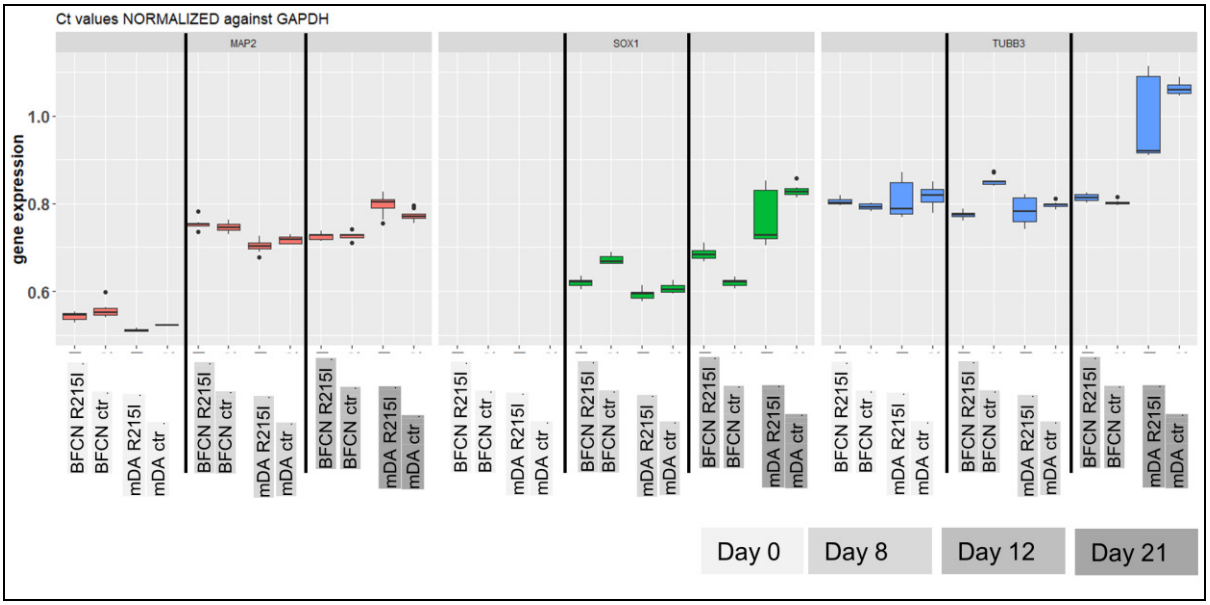

Figure 4.8 qPCR comparison between mDA and BFCN cell lines. Expression of MAP2, SOX1, *and* TUBB3 *indicates a similar neuronal differentiation pattern on Day 0 and Day 8 between both neuronal differentiations. Day 21 of the mDA differentiation is difficult to compare to the Day 12 of BFCN differentiation, as expression values differ. Expression levels are quantified in relation to GAPDH. Three biological replicates were examined for each cell line. Data are presented as mean ± SD, no statistically significant changes were detected using Mann-Whitney-Wilcoxon U-test with Benjamini-Hochberg correction.*

4.2.3 Single-cell RNA-sequencing

Single-cell RNA-sequencing has been performed using 10x Genomics for the BFCN Differentiation Day 0, Day 8, and Day 12 as described in the Methods Section 3.7. Quality control data are visualized in Supporting Section 8.4.

In total 38’439 cells were selected for downstream analysis after pre-processing and quality control. For the iPSC state 5’671 cells were selected from ctr, 7’292 cells from R215I. At Day 8 7’106 cells were selected from ctr, and 7’960 cells from R215I, and 5’450 for the control and 4’870 cells for R215I at Day 12.

The UMAP embedding of the data exhibits distinct cell types which correspond to neuronal development as shown Figure 4.9. Cells of similar differentiation state are closer to each other compared to cells collected at other timepoints. This indicates that gene expression was mostly determined by the stage of differentiation and not the cell line. An exemption is a cluster of cells containing cells from both, Differentiation Day 8 and Day 12, and a high share of cells from the isogenic control. This cluster will be discussed in the following Subsection.

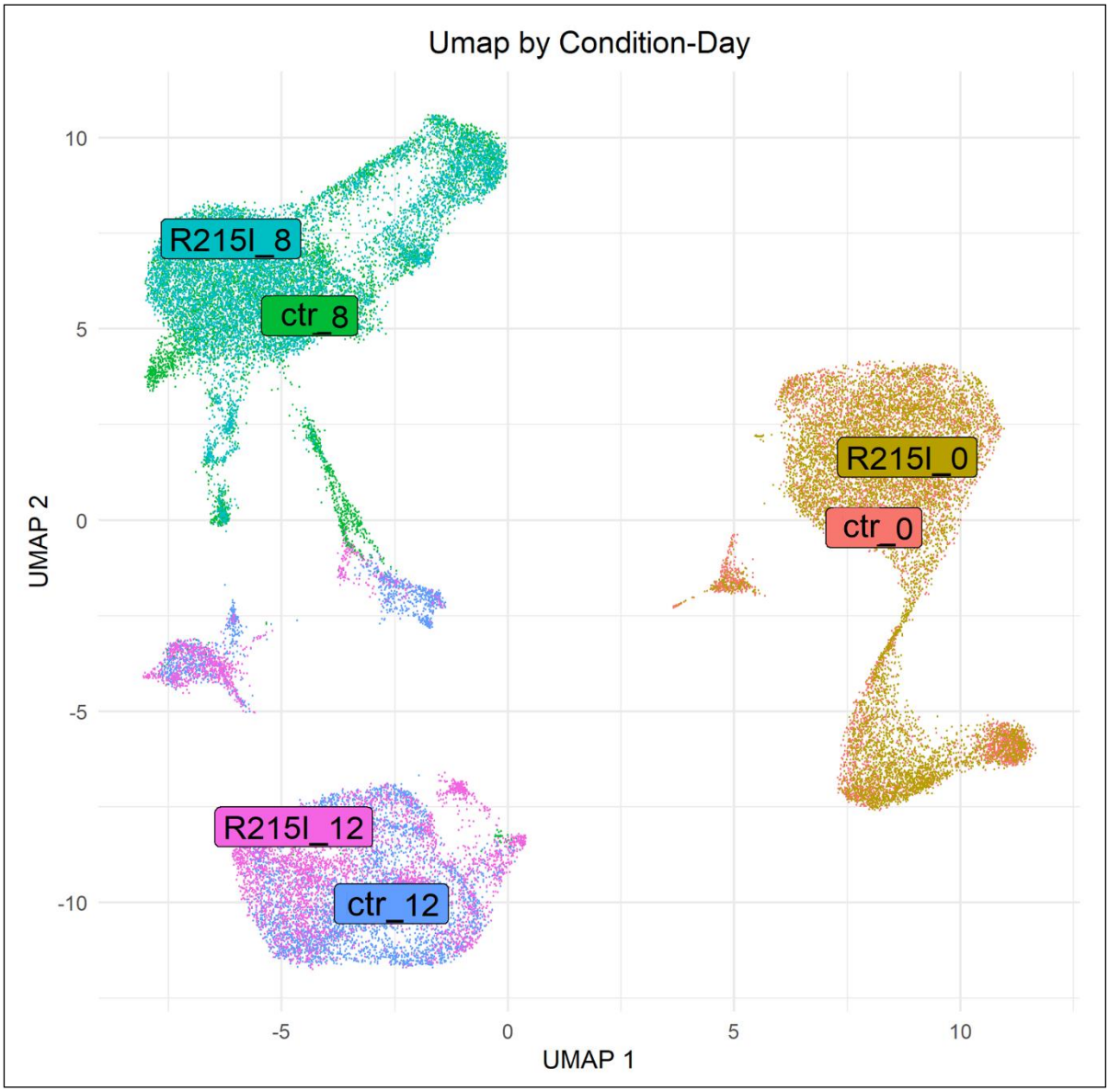

Figure 4.9 Representation of cells in UMAP space. Each dot represents a cell. Based on our sc-RNAseq data, cell lines cluster according to differentiation stage, indicating a similar development of R215I and the isogenic control.

4.2.3.1 Expression of genetic markers of neuronal development

UMAP dimensionality reduction revealed that R215I and ctr formed homogeneous clusters depending on the collection timepoint (Day 0, 8, 12), indicating that the cell lines developed into the same cell state. This allows for the detection of small changes induced by the mutation in *ADAM17*.

The differences in gene expression between the different days was used to verify the transition of the cells from pluripotency towards BFCN. At Day 0, cells express markers of pluripotency: *POU5F1, L1TD1, USP44, TDGF1, POLR3G, TERF1, DPPA4, PRDX1*, *NANOG, THY1,* and *CD9,*

as expected from literature (Goulburn *et al.*, 2011; Novak *et al.*, 2022). At Day 8 cells express neuronal fate and rosette markers *NES, PAX6,* and *OTX2* (Goulburn *et al.*, 2011). Towards Day 12, cells are showing markers of ventral progenitors, such as *SHH* and *NKX2-1,* with an expected decrease of *PAX6* expression (Bissonnette *et al.*, 2011; Goulburn *et al.*, 2011). For visual comparison of gene expression values refer to Figure 4.10.

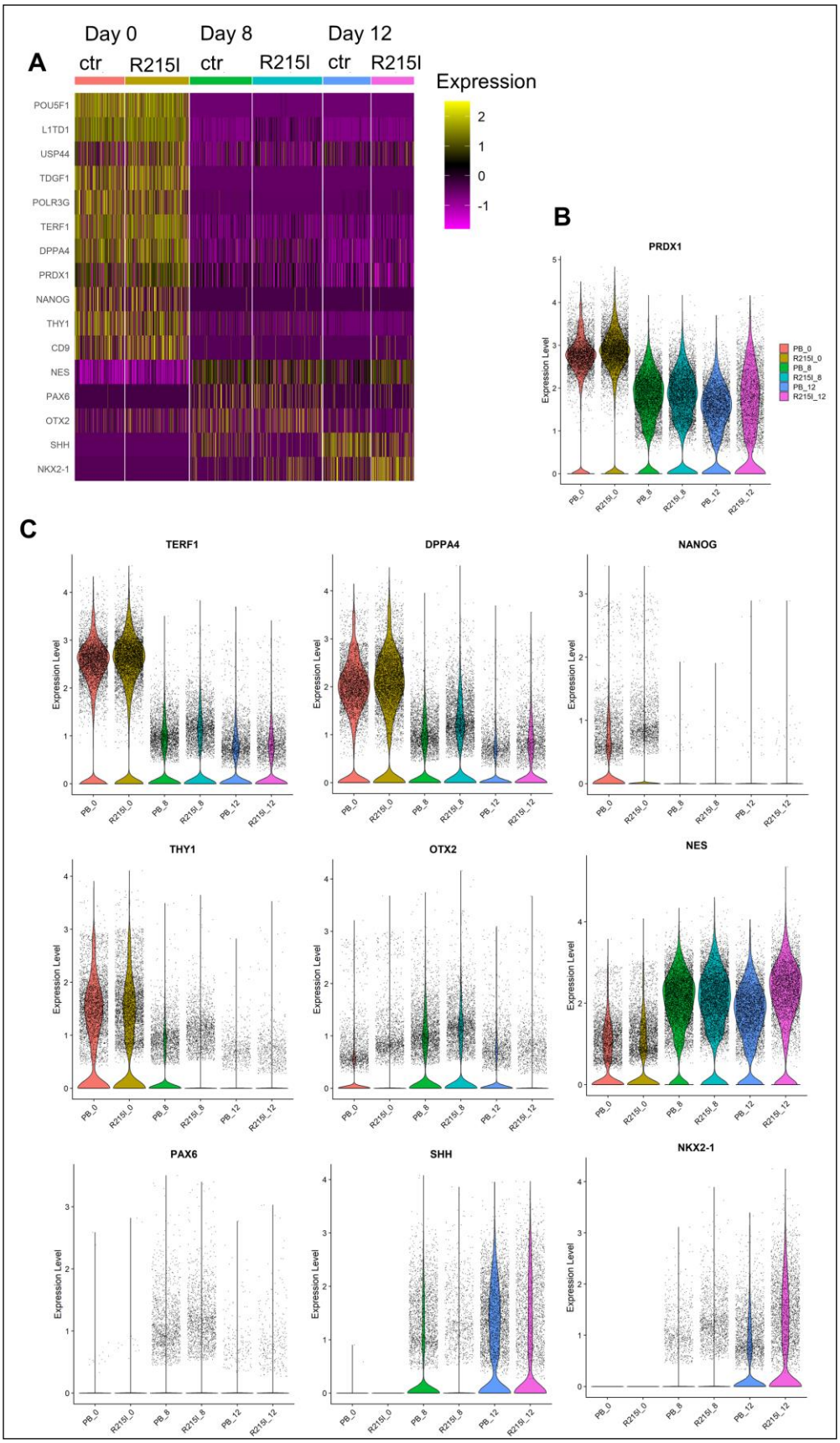

Figure 4.10 Heatmap and selected violone plots of neuronal development markers. Pluripotency markers POU5F1, L1TD1, USP44, TDGF1, POLR3G, TERF1, DPPA4, PRDX1, NANOG, THY1, *and* CD9 *are expressed at Day 0. At Day 8 cells express neuronal fate/ rosette markers* NES, PAX6, *and* OTX2. *Towards Day 12, markers of ventral progenitors, such as* SHH *and* NKX2-1 *are expressed. R215I is the mutant cell line, PB is the ctr.*
Violine plots of other development markers are depicted in Figure 8.4.

A marker for the basal forebrain, *FOS,* was expressed mostly at Day 8. The basal forebrain marker *NGFR* is expressed on a low level, with the highest expression at Day 8. Other marker for cholinergic neurons*, NTRK1, NTRK2, NTRK3* and *ACHE*, are overall expressed on a low level or are nearly absent. Figure 4.12 B in Results Subsection 4.2.3.2 shows a heatmap of *NGRF, NTRK1* and *NTRK2* expression depending on cell line. The low abundance of *NGFR* was indicated in the quantification of the cells via FACS and is not surprising, as the cells are neuronal progenitor cells.

Cells were assigned to clusters dependent on their similarity in gene expression. The analysis derived 10 clusters: each differentiation state is represented by 3 clusters (Figure 4.11 A). Cluster 7 is intriguing since it includes cells from the two differentiation Days 8 and 12. Most of the cells in Cluster 7 are cells of the control cell line. Interestingly, Cluster 7 seems to be the most relevant for BFCN cell fate. 18 genes were strongest expressed in Cluster 7 (*STMN2, TUBB3, NHLH1, ELAVL3, ONECUT2, NEFM, TAGLN3, SCG3, ELAVL4, TLCD3B, PCBP4, EPB41, NEUROD1, DCX, INA, GPC3, LHX5*, *SYP* and *OLIG2*), while GPC3 was the least expressed one (Figure 4.11 B). Functional profiling with g:Profiler (Raudvere *et al.*, 2019) showed that these genes are enriched in pathways pointing towards neuronal system development, cell differentiation, central nervous system neuron differentiation, generation of neurons, and forebrain development. Thus, it can be concluded that Cluster 7 contains most of the cells which will eventually develop a BFCN phenotype. However, *NGFR,* which transcripts are sorted for at Differentiation Day 12, is not differentially enriched at Day 8, which could be explained by the general low abundance of *NGFR* transcript detect in the sample (Figure 4.12 B); and no cluster is enriched in *NGFR* transcripts. NGFR positive cells can eventually generate mature BFCN phenotype. Composition of cells in Cluster 7 does not match the FACS sorting data. Only 3 % of R215I cells of Day 12 are found in Cluster 7, while FACS sorting reported 21.5 % NGFR positive cells. Cluster 7 contains 10 % ctr cells of Differentiation Day 12, however a reliable value for the FACS sorting as validation cannot be provided. The situation is similar at Day 8. Only 0.3 % of R215I cells of differentiation Day 8 are in Cluster 7, while 21.5 % of cells were NGFR positive in the FACS analysis. For the ctr, 7.5 % of cells collected at Day 8 are in Cluster 7, whereas 24.9 % showed NGRF positive in FACS. This difference may indicate the limited coverage in the sc-RNAseq data set which can result in false negative cell identification.

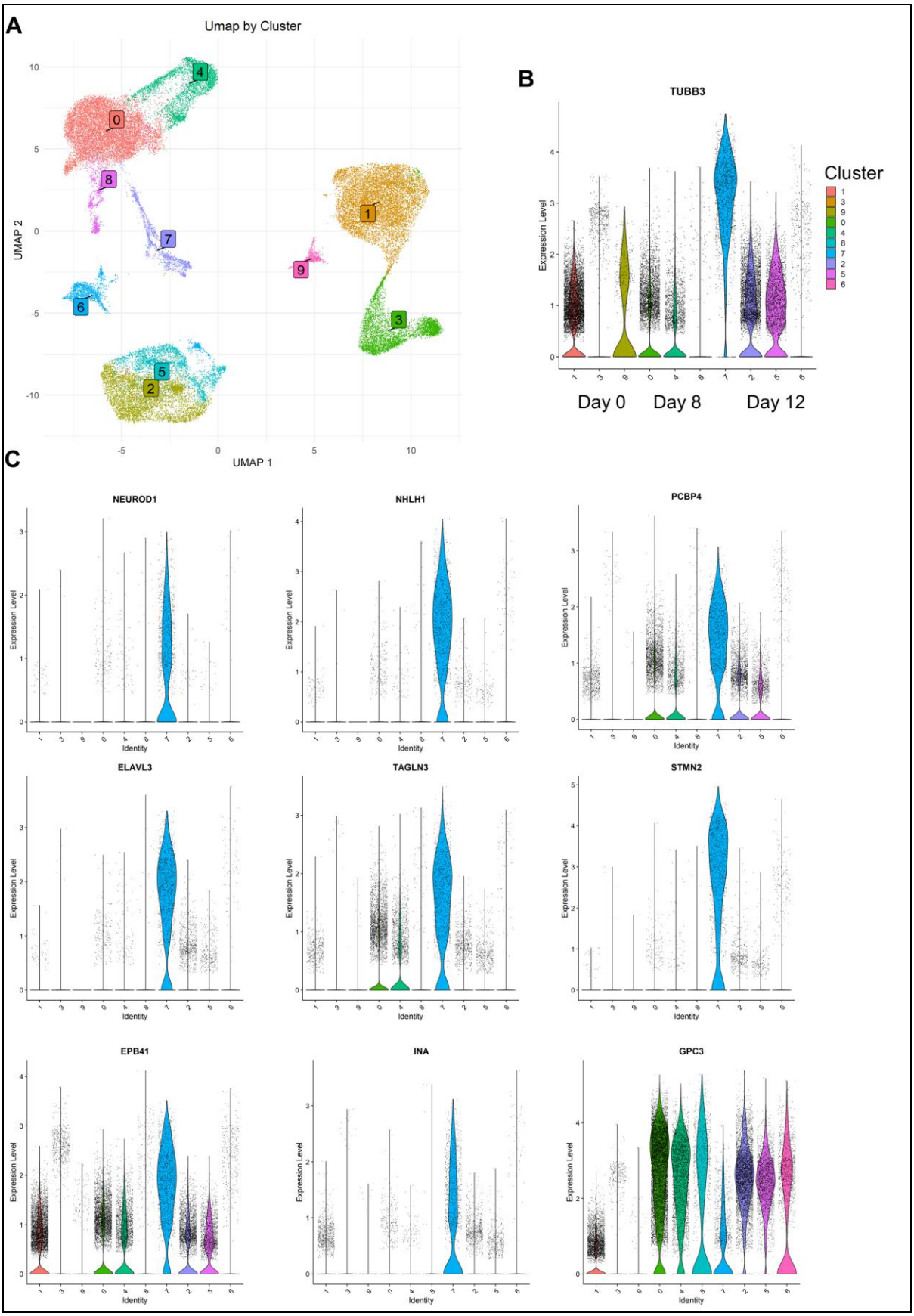
A
Umap by Cluster
UMAP 2
UMAP 1
B
TUBB3
Expression Level
Cluster
Day 0
Day 8
Day 12
C
NEUROD1
NHLH1
PCBP4
ELAVL3
TAGLN3
STMN2
EPB41
INA
GPC3
Identity

Figure 4.11 UMAP of clusters and violine plots characterising Cluster 7. ***(A)*** *UMAP is indicating different cell type clusters. Each differentiation state is represented by 3 clusters. Cluster 1, 3, and 9 contain iPSC. Cluster 0, 4, 8 contain cells of differentiation at Day 8, and cluster 2, 5, 6, contain cells of differentiation at Day 12. Apart from that, Cluster 7 contains cells from differentiation at Day 8 and Day 12 (see Figure 4.9).* ***(B+C)*** *Violine plots of representative DEGs with lower (*GPC3*) or higher expressed in Cluster 7 (compared to all others) (padj < 0.001). Violine plot of* TUBB3 *is used for annotation of the labels.*

4.2.3.2 Comparison of R215I and ctr mRNA expression

The number of differentially expressed genes between R215I and ctr increases during the course of differentiation from 22 DEGs at Day 0, to 95 DEGs at Day 8, and to 309 DEGs at Day 12. A list of all DEGs per timepoint can be found in Supporting Table 8.8. This trend could indicate an amplification of the effect introduced by the mutation. In total, 5 genes are differentially expressed (padj < 0.001) at all timepoints. *SMS* (spermine synthase; log_2FC 0.28, 0.74, and 0.8 on Day 0, Day 8, and Day 12, respectively), *BEX3* (brain expressed X-linked 3; log_2FC 0.34, 0.36, and 0.36 on Day 0, Day 8, and Day 12, respectively), *STAG2* (STAG2 cohesin complex component; log_2FC 0.34, 0.42, and 0.39 on Day 0, Day 8, and Day 12, respectively), *TCEAL9* (transcription elongation factor A like 9; log_2FC 0.32, 0.29, and 0.33 on Day 0, Day 8, and Day 12, respectively) are overexpressed in R215I compared to control, while *XIST* (X inactive specific transcript; log_2FC 1.22, 1.56, and 1.56 on Day 0, Day 8, and Day 12, respectively) is overexpressed in ctr compared to R215I. Despite not being statistically different at all three timepoints, 3 other DEGs exhibit a substantial fold change (log_2FC > |1|) at least at one timepoint. These are *SIX3 (*SIX homeobox 3)*, SIX6 (*SIX homeobox 6)*,* and *IGFBP5* (insulin-like growth factor binding protein 5). Both, *SIX6* and *IGFBP5,* are significantly higher expressed in R215I compared to control, with a log_2FC > 1 at Differentiation Day 12. *SIX3* is significantly higher expressed in R215I and it is the DEG with the highest fold change at Day 8 (log_2FC 0.95) and third highest fold change at Day 12 (log_2FC 0.81).

ADAM17 has previously been found to alter the expression of *APP*. However, in our dataset we did not find significant changes in *APP* expression between R215I and ctr (Figure 5.2 in the Discussion).

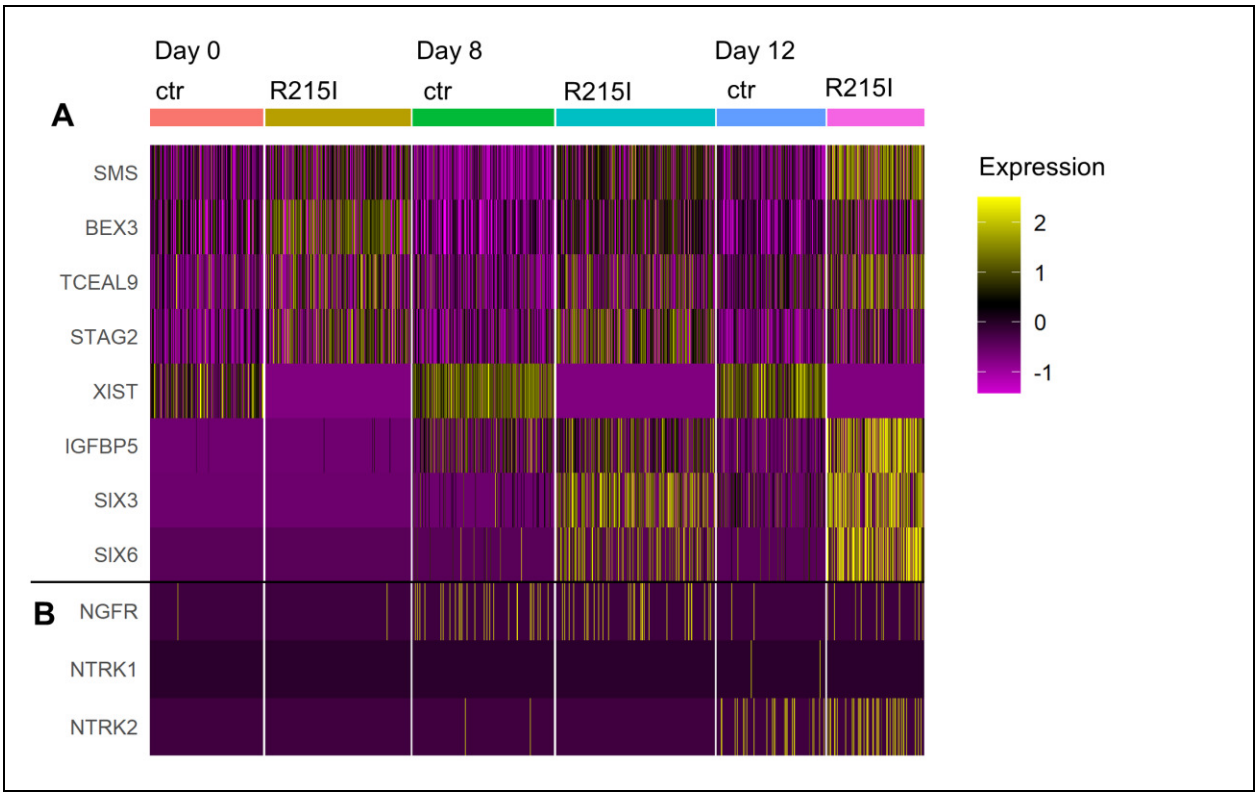

Figure 4.12 Heatmap of differential expressed genes between R15I and ctr. ***(A)*** *Upper part of the heatmap shows genes which have been differentially expressed during all timepoint of the differentiation (SMS, BEX3, TCEAL9, STAG2, and XIST), and genes which are differentially expressed with a high fold change at Differentiation Day 12 (SIX3/SIX6).* ***(B)*** *Lower part of the heatmap depicts genes relevant for BFCN cell fate which were overall detected with low sequencing depth.*

4.2.4 Metabolomic data

An untargeted metabolomics approach was used to investigate the influence of *ADAM17* rs142946965 on the metabolism of differentiating cells. Cellular extracts and medium collected at Day 0, Day 8, and Day 12 of the BFCN differentiation and Day 0 and Day 8 of the mDA differentiation were analysed with ICMS and HILIC. In total the HILIC approach included 175 compounds, of which 132 and 127 were recorded for the BFCN and mDA differentiation, respectively. The ICMS targeted 206 metabolites, of which 133 were detected for the BFCN differentiation and 135 for the mDA neuronal differentiation. In the following Subsections results of the metabolomic analysis will be presented.

4.2.4.1 Pathway enrichment for BFCN metabolites

For the BFCN differentiation, the maximum number of differentially abundant metabolites in the HILIC analysis was found at Day 0 (n = 73), and as the differentiation advanced, the number decreased to 53 metabolites at Day 8, and 30 metabolites at Day 12 (Supporting Table 8.2). This

does not necessarily imply that the influence of the mutation decreases with time. Another argument is that the investigated metabolites may not have been the most significant ones at the later timepoints. In total 105 metabolites were differentially abundant in at least one timepoint. The numbers are similar for the ICMS analysis. In total 133 metabolites were differentially abundant in at least one timepoint (54 compounds at Day 0, 38 compounds at Day 8, and 57 compounds at Day 12; Supporting Table 8.3)

Over Representation Analysis with MetaboAnalyst (Xia and Wishart, 2011; Lu, Pang and Xia, 2023) for the most differentially abundant metabolites in the HILIC measurements between R215I and control revealed in 96 pathways (most relevant illustrated in Figure 4.13). Among them, the pathways “Amino Sugar Metabolism”, “Ammonia Recycling”, “Arginine and Proline Metabolism”, “Aspartate Metabolism”, “Citric Acid Cycle”, “Glutamate Metabolism”, “Glycine and Serine Metabolism”, “Purine Metabolism”, “Urea Cycle”, and “Warburg Effect” are enriched at each of the three timepoints. Six of these pathways are also enriched at Day 0 and Day 12 for the ICMS metabolites (“Amino Sugar Metabolism”, “Arginine and Proline Metabolism”, “Aspartate metabolism”, “Glutamate metabolism”, and “Warburg Effect”). The pathways “Warburg Effect” and “Citrate Acid Cycle” indicate the transition in energy metabolism from glycolysis to oxidative phosphorylation during differentiation. Other enriched pathways are important for the biosynthesis of amino acids and purines, which are essential for cell growth and differentiation.

According to the comparison of enriched pathways between the differentiation days, all pathways enriched in metabolites less abundant in the mutant exhibit an enrichment in other metabolites of the same pathway. This indicates that some metabolites of a pathways are used by the mutant cells to produce products of the same pathway and point to some metabolic dysregulation. One notable exception is the pathway “De Novo Triacylglycerol Biosynthesis” which is only enriched for metabolites less abundant in the R215I at Day 8 (Figure 4.14). This could indicate that the compounds of this pathway are used up by other metabolic reactions in the R215I cell line.

The pathway “Spermine and Spermidine synthesis” is enriched for different abundant metabolites at all timepoints for BFCN differentiation. However, with no statistical significance (Supporting Table 8.6). This pathway is not enriched in the mDA differentiation at any timepoint.

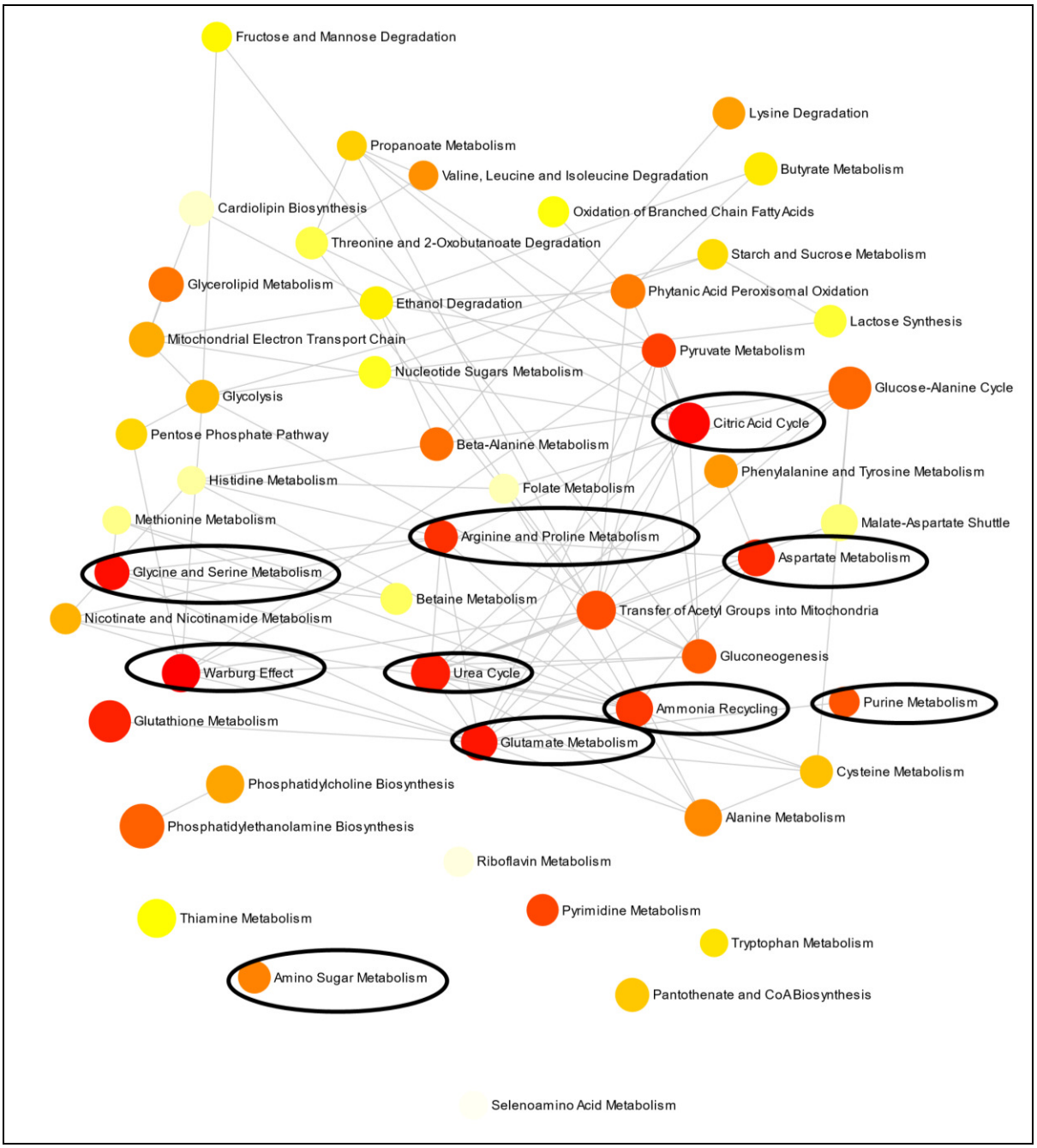

Figure 4.13 Network of pathways enriched for differentially abundant metabolites during BFCN differentiation. Pathways enriched at all differentiation days are circled. Image was created using MetaboAnalyst (Xia and Wishart, 2011; Lu, Pang and Xia, 2023). Colour indicates the significance (white least significant, red most significant) on an arbitrary scale.

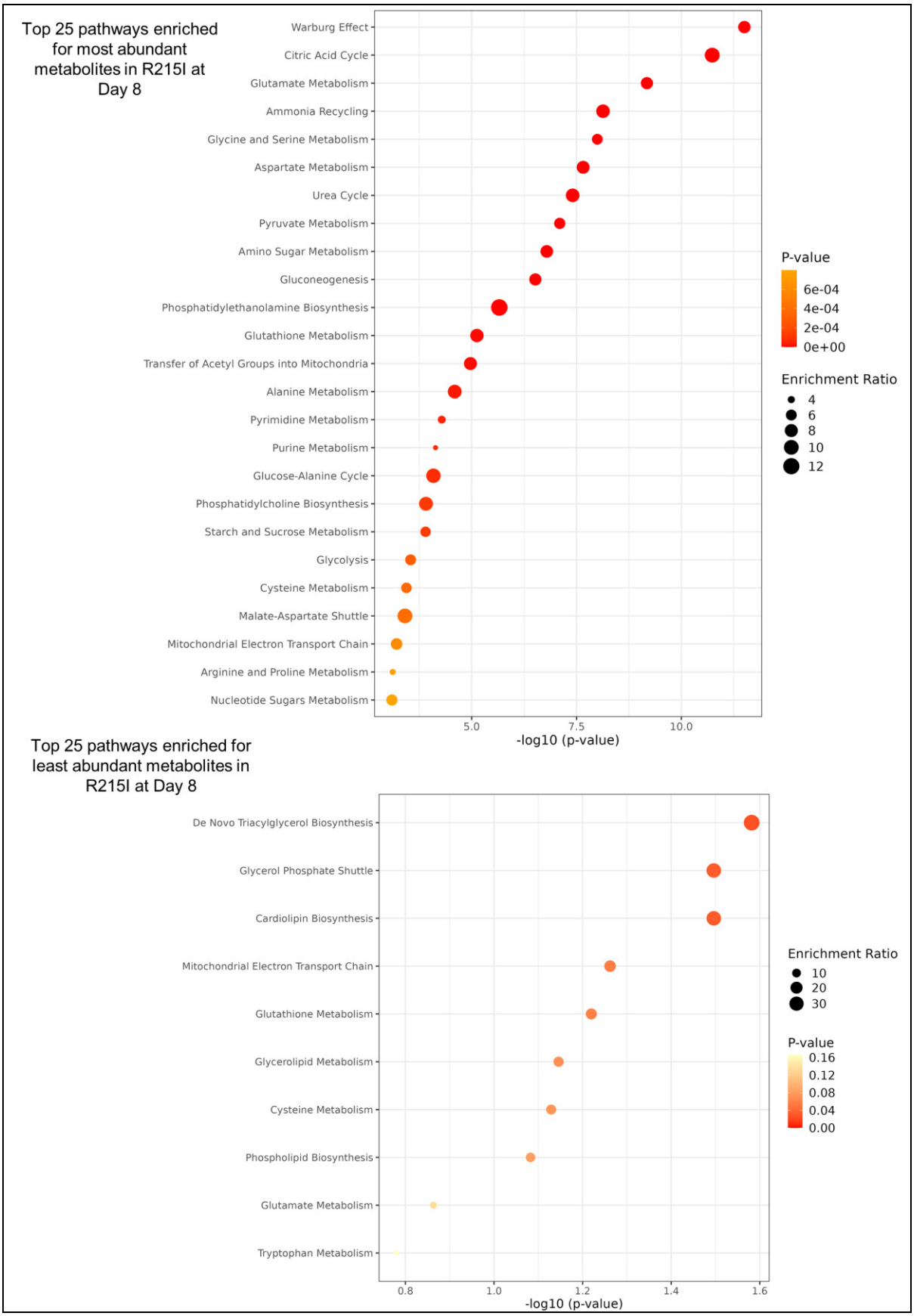
Top 25 pathways enriched for most abundant metabolites in R215I at Day 8
Warburg Effect
Citric Acid Cycle
Glutamate Metabolism
Ammonia Recycling
Glycine and Serine Metabolism
Aspartate Metabolism
Urea Cycle
Pyruvate Metabolism
Amino Sugar Metabolism
Gluconeogenesis
Phosphatidylethanolamine Biosynthesis
Glutathione Metabolism
Transfer of Acetyl Groups into Mitochondria
Alanine Metabolism
Pyrimidine Metabolism
Purine Metabolism
Glucose-Alanine Cycle
Phosphatidylcholine Biosynthesis
Starch and Sucrose Metabolism
Glycolysis
Cysteine Metabolism
Malate-Aspartate Shuttle
Mitochondrial Electron Transport Chain
Arginine and Proline Metabolism
Nucleotide Sugars Metabolism
5.0
7.5
10.0
-log10 (p-value)
P-value
6e-04
4e-04
2e-04
0e+00
Enrichment Ratio
4
6
8
10
12
Top 25 pathways enriched for least abundant metabolites in R215I at Day 8
De Novo Triacylglycerol Biosynthesis
Glycerol Phosphate Shuttle
Cardiolipin Biosynthesis
Mitochondrial Electron Transport Chain
Glutathione Metabolism
Glycerolipid Metabolism
Cysteine Metabolism
Phospholipid Biosynthesis
Glutamate Metabolism
Tryptophan Metabolism
0.8
1.0
1.2
1.4
1.6
-log10 (p-value)
Enrichment Ratio
10
20
30
P-value
0.16
0.12
0.08
0.04
0.00

*Figure 4.14 Pathways enriched for differential abundant metabolites at Day 8 of BFCN differentiation. Dot plots displays pathways enriched in metabolites significantly more abundant **(top)** or less abundant **(bottom)** in R215I compared to control. Metabolites less abundant in R215I are sharing same pathways with the more abundant, except for the "De Novo Triglycerol Biosynthesis" pathway which is unique to the less abundant metabolites. Image was created using MetaboAnalyst (Xia and Wishart, 2011; Lu, Pang and Xia, 2023).*

4.2.4.2 Metabolome of mDA reflects observations for BFCN metabolome

For the mDA differentiation, at Day 0 a total number of 21 metabolites were differentially abundant in the HILIC analysis, and 24 metabolites at Day 8. In total 35 metabolites were differentially abundant in at least one timepoint (Supporting Table 8.4). For the ICMS analysis, 43 metabolites were found differentially abundant in at least one timepoint, 31 compounds at Day 0, 16 compounds at Day 12 (Supporting Table 8.5).

Enrichment analysis with MetaboAnalyst (Xia and Wishart, 2011; Lu, Pang and Xia, 2023) for the most differentially abundant metabolites in the HILIC measurements between R215I and control revealed 57 pathways, which were similar to the once enriched in the BFCN differentiation (Figure 4.15). No pathway was significantly enriched for only mDA differentiation. None of the pathways was statistically significant for both timepoints. "Aspartate Metabolism" (p-value < 0.001, FDR 0.0141) and "Urea Cycle" (p-value < 0.001, FDR 0.011) were statistically significant enriched at Day 0.

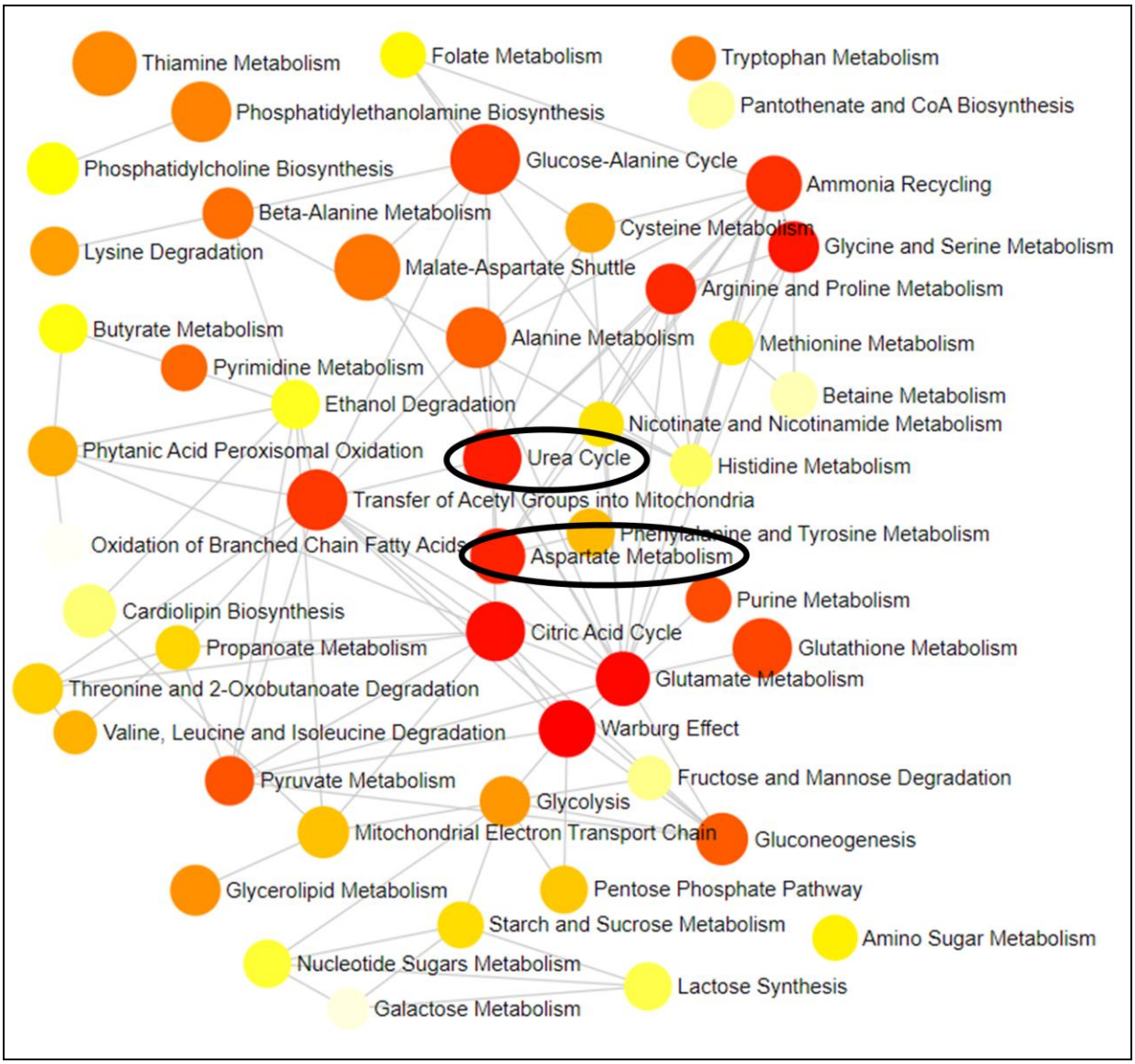

Figure 4.15 Network of pathways enriched for differentially abundant metabolites of mDA differentiation. Pathways significantly enriched at Day 0 are circled. Image was created using MetaboAnalyst (Xia and Wishart, 2011; Lu, Pang and Xia, 2023). Colour indicates the significance (white least significant, red most significant) on an arbitrary scale.

5 Discussion

NDA are tremendously detrimental to patients and society. The multi-faceted clinical symptoms and the gradual disease progression hinder timely diagnosis. Despite decades of intensive research, the underlying cause of NDA is often unknown and curative therapy is mostly not available (Wilson *et al.*, 2023). One especially intriguing NDA is AD, which is characterised by the co-occurrence of Aβ plaques and NFT. While both, modifiable lifestyle and genetic risk factors, are known, their mechanistic link and combined impact on disease onset and progression remains poorly understood. Recently, one SNV on *ADAM17* was discovered to be causative to AD in a Spanish family (Hartl *et al.*, 2018). Till today, ADAM17 is not well characterized in the context of AD, and the underlying mechanisms are not yet elucidated. Here, a cutting-edge approach combining iPSC differentiation into neuronal phenotypes and multi-omics integration is used to get insights into the effect of an AD-associated *ADAM17* mutation on early neuronal differentiation and to identify potentially disease triggering pathway modifications.

5.1 Generation of a stable iPSC cell line carrying rs142946965 in *ADAM17*

During the course of the PhD project two clones of the *ADAM17* rs142946965 mutation were generated following a FACS assisted strategy for heterozygous CRISPR/Cas gene editing (Jarazo, Qing and Schwamborn, 2019). While for clone 1, the targeted mutation could not be verified by sequencing, clone 2 carries the desired mutation G > T at position 34’569 on the reference gene. However, further mutations, most likely insertions or deletions, were introduced at the site of interest as shown in Figure 4.3 in Section 4.1.4. Both alterations are visible downstream the BTE, which indicates that the sgRNA and PAM site were chosen correctly for the intended mutation site. CRISPR/Cas9 is generally considered as an efficient and versatile way of gene editing, especially in comparison with earlier techniques such as zinc finger nucleases (ZFNs) and Transcription Activator-Like Effector Nucleases (TALENs) (Cong *et al.*, 2013; Jinek *et al.*, 2013; Mali *et al.*, 2013). The technique relies on the introduction of a double strand break at a desired target sequence in the genome. Endogenous DNA repair mechanisms include fast, error-prone non-homologous end joining or slower, more accurate homology directed repair. While the first mechanism is employed to generate targeted gene knockouts, the second one is used for gene insertions or base editing (Bae *et al.*, 2019).

In this work, the homology arms in the donor plasmid served as a template for homology directed repair. Sequencing data reveal that subsequent double strand breaks occurred despite the

inclusion of a mutation at the PAM that was supposed to prevent them. Of note, other methods of gene editing with CRISPR allow for a change of base pairs without the double-strand break and hence have a lower risk of insertions or deletions (Ran *et al.*, 2013; Komor *et al.*, 2016; Gaudelli *et al.*, 2017). However, these techniques do not allow for selection of heterozygous mutations. A combination of both systems, such as employing DNA nicking for the introduction of the DNA break and biallelic homology directed repair might increase the chances of harvesting the desired R215I mutation in *ADAM17.*

Western blot was performed to test whether the mutation rs142946965 alters the maturation of ADAM17. As the mutation induces a missense mutation changing the polarity of the protein close to the cleavage side of the inhibitory pro-domain. This pro-domain gets cleaved by furin at two cleavage sides during the transport of the enzyme through the trans-Golgi-network (TGN) towards the plasma membrane.

Different sizes of the ADAM17 have been reported in literature. Mature ADAM17 is known to have a molecular weight of approximately 70-100 kDa, depending on post-translational modifications such as glycosylation (Grell *et al.*, 1995; Dang *et al.*, 2013; Wong *et al.*, 2015; Pavlenko *et al.*, 2019). In our experiments, the mature ADAM17 is detected at approximately 70 kDA. The pro-form is reported as a 130 kDa protein (Gooz, 2010; Xu *et al.*, 2022), which corresponds to the work presented in Figure 4.4 in Subsection 4.1.6.

Western blot for R215I and its isogenic control showed no difference in band intensity, for both antibodies. One possible explanation could be an enhanced cleavage of ADAM17 at the boundary site between pro-domain and catalytic domain, as proposed by Wong *et al.*, 2015. If the cleavage at the pro-protein convertase cleavage motif (positions 211–214) occurs before an upstream cleavage at position 56-58, the inhibitory pro-domain can remain bound to the catalytic center and create a pseudo pro-form (Wong *et al.*, 2015). However, Hartl *et al.* which found alterations in pro-ADAM17 concentration in Western blot after overexpressing the rs142946965 mutation in SY-SHY cells (Hartl *et al.*, 2018).

For the clone 1 and clone 2 the picture is different. Both antibodies show decreased abundance of the pro-form compared to their wildtype control WTSIi010-A, independent of the antibody binding side. The expression of the mature form of ADAM17 was not altered. Possibly, cleavage of the pro-domain at the position 211-214 was enhanced, but the additional insertions and deletions of the pro-domain inhibited further attachment to the catalytic center.

During the further characterisation of clone 1 and clone 2 generated in the first part of the project, the independently generated and validated clone was employed for the second part, the characterisation of ADAM17 in early neurogenesis.

In this work healthy iPSC lines were used to insert the specific genetic polymorphism on *ADAM17.* This approach aimed to characterise the impact of *ADAM17* on neuronal development. A healthy cell line was preferred to a patient-derived one to exclude the potentially additional impact on disease altering by the genetic background. Following this approach several potential downstream implications of ADAM17 in neurogenesis were revealed, which should be followed up individually to understand the mechanistic link. Recently, another SNP in *ADAM17* has been associated with AD, elevating *ADAM17* to the status of a recognized risk gene for AD. With this new mutation a patient-derived iPSC model, comparing rs142946965 to the newly identified SNP, might be useful to validate the findings of this work and to target the potential effect of the genetic background.

5.2 ADAM17 in early neuronal development

Neurodegenerative disorders are characterized by the progressive death of neurons in the brain. Therefore, investigating how neurons develop and function physiologically helps to identify abnormal processes that occur in AD or PD. This can provide insights into the molecular and cellular mechanisms underlying the disease. To uncover the role of *ADAM17* in neuronal development, the SNV rs142946965 was introduced in a healthy iPSC line which was used for the differentiation to neuronal precursors of BFCN and mDA neurons, respectively. Differentiation of iPSC to neurons offers the unique possibility to investigate the differentiation dynamics and to identify early modifications which are typically not visible from patient samples since they represent a later disease stage at the time of diagnosis when neuronal loss has already been occurred.

BFCN are the main source of cholinergic input of the CNS and are among the first neurons to be affected by AD neurodegeneration. mDA are neurons specifically impacted in PD, another neurodegenerative disease with increasing incidence.

5.2.1 Verification of neuronal phenotypes

BFCN differentiation was performed following a previously published protocol (Ortiz-Virumbrales *et al.*, 2017). The BFCN development was verified by qPCR and FACS data (Figure 4.6 and Subsection 4.2.1.1 in the Results Section). Marker genes for neuronal development, such as *TUBB3, MAP2* and *SOX1*, are expressed at relevant timepoints of the differentiation. The pluripotency marker *POU5F1* is expressed at early days of the development and expression levels decrease over time. The BFCN phenotype is defined by the expression of *NGFR*. qPCR data reveal a surprisingly low level of *NGFR* at Day12 of differentiation, which is reflected in the data for FACS sorting (Subsection 4.2.1.1 in Section 4.2.1) and in the data for the sc-RNAseq (Figure 4.12). Optimisation of the BFCN differentiation regarding feeding times, medium volume and cell numbers was performed with cell line WTSIi010-A, which robustly showed the highest *NGFR* expression at Day 12 (data not shown). It was reported previously that individual cell lines can exhibit differences in differentiation efficacy (Hu *et al.*, 2010), which was likely a confounding factor in this experiment. Due to technical difficulties and time constraints, the optimal timepoint for FACS sorting could not be evaluated again for the new cell lines R215I and PB005.1.

mDA differentiation was performed following the adapted Kriks protocol (Novak *et al.*, 2022). As a first step, the mDA development was confirmed using qPCR and immunostaining (Figure 4.7 in Subsection 4.2.2 in the Results Section). Expression of the dopaminergic marker *TH*, the neuronal markers *TUBB3, MAP2* and *SOX1* was detected with qPCR at the expected timepoints (Novak *et al.*, 2022). mDA are characterized by the expression of *KCNJ6* and *LMX1A*, genes indicating the midbrain character. In the experiments, both markers were already expressed at Day 21 of differentiation in agreement with previous experiments (Novak *et al.*, 2022). Immunostaining revealed expression of TRA-1-60, a pluripotency marker, at Day 0. Imaging markers of dopaminergic neurons, such as TH and MAP2, were present at Day 21. DAT was not stably expressed at Day 21, which indicates the early neuronal phenotype. Overall, the characterization of the mDA neuronal differentiation indicated the successful generation of mDA neuronal progenitors.

5.2.2 Single-cell RNA-sequencing of BFCN progenitor cells

Based on the first validation of the differentiation, sc-RNAseq was subsequently employed to identify implications of *ADAM17* on gene expression and its impact on early neuronal development. The two in parallel differentiated cell lines were compared for differential expression at each time point in order to explore potential underlying mechanisms of the R215I mutation.

Genes that were found to be differently expressed at each of the four time points were then identified.

At iPSC state 34 DEGs (19 DEGs overexpressed in R215I, 13 DEGs in control) were detected, 95 DEGs (61 DEGs overexpressed in R215I, 34 DEGs in control) at Differentiation Day 8 and 309 DEGs at Differentiation Day 12 (157 DEGs overexpressed in R215I, 152 DEGs in control). Among them, five genes were differentially expressed on days 0, 8, and 12 of the basal forebrain cholinergic development. These genes are *SMS*, *BEX3*, *TCEAL9*, *STAG2* and *XIST*.

5.2.2.1 Spermine synthase (SMS)

SMS encodes for spermine synthase, the enzyme converting spermidine to spermine. *SMS* was upregulated in R215I compared to control (Figure 4.12 in Results Subsection 4.2.3.2). Spermine and the other physiological polyamines spermidine and putrescin are aliphatic molecules carrying multiple amine groups.

Physiologically, spermine production is depending on the activity of the rate-limiting enzymes ODC (ornithine decarboxylase) and MAT1 (s-adenosylmethionine synthase) to create the necessary precursors, putrescine, and SAM (s-adenoyslmethionine), which is further processed to dcSAM (decarboxylated s-adenosylmethioninamine). Thereafter, SRM (spermidine synthase) catalyses the production of spermidine from dcSAM and putrescine. Subsequent reaction of spermidine with dcSAM, catalysed by spermine synthase, gives rise to spermine. The polyamines spermine, putrescine and spermidine are best known for protecting the cell from ROS. Spermine is catabolized by SAT1 (diamine acetyltransferase 1) and SMOX (spermine oxidase), both reactions yield neurotoxic compounds, such as hydrogen peroxide and acrolein (Polis, Karasik and Samson, 2021; Sagar *et al.*, 2021). Anabolic and catabolic pathways involved in polyamine metabolism are illustrated in Figure 5.1. Interestingly, in our dataset, the expression of *ODC*, *MAT1* and *SMOX* did not differ between R215I and ctr. *SAT1* was found significantly overexpressed in R215I compared to ctr at Differentiation Day 8 (padj < 0.001, $\log_2$FC 0.62) and Day 12 (padj < 0.001, $\log_2$FC 0.26). *SRM* is significantly downregulated in R215I compared to ctr at Day12 (padj < 0.001, $\log_2$FC 0.28), indicating a potential compensatory reaction to halt the production of spermine (Figure 5.2).

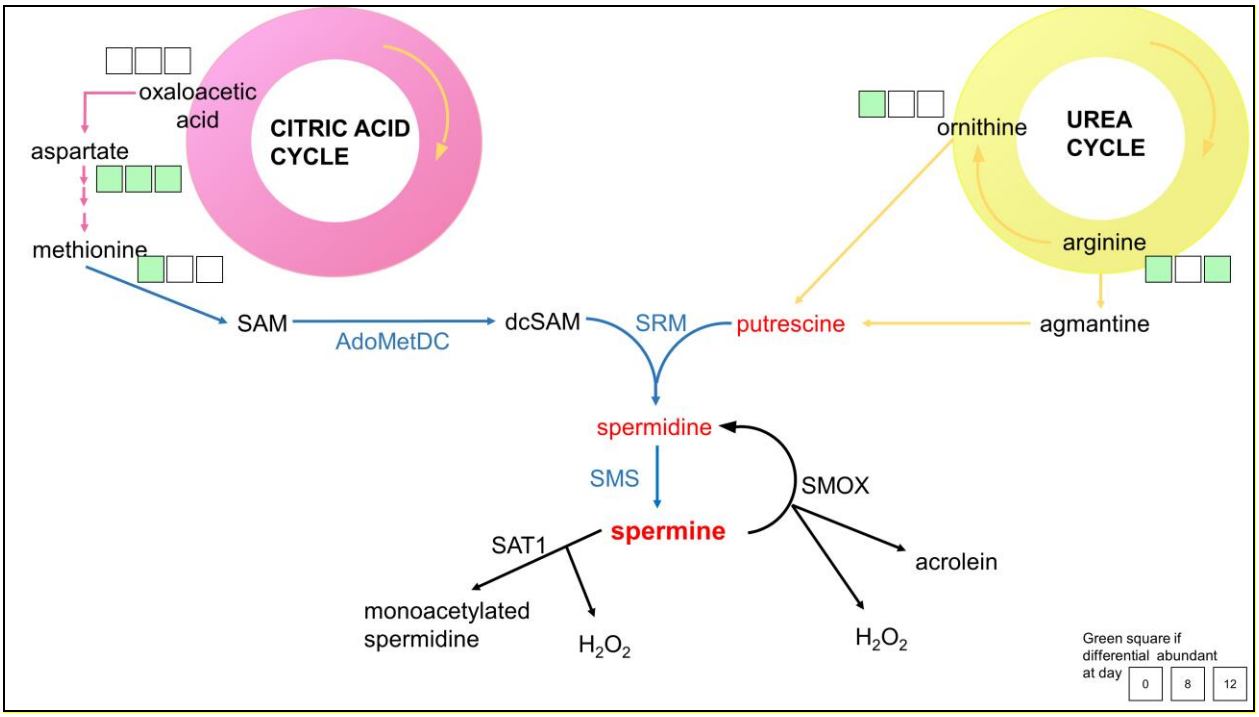

Figure 5.1 Schematic overview of the spermine metabolism in the human brain. Main suppliers of substrate of the "Spermine and Spermidine Biosynthesis pathway" are the citric acid cycle (pink) and the urea cycle (yellow). Anabolic enzymes of spermine are marked in blue, catabolic in black. The squares are filled green, if the metabolite was significantly altered at one timepoint, or white if it was detected but not altered between R215I and control. Compounds with no squares were not measured. Polyamines are highlighted in red. Abbreviations and description of the pathways is in the text above. Figure was inspired by Zou et al.*, 2022.*

Polyamines are usually positively charged under physiological conditions and hence interact with negatively charged nucleic acids and proteins (Polis, Karasik and Samson, 2021). Spermine and spermidine are proposed to stabilize the DNA double helix, and influence DNA transcription as well as RNA translation (Pegg, 2014; Polis, Karasik and Samson, 2021). Apart from this, polyamines can protect the cell from ROS damage. They can scavenge free radicals and stimulate expression of ROS protecting enzymes. Spermine is the most effective polyamine in this regard (Pegg, 2014). Furthermore, polyamines can influence the function of ion channels, such as potassium-channels, NMDA receptors, nicotinic acetylcholine receptor (nAChR), and voltage-gated sodium channels (Skatchkov, Woodbury-Fariña and Eaton, 2014; Polis, Karasik and Samson, 2021). Spermine and spermidine are agonists of the NMDA receptor at a distinct bindings site, which is different to those of L-glutamate (Williams *et al.*, 1990). In multiple experiments, spermine was shown to be more effective than spermidine (Pegg, 2014). The involvement of receptor regulation might explain the positive association of polyamines with facilitation of learning. In fact, spermidine supplement is promoted as beneficial for cognitive

impairment, cardiovascular strength and extended life-span (Madeo *et al.*, 2018; Senekowitsch *et al.*, 2023; Wortha *et al.*, 2023).

Alterations in *SMS* expression levels have previously been associated with AD. A “significant albeit modest elevation of SMS protein level” in *post mortem* AD brains has been identified via analysis of previously published proteomic data (Tao *et al.*, 2023). Furthermore, the same study identified the catabolic enzymes of spermine, SAT1 and SMOX, to be upregulated in AD brains. In contrast, another study on *post mortem* brain tissue found expression of *SRM*, an enzyme upstream to SMS, decreased in the entorhinal cortex and hippocampus in AD patients. Degrading enzymes of spermine, SAT1 and SMOX, were found to be increased or unaltered in AD brain (Mahajan *et al.*, 2020).

Metabolomic data support *SMS* as a relevant DEG (see Results Subsection 4.2.3.2). SMS is involved in the pathway “Spermine and Spermidine Biosynthesis”, which is enriched with differentially abundant metabolites at all investigated timepoints. Pathways upstream to the “Spermine and Spermidine synthesis” are also enriched. This includes the urea cycle, arginine and proline metabolism, and the citric acid cycle, which were significantly enriched over all 3 timepoints Figure 4.13 in the Results section 4.2.4.1. Notably, “Spermine and Spermidine Biosynthesis” was not enriched in the mDA differentiation.

Alterations in spermine metabolism were previously associated with AD. One example is a study combining metabolomic data of serum samples of AD patients, in which spermidine was found significantly enriched in two subsets (Horgusluoglu *et al.*, 2022). Of these subsets, one was top ranked based on its association with clinical AD pathological traits. Apart from this, a study of the metabolome of patients with AD and patients with mild cognitive impairment (MCI) found that MCI-patients prone to develop AD show significant increase of spermine and spermidine biosynthesis compared to MCI-patients which do not develop AD (Graham *et al.*, 2015). This might imply that these metabolic pathways play a significant role in the progression of healthy individuals to MCI and AD. In another study, metabolomic changes of spermine was one of the top markers in an AD prediction score, which is based on multi-omics AD signatures (Iturria-Medina *et al.*, 2022). Toledo *et al*. conducted a comprehensive metabolomic study on the serum of AD patients and non-cognitive impaired people. They adjusted for clinical data in case it was available. Three clinical outcome predictors were discovered among the major altered compounds. Surprisingly, two of these clinical indicators were linked to spermidine (Toledo *et al.*, 2017). In another study, CSF and plasma of elderly people was investigated targeted on metabolites of the “homocysteine-methionine” cycle. They found the concentration of SAM, a

compound upstream of spermine, decreased in both CSF and plasma (Guiraud *et al.*, 2017). SAM is a critical metabolite in the methionine cycle that is required for protein synthesis and the maintenance of cellular methylation of DNA, proteins, and neurotransmitters (Wilkins and Trushina, 2018). In a longitudinal study, the metabolome of female APP/PS1 mice was studied in plasma and brain tissue in a targeted approach compared to a healthy control. APP/PS1 mice have pathogenic mutations in the *APP* and *PSEN1* genes, resulting in cognitive impairment at the age of 3 months and Aβ accumulations at the age of 6 months. Significant changes in levels of spermine, spermidine and putrescine were detected in the brain metabolome after 6-8 months and in the plasma after 10-12 months (Pan *et al.*, 2016). Other metabolites of arginine, upstream of the spermine biosynthesis, such as creatinine, sarcosine, ornithine, proline or, hydroxyproline, were found either unaffected or only infrequently altered during the study (Pan *et al.*, 2016). The same is true for the BFCN dataset, in which proline, creatinine, and ornithine are found differentially abundant at some timepoints, but not consistently.

Spermine has been found to facilitate aggregation of hyperphosphorylated tau proteins. In a *drosophila* model, heterozygous loss-of-function of SMS significantly abated tau accumulation and ameliorated tauopathy. In the same study, *SMS* knock-down reduced tau accumulation in human neuronal or glial cell lines (Tao *et al.*, 2023). In a computational model, polyamines condensed tau protein accumulations, based on electrostatic interactions (Ivanov *et al.*, 2020).

Altered *SMS* expression has been linked to AD before, and so have alterations in the metabolic pathway of spermine and spermidine. This change in metabolomic pathways was additionally verified in the generated metabolomic dataset (Section 4.2.4.1). The current work reveals the involvement of *ADAM17* in this pathway.

5.2.2.2 Brain expressed X-linked 3 (BEX3) gene and transcription elongation factor A like 9 (TCEAL9)

BEX3 and *TCEAL9* have been found to be differentially expressed in all investigated timepoints in the BFCN differentiation (Figure 4.12 in Results Subsection 4.2.3.2). *BEX3* is of special interest, as it has been found to directly interact with NGFR, the defining receptor of BFCN.

The *BEX3* encoded protein NADE (Nerve growth factor receptor-associated protein 1) has been found to bind the intracellular domain of NGFR and induce apoptosis in a NGF dependent manner (Mukai *et al.*, 2000, 2002). It was hypothesized that after binding NGF-binding to the NGFR, NADE is recruited and binds the intracellular domain of NGFR. A conformational change of NADE then initiates a downstream apoptosis signalling cascade. Apart from the functional relation to NGFR, *BEX3* has been linked to AD in a single-nuclei transcriptomic study. *BEX3* expression has been

found elevated for both inhibitory and excitatory neurons in prefrontal cortex samples of AD patients compared to healthy individuals (Mathys *et al.*, 2019).

TCEAL9 encodes for a protein which has been proposed to act as a transcription factor. It has not yet been linked to neither AD, nor ADAM17. Notably, *BEX3* and *TCEAL9* are adjunct genes on the X chromosome location Xq22.2. Both belong to gene families which have been proposed to be highly relevant for forebrain development in mammals. These gene families share a non-coding sequence motif, which is restricted to the X chromosome (Winter and Ponting, 2005). *BEX3* and *TCEAL9* share a promotor, which located between the genes. This promotor has a binding site for ZNF121 (Fishilevich *et al.*, 2017).

In summary, *BEX3* as a DEG is an interesting finding. The encoded protein NADE is linked to NGFR, a substrate of ADAM17. Loss-of-function of ADAM17 could leave intact NGFR on the cell surface, allowing an enhanced binding of NGF, potentially indirectly enhancing a NADE-mediated apoptosis. Notably, NGF is supplemented to the medium in the BFCN differentiation protocol (Ortiz-Virumbrales *et al.*, 2017). Additionally, *BEX3* expression has been found altered in a previously published study of ÁD transcriptome (Mathys *et al.*, 2019). *TCEAL9*, which is highly co-expressed with *BEX3*, has not yet been associated with neither AD nor ADAM17.

5.2.2.3 STAG2 cohesin complex component (STAG2)

STAG2 is another gene discovered to be consistently overexpressed in R215I compared to controls (Figure 4.12 in Results Subsection 4.2.3.2). It encodes a cohesin component involved in sister chromatid cohesion during mitosis. In addition, cohesion is involved in gene expression of non-dividing cells (Schaaf *et al.*, 2013).

STAG2 mutations or duplications have been linked to mental retardation, such as intellectual disabilities and neurological abnormalities (Piché *et al.*, 2019). A recent study combined transcriptomic data with targeted blood metabolomic data from AD patients and control (Horgusluoglu *et al.*, 2022). The authors identified several metabolomic network modules which were altered in AD compared to control and investigated gene expression in the brain for genes associated with the strongest altered network. One of two genes identified was *ABCA1*, which was found co-expressed with *STAG2* and *IGFBP5.* The set of *ABCA1* and co-expressed genes is highly enriched with known AD signatures such as immune system processes, tyrosine kinase signalling, metabolic syndrome, synaptic signalling, and metabolic process (Horgusluoglu *et al.*, 2022).

This work creates an interesting link between *ADAM17* and *STAG2* expression. *STAG2* duplication has been found to dysregulate genes which critical for the development of the central nervous system (Kumar *et al.*, 2015). Hence, it can be speculated that *STAG2* plays a role for BFCN development.

5.2.2.4 X inactive specific transcript (XIST)

The *XIST* (*X inactive specific transcript*) gene was overexpressed in ctr compared to R215I with a high fold change ($log_2FC > 1$) at all 3 investigated timepoints (Figure 4.12 in Results Subsection 4.2.3.2). It is coding a long non-coding RNA (lnc RNA Xist), which has multiple functions including epigenetic silencing and regulation of gene expression.

Xist has been found previously to alter *ADAM17* expression in carcinoma (Shi *et al.*, 2020). This was found relevant in the context of nasopharyngeal carcinoma, where Xist upregulation caused miRNA-148a-3p downregulation and thereby an overexpression of *ADAM17* (Shi *et al.*, 2020). However, an influence of *ADAM17* on *XIST* expression had not yet been proposed.

XIST has also been associated to AD via several pathways. Exposure of hippocampal neurons to $A\beta_{25-35}$ increased *XIST* expression. Conversely, *XIST* knockdown abated oxidative stress and apoptosis induced by $A\beta_{25-35}$ treatment. The effects were proposed to be mediated via miR-132 (Wang *et al.*, 2018). Furthermore, upregulation of *XIST* has been found to enhance *BACE1* expression via miR-142 binding (Yue *et al.*, 2020). Apart from that, Xist was found to regulate the expression of *MME*, a gene coding an Aβ degrading enzyme (Yan *et al.*, 2022). In our sc-RNAseq dataset, neither *BACE1,* nor *MME* was not found differentially expressed between R215I and ctr, indicating the potential influence of other pathways or biological compensatory mechanisms.

Xist is an important regulator of X-chromosome dosage compensation by silencing one X chromosome in females. Remarkably, all DEGs which were found at all three points of the differentiation, lie on the chromosome. *STAG2, SMS, BEX3* and *TCEAL9* could potentially escape the X chromosome inactivation, which is common for some genes (Skuse, 2005; Lisik and Sieron, 2008). However, neither of these four genes has been verified as a potential escapee (Zhang *et al.*, 2013; Wainer Katsir and Linial, 2019).

To conclude, *XIST* has been associated with *ADAM17* expression and with AD via different pathways. While it in principle could be regulating the other 4 DEGs presented, this has not yet been reported before. The differential expression of Xist could partially explain the higher AD incidence in females compared to man.

5.2.2.5 Insulin-like growth factor-binding protein 5 (IGFBP5)

IGFBP5 gene was overexpressed in R215I compared to ctr with a high fold change ($log_2FC > 1$) at Day 12 (Figure 4.12 in Results Subsection - 78 -4.2.3.2). IGFBP-5 regulates availability of IGF (Insulin-like growth factor) by binding it with a higher affinity than the respective receptor. IGFBP-5 has a high influence on cell survival and differentiation via this pathway (Duan and Allard, 2020). IGFBP-5 is expressed in a variety of different tissues, depending on developmental stage. It has several functions independent of IGF, which it exerts depending on cell type and availability of IGF1 and IGF2. For example, it has been found to foster IL-6 induced ROS production and induce premature senescence in fibroblast (Sanada *et al.*, 2018). In vascular smooth muscle cells, IGFBP-5 promotes cell migration via IGF-independent binding to cell surface proteoglycans. Upregulation of *IGFBP5* leads to increased apoptosis (Duan and Allard, 2020). Due to various IGF independent reactions, it was speculated whether IGFBP-5 has its own receptor. As IFGBP-3, a close paralog of IGFPB-5, is binding to LRP-1, this receptor was suggested as a potential receptor for IGFBP-5 (Shian Huang *et al.*, 2004; Duan and Allard, 2020). Interestingly, LRP-1 is a substrate of ADAM17.

While *IGFBP5* is expressed during forebrain development (Bondy and Lee, 1993) and plays a crucial role in premature cell senescence (Sanada *et al.*, 2018), it has also been linked to Alzheimer's disease in previous studies. Thus, a recent RNA-seq study of the dorsal lateral prefrontal cortex used gene module–trait network analysis to identify coherent cellular processes that impact AD phenotypes. They identified 47 mutually exclusive modules, of which module m109 includes a set of genes which is strongly and directly linked to cognitive decline. Among others, this m109 contains *IGFBP5*, reinforcing its relevance to AD (Mostafavi *et al.*, 2018). In an *in vitro* study with SH-SY5Y soluble $A\beta_{42}$ was found to increase *IGFPB5* expression at low concentrations (Barucker *et al.*, 2015). The authors propose an effect of Aβ on *IGFPB5* as a potential driver of AD progression. In another multi-omics study, IGFBP5 was significantly enriched in AD patients compared to non-cognitive impaired control (Iturria-Medina *et al.*, 2022). Apart from this, it was found co-expressed with *STAG2* in a study combining transcriptomic and metabolomic data (Horgusluoglu *et al.*, 2022)., which has been described in Section 5.2.2.3 above.

5.2.2.6 *SIX homeoboxes 3/6 (SIX3 and SIX6)*

SIX3 and *SIX6* are members of the SINE class homeoboxes gene family and are essential transcriptional regulators during forebrain development (Bernier *et al.*, 2000; Ando *et al.*, 2005). SIX6 and SIX3 are paralogs with high sequence identity and similar expression patterns (Turcu,

Lillehaug and Seo, 2019). Changes in *SIX3* expression leads to holoprosencephaly, a defect in which the hemispheres of the forebrain are not properly segregated (Lee *et al.*, 2013).

SIX6 gene was found overexpressed in R215I compared to ctr with a high fold change (log_2FC > 1) at Day 12, while *SIX3* is one of the genes with highest fold change at Day 8 and Day 12 (Figure 4.12 in Results Subsection - 78 -4.2.3.2). There is an interestingly link between *SIX3*/*SIX6* expression and ADAM17. Combined downregulation of *SIX3* and *SIX6* was previously found to cause morphological abnormalities in murine multipotent neuronal precursors cells. These abnormalities were traced back to a decreased expression of *SOX2*, which downregulated the expression of *NOTCH1* (Diacou *et al.*, 2018). Notch1 is an important substrate of ADAM17 and involved in divers cell fate and differentiation processes. In the sc-RNAseq data set generated in this work, both *SIX3* and *SIX6* are significantly overexpressed in R215I compared to control at Differentiation Day 12 (*SIX3*: p-value < 0.0001, log2FC 1.1; *SIX6* p-value < 0.0001, log2FC 1.24). It can be speculated that this is an effect of a compensatory mechanism due to insufficient Notch1 cleavage due to decreased ADAM17 activity. *SOX2*, a target of SIX3 and SIX6, is overexpressed in R215I compared to control at Differentiation Day 8 and Day 12 (see Figure 4.5). *NOTCH1* expression was not detected in this experiment. Notch signalling is involved in neural development and function, angiogenesis, and maintenance of neuronal stem cells (Kapoor and Nation, 2021), and was found to support neuronal cell differentiation and inhibits cell death in neural stem/progenitor cells (Kim, Rhee and Paik, 2014). As Notch1 is an important target of ADAM17, the loss-of-function mutation R215I is expected to have a high influence on neuronal development.

SIX3 and SIX6 are highly involved in forebrain development and could be linked to ADAM17 function. The connection between *ADAM17* and *SIX3/6* should be explored further. It will be interesting to see, whether *SIX3* or *SIX6* are differentially expressed in the mDA differentiation as well.

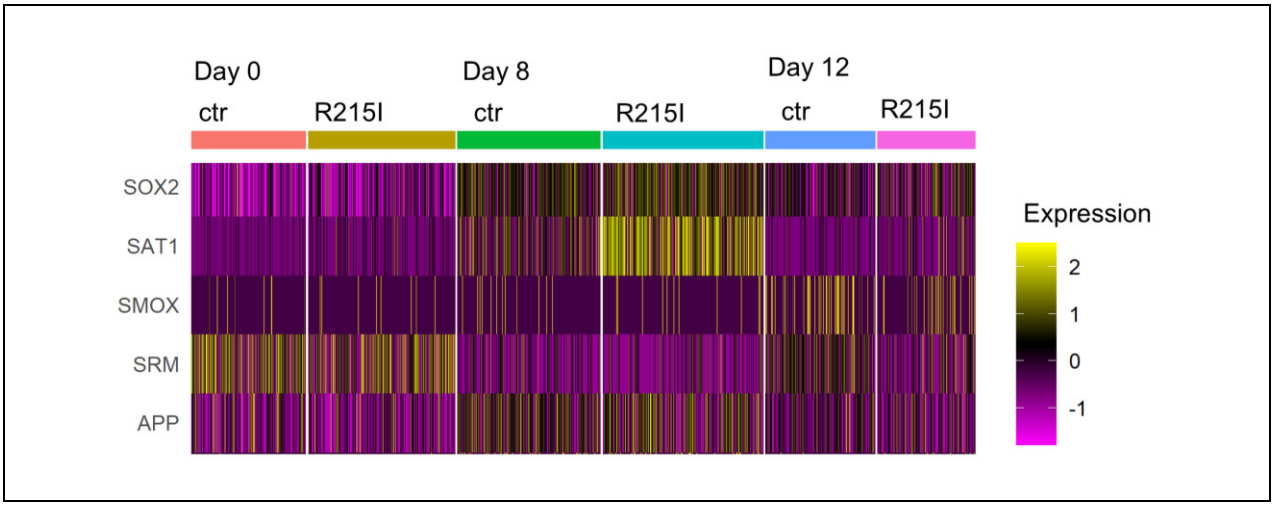

Figure 5.2 Heatmap depicting expression of genes relevant for the discussion of the Top 8 DEGs. **SOX2** *is overexpressed in R215I for Day 8 and Day 12, possibly by a mechanism caused by combined* SIX3/SIX6 *overexpression.* **SAT1**, **SMOX** *and* **SRM** *are coding for genes involved in spermine metabolism. Their expression could be influenced by overexpression of* SMS *in R215I.* **APP** *expression was previously found to be altered by loss-of-function ADAM17 (Hartl* et al.*, 2018), which was not replicated in our dataset.*

Taken together, sc-RNAseq revealed interesting connections between ADAM17 and early neuronal differentiation, which have not been established before. Sc-RNAseq - is a state-of-the-art method for deep phenotyping, especially in combination with other omic- experiments. However, sc-RNAseq comes with limitations. First, both 10x Genomics and Drop-seq have a low sequencing depth compared to other methods such as Smart-Seq2 (Picelli *et al.*, 2013) or SCRB-seq (Salomon *et al.*, 2019; Ni *et al.*, 2020). Second, the necessary UMAP technique for standard dimensionality reduction, followed by for identification of candidate genes and pathways, may miss essential underlying mechanisms compared to more integrative approaches.

5.2.3 Metabolomic characterization

The metabolomics characterization of the BFCN differentiation (Results Subsection 4.2.4.1) found the pathways “Amino Sugar Metabolism”, “Ammonia Recycling”, “Arginine and Proline Metabolism”, “Aspartate Metabolism”, “Citric Acid Cycle”, “Glutamate Metabolism”, “Glycine and Serine Metabolism”, “Purine Metabolism”, “Urea Cycle”, and “Warburg Effect” to be enriched at each of the three timepoints analysed.

For the mDA differentiation (Results Subsection 4.2.4.2) the pathways “Aspartate Metabolism” and “Urea Cycle” were statistically significant enriched at Day 0 whereas no pathways were found statistically significantly enriched at Day 8. Overall, less metabolites are differentially abundant in the mDA differentiation compared to the BFCN differentiation. This could be a confounding factor caused by the experimental setup. The medium of the BFCN experiment was collected after

24 hours, while the medium of the mDA experiment was changed after 12 hours accordingly to the different protocols. Naturally, this different feeding periods leave more time for the compounds to enrich in the BFCN medium, and subsequently to a higher number of detectable metabolites via HILIC and ICMS analysis. While the different media turnover may lead to different signatures, one might speculate that the first or main differences occur in “Aspartate metabolism” and “Urea Cycle” as these are already detectable after 12 hours. To account for change in cell numbers change during the neuronal development, adjustments are done regarding cell number and protein content (see Metabolomics Section 3.8 in Materials and Methods).

Metabolomic data for both neuronal differentiations support the qPCR findings, as pathways involved in differentiation are enriched in metabolites found. Among other functions, the identified pathways are relevant for neuronal differentiation. One example is the switch in energy metabolism. iPSC cells use mainly anaerobic glycolysis for their energy production, while neurons rely on ATP production via oxidative phosphorylation (Iwata and Vanderhaeghen, 2021). The change to aerobic glycolysis, known as the Warburg effect, is common for cells during differentiation (Vander Heiden, Cantley and Thompson, 2009). This is a necessary process of differentiating neurons to increase their cellular energy requirement and meet the needs of protein and membrane synthesis (Bifari *et al.*, 2020).

Other pathways are important to incorporate nutrients and produce biomass, important for cell proliferation and growth. Glutamate metabolism is involved in regulation growth and proliferation (Kim, Rhee and Paik, 2014) constitutes a main nitrogen donor for the biosynthesis of purines and pyrimidines and provides the amino group for most amino acids (Walker and van der Donk, 2016). Other main important pathways include metabolism of amino acids, which are essential for cell growth.

Other AD metabolomic studies find differences between AD and healthy control in pathways related to energy metabolism – mainly in “Citric Acid Cycle”, “Lipid Homeostasis”, and “Mitochondrial Ketone Bodies” pathways measured in CSF and plasma metabolome (Wilkins and Trushina, 2018; Hampel, Nisticò, *et al.*, 2021). In a small study, Paglia and colleagues found the metabolic pathways “Alanine, Aspartate, and Glutamate metabolism”, “Arginine and Proline metabolism”, “Cysteine and Methionine metabolism”, “Glycine, Serine, and Threonine metabolism”, “Purine metabolism”, and “Pantothenate and CoA biosynthesis” significantly altered in AD *post mortem* brains compared to healthy control. After identification of key drivers of these pathways, the authors conclude that defective mitochondria, and hence altered energy metabolism, are causal of the altered metabolic profiles between patients and controls (Paglia *et*

al., 2016). Alterations in energy metabolism were also found in our data set. However, as the energy flux during differentiation changes dramatically, this could be a confounding factor. Cells differentiating into neurons upregulate their energy metabolism to meet needs of enhanced biosynthesis (Bifari *et al.*, 2020). The sc-RNAseq data indicate a slower differentiation for the *ADAM17* mutant, which might influence the differences in the metabolomics data.

Additionally, metabolism of different amino acids was found altered in the metabolome of AD patients and mouse models. Namely, in a targeted approach histidine, leucine, valine, phenylalanine, and lysine have been found altered in APP/PS1 mice (Pan *et al.*, 2016). In humans, alterations in asparagine, proline, serine, threonine, tryptophane, tyrosine, alanine, histidine, glutamine, and valine have been found (Iturria-Medina *et al.*, 2022) to predict clinical progression. In our dataset, alterations in essential and non-essential amino acids were detected between R215I and control. However, this difference was not consistent across the timepoints.

Furthermore, sphingomyelins and phosphatidylcholines are often found perturbed in AD samples (Pan *et al.*, 2016; Toledo *et al.*, 2017; Wilkins and Trushina, 2018). Metabolites of this pathways are not targeted in our approach. Although ADAM17 is not expected to alter these pathways, a further targeted approach which includes relevant later timepoints of the differentiation could potentially shed more light into a potential influence of ADAM17 on the metabolism of these compounds.

Other pathways, commonly found to be altered between patients and controls are the “lipid homeostasis”, and “fatty acid biosynthesis”, “neurotransmitters” (González-Domínguez *et al.*, 2021; Hampel, Nisticò, *et al.*, 2021) but were not prominent in the present dataset. The focus on the early differentiation in this work is unlikely to reveal changes in neurotransmitters, as they are typically only expressed later in development.

Interestingly, both metabolomic and sc-RNAseq data indicate alterations in spermine biosynthesis. “Spermine and Spermidine biosynthesis” is a pathway enriched in differentially abundant metabolites discovered in the metabolomics data, although not significant. In line with that, the transcript of “spermine synthetase” was significantly overexpressed in all 3 timepoints of early BFCN differentiation. The DEG *SMS*, together with the metabolic pathways, suggesting a convergence of AD development in this network.

6 Conclusion and Outlook

This work characterised the influence of a specific AD-related mutation of *ADAM17 (*rs142946965) in iPSC and during early neuronal differentiation in a multi-omics approach.

In the first part of the project, clones carrying mutations in the inhibitory pro-domain of *ADAM17* were generated. Western blot revealed a decrease of the long ADAM17 pro-forms while the abundance of mature ADAM17 was not altered. This indicates a faster cleavage of the pro-domain in the mutant compared to wild type, in contrast to existing literature (Hartl *et al.*, 2018). One clone carrying the rs142946965 mutation in *ADAM17* was generated at the Murdoch Children´s Research Institute (Australia). This clone does not show alterations in pro-ADAM17 abundance in Western blot. These results can be partly explained by an enhanced cleavage of the pro-form, as altered sequence of cleavage can leave the cleaved pro-domain attached to the catalytic center, forming an inactive pseudo pro-form (Wong *et al.*, 2015).

In the second part of the project, the influence of the *ADAM17* rs142946965 mutation was investigated in the context of neuronal development. iPSC were differentiated into BFCN and mDA neurons, respectively. BFCN among the first affected by AD and constitute the main cholinergic input in the CNS. mDA neurons are specifically impacted by PD, another neurodegenerative disease with increasing incidence. Five genes were found differentially expressed between R215I and the isogenic control during all timepoints investigated in the analysis of BFCN sc-RNAseq dataset. These genes identified have been connected to AD progression and/or basal forebrain development earlier, however a link to ADAM17 has not previously been established. The metabolomic dataset does not only reflect changes due the neuronal development but underpins the findings of the sc-RNAseq. Spermine, a physiological polyamine, was found highly impacted by the ADAM17 loss-of-function. The “Spermine and Spermidine biosynthesis” metabolic pathway was found altered, and the spermine synthesising enzyme spermine synthase was found differentially expressed between R215I and isogenic control at all 3 timepoints of the differentiation. Metabolic alterations found in this ADAM17 centred project reflect signatures found in AD literature and provides therefore a potential mechanistic link of the *ADAM17* rs142946965 mutation to AD development which is already visible during the early differentiation.

Several datasets generated in this work are not yet complete and hence could not be integrated yet. For the mDA neuronal differentiation, data of the sc-RNAseq, and proteomic analysis were

not provided but are expected in the coming weeks. These datasets are crucial to validate the findings of this work.

Apart from that, improvement of the BFCN differentiation, to generate a generous amount of BFCN neurons for further analysis would boost the explanatory power of the work presented. Additionally, an analysis of the proteome of BFCN could be used to validate the impact of ADAM17 on early neurogenesis. Combined with a targeted metabolomic approach, the influence of ADAM17 on the spermine synthesis could be further investigated. For this project an untargeted approach was employed. By measuring approximately 200 compounds, this method aims to identify cell line specific metabolic fingerprints. Untargeted metabolomics is useful for identifying novel, unexpected pathways, but it may miss or underrepresent other pathways.

The multi-omic approach, combining genomics, proteomics, metabolomics, and transcriptomics, intends to characterise pools of biological molecules to unravel functional pathways and cellular dynamics implicated in progression of NDA (Menéndez-González, 2023). In this work, sc-RNAseq and untargeted metabolomics where combined to investigate the influence of *ADAM17* on early neuronal differentiation. To estimate the implications of the R215I mutation on early neuronal development different data sets were generated by sc-RNAseq, metabolomics and proteomics. A general limitation of the approach is the mechanistic data integration of the diverse data sets. The pathway analysis of each level individually and subsequent, independent cross-validation and may miss essential drivers of disease development was employed for the analysis of the data presented.

Overall, the findings generated in this project are relevant in AD and generate new links between *ADAM17* and AD related processes.

7 Bibliography

Abolhassani, N. *et al.* (2017) 'Molecular pathophysiology of impaired glucose metabolism, mitochondrial dysfunction, and oxidative DNA damage in Alzheimer's disease brain', *Mechanisms of Ageing and Development*, 161, pp. 95–104. Available at: https://doi.org/10.1016/j.mad.2016.05.005.

Abubakar, M.B. *et al.* (2022) 'Alzheimer's Disease: An Update and Insights Into Pathophysiology', *Frontiers in Aging Neuroscience*, 14, p. 742408. Available at: https://doi.org/10.3389/fnagi.2022.742408.

Acosta, C., Anderson, H.D. and Anderson, C.M. (2017) 'Astrocyte dysfunction in Alzheimer disease', *Journal of Neuroscience Research*, 95(12), pp. 2430–2447. Available at: https://doi.org/10.1002/jnr.24075.

Aikawa, T. *et al.* (2019) 'ABCA7 haplodeficiency disturbs microglial immune responses in the mouse brain', *Proceedings of the National Academy of Sciences*, 116(47), pp. 23790–23796. Available at: https://doi.org/10.1073/pnas.1908529116.

Aldana, B.I. *et al.* (2017) 'Characterization of energy and neurotransmitter metabolism in cortical glutamatergic neurons derived from human induced pluripotent stem cells: A novel approach to study metabolism in human neurons', *Neurochemistry International*, 106, pp. 48–61. Available at: https://doi.org/10.1016/j.neuint.2017.02.010.

Alvarez-Mora, M.I. *et al.* (2022) 'Heterozygous and Homozygous Variants in SORL1 Gene in Alzheimer's Disease Patients: Clinical, Neuroimaging and Neuropathological Findings', *International Journal of Molecular Sciences*, 23(8), p. 4230. Available at: https://doi.org/10.3390/ijms23084230.

Alzheimer's association (2022) '2022 Alzheimer's disease facts and figures', *Alzheimer's & Dementia*, 18(4), pp. 700–789. Available at: https://doi.org/10.1002/alz.12638.

Ando, H. *et al.* (2005) 'Lhx2 mediates the activity of Six3 in zebrafish forebrain growth', *Developmental Biology*, 287(2), pp. 456–468. Available at: https://doi.org/10.1016/j.ydbio.2005.09.023.

Ando, K. *et al.* (2013) 'Clathrin adaptor CALM/PICALM is associated with neurofibrillary tangles and is cleaved in Alzheimer's brains', *Acta Neuropathologica*, 125(6), pp. 861–878. Available at: https://doi.org/10.1007/s00401-013-1111-z.

Arias-Fuenzalida, J. *et al.* (2017) 'FACS-Assisted CRISPR-Cas9 Genome Editing Facilitates Parkinson's Disease Modeling', *Stem Cell Reports*, 9(5), pp. 1423–1431. Available at: https://doi.org/10.1016/j.stemcr.2017.08.026.

Armstrong, R.A. (2019) 'Risk factors for Alzheimer's disease', *Folia Neuropathologica*, 57(2), pp. 87–105. Available at: https://doi.org/10.5114/fn.2019.85929.

Arranz, A.M. and De Strooper, B. (2019) 'The role of astroglia in Alzheimer's disease: pathophysiology and clinical implications', *The Lancet Neurology*, 18(4), pp. 406–414. Available at: https://doi.org/10.1016/S1474-4422(18)30490-3.

Ata, S.K. *et al.* (2021) 'Recent advances in network-based methods for disease gene prediction', *Briefings in Bioinformatics*, 22(4), p. bbaa303. Available at: https://doi.org/10.1093/bib/bbaa303.

Ayodele, T. *et al.* (2021) 'Early-Onset Alzheimer's Disease: What Is Missing in Research?', *Current Neurology and Neuroscience Reports*, 21(2), p. 4. Available at: https://doi.org/10.1007/s11910-020-01090-y.

Bae, T. *et al.* (2019) 'Recent trends in CRISPR-Cas system: genome, epigenome, and transcriptome editing and CRISPR delivery systems', *Genes & Genomics*, 41(8), pp. 871–877. Available at: https://doi.org/10.1007/s13258-019-00830-w.

Bajanca, F. *et al.* (2015) 'Editorial: Cell adhesion in development', *Developmental Biology*, 401(1), p. 1. Available at: https://doi.org/10.1016/j.ydbio.2015.02.015.

Baker-Nigh, A. *et al.* (2015) 'Neuronal amyloid-β accumulation within cholinergic basal forebrain in ageing and Alzheimer's disease', *Brain*, 138(6), pp. 1722–1737. Available at: https://doi.org/10.1093/brain/awv024.

Barnes, D.E. and Yaffe, K. (2011) 'The projected effect of risk factor reduction on Alzheimer's disease prevalence', *The Lancet Neurology*, 10(9), pp. 819–828. Available at: https://doi.org/10.1016/S1474-4422(11)70072-2.

Barnes, J. *et al.* (2015) 'Alzheimer's disease first symptoms are age dependent: Evidence from the NACC dataset', *Alzheimer's & Dementia*, 11(11), pp. 1349–1357. Available at: https://doi.org/10.1016/j.jalz.2014.12.007.

Barucker, C. *et al.* (2015) 'Alzheimer Amyloid Peptide Aβ42 Regulates Gene Expression of Transcription and Growth Factors', *Journal of Alzheimer's Disease*, 44(2), pp. 613–624. Available at: https://doi.org/10.3233/JAD-141902.

Bekris, L.M. *et al.* (2010) 'Genetics of Alzheimer Disease', *Journal of geriatric psychiatry and neurology*, 23(4), p. 213. Available at: https://doi.org/10.1177/0891988710383571.

Bellenguez, C. *et al.* (2022) 'New insights into the genetic etiology of Alzheimer's disease and related dementias', *Nature Genetics*, 54(4), pp. 412–436. Available at: https://doi.org/10.1038/s41588-022-01024-z.

Bellenguez, C., Grenier-Boley, B. and Lambert, J.-C. (2020) 'Genetics of Alzheimer's disease: where we are, and where we are going', *Current Opinion in Neurobiology*, 61, pp. 40–48. Available at: https://doi.org/10.1016/j.conb.2019.11.024.

Bernier, G. *et al.* (2000) 'Expanded retina territory by midbrain transformation upon overexpression of Six6 (Optx2) in Xenopus embryos', *Mechanisms of Development*, 93(1), pp. 59–69. Available at: https://doi.org/10.1016/S0925-4773(00)00271-9.

Bian, H. *et al.* (2016) 'RNA Interference Silencing of Glycogen Synthase Kinase 3β Inhibites Tau Phosphorylation in Mice with Alzheimer Disease', *Neurochemical Research*, 41(9), pp. 2470–2480. Available at: https://doi.org/10.1007/s11064-016-1960-7.

Bickel, D.R. (2002) 'Robust estimators of the mode and skewness of continuous data', *Computational Statistics & Data Analysis*, 39(2), pp. 153–163. Available at: https://doi.org/10.1016/S0167-9473(01)00057-3.

Bidesi, N.S.R. *et al.* (2021) 'The role of neuroimaging in Parkinson's disease', *Journal of Neurochemistry*, 159(4), pp. 660–689. Available at: https://doi.org/10.1111/jnc.15516.

Bien, S.A. *et al.* (2019) 'The Future of Genomic Studies Must Be Globally Representative: Perspectives from PAGE', *Annual Review of Genomics and Human Genetics*, 20(1), pp. 181–200. Available at: https://doi.org/10.1146/annurev-genom-091416-035517.

Biessels, G.J. and Despa, F. (2018) 'Cognitive decline and dementia in diabetes mellitus: mechanisms and clinical implications', *Nature Reviews Endocrinology*, 14(10), pp. 591–604. Available at: https://doi.org/10.1038/s41574-018-0048-7.

Bifari, F. *et al.* (2020) 'Complete neural stem cell (NSC) neuronal differentiation requires a branched chain amino acids-induced persistent metabolic shift towards energy metabolism', *Pharmacological Research*, 158, p. 104863. Available at: https://doi.org/10.1016/j.phrs.2020.104863.

Bissonnette, C.J. *et al.* (2011) 'The Controlled Generation of Functional Basal Forebrain Cholinergic Neurons from Human Embryonic Stem Cells: The Controlled Generation of Human BFCN from hESC', *STEM CELLS*, 29(5), pp. 802–811. Available at: https://doi.org/10.1002/stem.626.

Boeve, B.F. *et al.* (2022) 'Advances and controversies in frontotemporal dementia: diagnosis, biomarkers, and therapeutic considerations', *The Lancet Neurology*, 21(3), pp. 258–272. Available at: https://doi.org/10.1016/S1474-4422(21)00341-0.

Bondy, C. and Lee, W. (1993) 'Correlation between insulin-like growth factor (IGF)-binding protein 5 and IGF-I gene expression during brain development', *The Journal of Neuroscience*, 13(12), pp. 5092–5104. Available at: https://doi.org/10.1523/JNEUROSCI.13-12-05092.1993.

Boskovic, Z. *et al.* (2019) 'Regulation of cholinergic basal forebrain development, connectivity, and function by neurotrophin receptors', *Neuronal Signaling*, 3(1), p. NS20180066. Available at: https://doi.org/10.1042/NS20180066.

Braak, H. and Braak, E. (1991) 'Neuropathological stageing of Alzheimer-related changes', *Acta Neuropathologica*, 82(4), pp. 239–259. Available at: https://doi.org/10.1007/BF00308809.

Brai, E., Alina Raio, N. and Alberi, L. (2016) 'Notch1 hallmarks fibrillary depositions in sporadic Alzheimer's disease', *Acta Neuropathologica Communications*, 4(1), p. 64. Available at: https://doi.org/10.1186/s40478-016-0327-2.

Brueggen, K. *et al.* (2015) 'Basal Forebrain and Hippocampus as Predictors of Conversion to Alzheimer's Disease in Patients with Mild Cognitive Impairment – A Multicenter DTI and Volumetry Study', *Journal of Alzheimer's Disease*, 48(1), pp. 197–204. Available at: https://doi.org/10.3233/JAD-150063.

Buchhave, P. *et al.* (2012) 'Cerebrospinal Fluid Levels ofβ-Amyloid 1-42, but Not of Tau, Are Fully Changed Already 5 to 10 Years Before the Onset of Alzheimer Dementia', *Archives of General Psychiatry*, 69(1), pp. 98–106. Available at: https://doi.org/10.1001/archgenpsychiatry.2011.155.

Buell, A.K. (2022) 'Stability matters, too – the thermodynamics of amyloid fibril formation', *Chemical Science*, 13(35), pp. 10177–10192. Available at: https://doi.org/10.1039/D1SC06782F.

Bukhari, H. *et al.* (2017) 'Small things matter: Implications of APP intracellular domain AICD nuclear signaling in the progression and pathogenesis of Alzheimer's disease', *Progress in Neurobiology*, 156, pp. 189–213. Available at: https://doi.org/10.1016/j.pneurobio.2017.05.005.

Bull, N.D. *et al.* (2012) 'Reduced Axonal Transport and Increased Excitotoxic Retinal Ganglion Cell Degeneration in Mice Transgenic for Human Mutant P301S Tau', *PLoS ONE*. Edited by J. Götz, 7(4), p. e34724. Available at: https://doi.org/10.1371/journal.pone.0034724.

Busche, M.A. and Hyman, B.T. (2020) 'Synergy between amyloid-β and tau in Alzheimer's disease', *Nature Neuroscience*, 23(10), pp. 1183–1193. Available at: https://doi.org/10.1038/s41593-020-0687-6.

Butterfield, D.A. and Halliwell, B. (2019) 'Oxidative stress, dysfunctional glucose metabolism and Alzheimer disease', *Nature Reviews Neuroscience*, 20(3), pp. 148–160. Available at: https://doi.org/10.1038/s41583-019-0132-6.

Cacace, R., Sleegers, K. and Van Broeckhoven, C. (2016) 'Molecular genetics of early-onset Alzheimer's disease revisited', *Alzheimer's & Dementia*, 12(6), pp. 733–748. Available at: https://doi.org/10.1016/j.jalz.2016.01.012.

Cahill, S., Chandola, T. and Hager, R. (2022) 'Genetic Variants Associated With Resilience in Human and Animal Studies', *Frontiers in Psychiatry*, 13. Available at: https://www.frontiersin.org/articles/10.3389/fpsyt.2022.840120 (Accessed: 7 March 2023).

Cai, Q. and Tammineni, P. (2017) 'Mitochondrial Aspects of Synaptic Dysfunction in Alzheimer's Disease', *Journal of Alzheimer's disease : JAD*, 57(4), pp. 1087–1103. Available at: https://doi.org/10.3233/JAD-160726.

Calabrò, M. *et al.* (2021) 'The biological pathways of Alzheimer disease: a review', *AIMS Neuroscience*, 8(1), pp. 86–132. Available at: https://doi.org/10.3934/Neuroscience.2021005.

Caldwell, K.A., Willicott, C.W. and Caldwell, G.A. (2020) 'Modeling neurodegeneration in Caenorhabditis elegans', *Disease Models & Mechanisms*, 13(10), p. dmm046110. Available at: https://doi.org/10.1242/dmm.046110.

Calligaris, M. *et al.* (2021) 'Strategies to Target ADAM17 in Disease: From Its Discovery to the iRhom Revolution', *Molecules*, 26(4), p. 944. Available at: https://doi.org/10.3390/molecules26040944.

Campion, D., Charbonnier, C. and Nicolas, G. (2019) 'SORL1 genetic variants and Alzheimer disease risk: a literature review and meta-analysis of sequencing data', *Acta Neuropathologica*, 138(2), pp. 173–186. Available at: https://doi.org/10.1007/s00401-019-01991-4.

Cavadas, M. *et al.* (2017) 'Phosphorylation of iRhom2 Controls Stimulated Proteolytic Shedding by the Metalloprotease ADAM17/TACE', *Cell Reports*, 21(3), pp. 745–757. Available at: https://doi.org/10.1016/j.celrep.2017.09.074.

Cavedo, E. *et al.* (2016) 'Reduced Regional Cortical Thickness Rate of Change in Donepezil-Treated Subjects With Suspected Prodromal Alzheimer's Disease', *Journal of Clinical Psychiatry* [Preprint]. Available at: https://doi.org/10.4088/JCP.15m10413.

Cavedo, E. *et al.* (2017) 'Reduced basal forebrain atrophy progression in a randomized Donepezil trial in prodromal Alzheimer's disease', *Scientific Reports*, 7(1), p. 11706. Available at: https://doi.org/10.1038/s41598-017-09780-3.

Cenini, G. *et al.* (2016) 'Amyloid β-peptides interfere with mitochondrial preprotein import competence by a coaggregation process', *Molecular Biology of the Cell*, 27(21), pp. 3257–3272. Available at: https://doi.org/10.1091/mbc.E16-05-0313.

Cenini, G. and Voos, W. (2019) 'Mitochondria as Potential Targets in Alzheimer Disease Therapy: An Update', *Frontiers in Pharmacology*, 10, p. 902. Available at: https://doi.org/10.3389/fphar.2019.00902.

Chen, X.-Q. and Mobley, W.C. (2019) 'Exploring the Pathogenesis of Alzheimer Disease in Basal Forebrain Cholinergic Neurons: Converging Insights From Alternative Hypotheses', *Frontiers in Neuroscience*, 13. Available at: https://www.frontiersin.org/articles/10.3389/fnins.2019.00446 (Accessed: 10 March 2023).

Christova, Y. *et al.* (2013) 'Mammalian iRhoms have distinct physiological functions including an essential role in TACE regulation', *EMBO reports*, 14(10), pp. 884–890. Available at: https://doi.org/10.1038/embor.2013.128.

Cochran, J.N. *et al.* (2015) 'The Alzheimer's disease risk factor CD2AP maintains blood–brain barrier integrity', *Human Molecular Genetics*, 24(23), pp. 6667–6674. Available at: https://doi.org/10.1093/hmg/ddv371.

Colucci-D'Amato, L., Speranza, L. and Volpicelli, F. (2020) 'Neurotrophic Factor BDNF, Physiological Functions and Therapeutic Potential in Depression, Neurodegeneration and Brain Cancer', *International Journal of Molecular Sciences*, 21(20), p. 7777. Available at: https://doi.org/10.3390/ijms21207777.

Concordet, J.-P. and Haeussler, M. (2018) 'CRISPOR: intuitive guide selection for CRISPR/Cas9 genome editing experiments and screens', *Nucleic Acids Research*, 46(W1), pp. W242–W245. Available at: https://doi.org/10.1093/nar/gky354.

Cong, L. *et al.* (2013) 'Multiplex Genome Engineering Using CRISPR/Cas Systems', *Science*, 339(6121), pp. 819–823. Available at: https://doi.org/10.1126/science.1231143.

Conroy, J.N. and Coulson, E.J. (2022) 'High-affinity TrkA and p75 neurotrophin receptor complexes: A twisted affair', *The Journal of Biological Chemistry*, 298(3), p. 101568. Available at: https://doi.org/10.1016/j.jbc.2022.101568.

Constantin, A.-E. and Patil, I. (2021) 'ggsignif: R Package for Displaying Significance Brackets for "ggplot2"', *PsyArxiv* [Preprint]. Available at: https://doi.org/10.31234/osf.io/7awm6.

Cox, J. *et al.* (2011) 'Andromeda: A Peptide Search Engine Integrated into the MaxQuant Environment', *Journal of Proteome Research*, 10(4), pp. 1794–1805. Available at: https://doi.org/10.1021/pr101065j.

Cox, J. *et al.* (2014) 'Accurate Proteome-wide Label-free Quantification by Delayed Normalization and Maximal Peptide Ratio Extraction, Termed MaxLFQ*', *Molecular & Cellular Proteomics*, 13(9), pp. 2513–2526. Available at: https://doi.org/10.1074/mcp.M113.031591.

Cox, J. and Mann, M. (2008) 'MaxQuant enables high peptide identification rates, individualized p.p.b.-range mass accuracies and proteome-wide protein quantification', *Nature Biotechnology*, 26(12), pp. 1367–1372. Available at: https://doi.org/10.1038/nbt.1511.

Crompton, L.A. *et al.* (2013) 'Stepwise, non-adherent differentiation of human pluripotent stem cells to generate basal forebrain cholinergic neurons via hedgehog signaling', *Stem Cell Research*, 11(3), pp. 1206–1221. Available at: https://doi.org/10.1016/j.scr.2013.08.002.

Cruchaga, C. *et al.* (2012) 'Rare Variants in APP, PSEN1 and PSEN2 Increase Risk for AD in Late-Onset Alzheimer's Disease Families', *PLoS ONE*. Edited by M. Toft, 7(2), p. e31039. Available at: https://doi.org/10.1371/journal.pone.0031039.

Culig, L., Chu, X. and Bohr, V.A. (2022) 'Neurogenesis in aging and age-related neurodegenerative diseases', *Ageing Research Reviews*, 78, p. 101636. Available at: https://doi.org/10.1016/j.arr.2022.101636.

Cunnane, S.C. *et al.* (2020) 'Brain energy rescue: an emerging therapeutic concept for neurodegenerative disorders of ageing', *Nature Reviews Drug Discovery*, 19(9), pp. 609–633. Available at: https://doi.org/10.1038/s41573-020-0072-x.

Dang, M. *et al.* (2013) 'Regulated ADAM17-dependent EGF family ligand release by substrate-selecting signaling pathways', *Proceedings of the National Academy of Sciences*, 110(24), pp. 9776–9781. Available at: https://doi.org/10.1073/pnas.1307478110.

D'Argenio, V. and Sarnataro, D. (2020) 'New Insights into the Molecular Bases of Familial Alzheimer's Disease', *Journal of Personalized Medicine*, 10(2), p. 26. Available at: https://doi.org/10.3390/jpm10020026.

Davis, M.W. and Jorgensen, E.M. (2022) 'ApE, A Plasmid Editor: A Freely Available DNA Manipulation and Visualization Program', *Frontiers in Bioinformatics*, 2. Available at: https://www.frontiersin.org/articles/10.3389/fbinf.2022.818619 (Accessed: 3 January 2023).

Delenclos, M. *et al.* (2019) 'Cellular models of alpha-synuclein toxicity and aggregation', *Journal of Neurochemistry*, 150(5), pp. 566–576. Available at: https://doi.org/10.1111/jnc.14806.

Diacou, R. *et al.* (2018) 'Six3 and Six6 Are Jointly Required for the Maintenance of Multipotent Retinal Progenitors through Both Positive and Negative Regulation', *Cell Reports*, 25(9), pp. 2510-2523.e4. Available at: https://doi.org/10.1016/j.celrep.2018.10.106.

Dib, S., Pahnke, J. and Gosselet, F. (2021) 'Role of ABCA7 in Human Health and in Alzheimer's Disease', *International Journal of Molecular Sciences*, 22(9), p. 4603. Available at: https://doi.org/10.3390/ijms22094603.

Dirkse, A. *et al.* (2019) 'Stem cell-associated heterogeneity in Glioblastoma results from intrinsic tumor plasticity shaped by the microenvironment', *Nature Communications*, 10(1), p. 1787. Available at: https://doi.org/10.1038/s41467-019-09853-z.

Doench, J.G. *et al.* (2016) 'Optimized sgRNA design to maximize activity and minimize off-target effects of CRISPR-Cas9', *Nature Biotechnology*, 34(2), pp. 184–191. Available at: https://doi.org/10.1038/nbt.3437.

Dourlen, P. *et al.* (2019) 'The new genetic landscape of Alzheimer's disease: from amyloid cascade to genetically driven synaptic failure hypothesis?', *Acta Neuropathologica*, 138(2), pp. 221–236. Available at: https://doi.org/10.1007/s00401-019-02004-0.

Du, H. *et al.* (2010) 'Early deficits in synaptic mitochondria in an Alzheimer's disease mouse model', *Proceedings of the National Academy of Sciences*, 107(43), pp. 18670–18675. Available at: https://doi.org/10.1073/pnas.1006586107.

Duan, C. and Allard, J.B. (2020) 'Insulin-Like Growth Factor Binding Protein-5 in Physiology and Disease', *Frontiers in Endocrinology*, 11. Available at: https://www.frontiersin.org/articles/10.3389/fendo.2020.00100 (Accessed: 2 June 2023).

Durkee, C.A. and Araque, A. (2019) 'Diversity and Specificity of Astrocyte–neuron Communication', *Neuroscience*, 396, pp. 73–78. Available at: https://doi.org/10.1016/j.neuroscience.2018.11.010.

Düsterhöft, S. *et al.* (2015) 'Extracellular Juxtamembrane Segment of ADAM17 Interacts with Membranes and Is Essential for Its Shedding Activity', *Biochemistry*, 54(38), pp. 5791–5801. Available at: https://doi.org/10.1021/acs.biochem.5b00497.

Edwards III, G.A. *et al.* (2019) 'Modifiable Risk Factors for Alzheimer's Disease', *Frontiers in Aging Neuroscience*, 11, p. 146. Available at: https://doi.org/10.3389/fnagi.2019.00146.

Efthymiou, A.G. and Goate, A.M. (2017) 'Late onset Alzheimer's disease genetics implicates microglial pathways in disease risk', *Molecular Neurodegeneration*, 12(1), p. 43. Available at: https://doi.org/10.1186/s13024-017-0184-x.

Esquerda-Canals, G. *et al.* (2017) 'Mouse Models of Alzheimer's Disease', *Journal of Alzheimer's Disease*, 57(4), pp. 1171–1183. Available at: https://doi.org/10.3233/JAD-170045.

Fang, E.F. *et al.* (2019) 'Mitophagy inhibits amyloid-β and tau pathology and reverses cognitive deficits in models of Alzheimer's disease', *Nature Neuroscience*, 22(3), pp. 401–412. Available at: https://doi.org/10.1038/s41593-018-0332-9.

Farh, K.K.-H. *et al.* (2015) 'Genetic and epigenetic fine mapping of causal autoimmune disease variants', *Nature*, 518(7539), pp. 337–343. Available at: https://doi.org/10.1038/nature13835.

Ferrer, I. (2023) 'Hypothesis review: Alzheimer's overture guidelines', *Brain Pathology*, 33(1), p. e13122. Available at: https://doi.org/10.1111/bpa.13122.

Figiel-Dabrowska, A. *et al.* (2021) 'Neurogenic and Neuroprotective Potential of Stem/Stromal Cells Derived from Adipose Tissue', *Cells*, 10(6), p. 1475. Available at: https://doi.org/10.3390/cells10061475.

Finneran, D.J. and Nash, K.R. (2019) 'Neuroinflammation and fractalkine signaling in Alzheimer's disease', *Journal of Neuroinflammation*, 16(1), p. 30. Available at: https://doi.org/10.1186/s12974-019-1412-9.

Fishel, M.A. *et al.* (2005) 'Hyperinsulinemia Provokes Synchronous Increases in Central Inflammation and β-Amyloid in Normal Adults', *Archives of Neurology*, 62(10), pp. 1539–1544. Available at: https://doi.org/10.1001/archneur.62.10.noc50112.

Fishilevich, S. *et al.* (2017) 'GeneHancer: genome-wide integration of enhancers and target genes in GeneCards', *Database*, 2017, p. bax028. Available at: https://doi.org/10.1093/database/bax028.

Fixemer, S. *et al.* (2022) 'Microglia phenotypes are associated with subregional patterns of concomitant tau, amyloid-β and α-synuclein pathologies in the hippocampus of patients with Alzheimer's disease and dementia with Lewy bodies', *Acta Neuropathologica Communications*, 10(1), p. 36. Available at: https://doi.org/10.1186/s40478-022-01342-7.

Flannery, P.J. and Trushina, E. (2019) 'Mitochondrial dynamics and transport in Alzheimer's disease', *Molecular and Cellular Neuroscience*, 98, pp. 109–120. Available at: https://doi.org/10.1016/j.mcn.2019.06.009.

Forloni, G. and Balducci, C. (2018) 'Alzheimer's Disease, Oligomers, and Inflammation', *Journal of Alzheimer's Disease*, 62(3), pp. 1261–1276. Available at: https://doi.org/10.3233/JAD-170819.

Foster, E.M. *et al.* (2019) 'Clusterin in Alzheimer's Disease: Mechanisms, Genetics, and Lessons From Other Pathologies', *Frontiers in Neuroscience*, 13. Available at: https://www.frontiersin.org/articles/10.3389/fnins.2019.00164 (Accessed: 31 March 2023).

Frederiksen, H.R. *et al.* (2021) 'Non-immunogenic Induced Pluripotent Stem Cells, a Promising Way Forward for Allogenic Transplantations for Neurological Disorders', *Frontiers in Genome Editing*, 2. Available at: https://www.frontiersin.org/articles/10.3389/fgeed.2020.623717 (Accessed: 9 January 2023).

Fu, H., Hardy, J. and Duff, K.E. (2018) 'Selective vulnerability in neurodegenerative diseases', *Nature Neuroscience*, 21(10), pp. 1350–1358. Available at: https://doi.org/10.1038/s41593-018-0221-2.

Gabbouj, S. *et al.* (2019) 'Altered Insulin Signaling in Alzheimer's Disease Brain – Special Emphasis on PI3K-Akt Pathway', *Frontiers in Neuroscience*, 13. Available at: https://www.frontiersin.org/articles/10.3389/fnins.2019.00629 (Accessed: 13 February 2023).

Gadhave, K. *et al.* (2020) 'The dark side of Alzheimer's disease: unstructured biology of proteins from the amyloid cascade signaling pathway', *Cellular and Molecular Life Sciences*, 77(20), pp. 4163–4208. Available at: https://doi.org/10.1007/s00018-019-03414-9.

Gao, P. *et al.* (2021) 'The Mechanistic Role of Bridging Integrator 1 (BIN1) in Alzheimer's Disease', *Cellular and Molecular Neurobiology*, 41(7), pp. 1431–1440. Available at: https://doi.org/10.1007/s10571-020-00926-y.

García-Casares, N. *et al.* (2014) 'Structural and Functional Brain Changes in Middle-Aged Type 2 Diabetic Patients: A Cross-Sectional Study', *Journal of Alzheimer's Disease*, 40(2), pp. 375–386. Available at: https://doi.org/10.3233/JAD-131736.

Gatz, M. *et al.* (2006) 'Role of Genes and Environments for Explaining Alzheimer Disease', *Archives of General Psychiatry*, 63(2), p. 168. Available at: https://doi.org/10.1001/archpsyc.63.2.168.

Gaudelli, N.M. *et al.* (2017) 'Programmable base editing of A•T to G•C in genomic DNA without DNA cleavage', *Nature*, 551(7681), pp. 464–471. Available at: https://doi.org/10.1038/nature24644.

Ge, W.-Y. *et al.* (2023) 'Amyloid Protein Cross-Seeding Provides a New Perspective on Multiple Diseases *In Vivo*', *Biomacromolecules*, 24(1), pp. 1–18. Available at: https://doi.org/10.1021/acs.biomac.2c01233.

Ghasemi, R. *et al.* (2013) 'Insulin in the Brain: Sources, Localization and Functions', *Molecular Neurobiology*, 47(1), pp. 145–171. Available at: https://doi.org/10.1007/s12035-012-8339-9.

Giacobini, E., Cuello, A.C. and Fisher, A. (2022) 'Reimagining cholinergic therapy for Alzheimer's disease', *Brain*, 145(7), pp. 2250–2275. Available at: https://doi.org/10.1093/brain/awac096.

Ginsberg, S.D. *et al.* (2006) 'Down regulation of trk but not p75NTR gene expression in single cholinergic basal forebrain neurons mark the progression of Alzheimer's disease', *Journal of Neurochemistry*, 97(2), pp. 475–487. Available at: https://doi.org/10.1111/j.1471-4159.2006.03764.x.

Giuffrida, M.L. *et al.* (2015) 'Monomeric ß-amyloid interacts with type-1 insulin-like growth factor receptors to provide energy supply to neurons', *Frontiers in Cellular Neuroscience*, 9. Available at: https://www.frontiersin.org/articles/10.3389/fncel.2015.00297 (Accessed: 10 March 2023).

Glerup, S. *et al.* (2013) 'SorLA Controls Neurotrophic Activity by Sorting of GDNF and Its Receptors GFRα1 and RET', *Cell Reports*, 3(1), pp. 186–199. Available at: https://doi.org/10.1016/j.celrep.2012.12.011.

Goard, M. and Dan, Y. (2009) 'Basal Forebrain Activation Enhances Cortical Coding of Natural Scenes', *Nature neuroscience*, 12(11), pp. 1444–1449. Available at: https://doi.org/10.1038/nn.2402.

Gomez-Arboledas, A. *et al.* (2018) 'Phagocytic clearance of presynaptic dystrophies by reactive astrocytes in Alzheimer's disease', *Glia*, 66(3), pp. 637–653. Available at: https://doi.org/10.1002/glia.23270.

Gómez-Isla, T. and Frosch, M.P. (2022) 'Lesions without symptoms: understanding resilience to Alzheimer disease neuropathological changes', *Nature Reviews Neurology*, 18(6), pp. 323–332. Available at: https://doi.org/10.1038/s41582-022-00642-9.

González-Domínguez, R. *et al.* (2021) 'Mechanistic Insights into Alzheimer's Disease Unveiled through the Investigation of Disturbances in Central Metabolites and Metabolic Pathways', *Biomedicines*, 9(3), p. 298. Available at: https://doi.org/10.3390/biomedicines9030298.

Gooz, M. (2010) 'ADAM-17: the enzyme that does it all', *Critical Reviews in Biochemistry and Molecular Biology*, 45(2), pp. 146–169. Available at: https://doi.org/10.3109/10409231003628015.

Gordon, B.A. *et al.* (2018) 'Spatial patterns of neuroimaging biomarker change in individuals from families with autosomal dominant Alzheimer's disease: a longitudinal study', *The Lancet Neurology*, 17(3), pp. 241–250. Available at: https://doi.org/10.1016/S1474-4422(18)30028-0.

Götz, A. *et al.* (2019) 'Increased H-Bond Stability Relates to Altered ε-Cleavage Efficiency and Aβ Levels in the I45T Familial Alzheimer's Disease Mutant of APP', *Scientific Reports*, 9(1), p. 5321. Available at: https://doi.org/10.1038/s41598-019-41766-1.

Goulburn, A.L. *et al.* (2011) 'A Targeted NKX2.1 Human Embryonic Stem Cell Reporter Line Enables Identification of Human Basal Forebrain Derivatives', *Stem Cells*, 29(3), pp. 462–473. Available at: https://doi.org/10.1002/stem.587.

Graff-Radford, J. *et al.* (2021) 'New insights into atypical Alzheimer's disease in the era of biomarkers', *The Lancet Neurology*, 20(3), pp. 222–234. Available at: https://doi.org/10.1016/S1474-4422(20)30440-3.

Graham, S.F. *et al.* (2015) 'Untargeted Metabolomic Analysis of Human Plasma Indicates Differentially Affected Polyamine and L-Arginine Metabolism in Mild Cognitive Impairment Subjects Converting to Alzheimer's Disease', *PLOS ONE*, 10(3), p. e0119452. Available at: https://doi.org/10.1371/journal.pone.0119452.

Grell, M. *et al.* (1995) 'The transmembrane form of tumor necrosis factor is the prime activating ligand of the 80 kDa tumor necrosis factor receptor', *Cell*, 83(5), pp. 793–802. Available at: https://doi.org/10.1016/0092-8674(95)90192-2.

Griffith, C.M. *et al.* (2018) 'Evidence for altered insulin receptor signaling in Alzheimer's disease', *Neuropharmacology*, 136, pp. 202–215. Available at: https://doi.org/10.1016/j.neuropharm.2018.01.008.

Guiraud, S.P. *et al.* (2017) 'High-throughput and simultaneous quantitative analysis of homocysteine–methionine cycle metabolites and co-factors in blood plasma and cerebrospinal fluid by isotope dilution LC–MS/MS', *Analytical and Bioanalytical Chemistry*, 409(1), pp. 295–305. Available at: https://doi.org/10.1007/s00216-016-0003-1.

Guo, T. *et al.* (2020) 'Molecular and cellular mechanisms underlying the pathogenesis of Alzheimer's disease', *Molecular Neurodegeneration*, 15(1), p. 40. Available at: https://doi.org/10.1186/s13024-020-00391-7.

Guo, W. *et al.* (2011) 'An ALS-associated mutation affecting TDP-43 enhances protein aggregation, fibril formation and neurotoxicity', *Nature Structural & Molecular Biology*, 18(7), pp. 822–830. Available at: https://doi.org/10.1038/nsmb.2053.

Hall, A.M. *et al.* (2008) 'Basal forebrain atrophy is a presymptomatic marker for Alzheimer's disease', *Alzheimer's & Dementia*, 4(4), pp. 271–279. Available at: https://doi.org/10.1016/j.jalz.2008.04.005.

Hampel, H. *et al.* (2018) 'REVISITING THE CHOLINERGIC HYPOTHESIS IN ALZHEIMER'S DISEASE: EMERGING EVIDENCE FROM TRANSLATIONAL AND CLINICAL RESEARCH', *The Journal Of Prevention of Alzheimer's Disease*, pp. 1–14. Available at: https://doi.org/10.14283/jpad.2018.43.

Hampel, H., Nisticò, R., *et al.* (2021) 'Omics sciences for systems biology in Alzheimer's disease: State-of-the-art of the evidence', *Ageing Research Reviews*, 69, p. 101346. Available at: https://doi.org/10.1016/j.arr.2021.101346.

Hampel, H., Hardy, J., *et al.* (2021) 'The Amyloid-β Pathway in Alzheimer's Disease', *Molecular Psychiatry*, 26(10), pp. 5481–5503. Available at: https://doi.org/10.1038/s41380-021-01249-0.

Hanseeuw, B.J. *et al.* (2019) 'Association of Amyloid and Tau With Cognition in Preclinical Alzheimer Disease: A Longitudinal Study', *JAMA Neurology*, 76(8), pp. 915–924. Available at: https://doi.org/10.1001/jamaneurol.2019.1424.

Hao, Y. *et al.* (2021) 'Integrated analysis of multimodal single-cell data', *Cell*, 184(13), pp. 3573-3587.e29. Available at: https://doi.org/10.1016/j.cell.2021.04.048.

Harold, D. *et al.* (2009) 'Genome-wide association study identifies variants at CLU and PICALM associated with Alzheimer's disease', *Nature Genetics*, 41(10), pp. 1088–1093. Available at: https://doi.org/10.1038/ng.440.

Harris, S.S. *et al.* (2020) 'Tipping the Scales: Peptide-Dependent Dysregulation of Neural Circuit Dynamics in Alzheimer's Disease', *Neuron*, 107(3), pp. 417–435. Available at: https://doi.org/10.1016/j.neuron.2020.06.005.

Hartl, D. *et al.* (2018) 'A rare loss-of-function variant of ADAM17 is associated with late-onset familial Alzheimer disease', *Molecular Psychiatry* [Preprint]. Available at: https://doi.org/10.1038/s41380-018-0091-8.

He, Z. *et al.* (2018) 'Amyloid-β plaques enhance Alzheimer's brain tau-seeded pathologies by facilitating neuritic plaque tau aggregation', *Nature Medicine*, 24(1), pp. 29–38. Available at: https://doi.org/10.1038/nm.4443.

Hendrie, H.C. *et al.* (2018) 'The Association of Early Life Factors and Declining Incidence Rates of Dementia in an Elderly Population of African Americans', *The Journals of Gerontology: Series B*, 73(suppl_1), pp. S82–S89. Available at: https://doi.org/10.1093/geronb/gbx143.

Heneka, M.T. *et al.* (2015) 'Neuroinflammation in Alzheimer's disease', *The Lancet Neurology*, 14(4), pp. 388–405. Available at: https://doi.org/10.1016/S1474-4422(15)70016-5.

Henjum, K. *et al.* (2018) 'CSF sTREM2 in delirium—relation to Alzheimer's disease CSF biomarkers Aβ42, t-tau and p-tau', *Journal of Neuroinflammation*, 15(1), p. 304. Available at: https://doi.org/10.1186/s12974-018-1331-1.

Hollmann, P. (2022) 'Update: FDA approval of Biogen's aducanumab', *Geriatric Nursing*, 43, pp. 318–319. Available at: https://doi.org/10.1016/j.gerinurse.2021.12.018.

Hoogmartens, J., Cacace, R. and Van Broeckhoven, C. (2021) 'Insight into the genetic etiology of Alzheimer's disease: A comprehensive review of the role of rare variants', *Alzheimer's & Dementia: Diagnosis, Assessment & Disease Monitoring*, 13(1), p. e12155. Available at: https://doi.org/10.1002/dad2.12155.

Horgusluoglu, E. *et al.* (2022) 'Integrative metabolomics-genomics approach reveals key metabolic pathways and regulators of Alzheimer's disease', *Alzheimer's & Dementia*, 18(6), pp. 1260–1278. Available at: https://doi.org/10.1002/alz.12468.

Hou, J. *et al.* (2022) 'TREM2 dependent and independent functions of microglia in Alzheimer's disease', *Molecular Neurodegeneration*, 17(1), p. 84. Available at: https://doi.org/10.1186/s13024-022-00588-y.

Hu, B.-Y. *et al.* (2010) 'Neural differentiation of human induced pluripotent stem cells follows developmental principles but with variable potency', *Proceedings of the National Academy of Sciences of the United States of America*, 107(9), pp. 4335–4340. Available at: https://doi.org/10.1073/pnas.0910012107.

Huang, Y.-W.A. *et al.* (2017) 'ApoE2, ApoE3, and ApoE4 Differentially Stimulate APP Transcription and Aβ Secretion', *Cell*, 168(3), pp. 427-441.e21. Available at: https://doi.org/10.1016/j.cell.2016.12.044.

Huang, Z. *et al.* (2020) 'Blood-brain barrier integrity in the pathogenesis of Alzheimer's disease', *Frontiers in Neuroendocrinology*, 59, p. 100857. Available at: https://doi.org/10.1016/j.yfrne.2020.100857.

Imbimbo, B.P. *et al.* (2022) 'Should we lower or raise levels of amyloid-β in the brains of Alzheimer patients?', *Pharmacological Research*, 183, p. 106390. Available at: https://doi.org/10.1016/j.phrs.2022.106390.

Iturria-Medina, Y. *et al.* (2022) 'Unified epigenomic, transcriptomic, proteomic, and metabolomic taxonomy of Alzheimer's disease progression and heterogeneity', *Science Advances*, 8(46), p. eabo6764. Available at: https://doi.org/10.1126/sciadv.abo6764.

Ivanov, S.M. *et al.* (2020) 'Cellular polyamines condense hyperphosphorylated Tau, triggering Alzheimer's disease', *Scientific Reports*, 10(1), p. 10098. Available at: https://doi.org/10.1038/s41598-020-67119-x.

Iwata, R. and Vanderhaeghen, P. (2021) 'Regulatory roles of mitochondria and metabolism in neurogenesis', *Current Opinion in Neurobiology*, 69, pp. 231–240. Available at: https://doi.org/10.1016/j.conb.2021.05.003.

Jack, C.R. *et al.* (2018) 'NIA-AA Research Framework: Toward a biological definition of Alzheimer's disease', *Alzheimer's & Dementia*, 14(4), pp. 535–562. Available at: https://doi.org/10.1016/j.jalz.2018.02.018.

Jarazo, J., Qing, X. and Schwamborn, J.C. (2019) 'Guidelines for Fluorescent Guided Biallelic HDR Targeting Selection With PiggyBac System Removal for Gene Editing', *Frontiers in Genetics*, 10, p. 190. Available at: https://doi.org/10.3389/fgene.2019.00190.

Jay, T.R. *et al.* (2017) 'Disease Progression-Dependent Effects of TREM2 Deficiency in a Mouse Model of Alzheimer's Disease', *Journal of Neuroscience*, 37(3), pp. 637–647. Available at: https://doi.org/10.1523/JNEUROSCI.2110-16.2016.

Jayaswamy, P.K. *et al.* (2023) 'Implicative role of epidermal growth factor receptor and its associated signaling partners in the pathogenesis of Alzheimer's disease', *Ageing Research Reviews*, 83, p. 101791. Available at: https://doi.org/10.1016/j.arr.2022.101791.

Jiang, X. *et al.* (2009) 'Isolation and Characterization of Neural Crest Stem Cells Derived From In Vitro–Differentiated Human Embryonic Stem Cells', *Stem Cells and Development*, 18(7), pp. 1059–1071. Available at: https://doi.org/10.1089/scd.2008.0362.

Jinek, M. *et al.* (2013) 'RNA-programmed genome editing in human cells', *eLife*. Edited by D. Weigel, 2, p. e00471. Available at: https://doi.org/10.7554/eLife.00471.

Jónsdóttir, M.K., Harrison, J. and Hannesdóttir, K.I. (2023) 'The ambivalence toward neuropsychology in dementia research, diagnosis, and drug development: Myths and misconceptions', *Alzheimer's & Dementia*, p. alz.12909. Available at: https://doi.org/10.1002/alz.12909.

Jonsson, T. *et al.* (2012) 'A mutation in APP protects against Alzheimer's disease and age-related cognitive decline', *Nature*, 488(7409), pp. 96–99. Available at: https://doi.org/10.1038/nature11283.

Joshi, A.U. *et al.* (2019) 'Fragmented mitochondria released from microglia trigger A1 astrocytic response and propagate inflammatory neurodegeneration', *Nature Neuroscience*, 22(10), pp. 1635–1648. Available at: https://doi.org/10.1038/s41593-019-0486-0.

Kamboh, M.I. (2022) 'Genomics and Functional Genomics of Alzheimer's Disease', *Neurotherapeutics*, 19(1), pp. 152–172. Available at: https://doi.org/10.1007/s13311-021-01152-0.

Kapoor, A. and Nation, D.A. (2021) 'Role of Notch signaling in neurovascular aging and Alzheimer's disease', *Seminars in Cell & Developmental Biology*, 116, pp. 90–97. Available at: https://doi.org/10.1016/j.semcdb.2020.12.011.

Kerr, J.S. *et al.* (2017) 'Mitophagy and Alzheimer's Disease: Cellular and Molecular Mechanisms', *Trends in Neurosciences*, 40(3), pp. 151–166. Available at: https://doi.org/10.1016/j.tins.2017.01.002.

Khan, S., Barve, K.H. and Kumar, M.S. (2020) 'Recent Advancements in Pathogenesis, Diagnostics and Treatment of Alzheimer's Disease', *Current Neuropharmacology*, 18(11), pp. 1106–1125. Available at: https://doi.org/10.2174/1570159X18666200528142429.

Kim, D.-Y., Rhee, I. and Paik, J. (2014) 'Metabolic circuits in neural stem cells', *Cellular and Molecular Life Sciences*, 71(21), pp. 4221–4241. Available at: https://doi.org/10.1007/s00018-014-1686-0.

Kim, K. *et al.* (2010) 'Epigenetic memory in induced pluripotent stem cells', *Nature*, 467(7313), pp. 285–290. Available at: https://doi.org/10.1038/nature09342.

Knupp, A. *et al.* (2020) 'Depletion of the AD Risk Gene SORL1 Selectively Impairs Neuronal Endosomal Traffic Independent of Amyloidogenic APP Processing', *Cell Reports*, 31(9), p. 107719. Available at: https://doi.org/10.1016/j.celrep.2020.107719.

Komor, A.C. *et al.* (2016) 'Programmable editing of a target base in genomic DNA without double-stranded DNA cleavage', *Nature*, 533(7603), pp. 420–424. Available at: https://doi.org/10.1038/nature17946.

Kriks, S. *et al.* (2011) 'Dopamine neurons derived from human ES cells efficiently engraft in animal models of Parkinson's disease', *Nature*, 480(7378), pp. 547–551. Available at: https://doi.org/10.1038/nature10648.

Kuhn, P.-H. *et al.* (2010) 'ADAM10 is the physiologically relevant, constitutive α-secretase of the amyloid precursor protein in primary neurons', *The EMBO Journal*, 29(17), pp. 3020–3032. Available at: https://doi.org/10.1038/emboj.2010.167.

Kulas, J.A., Weigel, T.K. and Ferris, H.A. (2020) 'Insulin resistance and impaired lipid metabolism as a potential link between diabetes and Alzheimer's disease', *Drug Development Research*, 81(2), pp. 194–205. Available at: https://doi.org/10.1002/ddr.21643.

Kumar, R. *et al.* (2015) 'Increased *STAG2* dosage defines a novel cohesinopathy with intellectual disability and behavioral problems', *Human Molecular Genetics*, 24(25), pp. 7171–7181. Available at: https://doi.org/10.1093/hmg/ddv414.

Kunkle, B.W. *et al.* (2019) 'Genetic meta-analysis of diagnosed Alzheimer's disease identifies new risk loci and implicates Aβ, tau, immunity and lipid processing', *Nature Genetics*, 51(3), pp. 414–430. Available at: https://doi.org/10.1038/s41588-019-0358-2.

Künzel, U. *et al.* (2018) 'FRMD8 promotes inflammatory and growth factor signalling by stabilising the iRhom/ADAM17 sheddase complex', *eLife*. Edited by C.G. Burd, 7, p. e35012. Available at: https://doi.org/10.7554/eLife.35012.

LaFerla, F.M., Green, K.N. and Oddo, S. (2007) 'Intracellular amyloid-β in Alzheimer's disease', *Nature Reviews Neuroscience*, 8(7), pp. 499–509. Available at: https://doi.org/10.1038/nrn2168.

Lambert, J.-C. *et al.* (2009) 'Genome-wide association study identifies variants at CLU and CR1 associated with Alzheimer's disease', *Nature Genetics*, 41(10), pp. 1094–1099. Available at: https://doi.org/10.1038/ng.439.

Lambert, J.-C. *et al.* (2013) 'Meta-analysis of 74,046 individuals identifies 11 new susceptibility loci for Alzheimer's disease', *Nature Genetics*, 45(12), pp. 1452–1458. Available at: https://doi.org/10.1038/ng.2802.

Lambrecht, B.N., Vanderkerken, M. and Hammad, H. (2018) 'The emerging role of ADAM metalloproteinases in immunity', *Nature Reviews Immunology*, 18(12), pp. 745–758. Available at: https://doi.org/10.1038/s41577-018-0068-5.

Lee, B. *et al.* (2013) 'Genomic code for Sox2 binding uncovers its regulatory role in Six3 activation in the forebrain', *Developmental Biology*, 381(2), pp. 491–501. Available at: https://doi.org/10.1016/j.ydbio.2013.06.016.

Lee, R. *et al.* (2001) 'Regulation of Cell Survival by Secreted Proneurotrophins', *Science*, 294(5548), pp. 1945–1948. Available at: https://doi.org/10.1126/science.1065057.

Lenz, K.M. and Nelson, L.H. (2018) 'Microglia and Beyond: Innate Immune Cells As Regulators of Brain Development and Behavioral Function', *Frontiers in Immunology*, 9. Available at: https://www.frontiersin.org/articles/10.3389/fimmu.2018.00698 (Accessed: 30 March 2023).

Lichtenthaler, S.F., Tschirner, S.K. and Steiner, H. (2022) 'Secretases in Alzheimer's disease: Novel insights into proteolysis of APP and TREM2', *Current Opinion in Neurobiology*, 72, pp. 101–110. Available at: https://doi.org/10.1016/j.conb.2021.09.003.

Lim, E.W. *et al.* (2019) 'Amyloid-β and Parkinson's disease', *Journal of Neurology*, 266(11), pp. 2605–2619. Available at: https://doi.org/10.1007/s00415-018-9100-8.

Lisik, M.Z. and Sieron, A.L. (2008) 'X-linked mental retardation', *Med Sci Monit* [Preprint].

Liu, J.Z., Erlich, Y. and Pickrell, J.K. (2017) 'Case–control association mapping by proxy using family history of disease', *Nature Genetics*, 49(3), pp. 325–331. Available at: https://doi.org/10.1038/ng.3766.

Liu, W. *et al.* (2011) 'Pink1 regulates the oxidative phosphorylation machinery via mitochondrial fission', *Proceedings of the National Academy of Sciences*, 108(31), pp. 12920–12924. Available at: https://doi.org/10.1073/pnas.1107332108.

Liu, X. *et al.* (2020) 'SOX1 Is Required for the Specification of Rostral Hindbrain Neural Progenitor Cells from Human Embryonic Stem Cells', *iScience*, 23(9), p. 101475. Available at: https://doi.org/10.1016/j.isci.2020.101475.

Lopez-Rodriguez, A.B. *et al.* (2021) 'Acute systemic inflammation exacerbates neuroinflammation in Alzheimer's disease: IL-1β drives amplified responses in primed astrocytes and neuronal network dysfunction', *Alzheimer's & Dementia*, 17(10), pp. 1735–1755. Available at: https://doi.org/10.1002/alz.12341.

Lord, A. *et al.* (2009) 'Amyloid-β protofibril levels correlate with spatial learning in Arctic Alzheimer's disease transgenic mice', *The FEBS Journal*, 276(4), pp. 995–1006. Available at: https://doi.org/10.1111/j.1742-4658.2008.06836.x.

Lourenco, M.V. *et al.* (2013) 'TNF-α Mediates PKR-Dependent Memory Impairment and Brain IRS-1 Inhibition Induced by Alzheimer's β-Amyloid Oligomers in Mice and Monkeys', *Cell Metabolism*, 18(6), pp. 831–843. Available at: https://doi.org/10.1016/j.cmet.2013.11.002.

Loy, C.T. *et al.* (2014) 'Genetics of dementia', *The Lancet*, 383(9919), pp. 828–840. Available at: https://doi.org/10.1016/S0140-6736(13)60630-3.

Lu, Y., Pang, Z. and Xia, J. (2023) 'Comprehensive investigation of pathway enrichment methods for functional interpretation of LC–MS global metabolomics data', *Briefings in Bioinformatics*, 24(1), p. bbac553. Available at: https://doi.org/10.1093/bib/bbac553.

Ma, S. *et al.* (2020) 'Aging-relevant human basal forebrain cholinergic neurons as a cell model for Alzheimer's disease', *Molecular Neurodegeneration*, 15, p. 61. Available at: https://doi.org/10.1186/s13024-020-00411-6.

Macosko, E.Z. *et al.* (2015) 'Highly Parallel Genome-wide Expression Profiling of Individual Cells Using Nanoliter Droplets', *Cell*, 161(5), pp. 1202–1214. Available at: https://doi.org/10.1016/j.cell.2015.05.002.

Madeo, F. *et al.* (2018) 'Spermidine in health and disease', *Science*, 359(6374), p. eaan2788. Available at: https://doi.org/10.1126/science.aan2788.

Mahajan, U.V. *et al.* (2020) 'Dysregulation of multiple metabolic networks related to brain transmethylation and polyamine pathways in Alzheimer disease: A targeted metabolomic and transcriptomic study', *PLOS Medicine*, 17(1), p. e1003012. Available at: https://doi.org/10.1371/journal.pmed.1003012.

Mali, P. *et al.* (2013) 'CAS9 transcriptional activators for target specificity screening and paired nickases for cooperative genome engineering', *Nature Biotechnology*, 31(9), pp. 833–838. Available at: https://doi.org/10.1038/nbt.2675.

Maretzky, T. *et al.* (2013) 'iRhom2 controls the substrate selectivity of stimulated ADAM17-dependent ectodomain shedding', *Proceedings of the National Academy of Sciences*, 110(28), pp. 11433–11438. Available at: https://doi.org/10.1073/pnas.1302553110.

Marsh, S.E. and Blurton-Jones, M. (2012) 'Examining the mechanisms that link β-amyloid and α-synuclein pathologies', *Alzheimer's Research & Therapy*, 4(2), p. 11. Available at: https://doi.org/10.1186/alzrt109.

Mathys, H. *et al.* (2019) 'Single-cell transcriptomic analysis of Alzheimer's disease', *Nature*, 570(7761), pp. 332–337. Available at: https://doi.org/10.1038/s41586-019-1195-2.

Maurano, M.T. *et al.* (2012) 'Systematic Localization of Common Disease-Associated Variation in Regulatory DNA', *Science*, 337(6099), pp. 1190–1195. Available at: https://doi.org/10.1126/science.1222794.

McAvoy, K.M. *et al.* (2019) 'Cell-autonomous and non-cell autonomous effects of neuronal BIN1 loss in vivo', *PLOS ONE*, 14(8), p. e0220125. Available at: https://doi.org/10.1371/journal.pone.0220125.

McDade, E. *et al.* (2018) 'Longitudinal cognitive and biomarker changes in dominantly inherited Alzheimer disease', *Neurology*, 91(14), pp. e1295–e1306. Available at: https://doi.org/10.1212/WNL.0000000000006277.

McGirr, S., Venegas, C. and Swaminathan, A. (2020) 'Alzheimers Disease: A Brief Review', *Journal of Experimental Neurology*, Volume 1(Issue 3), pp. 89–98. Available at: https://doi.org/10.33696/Neurol.1.015.

Medway, C. and Morgan, K. (2014) 'Review: The genetics of Alzheimer's disease; putting flesh on the bones: The genetics of Alzheimer's disease', *Neuropathology and Applied Neurobiology*, 40(2), pp. 97–105. Available at: https://doi.org/10.1111/nan.12101.

Meeker, R. and Williams, K. (2015) 'The p75 neurotrophin receptor: at the crossroad of neural repair and death', *Neural Regeneration Research*, 10(5), p. 721. Available at: https://doi.org/10.4103/1673-5374.156967.

Menéndez-González, M. (2023) 'Toward a new nosology of neurodegenerative diseases', *Alzheimer's & Dementia*, p. alz.13041. Available at: https://doi.org/10.1002/alz.13041.

Mesulam, M. *et al.* (2004) 'Cholinergic nucleus basalis tauopathy emerges early in the aging-MCI-AD continuum', *Annals of Neurology*, 55(6), pp. 815–828. Available at: https://doi.org/10.1002/ana.20100.

Miller, J.D. *et al.* (2013) 'Human iPSC-Based Modeling of Late-Onset Disease via Progerin-Induced Aging', *Cell Stem Cell*, 13(6), pp. 691–705. Available at: https://doi.org/10.1016/j.stem.2013.11.006.

Mitchell, R.A., Luwor, R.B. and Burgess, A.W. (2018) 'Epidermal growth factor receptor: Structure-function informing the design of anticancer therapeutics', *Experimental Cell Research*, 371(1), pp. 1–19. Available at: https://doi.org/10.1016/j.yexcr.2018.08.009.

Miyagawa, T. *et al.* (2016) 'BIN1 regulates BACE1 intracellular trafficking and amyloid-β production', *Human Molecular Genetics*, p. ddw146. Available at: https://doi.org/10.1093/hmg/ddw146.

Modamio, J. *et al.* (2021) 'Synaptic decline precedes dopaminergic neuronal loss in human midbrain organoids harboring a triplication of the SNCA gene'. bioRxiv, p. 2021.07.15.452499. Available at: https://doi.org/10.1101/2021.07.15.452499.

Montagne, A., Zhao, Z. and Zlokovic, B.V. (2017) 'Alzheimer's disease: A matter of blood–brain barrier dysfunction?', *Journal of Experimental Medicine*, 214(11), pp. 3151–3169. Available at: https://doi.org/10.1084/jem.20171406.

de la Monte, S.M. and Wands, J.R. (2008) 'Alzheimer's Disease is Type 3 Diabetes—Evidence Reviewed', *Journal of Diabetes Science and Technology*, 2(6), pp. 1101–1113. Available at: https://doi.org/10.1177/193229680800200619.

Moreno-Jiménez, E.P. *et al.* (2019) 'Adult hippocampal neurogenesis is abundant in neurologically healthy subjects and drops sharply in patients with Alzheimer's disease', *Nature Medicine*, 25(4), pp. 554–560. Available at: https://doi.org/10.1038/s41591-019-0375-9.

Morley, J.E. *et al.* (2019) 'What is the Physiological Function of Amyloid-Beta Protein?', *The journal of nutrition, health & aging*, 23(3), pp. 225–226. Available at: https://doi.org/10.1007/s12603-019-1162-5.

Mostafavi, S. *et al.* (2018) 'A molecular network of the aging human brain provides insights into the pathology and cognitive decline of Alzheimer's disease', *Nature Neuroscience*, 21(6), pp. 811–819. Available at: https://doi.org/10.1038/s41593-018-0154-9.

Mucke, L. and Selkoe, D.J. (2012) 'Neurotoxicity of Amyloid β-Protein: Synaptic and Network Dysfunction', *Cold Spring Harbor Perspectives in Medicine*, 2(7), p. a006338. Available at: https://doi.org/10.1101/cshperspect.a006338.

Mukai, J. *et al.* (2000) 'NADE, a p75NTR-associated Cell Death Executor, Is Involved in Signal Transduction Mediated by the Common Neurotrophin Receptor p75NTR', *Journal of Biological Chemistry*, 275(23), pp. 17566–17570. Available at: https://doi.org/10.1074/jbc.C000140200.

Mukai, J. *et al.* (2002) 'Structure-Function Analysis of NADE: IDENTIFICATION OF REGIONS THAT MEDIATE NERVE GROWTH FACTOR-INDUCED APOPTOSIS*', *Journal of Biological Chemistry*, 277(16), pp. 13973–13982. Available at: https://doi.org/10.1074/jbc.M106342200.

Murdaca, G. *et al.* (2022) 'Neuro-Inflammaging and Psychopathological Distress', *Biomedicines*, 10(9), p. 2133. Available at: https://doi.org/10.3390/biomedicines10092133.

Naj, A.C., Schellenberg, G.D., and for the Alzheimer's Disease Genetics Consortium (ADGC) (2017) 'Genomic variants, genes, and pathways of Alzheimer's disease: An overview', *American Journal of Medical Genetics Part B: Neuropsychiatric Genetics*, 174(1), pp. 5–26. Available at: https://doi.org/10.1002/ajmg.b.32499.

Narayan, P. *et al.* (2020) 'PICALM Rescues Endocytic Defects Caused by the Alzheimer's Disease Risk Factor APOE4', *Cell Reports*, 33(1), p. 108224. Available at: https://doi.org/10.1016/j.celrep.2020.108224.

Ni, J. *et al.* (2020) 'Significant improvement in data quality with simplified SCRB-seq', *Acta Biochimica et Biophysica Sinica*, 52(4), pp. 457–459. Available at: https://doi.org/10.1093/abbs/gmaa007.

Nicolas, G. *et al.* (2016) 'SORL1 rare variants: a major risk factor for familial early-onset Alzheimer's disease', *Molecular Psychiatry*, 21(6), pp. 831–836. Available at: https://doi.org/10.1038/mp.2015.121.

Nishimura, A. *et al.* (2017) 'Characterization of APOE and TOMM40 allele frequencies in the Japanese population', *Alzheimer's & Dementia : Translational Research & Clinical Interventions*, 3(4), pp. 524–530. Available at: https://doi.org/10.1016/j.trci.2017.07.003.

Norton, S. *et al.* (2014) 'Potential for primary prevention of Alzheimer's disease: an analysis of population-based data', *The Lancet Neurology*, 13(8), pp. 788–794. Available at: https://doi.org/10.1016/S1474-4422(14)70136-X.

Novak, G. *et al.* (2022) 'Single-cell transcriptomics of human iPSC differentiation dynamics reveal a core molecular network of Parkinson's disease', *Communications Biology*, 5(1), p. 49. Available at: https://doi.org/10.1038/s42003-021-02973-7.

Okumura, T. *et al.* (2003) 'Neurotrophin receptor p75NTR characterizes human esophageal keratinocyte stem cells in vitro', *Oncogene*, 22(26), pp. 4017–4026. Available at: https://doi.org/10.1038/sj.onc.1206525.

O'Nuallain, B. *et al.* (2010) 'Amyloid β-Protein Dimers Rapidly Form Stable Synaptotoxic Protofibrils', *The Journal of Neuroscience*, 30(43), pp. 14411–14419. Available at: https://doi.org/10.1523/JNEUROSCI.3537-10.2010.

Onyango, I.G. *et al.* (2021) 'Neuroinflammation in Alzheimer's Disease', *Biomedicines*, 9(5), p. 524. Available at: https://doi.org/10.3390/biomedicines9050524.

Ortiz-Virumbrales, M. *et al.* (2017) 'CRISPR/Cas9-Correctable mutation-related molecular and physiological phenotypes in iPSC-derived Alzheimer's PSEN2 N141I neurons', *Acta Neuropathologica Communications*, 5(1), p. 77. Available at: https://doi.org/10.1186/s40478-017-0475-z.

Osorio, D. and Cai, J.J. (2021) 'Systematic determination of the mitochondrial proportion in human and mice tissues for single-cell RNA-sequencing data quality control', *Bioinformatics*. Edited by A. Mathelier, 37(7), pp. 963–967. Available at: https://doi.org/10.1093/bioinformatics/btaa751.

Ovsepian, S.V. *et al.* (2014) 'Neurotrophin receptor p75 mediates the uptake of the amyloid beta (Aβ) peptide, guiding it to lysosomes for degradation in basal forebrain cholinergic neurons', *Brain Structure and Function*, 219(5), pp. 1527–1541. Available at: https://doi.org/10.1007/s00429-013-0583-x.

Oyarzabal, A. and Marin-Valencia, I. (2019) 'Synaptic energy metabolism and neuronal excitability, in sickness and health', *Journal of Inherited Metabolic Disease*, 42(2), pp. 220–236. Available at: https://doi.org/10.1002/jimd.12071.

Paglia, G. *et al.* (2016) 'Unbiased Metabolomic Investigation of Alzheimer's Disease Brain Points to Dysregulation of Mitochondrial Aspartate Metabolism', *Journal of Proteome Research*, 15(2), pp. 608–618. Available at: https://doi.org/10.1021/acs.jproteome.5b01020.

Pan, X. *et al.* (2016) 'Alzheimer's disease–like pathology has transient effects on the brain and blood metabolome', *Neurobiology of Aging*, 38, pp. 151–163. Available at: https://doi.org/10.1016/j.neurobiolaging.2015.11.014.

Paolicelli, R.C. *et al.* (2011) 'Synaptic Pruning by Microglia Is Necessary for Normal Brain Development', *Science*, 333(6048), pp. 1456–1458. Available at: https://doi.org/10.1126/science.1202529.

Pavlenko, E. *et al.* (2019) 'Functional Characterization of Colon Cancer-Associated Mutations in ADAM17: Modifications in the Pro-Domain Interfere with Trafficking and Maturation', *International Journal of Molecular Sciences*, 20(9), p. 2198. Available at: https://doi.org/10.3390/ijms20092198.

Pedersen, T.L. (2022) *patchwork: The Composer of Plots*. Available at: https://CRAN.R-project.org/package=patchwork.

Pegg, A.E. (2014) 'The function of spermine', *IUBMB Life*, 66(1), pp. 8–18. Available at: https://doi.org/10.1002/iub.1237.

Perry, V.H. and Holmes, C. (2014) 'Microglial priming in neurodegenerative disease', *Nature Reviews Neurology*, 10(4), pp. 217–224. Available at: https://doi.org/10.1038/nrneurol.2014.38.

Picelli, S. *et al.* (2013) 'Smart-seq2 for sensitive full-length transcriptome profiling in single cells', *Nature Methods*, 10(11), pp. 1096–1098. Available at: https://doi.org/10.1038/nmeth.2639.

Piché, J. *et al.* (2019) 'The expanding phenotypes of cohesinopathies: one ring to rule them all!', *Cell Cycle*, 18(21), pp. 2828–2848. Available at: https://doi.org/10.1080/15384101.2019.1658476.

Pini, L. *et al.* (2016) 'Brain atrophy in Alzheimer's Disease and aging', *Ageing Research Reviews*, 30, pp. 25–48. Available at: https://doi.org/10.1016/j.arr.2016.01.002.

Polis, B., Karasik, D. and Samson, A.O. (2021) 'Alzheimer's disease as a chronic maladaptive polyamine stress response', *Aging*, 13(7), pp. 10770–10795. Available at: https://doi.org/10.18632/aging.202928.

Preman, P. *et al.* (2021) 'Astrocytes in Alzheimer's Disease: Pathological Significance and Molecular Pathways', *Cells*, 10(3), p. 540. Available at: https://doi.org/10.3390/cells10030540.

Qian, M., Shen, X. and Wang, H. (2016) 'The Distinct Role of ADAM17 in APP Proteolysis and Microglial Activation Related to Alzheimer's Disease', *Cellular and Molecular Neurobiology*, 36(4), pp. 471–482. Available at: https://doi.org/10.1007/s10571-015-0232-4.

de Queiroz, T.M., Lakkappa, N. and Lazartigues, E. (2020) 'ADAM17-Mediated Shedding of Inflammatory Cytokines in Hypertension', *Frontiers in Pharmacology*, 11. Available at: https://www.frontiersin.org/articles/10.3389/fphar.2020.01154 (Accessed: 14 April 2023).

R Core Team (2022) 'R: A Language and Environment for Statistical Computing'. Vienna, Austria: R Foundation for Statistical Computing. Available at: https://www.R-project.org/.

Rabinovici, G.D. (2019) 'Late-onset Alzheimer Disease', *Continuum : Lifelong Learning in Neurology*, 25(1), pp. 14–33. Available at: https://doi.org/10.1212/CON.0000000000000700.

Rajan, K.B. *et al.* (2017) 'Racial Differences in the Association Between Apolipoprotein E Risk Alleles and Overall and Total Cardiovascular Mortality Over 18 Years', *Journal of the American Geriatrics Society*, 65(11), pp. 2425–2430. Available at: https://doi.org/10.1111/jgs.15059.

Ran, F.A. *et al.* (2013) 'Double Nicking by RNA-Guided CRISPR Cas9 for Enhanced Genome Editing Specificity', *Cell*, 154(6), pp. 1380–1389. Available at: https://doi.org/10.1016/j.cell.2013.08.021.

Raudvere, U. *et al.* (2019) 'g:Profiler: a web server for functional enrichment analysis and conversions of gene lists (2019 update)', *Nucleic Acids Research*, 47(W1), pp. W191–W198. Available at: https://doi.org/10.1093/nar/gkz369.

Rea, I.M. *et al.* (2018) 'Age and Age-Related Diseases: Role of Inflammation Triggers and Cytokines', *Frontiers in Immunology*, 9. Available at: https://www.frontiersin.org/articles/10.3389/fimmu.2018.00586 (Accessed: 30 March 2023).

Ribarič, S. (2023) 'Detecting Early Cognitive Decline in Alzheimer's Disease with Brain Synaptic Structural and Functional Evaluation', *Biomedicines*, 11(2), p. 355. Available at: https://doi.org/10.3390/biomedicines11020355.

Ricciarelli, R. and Fedele, E. (2017) 'The Amyloid Cascade Hypothesis in Alzheimer's Disease: It's Time to Change Our Mind', *Current Neuropharmacology*, 15(6), pp. 926–935. Available at: https://doi.org/10.2174/1570159X15666170116143743.

Ridge, P.G. *et al.* (2016) 'Assessment of the genetic variance of late-onset Alzheimer's disease', *Neurobiology of Aging*, 41, p. 200.e13-200.e20. Available at: https://doi.org/10.1016/j.neurobiolaging.2016.02.024.

Rohe, M. *et al.* (2013) 'SORLA-Mediated Trafficking of TrkB Enhances the Response of Neurons to BDNF', *PLOS ONE*, 8(8), p. e72164. Available at: https://doi.org/10.1371/journal.pone.0072164.

Rose-John, S. (2020) 'Interleukin-6 signalling in health and disease'. F1000Research. Available at: https://doi.org/10.12688/f1000research.26058.1.

Ruitenberg, A. *et al.* (2001) 'Incidence of dementia: does gender make a difference?', *Neurobiology of Aging*, 22(4), pp. 575–580. Available at: https://doi.org/10.1016/S0197-4580(01)00231-7.

Saad, M.I., Rose-John, S. and Jenkins, B.J. (2019) 'ADAM17: An Emerging Therapeutic Target for Lung Cancer', *Cancers*, 11(9), p. 1218. Available at: https://doi.org/10.3390/cancers11091218.

Sagar, N.A. *et al.* (2021) 'Polyamines: Functions, Metabolism, and Role in Human Disease Management', *Medical Sciences*, 9(2), p. 44. Available at: https://doi.org/10.3390/medsci9020044.

Sala Frigerio, C. *et al.* (2019) 'The Major Risk Factors for Alzheimer's Disease: Age, Sex, and Genes Modulate the Microglia Response to Aβ Plaques', *Cell Reports*, 27(4), pp. 1293-1306.e6. Available at: https://doi.org/10.1016/j.celrep.2019.03.099.

Salazar, J.L., Yang, S.-A. and Yamamoto, S. (2020) 'Post-Developmental Roles of Notch Signaling in the Nervous System', *Biomolecules*, 10(7), p. 985. Available at: https://doi.org/10.3390/biom10070985.

Salomon, R. *et al.* (2019) 'Droplet-based single cell RNAseq tools: a practical guide', *Lab on a Chip*, 19(10), pp. 1706–1727. Available at: https://doi.org/10.1039/C8LC01239C.

Sanada, F. *et al.* (2018) 'IGF Binding Protein-5 Induces Cell Senescence', *Frontiers in Endocrinology*, 9. Available at: https://www.frontiersin.org/articles/10.3389/fendo.2018.00053 (Accessed: 2 June 2023).

Sanson, K.R. *et al.* (2018) 'Optimized libraries for CRISPR-Cas9 genetic screens with multiple modalities', *Nature Communications*, 9(1), p. 5416. Available at: https://doi.org/10.1038/s41467-018-07901-8.

Sartori, M. *et al.* (2019) 'BIN1 recovers tauopathy-induced long-term memory deficits in mice and interacts with Tau through Thr348 phosphorylation', *Acta Neuropathologica*, 138(4), pp. 631–652. Available at: https://doi.org/10.1007/s00401-019-02017-9.

Sato, C. *et al.* (2018) 'Tau Kinetics in Neurons and the Human Central Nervous System', *Neuron*, 97(6), pp. 1284-1298.e7. Available at: https://doi.org/10.1016/j.neuron.2018.02.015.

Satoh, K. *et al.* (2015) 'ATP-binding Cassette Transporter A7 (ABCA7) Loss of Function Alters Alzheimer Amyloid Processing*', *Journal of Biological Chemistry*, 290(40), pp. 24152–24165. Available at: https://doi.org/10.1074/jbc.M115.655076.

Saul, D. and Kosinsky, R.L. (2021) 'Epigenetics of Aging and Aging-Associated Diseases', *International Journal of Molecular Sciences*, 22(1), p. 401. Available at: https://doi.org/10.3390/ijms22010401.

Sawa, M. *et al.* (2022) 'Impact of increased *APP* gene dose in Down syndrome and the Dp16 mouse model', *Alzheimer's & Dementia*, 18(6), pp. 1203–1234. Available at: https://doi.org/10.1002/alz.12463.

Schaaf, C.A. *et al.* (2013) 'Genome-Wide Control of RNA Polymerase II Activity by Cohesin', *PLoS Genetics*. Edited by B. Ren, 9(3), p. e1003382. Available at: https://doi.org/10.1371/journal.pgen.1003382.

Schindelin, J. *et al.* (2012) 'Fiji: an open-source platform for biological-image analysis', *Nature Methods*, 9(7), pp. 676–682. Available at: https://doi.org/10.1038/nmeth.2019.

Schlepckow, K. *et al.* (2017) 'An Alzheimer-associated TREM2 variant occurs at the ADAM cleavage site and affects shedding and phagocytic function', *EMBO Molecular Medicine*, 9(10), pp. 1356–1365. Available at: https://doi.org/10.15252/emmm.201707672.

Schöll, M. *et al.* (2015) 'Early astrocytosis in autosomal dominant Alzheimer's disease measured in vivo by multi-tracer positron emission tomography', *Scientific Reports*, 5(1), p. 16404. Available at: https://doi.org/10.1038/srep16404.

Schubert, M. *et al.* (2004) 'Role for neuronal insulin resistance in neurodegenerative diseases', *Proceedings of the National Academy of Sciences*, 101(9), pp. 3100–3105. Available at: https://doi.org/10.1073/pnas.0308724101.

Schumacher, N. and Rose-John, S. (2022) 'ADAM17 orchestrates Interleukin-6, TNFα and EGF-R signaling in inflammation and cancer', *Biochimica et Biophysica Acta (BBA) - Molecular Cell Research*, 1869(1), p. 119141. Available at: https://doi.org/10.1016/j.bbamcr.2021.119141.

Schymanski, E.L. *et al.* (2014) 'Identifying Small Molecules via High Resolution Mass Spectrometry: Communicating Confidence', *Environmental Science & Technology*, 48(4), pp. 2097–2098. Available at: https://doi.org/10.1021/es5002105.

Selkoe, D.J. and Hardy, J. (2016) 'The amyloid hypothesis of Alzheimer's disease at 25 years', *EMBO Molecular Medicine*, 8(6), pp. 595–608. Available at: https://doi.org/10.15252/emmm.201606210.

Senekowitsch, S. *et al.* (2023) 'High-Dose Spermidine Supplementation Does Not Increase Spermidine Levels in Blood Plasma and Saliva of Healthy Adults: A Randomized Placebo-Controlled Pharmacokinetic and Metabolomic Study', *Nutrients*, 15(8), p. 1852. Available at: https://doi.org/10.3390/nu15081852.

Serrano-Pozo, A. *et al.* (2011) 'Reactive Glia not only Associates with Plaques but also Parallels Tangles in Alzheimer's Disease', *The American Journal of Pathology*, 179(3), pp. 1373–1384. Available at: https://doi.org/10.1016/j.ajpath.2011.05.047.

Shankar, G.M. *et al.* (2008) 'Amyloid-β protein dimers isolated directly from Alzheimer's brains impair synaptic plasticity and memory', *Nature Medicine*, 14(8), pp. 837–842. Available at: https://doi.org/10.1038/nm1782.

Shaw, C. *et al.* (2021) 'Evaluation of Selective Survival and Sex/Gender Differences in Dementia Incidence Using a Simulation Model', *JAMA Network Open*, 4(3), p. e211001. Available at: https://doi.org/10.1001/jamanetworkopen.2021.1001.

Shi, J. *et al.* (2020) 'LncRNA XIST knockdown suppresses the malignancy of human nasopharyngeal carcinoma through XIST/miRNA-148a-3p/ADAM17 pathway in vitro and in vivo', *Biomedicine & Pharmacotherapy*, 121, p. 109620. Available at: https://doi.org/10.1016/j.biopha.2019.109620.

Shi, Y. and Holtzman, D.M. (2018) 'Interplay between innate immunity and Alzheimer disease: APOE and TREM2 in the spotlight', *Nature Reviews Immunology*, 18(12), pp. 759–772. Available at: https://doi.org/10.1038/s41577-018-0051-1.

Shian Huang, S. *et al.* (2004) 'Identification of insulin receptor substrate proteins as key molecules for the TβR-V/LRP-1-mediated growth inhibitory signaling cascade in epithelial and myeloid cells', *The FASEB Journal*, 18(14), pp. 1719–1721. Available at: https://doi.org/10.1096/fj.04-1872fje.

Sims, R., Hill, M. and Williams, J. (2020) 'The multiplex model of the genetics of Alzheimer's disease', *Nature Neuroscience*, 23(3), pp. 311–322. Available at: https://doi.org/10.1038/s41593-020-0599-5.

Skaper, S.D. *et al.* (2018) 'An Inflammation-Centric View of Neurological Disease: Beyond the Neuron', *Frontiers in Cellular Neuroscience*, 12. Available at: https://www.frontiersin.org/articles/10.3389/fncel.2018.00072 (Accessed: 29 March 2023).

Skatchkov, S.N., Woodbury-Fariña, M.A. and Eaton, M. (2014) 'The Role of Glia in Stress', *Psychiatric Clinics of North America*, 37(4), pp. 653–678. Available at: https://doi.org/10.1016/j.psc.2014.08.008.

Skuse, D.H. (2005) 'X-linked genes and mental functioning', *Human Molecular Genetics*, 14(suppl_1), pp. R27–R32. Available at: https://doi.org/10.1093/hmg/ddi112.

Slanzi, A. *et al.* (2020) 'In vitro Models of Neurodegenerative Diseases', *Frontiers in Cell and Developmental Biology*, 8. Available at: https://www.frontiersin.org/articles/10.3389/fcell.2020.00328 (Accessed: 29 April 2023).

Smajić, S. *et al.* (2022) 'Single-cell sequencing of human midbrain reveals glial activation and a Parkinson-specific neuronal state', *Brain*, p. awab446. Available at: https://doi.org/10.1093/brain/awab446.

Smit, A., Hubley, R. and Green, P. (2013) 'RepeatMasker Open-4.0'. Available at: http://www.repeatmasker.org (Accessed: 4 April 2023).

Sommer, A. *et al.* (2016) 'Phosphatidylserine exposure is required for ADAM17 sheddase function', *Nature Communications*, 7(1), p. 11523. Available at: https://doi.org/10.1038/ncomms11523.

Sousa, C. *et al.* (2018) 'Single-cell transcriptomics reveals distinct inflammation-induced microglia signatures', *EMBO reports*, 19(11), p. e46171. Available at: https://doi.org/10.15252/embr.201846171.

Subedi, S. *et al.* (2022) 'Amyloid Cross-Seeding: Mechanism, Implication, and Inhibition', *Molecules*, 27(6), p. 1776. Available at: https://doi.org/10.3390/molecules27061776.

Suh, J. *et al.* (2013) 'ADAM10 Missense Mutations Potentiate β-Amyloid Accumulation by Impairing Prodomain Chaperone Function', *Neuron*, 80(2), pp. 385–401. Available at: https://doi.org/10.1016/j.neuron.2013.08.035.

Sun, B. *et al.* (2021) 'Critical thinking on amyloid-beta-targeted therapy: challenges and perspectives', *Science China Life Sciences*, 64(6), pp. 926–937. Available at: https://doi.org/10.1007/s11427-020-1810-y.

Sweeney, M.D., Sagare, A.P. and Zlokovic, B.V. (2018) 'Blood–brain barrier breakdown in Alzheimer disease and other neurodegenerative disorders', *Nature Reviews Neurology*, 14(3), pp. 133–150. Available at: https://doi.org/10.1038/nrneurol.2017.188.

Swerdlow, R.H. (2018) 'Mitochondria and Mitochondrial Cascades in Alzheimer's Disease', *Journal of Alzheimer's Disease*. Edited by G. Perry et al., 62(3), pp. 1403–1416. Available at: https://doi.org/10.3233/JAD-170585.

Swerdlow, R.H. and Khan, S.M. (2004) 'A "mitochondrial cascade hypothesis" for sporadic Alzheimer's disease', *Medical Hypotheses*, 63(1), pp. 8–20. Available at: https://doi.org/10.1016/j.mehy.2003.12.045.

Szabo, M.P. *et al.* (2022) 'The role of Alzheimer's disease risk genes in endolysosomal pathways', *Neurobiology of Disease*, 162, p. 105576. Available at: https://doi.org/10.1016/j.nbd.2021.105576.

Talbot, K. *et al.* (2012) 'Demonstrated brain insulin resistance in Alzheimer's disease patients is associated with IGF-1 resistance, IRS-1 dysregulation, and cognitive decline', *The Journal of Clinical Investigation*, 122(4), pp. 1316–1338. Available at: https://doi.org/10.1172/JCI59903.

Tansey, M.G. *et al.* (2022) 'Inflammation and immune dysfunction in Parkinson disease', *Nature Reviews Immunology*, 22(11), pp. 657–673. Available at: https://doi.org/10.1038/s41577-022-00684-6.

Tao, X. *et al.* (2023) 'Reduction of Spermine Synthase Suppresses Tau Accumulation Through Autophagy Modulation in Tauopathy'. Available at: https://doi.org/10.1101/2023.03.17.533015.

Tatulian, S.A. (2022) 'Challenges and hopes for Alzheimer's disease', *Drug Discovery Today*, 27(4), pp. 1027–1043. Available at: https://doi.org/10.1016/j.drudis.2022.01.016.

THE BRAINSTORM CONSORTIUM *et al.* (2018) 'Analysis of shared heritability in common disorders of the brain', *Science*, 360(6395), p. eaap8757. Available at: https://doi.org/10.1126/science.aap8757.

Toledo, J.B. *et al.* (2017) 'Metabolic network failures in Alzheimer's disease: A biochemical road map', *Alzheimer's & Dementia*, 13(9), pp. 965–984. Available at: https://doi.org/10.1016/j.jalz.2017.01.020.

Tomishima, M. (2012) *Midbrain dopamine neurons from hESCs*, *StemBook [Internet]*. Harvard Stem Cell Institute. Available at: https://doi.org/10.3824/stembook.1.70.1.

Tomiyama, T. *et al.* (2008) 'A new amyloid β variant favoring oligomerization in Alzheimer's-type dementia', *Annals of Neurology*, 63(3), pp. 377–387. Available at: https://doi.org/10.1002/ana.21321.

Tomizawa, M. *et al.* (2018) 'Oct3/4 is potentially useful for the suppression of the proliferation and motility of hepatocellular carcinoma cells', *Oncology Letters*, 16(4), pp. 5243–5248. Available at: https://doi.org/10.3892/ol.2018.9292.

Tondo, G. *et al.* (2020) 'The combined effects of microglia activation and brain glucose hypometabolism in early-onset Alzheimer's disease', *Alzheimer's Research & Therapy*, 12(1), p. 50. Available at: https://doi.org/10.1186/s13195-020-00619-0.

Trapnell, C. *et al.* (2014) 'The dynamics and regulators of cell fate decisions are revealed by pseudotemporal ordering of single cells', *Nature Biotechnology*, 32(4), pp. 381–386. Available at: https://doi.org/10.1038/nbt.2859.

Tsoi, P.S. *et al.* (2023) 'Aggregation of Disordered Proteins Associated with Neurodegeneration', *International Journal of Molecular Sciences*, 24(4), p. 3380. Available at: https://doi.org/10.3390/ijms24043380.

Turcu, D.C., Lillehaug, J.R. and Seo, H.-C. (2019) 'SIX3 and SIX6 interact with GEMININ via C-terminal regions', *Biochemistry and Biophysics Reports*, 20, p. 100695. Available at: https://doi.org/10.1016/j.bbrep.2019.100695.

Ubelmann, F. *et al.* (2017) 'Bin1 and CD2AP polarise the endocytic generation of beta-amyloid', *EMBO reports*, 18(1), pp. 102–122. Available at: https://doi.org/10.15252/embr.201642738.

Vagnozzi, A.N. and Praticò, D. (2019) 'Endosomal sorting and trafficking, the retromer complex and neurodegeneration', *Molecular Psychiatry*, 24(6), pp. 857–868. Available at: https://doi.org/10.1038/s41380-018-0221-3.

Valdes, P. *et al.* (2022) *Integrative multiomics reveals common endotypes across PSEN1, PSEN2, and APP mutations in familial Alzheimer's disease*. preprint. In Review. Available at: https://doi.org/10.21203/rs.3.rs-2356131/v1.

Van Der Heide, L.P. *et al.* (2005) 'Insulin modulates hippocampal activity-dependent synaptic plasticity in a N-methyl-d-aspartate receptor and phosphatidyl-inositol-3-kinase-dependent manner: Insulin modulates LTP and LTD', *Journal of Neurochemistry*, 94(4), pp. 1158–1166. Available at: https://doi.org/10.1111/j.1471-4159.2005.03269.x.

Van Eldik, L.J. *et al.* (2016) 'The roles of inflammation and immune mechanisms in Alzheimer's disease', *Alzheimer's & Dementia : Translational Research & Clinical Interventions*, 2(2), pp. 99–109. Available at: https://doi.org/10.1016/j.trci.2016.05.001.

Vander Heiden, M.G., Cantley, L.C. and Thompson, C.B. (2009) 'Understanding the Warburg Effect: The Metabolic Requirements of Cell Proliferation', *Science*, 324(5930), pp. 1029–1033. Available at: https://doi.org/10.1126/science.1160809.

Veitch, D.P. *et al.* (2019) 'Understanding disease progression and improving Alzheimer's disease clinical trials: Recent highlights from the Alzheimer's Disease Neuroimaging Initiative', *Alzheimer's & Dementia*, 15(1), pp. 106–152. Available at: https://doi.org/10.1016/j.jalz.2018.08.005.

Verkhratsky, A. *et al.* (2017) 'Astroglial calcium signalling in Alzheimer's disease', *Biochemical and Biophysical Research Communications*, 483(4), pp. 1005–1012. Available at: https://doi.org/10.1016/j.bbrc.2016.08.088.

Vlahos, K. *et al.* (2019) 'Generation of iPSC lines from peripheral blood mononuclear cells from 5 healthy adults', *Stem Cell Research*, 34, p. 101380. Available at: https://doi.org/10.1016/j.scr.2018.101380.

Wadhwani, A.R. *et al.* (2019) 'Neuronal apolipoprotein E4 increases cell death and phosphorylated tau release in alzheimer disease', *Annals of Neurology*, 85(5), pp. 726–739. Available at: https://doi.org/10.1002/ana.25455.

Wainer Katsir, K. and Linial, M. (2019) 'Human genes escaping X-inactivation revealed by single cell expression data', *BMC Genomics*, 20(1), p. 201. Available at: https://doi.org/10.1186/s12864-019-5507-6.

Wake, H. *et al.* (2009) 'Resting Microglia Directly Monitor the Functional State of Synapses In Vivo and Determine the Fate of Ischemic Terminals', *Journal of Neuroscience*, 29(13), pp. 3974–3980. Available at: https://doi.org/10.1523/JNEUROSCI.4363-08.2009.

Walker, M.C. and van der Donk, W.A. (2016) 'The Many Roles of Glutamate in Metabolism', *Journal of industrial microbiology & biotechnology*, 43(0), pp. 419–430. Available at: https://doi.org/10.1007/s10295-015-1665-y.

Wang, A., Luan, H.H. and Medzhitov, R. (2019) 'An evolutionary perspective on immunometabolism', *Science*, 363(6423), p. eaar3932. Available at: https://doi.org/10.1126/science.aar3932.

Wang, W.-Y. *et al.* (2015) 'Role of pro-inflammatory cytokines released from microglia in Alzheimer's disease', *Annals of Translational Medicine*, 3(10), pp. 136–136. Available at: https://doi.org/10.3978/j.issn.2305-5839.2015.03.49.

Wang, X. *et al.* (2008) 'Amyloid-β overproduction causes abnormal mitochondrial dynamics via differential modulation of mitochondrial fission/fusion proteins', *Proceedings of the National Academy of Sciences*, 105(49), pp. 19318–19323. Available at: https://doi.org/10.1073/pnas.0804871105.

Wang, X. *et al.* (2018) 'LncRNA XIST knockdown attenuates Aβ25-35-induced toxicity, oxidative stress, and apoptosis in primary cultured rat hippocampal neurons by targeting miR-132', *International Journal of Clinical and Experimental Pathology*, 11(8), pp. 3915–3924. Available at: https://www.ncbi.nlm.nih.gov/pmc/articles/PMC6962802/ (Accessed: 29 May 2023).

Wang, Y. *et al.* (2020) 'Enzyme Kinetics by Isothermal Titration Calorimetry: Allostery, Inhibition, and Dynamics', *Frontiers in Molecular Biosciences*, 7, p. 583826. Available at: https://doi.org/10.3389/fmolb.2020.583826.

Wang, Y.-J. (2014) 'Lessons from immunotherapy for Alzheimer disease', *Nature Reviews Neurology*, 10(4), pp. 188–189. Available at: https://doi.org/10.1038/nrneurol.2014.44.

Westermark, P. and Westermark, G.T. (2013) 'Seeding and Cross-seeding in Amyloid Diseases', in M. Jucker and Y. Christen (eds) *Proteopathic Seeds and Neurodegenerative Diseases*. Berlin, Heidelberg: Springer (Research and Perspectives in Alzheimer's Disease), pp. 47–60. Available at: https://doi.org/10.1007/978-3-642-35491-5_4.

WHO (2022) *Fact sheets - Dementia*. Available at: https://www.who.int/news-room/fact-sheets/detail/dementia (Accessed: 19 January 2023).

Wickham, H. (2016) *ggplot2: Elegant Graphics for Data Analysis*. Springer-Verlag New York. Available at: https://ggplot2.tidyverse.org.

Wickham, H. *et al.* (2019) 'Welcome to the tidyverse', *Journal of Open Source Software*, 4(43), p. 1686. Available at: https://doi.org/10.21105/joss.01686.

Wickham, H. *et al.* (2023) *dplyr: A Grammar of Data Manipulation*. Available at: https://CRAN.R-project.org/package=dplyr.

Wilke, C.O. and Wiernik, B.M. (2022) *ggtext: Improved Text Rendering Support for 'ggplot2'*. Available at: https://CRAN.R-project.org/package=ggtext.

Wilkins, J.M. and Trushina, E. (2018) 'Application of Metabolomics in Alzheimer's Disease', *Frontiers in Neurology*, 8. Available at: https://www.frontiersin.org/articles/10.3389/fneur.2017.00719 (Accessed: 3 June 2023).

Williams, K. *et al.* (1990) 'Characterization of polyamines having agonist, antagonist, and inverse agonist effects at the polyamine recognition site of the NMDA receptor', *Neuron*, 5(2), pp. 199–208. Available at: https://doi.org/10.1016/0896-6273(90)90309-4.

Wilson, D.M. *et al.* (2023) 'Hallmarks of neurodegenerative diseases', *Cell*, 186(4), pp. 693–714. Available at: https://doi.org/10.1016/j.cell.2022.12.032.

Wingett, S.W. and Andrews, S. (2018) 'FastQ Screen: A tool for multi-genome mapping and quality control', *F1000Research*, 7, p. 1338. Available at: https://doi.org/10.12688/f1000research.15931.2.

Wingo, T.S. *et al.* (2012) 'Autosomal Recessive Causes Likely in Early-Onset Alzheimer Disease', *Archives of Neurology*, 69(1), pp. 59–64. Available at: https://doi.org/10.1001/archneurol.2011.221.

Winter, E.E. and Ponting, C.P. (2005) 'Mammalian BEX, WEX and GASP genes: Coding and non-coding chimaerism sustained by gene conversion events', *BMC Evolutionary Biology*, 5(1), p. 54. Available at: https://doi.org/10.1186/1471-2148-5-54.

Wong, E. *et al.* (2015) 'The Functional Maturation of A Disintegrin and Metalloproteinase (ADAM) 9, 10, and 17 Requires Processing at a Newly Identified Proprotein Convertase (PC) Cleavage Site', *Journal of Biological Chemistry*, 290(19), pp. 12135–12146. Available at: https://doi.org/10.1074/jbc.M114.624072.

Wortha, S.M. *et al.* (2023) 'Association of spermidine plasma levels with brain aging in a population-based study', *Alzheimer's & Dementia*, 19(5), pp. 1832–1840. Available at: https://doi.org/10.1002/alz.12815.

Wu, H., Williams, J. and Nathans, J. (2014) 'Complete morphologies of basal forebrain cholinergic neurons in the mouse', *eLife*. Edited by F. Polleux, 3, p. e02444. Available at: https://doi.org/10.7554/eLife.02444.

Xia, J. and Wishart, D.S. (2011) 'Web-based inference of biological patterns, functions and pathways from metabolomic data using MetaboAnalyst', *Nature Protocols*, 6(6), pp. 743–760. Available at: https://doi.org/10.1038/nprot.2011.319.

Xia, Q. *et al.* (2021) 'The Protective A673T Mutation of Amyloid Precursor Protein (APP) in Alzheimer's Disease', *Molecular Neurobiology*, 58(8), pp. 4038–4050. Available at: https://doi.org/10.1007/s12035-021-02385-y.

Xie, H. *et al.* (2013) 'Mitochondrial Alterations near Amyloid Plaques in an Alzheimer's Disease Mouse Model', *The Journal of Neuroscience*, 33(43), p. 17042. Available at: https://doi.org/10.1523/JNEUROSCI.1836-13.2013.

Xie, J. *et al.* (2017) 'Microglia-Synapse Pathways: Promising Therapeutic Strategy for Alzheimer's Disease', *BioMed Research International*, 2017, p. e2986460. Available at: https://doi.org/10.1155/2017/2986460.

Xie, L. *et al.* (2002) 'Alzheimer's β-Amyloid Peptides Compete for Insulin Binding to the Insulin Receptor', *The Journal of Neuroscience*, 22(10), pp. RC221–RC221. Available at: https://doi.org/10.1523/JNEUROSCI.22-10-j0001.2002.

Xu, M. *et al.* (2022) 'The E3 ubiquitin-protein ligase Trim31 alleviates non-alcoholic fatty liver disease by targeting Rhbdf2 in mouse hepatocytes', *Nature Communications*, 13(1), p. 1052. Available at: https://doi.org/10.1038/s41467-022-28641-w.

Yamazaki, Y. *et al.* (2019) 'Apolipoprotein E and Alzheimer disease: pathobiology and targeting strategies', *Nature Reviews Neurology*, 15(9), pp. 501–518. Available at: https://doi.org/10.1038/s41582-019-0228-7.

Yan, X.-W. *et al.* (2022) 'lncRNA XIST induces Aβ accumulation and neuroinflammation by the epigenetic repression of NEP in Alzheimer's disease', *Journal of Neurogenetics*, 36(1), pp. 11–20. Available at: https://doi.org/10.1080/01677063.2022.2028784.

Yang, G. *et al.* (2021) 'Molecular switch in human diseases-disintegrin and metalloproteinases, ADAM17', *Aging*, 13(12), pp. 16859–16872. Available at: https://doi.org/10.18632/aging.203200.

Yang, H. *et al.* (2022) 'Based on molecular structures: Amyloid-β generation, clearance, toxicity and therapeutic strategies', *Frontiers in Molecular Neuroscience*, 15. Available at: https://www.frontiersin.org/articles/10.3389/fnmol.2022.927530 (Accessed: 2 March 2023).

Yang, J. *et al.* (2020) 'TREM2 ectodomain and its soluble form in Alzheimer's disease', *Journal of Neuroinflammation*, 17(1), p. 204. Available at: https://doi.org/10.1186/s12974-020-01878-2.

Yao, X.-Q. *et al.* (2015) 'p75NTR ectodomain is a physiological neuroprotective molecule against amyloid-beta toxicity in the brain of Alzheimer's disease', *Molecular Psychiatry*, 20(11), pp. 1301–1310. Available at: https://doi.org/10.1038/mp.2015.49.

Ye, C. *et al.* (2023) 'Drosophila melanogaster as a model to study age and sex differences in brain injury and neurodegeneration after mild head trauma', *Frontiers in Neuroscience*, 17. Available at: https://www.frontiersin.org/articles/10.3389/fnins.2023.1150694 (Accessed: 29 April 2023).

Yeh, F.L. *et al.* (2016) 'TREM2 Binds to Apolipoproteins, Including APOE and CLU/APOJ, and Thereby Facilitates Uptake of Amyloid-Beta by Microglia', *Neuron*, 91(2), pp. 328–340. Available at: https://doi.org/10.1016/j.neuron.2016.06.015.

Yu, L. *et al.* (2015) 'Association of Brain DNA Methylation in SORL1, ABCA7, HLA-DRB5, SLC24A4, and BIN1 With Pathological Diagnosis of Alzheimer Disease', *JAMA Neurology*, 72(1), pp. 15–24. Available at: https://doi.org/10.1001/jamaneurol.2014.3049.

Yu, T., Robotham, J.L. and Yoon, Y. (2006) 'Increased production of reactive oxygen species in hyperglycemic conditions requires dynamic change of mitochondrial morphology', *Proceedings of the National Academy of Sciences of the United States of America*, 103(8), pp. 2653–2658. Available at: https://doi.org/10.1073/pnas.0511154103.

Yue, D. *et al.* (2020) 'Silencing of long noncoding RNA XIST attenuated Alzheimer's disease-related BACE1 alteration through miR-124', *Cell Biology International*, 44(2), pp. 630–636. Available at: https://doi.org/10.1002/cbin.11263.

Yvanka de Soysa, T. *et al.* (2022) 'Redefining microglia states: Lessons and limits of human and mouse models to study microglia states in neurodegenerative diseases', *Seminars in Immunology*, 60, p. 101651. Available at: https://doi.org/10.1016/j.smim.2022.101651.

Zhang, Y. *et al.* (2013) 'Genes That Escape X-Inactivation in Humans Have High Intraspecific Variability in Expression, Are Associated with Mental Impairment but Are Not Slow Evolving', *Molecular Biology and Evolution*, 30(12), pp. 2588–2601. Available at: https://doi.org/10.1093/molbev/mst148.

Zhang, Y. *et al.* (2022) 'Tauopathies: new perspectives and challenges', *Molecular Neurodegeneration*, 17(1), p. 28. Available at: https://doi.org/10.1186/s13024-022-00533-z.

Zimbone, S. *et al.* (2018) 'Amyloid Beta monomers regulate cyclic adenosine monophosphate response element binding protein functions by activating type-1 insulin-like growth factor receptors in neuronal cells', *Aging Cell*, 17(1), p. e12684. Available at: https://doi.org/10.1111/acel.12684.

Zou, D. *et al.* (2022) 'A comprehensive review of spermidine: Safety, health effects, absorption and metabolism, food materials evaluation, physical and chemical processing, and bioprocessing', *Comprehensive Reviews in Food Science and Food Safety*, 21(3), pp. 2820–2842. Available at: https://doi.org/10.1111/1541-4337.12963.

Zunke, F. and Rose-John, S. (2017) 'The shedding protease ADAM17: Physiology and pathophysiology', *Biochimica et Biophysica Acta (BBA) - Molecular Cell Research*, 1864(11), pp. 2059–2070. Available at: https://doi.org/10.1016/j.bbamcr.2017.07.001.

8 Appendix: Supporting Material

8.1 Sequence of the homology arms

Left homology arm (351bp)

TTTCATCATGTTGGCCAGGCTGGTCTCGAACTCCCGTCCTCAGGTGATTCACCCACCTTGGCCTCGCAAAGTGC
TGGGATTACAGGCCTGAGCCAACATGCCCGGCCTTACTCTGTTGAGCACTTTTTAAAGTTTCTGTATTGGAAAAA
TTAAAGAGGCACTTGTCCTTGGTTTTGAATTCTACAGTGTTTTAACTTTATGTTACTTTTCACTTTTCTGTCTTCCTC
CAAATTATTTTTTGTTGTTGTTCAGAATCCTTTAGTGATATTAAGCTCACATAATGTTTGTTTCAAAAATATGTTAGA
TTTAAAGTGTTACCATAAAACTCCTTGTTTTGGTGAATTTTGATTT

Right homology arm_1 (953bp) (RHA_sgRNA1_EGFP)

AATAGTGCATACAAATTCATATTAGAGCTTGTTCATCGAGTGAAAAGAATAGCTGACCCAGATCCTATGAAGAACA
CGTGTAAATTATTGGTGGTAGCAGATCATCGCTTCTACAGATACATGGGCAGAGGGGAAGAGAGTACAACTACA
AATTACTTAGTAAGTATTTGATATTGCATCGAGTAATTGAAAAAAAAAATTTGGGTGGGTACATTCCATGAAACTTAA
TGCAACCAGATCTGTTCCAGATACTCTGTTATTTCCCTAAAATATTTGAGGGATATTCTCTGAGGTTTTTATGTTAC
TGTATGGAAATTATAGTTTCAAATTTGTGACAACCCATTTTACCCTTGAACTAATATTTTCTGCATGTTAGAATTTAT
GCATATAGGGTTTGGGAGAGGTTATAATGTAGTCCTTCCTCCTTGATATAAGTGAGTTCTTTAAAAACATCACTGC
TATCATGGTAGTGAACCTGTGGTGTCACATGTGAATGTAAAAATATGTATTTGCATGAACCCATGTTTTTCTTTTG
CTTATATGTATATTTCAGAGAGGAAGGCGAGTTTTGTTTGTCATGTTAAAGACCTAATCATTGGACTTCACTTGAA
ATAGGTGGGACTTTCATGGTCATAACTAGTTCTAGGGCACAGAAGTGAAGGAAAGATGTAAGAAGTGATGATACT
GGATTTTTAAGTATGAACTATTATGATTTTTGAAGTCTGGGGAATCATTTTTCATTGACATTTTTTGCTAGTGTGAC
TTCATTCGTCATGATTACTTGGCACTGACCAAAATGTTGTTACTGAGGGAATAATGGAGAATGCAGCTATTCATGA
AGCAAGAAGAAGCTGGTGCAGTAAAGATGTCTTTCTCATTGCCTTGCTTTTCCCATGCTGTCCATTTTATTCATAC
CCTCCCAACTTCTTTCCCTTCCCTTTCATGTCAAGTGGA

Right homology arm_2 (953bp) (RHA_sgRNA2_EGFP)

AATAGTGCATACAAATTCATATTAGAGCTTGTTCATCGAGTGAAAAGAATAGCTGACCTAGATCCCATGAAGAACA
CGTGTAAATTATTGGTGGTAGCAGATCATCGCTTCTACAGATACATGGGCAGAGGGGAAGAGAGTACAACTACA
AATTACTTAGTAAGTATTTGATATTGCATCGAGTAATTGAAAAAAAAAATTTGGGTGGGTACATTCCATGAAACTTAA
TGCAACCAGATCTGTTCCAGATACTCTGTTATTTCCCTAAAATATTTGAGGGATATTCTCTGAGGTTTTTATGTTAC
TGTATGGAAATTATAGTTTCAAATTTGTGACAACCCATTTTACCCTTGAACTAATATTTTCTGCATGTTAGAATTTAT
GCATATAGGGTTTGGGAGAGGTTATAATGTAGTCCTTCCTCCTTGATATAAGTGAGTTCTTTAAAAACATCACTGC
TATCATGGTAGTGAACCTGTGGTGTCACATGTGAATGTAAAAATATGTATTTGCATGAACCCATGTTTTTCTTTTG
CTTATATGTATATTTCAGAGAGGAAGGCGAGTTTTGTTTGTCATGTTAAAGACCTAATCATTGGACTTCACTTGAA
ATAGGTGGGACTTTCATGGTCATAACTAGTTCTAGGGCACAGAAGTGAAGGAAAGATGTAAGAAGTGATGATACT
GGATTTTTAAGTATGAACTATTATGATTTTTGAAGTCTGGGGAATCATTTTTCATTGACATTTTTTGCTAGTGTGAC
TTCATTCGTCATGATTACTTGGCACTGACCAAAATGTTGTTACTGAGGGAATAATGGAGAATGCAGCTATTCATGA
AGCAAGAAGAAGCTGGTGCAGTAAAGATGTCTTTCTCATTGCCTTGCTTTTCCCATGCTGTCCATTTTATTCATAC
CCTCCCAACTTCTTTCCCTTCCCTTTCATGTCAAGTGGA

Right homology arm_dTomato (953bp) (RHA_sgRNA1_dTomato)

AATAGTGCATACAAATTCATATTAGAGCTTGTTCATCGAGTGAAAAGAAGAGCTGACCCAGATCCTATGAAGAAC
ACGTGTAAATTATTGGTGGTAGCAGATCATCGCTTCTACAGATACATGGGCAGAGGGGAAGAGAGTACAACTAC
AAATTACTTAGTAAGTATTTGATATTGCATCGAGTAATTGAAAAAAAAAATTTGGGTGGGTACATTCCATGAAACTTA
ATGCAACCAGATCTGTTCCAGATACTCTGTTATTTCCCTAAAATATTTGAGGGATATTCTCTGAGGTTTTTATGTTA
CTGTATGGAAATTATAGTTTCAAATTTGTGACAACCCATTTTACCCTTGAACTAATATTTTCTGCATGTTAGAATTTA
TGCATATAGGGTTTGGGAGAGGTTATAATGTAGTCCTTCCTCCTTGATATAAGTGAGTTCTTTAAAAACATCACTG
CTATCATGGTAGTGAACCTGTGGTGTCACATGTGAATGTAAAAATATGTATTTGCATGAACCCATGTTTTTCTTTT
GCTTATATGTATATTTCAGAGAGGAAGGCGAGTTTTGTTTGTCATGTTAAAGACCTAATCATTGGACTTCACTTGA
AATAGGTGGGACTTTCATGGTCATAACTAGTTCTAGGGCACAGAAGTGAAGGAAAGATGTAAGAAGTGATGATAC
TGGATTTTTAAGTATGAACTATTATGATTTTTGAAGTCTGGGGAATCATTTTTCATTGACATTTTTTGCTAGTGTGA
CTTCATTCGTCATGATTACTTGGCACTGACCAAAATGTTGTTACTGAGGGAATAATGGAGAATGCAGCTATTCATG
AAGCAAGAAGAAGCTGGTGCAGTAAAGATGTCTTTCTCATTGCCTTGCTTTTCCCATGCTGTCCATTTTATTCATA
CCCTCCCAACTTCTTTCCCTTCCCTTTCATGTCAAGTGGA

Right homology arm_dTomato (953bp) (RHA_sgRNA2_dTomato)

AATAGTGCATACAAATTCATATTAGAGCTTGTTCATCGAGTGAAAAGAAGAGCTGACCTAGATCCCATGAAGAAC
ACGTGTAAATTATTGGTGGTAGCAGATCATCGCTTCTACAGATACATGGGCAGAGGGGAAGAGAGTACAACTAC
AAATTACTTAGTAAGTATTTGATATTGCATCGAGTAATTGAAAAAAAAAATTTGGGTGGGTACATTCCATGAAACTTA
ATGCAACCAGATCTGTTCCAGATACTCTGTTATTTCCCTAAAATATTTGAGGGATATTCTCTGAGGTTTTTATGTTA
CTGTATGGAAATTATAGTTTCAAATTTGTGACAACCCATTTTACCCTTGAACTAATATTTTCTGCATGTTAGAATTTA
TGCATATAGGGTTTGGGAGAGGTTATAATGTAGTCCTTCCTCCTTGATATAAGTGAGTTCTTTAAAAACATCACTG
CTATCATGGTAGTGAACCTGTGGTGTCACATGTGAATGTAAAAATATGTATTTGCATGAACCCATGTTTTTCTTTT
GCTTATATGTATATTTCAGAGAGGAAGGCGAGTTTTGTTTGTCATGTTAAAGACCTAATCATTGGACTTCACTTGA
AATAGGTGGGACTTTCATGGTCATAACTAGTTCTAGGGCACAGAAGTGAAGGAAAGATGTAAGAAGTGATGATAC
TGGATTTTTAAGTATGAACTATTATGATTTTTGAAGTCTGGGGAATCATTTTTCATTGACATTTTTTGCTAGTGTGA
CTTCATTCGTCATGATTACTTGGCACTGACCAAAATGTTGTTACTGAGGGAATAATGGAGAATGCAGCTATTCATG
AAGCAAGAAGAAGCTGGTGCAGTAAAGATGTCTTTCTCATTGCCTTGCTTTTCCCATGCTGTCCATTTTATTCATA
CCCTCCCAACTTCTTTCCCTTCCCTTTCATGTCAAGTGGA

8.2 Results of the Karyotyping

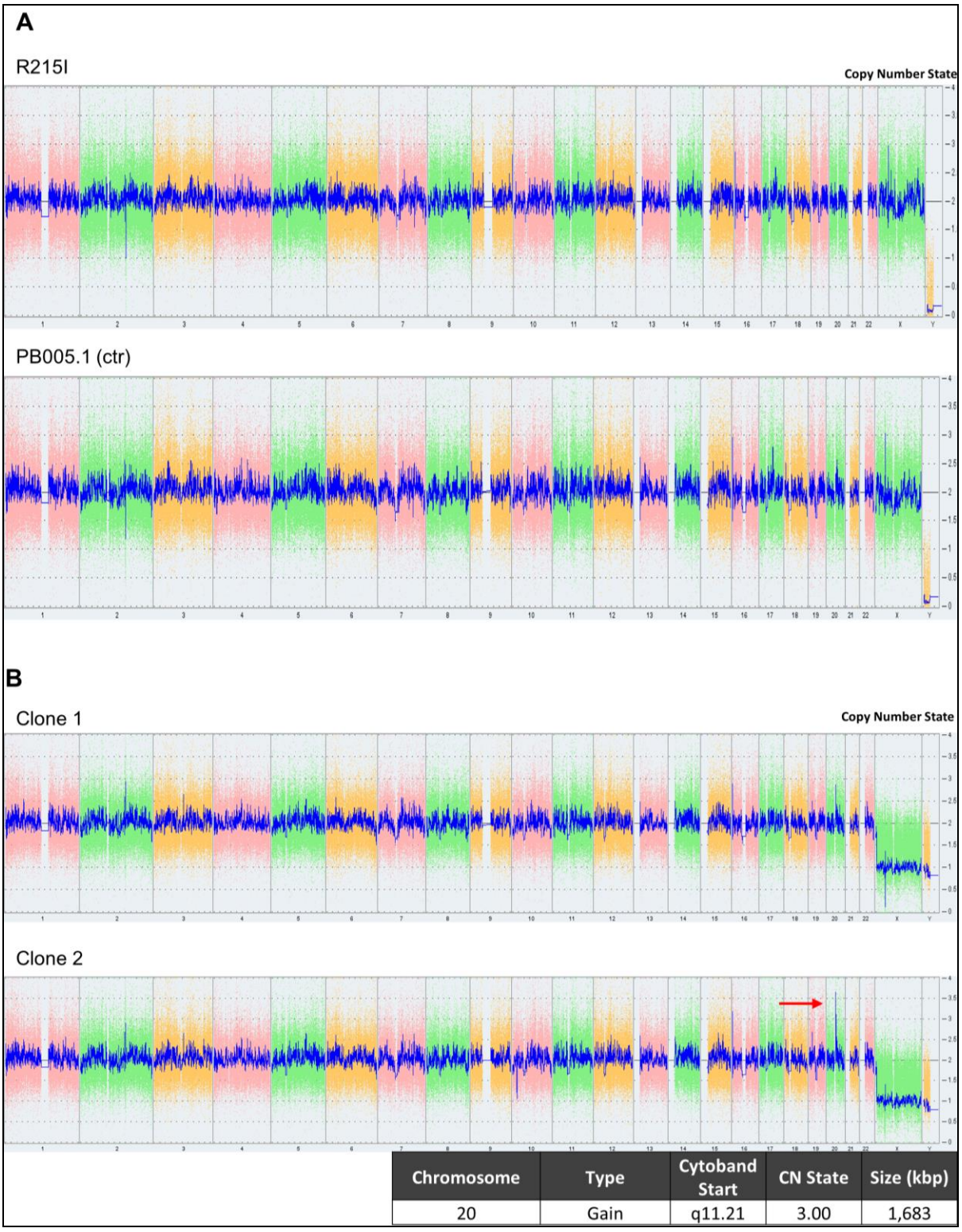

Chromosome	Type	Cytoband Start	CN State	Size (kbp)
20	Gain	q11.21	3.00	1,683

Figure 8.1 Results of the Karyotyping. ***(A)*** *Whole genome view of the isogenic pair generated by the Murdoch' Children´s Research Institute (Australia).* ***(B)*** *Whole genome view for the ADAM17 rs142946965 clone during this project. Clone 2 shows an insertion at chromosome 20 (red arrow). The log2 ratios, which represent the signal*

intensities of probes on the microarray, are smoothed to provide the smooth signal plot (right y-axis). Normal copy number condition is represented by a value of 2, whereas chromosomal gain is represented by a value of 3. The raw signal for each individual chromosomal probe is shown in pink, green, and yellow, and the normalized probe signal, which is used to determine copy number and aberrations (if any), is shown in blue.

8.3 Supplementary information regarding the metabolomics experiments

8.3.1 Reconstitution volumes for metabolic analysis

Sample	Cell number/well	Number of cells (million)	Correction Factor	Recon volume HILIC (µl)	Recon volume ICMS (µl)
R215I-BFCN-D12-3ml	6.95	2.06	3.4	101	135
ctr-BFCN-D0-3ml	7.89	2.06	3.8	115	153
R215I-BFCN-D8-3ml	11.075	2.06	5.4	161	215
ctr-BFCN-D8-3ml	9.178	2.06	4.5	134	178
R215I-BFCN-D0-3ml	2.49	2.06	1.2	36	48
ctr-BFCN-D0-3ml	3.513	2.06	1.7	51	68
R215I-mDA-D0	3.66	2.06	1.8	53	71
ctr-mDA-D0	3.99	2.06	1.9	58	77
R215I-mDA-D8	3.96	2.06	1.9	58	77
ctr-mDA-D8	2.93	2.06	1.4	43	57

Table 8.1 Reconstitution volumes for BFCN samples for the analysis of the metabolite extracts with HILIC and ICMS respectively.

8.3.2 Differential abundant metabolites (BFCN)

	Metabolites differentially more abundant in R215I	Metabolites differentially less abundant in R215I
Day 0	**2-Hydroxyadipic acid** 4-Hydroxyproline **Acetyl-CoA** Acetylcysteine Adenosine monophosphate **Adenosine triphosphate** **ADP** CDP Creatine **Cytidine triphosphate** D-Glucuronic acid **Deoxyadenosine triphosphate** **FAD** Flavine mononucleotide Fructose 1,6-bisphosphate Fumaric acid	Adenine cis-Aconitic acid Citric acid Creatinine Cytidine monophosphate D-Glycerate 3-phosphate Indoleacetaldehyde Inosine Inosinic acid Isocitric acid

	Galacturonic acid Gluconic acid Glutathione Glyceric acid **Guanosine diphosphate** **Guanosine diphosphate mannose** Guanosine monophosphate **Guanosine triphosphate** **Ketoleucine** L-Alanine L-Arginine L-Asparagine L-Aspartic acid L-Isoleucine **L-Kynurenine** L-Lactic acid L-Leucine L-Lysine L-Malic acid L-Methionine L-Phenylalanine L-Serine L-Tryptophan L-Tyrosine L-Valine N-Formyl-L-methionine NAD NADP **NADPH** Niacinamide O-Acetylserine Ornithine **Oxidized glutathione** Pantothenic acid Phosphoserine Pyridoxal Pyridoxine Pyroglutamic acid **Pyruvic acid** Succinic acid Taurine Thiamine pyrophosphate **Thymidine 5'-triphosphate** **Uridine 5'-diphosphate** Uridine 5'-monophosphate **Uridine diphosphategalactose** **Uridine triphosphate**	

Day 8	**4-Hydroxyproline** **Acetyl-CoA** Acetylcysteine **Adenosine triphosphate** ADP Betaine CDP Choline cis-Aconitic acid Citric acid **Cytidine triphosphate** **Cytosine** **D-Glucuronic acid** D-Glycerate 3-phosphate **FAD** Fumaric acid **Galacturonic acid** Gamma Glutamylglutamic acid **Gluconic acid** Glutathione **Guanosine diphosphate** Guanosine diphosphate mannose Guanosine monophosphate **Guanosine triphosphate** L-Alanine L-Asparagine L-Aspartic acid L-Cystathionine L-Glutamic acid L-Glutamine L-Lactic acid L-Malic acid **L-Serine** Myo-inositol 1-phosphate N-Acetyl-L-aspartic acid NAD O-Acetylserine **O-Phosphoethanolamine** **Oxidized glutathione** Oxoglutaric acid Phosphoenolpyruvic acid **Phosphoserine** Pyruvic acid Thymine Threonic acid Uridine Uridine 5'-diphosphate Uridine diphosphategalactose **Uridine triphosphate**	**Gamma-Glutamylcysteine** Glycerol 3-phosphate Indoleacetaldehyde **L-Cystine**

Day 12	4-Hydroxyproline Adenosine triphosphate cis-Aconitic acid Citric acid D-2-Hydroxyglutaric acid dUMP Glucaric acid Gluconic acid Glutathione **Inosinic acid** Isocitric acid **L-Acetylcarnitine** L-Arginine L-Aspartic acid L-Cystathionine L-Glutamic acid L-Glutamine Phosphoenolpyruvic acid **Phosphoserine** L-Lysine L-Threonine Uridine 5'-diphosphate **Uridine diphosphategalactose**	**3-Hydroxyglutaric acid** Cytosine **Glutaric acid** Guanine L-Proline N-Acetyl-L-aspartic acid **Phenylpyruvic acid**

Table 8.2 Differential abundant metabolites of the BFCN differentiation (HILIC analysis). Metabolites listed here are differentially abundant between R215I and ctr with padj <0.5 and log_2FC > |0.25|. Compounds marked in bold have a log_2FC > |1|.

	Metabolites differentially more abundant in R215I	Metabolites differentially less abundant in R215I
Day 0	5-Thymidylic acid **Adenosine triphosphate** ADP **Cytidine monophosphate N-acetylneuraminic acid** **Cytidine triphosphate** D-Aspartic acid D-Glucuronic acid D-Glyceraldehyde 3-phosphate D-Ribulose 1,5-bisphosphate **dADP** **dCTP** **Deoxyadenosine triphosphate** Deoxyribose 5-phosphate DL-O-Phosphoserine dTDP Fructose 1,6-bisphosphate Fumaric acid **Guanosine diphosphate** **Guanosine diphosphate mannose** **Guanosine triphosphate** Ketoleucine	1-Pyrroline-2-carboxylic acid 2-Phospho-D-glyceric acid 3-Phosphoglyceric acid 3-Sulfinoalanine 3,4-Dihydroxybenzeneacetic acid 4-Hydroxy-L-proline **Adenosine diphosphate ribose** Adenosine monophosphate Citric acid Cytidine monophosphate D-Ribose 5-phosphate D-Sedoheptulose 7-phosphate **Hypotaurine** **Inosinic acid** Isocitric acid L-Glutamic acid N-Acetyl-L-aspartic acid N-Acetylglutamic acid N-Acetylneuraminic acid N-Acetylserine Oxoglutaric acid Pantothenic acid

	NADPH O-Phosphoethanolamine Phosphoserine Pyruvic acid **Uridine 5'-diphosphate** **Uridine 5'-monophosphate** Uridine diphosphate-N-acetylgalactosamine Uridine diphosphate-N-acetylglucosamine **Uridine triphosphate**	Phosphoric acid Succinic acid
Day 8	**2,3-Diphosphoglyceric acid** **Guanosine triphosphate** **Uridine diphosphate glucuronic acid** **Phosphocreatine** **D-Glucuronic acid** **Gluconic acid** Phosphoserine 2-Hydroxyadipic acid 3-Hydroxymethylglutaric acid DL-O-Phosphoserine Glycerophosphorylethanolamine Aminoadipic acid 5-Thymidylic acid Acetylglycine Uridine	Pyroglutamic acid Taurine N-Acetyl-L-methionine N-Acetylglutamic acid N-Formyl-L-methionine Pantothenic acid Citramalic acid D-2-Hydroxyglutaric acid 3-Hydroxyglutaric acid Fructose 1,6-bisphosphate N-Acetylglucosamine 6-phosphate Glyceric acid Ethylmalonic acid Mannose 6-phosphate Beta-Glycerophosphoric acid Glycerol 3-phosphate Hydroxyphenyllactic acid Succinic acid D-Sedoheptulose 7-phosphate Dehydroascorbic acid D-Ribose-1-Phosphate **D-Ribose 5-phosphate** **3,4-Dihydroxybenzeneacetic acid**
Day 12	3-Sulfinoalanine Adenosine triphosphate ADP Cytidine triphosphate D-Aspartic acid dADP dCTP Glutathione **Inosinic acid** L-Glutamic acid Pectin Uridine 5'-monophosphate **Uridine diphosphate glucose** Uridine diphosphate glucuronic acid **Uridine diphosphategalactose**	1-Pyrroline-2-carboxylic acid **2-Hydroxyadipic acid** 2-Hydroxybutyric acid 2-Phospho-D-glyceric acid **3-Hydroxyglutaric acid** **3-Hydroxymethylglutaric acid** 3-Phosphoglyceric acid 3,4-Dihydroxybenzeneacetic acid 4-Hydroxy-L-proline 5-Thymidylic acid Acetylglycine Adenosine diphosphate ribose Aminoadipic acid Butyric acid Citramalic acid Cysteic acid Cytidine monophosphate N-acetylneuraminic acid

		D-2-Hydroxyglutaric acid D-Glucuronic acid D-Mannose 1-phosphate **Ethylmalonic acid** **Glutaric acid** **Hydroxyphenyllactic acid** Hypotaurine Ketoleucine N-Acetyl-L-alanine N-Acetyl-L-aspartic acid N-Acetyl-L-methionine N-Acetyl-L-phenylalanine N-Acetylasparagine N-Acetylglutamic acid N-Acetylserine N-Formyl-L-methionine O-Phosphoethanolamine Orotic acid Oxalic acid **Oxoadipic acid** Phosphoric acid Succinic acid Thiamine pyrophosphate Uracil 5-carboxylate Uridine

Table 8.3 Differential abundant metabolites of the BFCN differentiation (ICMS analysis). Metabolites listed here are differentially abundant between R215I and ctr with padj <0.5 and $log_2FC > |0.25|$. Compounds marked in bold have a $log_2FC > |1|$.

8.3.3 Differential abundant metabolites (mDA)

	Metabolites differentially more abundant in R215I	Metabolites differentially less abundant in R215I
Day 0	Creatine Choline Glycerol 3-phosphate Pantothenic acid Betaine Gamma Glutamylglutamic acid **L-Kynurenine** **Galacturonic acid**	L-Alanine N-Acetylglutamic acid L-Tyrosine L-Malic acid **Orotic acid** L-Valine L-Glutamine L-Histidine L-Threonine L-Asparagine Cytidine triphosphate Fumaric acid Uridine 5'-diphosphate

Day 8	**Cytosine** Fumaric acid Gamma Glutamylglutamic acid L-Alanine L-Glutamine L-Aspartic acid L-Glutamic acid **Phosphoserine** L-Proline Galacturonic acid L-Malic acid Thymine Uracil	Guanosine diphosphate mannose Acetylcysteine CDP Glyceric acid Glycerol 3-phosphate Inosinic acid Ketoleucine L-Cystathionine L-Lactic acid N-Acetylglutamic acid Uridine 5'-diphosphate

Table 8.4 Differential abundant metabolites of the mDA differentiation (HILIC analysis). Metabolites listed here are differentially abundant between R215I and ctr with padj <0.5 and log_2FC > |0.25|. Compounds marked in bold have a log_2FC > |1|.

	Metabolites differentially more abundant in R215I	Metabolites differentially less abundant in R215I
Day 0	**N-Acetyl-L-phenylalanine** 2-Hydroxybutyric acid Ascorbic acid Deoxyribose 5-phosphate D-Glucuronic acid DL-O-Phosphoserine Gluconic acid **Glycerophosphorylethanolamine** Hydroxyphenyllactic acid Phosphocreatine Phosphoserine	**3-Sulfinoalanine** 2-Hydroxyadipic acid 3,4-Dihydroxybenzeneacetic acid 3-Hydroxymethylglutaric acid **4,5-Dihydroorotic acid** CDP Cysteic acid Cytidine triphosphate dCDP dCTP Fumaric acid Hypotaurine N-Acetylglucosamine 6-phosphate N-Acetylglutamic acid NADPH Orotic acid Uracil-5-carboxylate Uridine 5'-diphosphate Uridine diphosphate glucuronic acid Uridine triphosphate
Day 8	**Phosphoserine** Biotin **DL-O-Phosphoserine** L-Glutamic acid N-Acetylneuraminic acid O-Phosphoethanolamine Pantothenic acid Uridine	**3,4-Dihydroxybenzeneacetic acid** Acetylcysteine Beta-Glycerophosphoric acid Dehydroascorbic acid Glycerol 3-phosphate **Hypotaurine** Phosphocreatine Thiamine pyrophosphate

Table 8.5 Differential abundant metabolites of the mDA differentiation (ICMS analysis). Metabolites listed here are differentially abundant between R215I and ctr with padj <0.5 and log_2FC > |0.25|. Compounds marked in bold have a log_2FC > |1|.

8.3.4 Pathways enriched for differential abundant metabolites (BFCN)

Pathway	Day	Raw p	FDR
Alanine Metabolism	0	0.00302	0.00953
	8	4.42E-05	0.00031
	12	0.0535	0.25
Amino Sugar Metabolism	0	0.00343	0.01
	8	4.22E-07	4.60E-06
	12	0.00057	0.0185
Ammonia Recycling	0	8.40E-05	0.00059
	8	2.20E-08	5.38E-07
	12	0.00459	0.0497
Androgen and Estrogen Metabolism	0	0.152	0.195
	8	0.431	0.509
	12	0.533	0.726
Androstenedione Metabolism	0	0.0601	0.0965
	8	0.285	0.367
	12	0.424	0.695
Arachidonic Acid Metabolism	0	0.653	0.681
	8	0.597	0.65
	12	0.467	0.695
Arginine and Proline Metabolism	0	1.49E-06	1.89E-05
	8	0.00028	0.00125
	12	0.00507	0.0497
Aspartate Metabolism	0	2.76E-05	0.00025
	8	6.45E-08	1.05E-06
	12	4.86E-06	0.00048
Beta Oxidation of Very Long Chain Fatty Acids	0	0.0877	0.132
	8	0.035	0.0624
	12	0.0535	0.25
Beta-Alanine Metabolism	0	0.00083	0.00325
	8	0.00272	0.00861
	12	0.176	0.505
Betaine Metabolism	0	0.039	0.0683
	8	0.00157	0.0055
	12	0.382	0.682
Bile Acid Biosynthesis	0	0.11	0.154
	8	0.318	0.395
	12	0.782	1
Biotin Metabolism	0	0.0867	0.132
	8	0.303	0.385

	12	0.0125	0.0939
Butyrate Metabolism	0	0.00073	0.00312
	8	0.00778	0.0191
	12	0.353	0.682
Caffeine Metabolism	0	0.191	0.234
	8	0.0842	0.125
Cardiolipin Biosynthesis	0	0.0279	0.0526
	8	0.0102	0.0228
Carnitine Synthesis	0	0.159	0.202
	8	0.251	0.337
	12	0.397	0.682
Catecholamine Biosynthesis	0	0.734	0.757
Citric Acid Cycle	0	5.28E-11	5.18E-09
	8	7.08E-11	3.47E-09
	12	0.00459	0.0497
Cysteine Metabolism	0	0.0205	0.0427
	8	6.90E-05	0.00045
	12	0.113	0.396
D-Arginine and D-Ornithine Metabolism	0	0.516	0.562
	8	0.392	0.468
De Novo Triacylglycerol Biosynthesis	0	0.447	0.504
	8	0.0559	0.0869
Degradation of Superoxides	0	0.516	0.562
Estrone Metabolism	0	0.0601	0.0965
	8	0.285	0.367
	12	0.424	0.695
Ethanol Degradation	0	0.00073	0.00312
	8	0.0469	0.0807
	12	0.353	0.682
Fatty Acid Biosynthesis	0	0.903	0.922
	8	0.798	0.86
Fatty Acid Elongation In Mitochondria	0	0.177	0.219
	8	0.462	0.532
Fatty acid Metabolism	0	0.131	0.178
	8	0.115	0.163
	12	0.631	0.836
Folate Metabolism	0	0.00774	0.0181
	8	0.00704	0.0182
	12	0.136	0.459
Fructose and Mannose Degradation	0	0.00053	0.00261
	8	0.0108	0.0236
	12	0.522	0.726
Galactose Metabolism	0	0.0286	0.0529

	8	0.00489	0.0137
	12	0.05	0.25
Gluconeogenesis	0	0.00018	0.00105
	8	7.85E-07	7.69E-06
	12	0.184	0.505
Glucose-Alanine Cycle	0	0.00077	0.00313
	8	0.00013	0.00071
	12	0.257	0.572
Glutamate Metabolism	0	6.45E-08	1.58E-06
	8	2.08E-10	6.80E-09
	12	0.00358	0.0497
Glutathione Metabolism	0	1.55E-06	1.89E-05
	8	9.79E-07	8.72E-06
	12	0.0101	0.0826
Glycerol Phosphate Shuttle	0	0.151	0.195
	8	0.0102	0.0228
Glycerolipid Metabolism	0	7.83E-05	0.00059
	8	0.00048	0.00198
	12	0.437	0.695
Glycine and Serine Metabolism	0	1.48E-07	2.90E-06
	8	4.01E-08	7.86E-07
	12	0.00133	0.026
Glycolysis	0	0.00353	0.01
	8	0.00048	0.00198
	12	0.106	0.396
Histidine Metabolism	0	0.0155	0.0346
	8	0.036	0.063
	12	0.251	0.572
Homocysteine Degradation	0	0.447	0.504
	8	0.0559	0.0869
	12	0.186	0.505
Inositol Metabolism	0	0.152	0.195
	8	0.0123	0.0263
	12	0.533	0.726
Inositol Phosphate Metabolism	0	0.225	0.266
	8	0.024	0.0479
	12	0.45	0.695
Ketone Body Metabolism	0	0.0442	0.0759
	8	0.108	0.156
Lactose Degradation	0	0.107	0.152
	8	0.0559	0.0869
	12	0.186	0.505
Lactose Synthesis	0	0.001	0.00375

	8	0.00124	0.0045
	12	0.0088	0.0784
Lysine Degradation	0	0.0019	0.00643
	8	0.00818	0.0195
	12	0.144	0.469
Malate-Aspartate Shuttle	0	0.128	0.177
	8	0.00057	0.00221
	12	0.0195	0.127
Methionine Metabolism	0	0.0492	0.0831
	8	0.00191	0.00625
	12	0.251	0.572
Mitochondrial Beta-Oxidation of Long Chain Saturated Fatty Acids	0	0.0278	0.0526
	8	0.0308	0.0569
	12	0.475	0.695
Mitochondrial Beta-Oxidation of Medium Chain Saturated Fatty Acids	0	0.0239	0.0469
	8	0.0272	0.0513
	12	0.463	0.695
Mitochondrial Beta-Oxidation of Short Chain Saturated Fatty Acids	0	0.0239	0.0469
	8	0.0272	0.0513
	12	0.463	0.695
Mitochondrial Electron Transport Chain	0	0.00073	0.00312
	8	9.07E-05	0.00056
	12	0.353	0.682
Nicotinate and Nicotinamide Metabolism	0	0.00151	0.00529
	8	0.00426	0.0124
	12	0.0467	0.25
Nucleotide Sugars Metabolism	0	0.00651	0.0159
	8	0.00124	0.0045
	12	0.0718	0.306
Oxidation of Branched Chain Fatty Acids	0	0.0205	0.0427
	8	0.024	0.0479
	12	0.113	0.396
Pantothenate and CoA Biosynthesis	0	0.00017	0.00105
	8	0.0606	0.0928
	12	0.382	0.682
Pentose Phosphate Pathway	0	0.00774	0.0181
	8	0.367	0.445
	12	0.487	0.696
Phenylacetate Metabolism	0	0.107	0.152
	8	0.0559	0.0869
	12	0.0158	0.111
Phenylalanine and Tyrosine Metabolism	0	0.00645	0.0159
	8	0.00602	0.016

	12	0.0225	0.138
Phosphatidylcholine Biosynthesis	0	0.00914	0.0208
	8	0.0002	0.00096
	12	0.274	0.597
Phosphatidylethanolamine Biosynthesis	0	0.0005	0.00256
	8	3.90E-06	3.19E-05
	12	0.24	0.572
Phosphatidylinositol Phosphate Metabolism	0	0.0877	0.132
	8	0.169	0.234
	12	0.322	0.682
Phospholipid Biosynthesis	0	0.561	0.591
	8	0.0346	0.0624
Phytanic Acid Peroxisomal Oxidation	0	0.00011	0.0007
	8	0.00431	0.0124
	12	0.45	0.695
Plasmalogen Synthesis	0	0.0205	0.0427
	8	0.318	0.395
Porphyrin Metabolism	0	0.473	0.527
	8	0.255	0.338
	12	0.604	0.811
Propanoate Metabolism	0	0.00357	0.01
	8	0.00166	0.0056
	12	0.242	0.572
Pterine Biosynthesis	0	0.106	0.152
	8	0.367	0.445
Purine Metabolism	0	4.37E-06	4.28E-05
	8	0.00018	0.00095
	12	0.00437	0.0497
Pyrimidine Metabolism	0	3.34E-05	0.00027
	8	0.00012	0.00071
	12	0.0386	0.223
Pyruvaldehyde Degradation	0	0.0213	0.0434
	8	0.00767	0.0191
	12	0.204	0.54
Pyruvate Metabolism	0	4.70E-08	1.54E-06
	8	2.53E-07	3.10E-06
	12	0.0886	0.347
Retinol Metabolism	0	0.203	0.243
	8	0.491	0.554
Riboflavin Metabolism	0	0.00651	0.0159
	8	0.0536	0.0869
	12	0.368	0.682
Selenoamino Acid Metabolism	0	0.00645	0.0159

	8	0.00602	0.016
	12	0.475	0.695
Spermidine and Spermine Biosynthesis	0	0.101	0.149
	8	0.558	0.621
	12	0.338	0.682
Sphingolipid Metabolism	0	0.036	0.0641
	8	0.0271	0.0513
	12	0.226	0.567
Starch and Sucrose Metabolism	0	0.00234	0.00763
	8	0.00023	0.00109
	12	0.151	0.479
Steroid Biosynthesis	0	0.0771	0.122
	8	0.155	0.217
	12	0.673	0.879
Steroidogenesis	0	0.523	0.563
	8	0.861	0.917
Sulfate/Sulfite Metabolism	0	0.413	0.476
	8	0.251	0.337
	12	0.397	0.682
Taurine and Hypotaurine Metabolism	0	0.547	0.582
Thiamine Metabolism	0	0.00147	0.00529
	8	0.0559	0.0869
	12	0.186	0.505
Threonine and 2-Oxobutanoate Degradation	0	0.00651	0.0159
	8	0.00942	0.022
	12	0.0718	0.306
Thyroid hormone synthesis	0	0.197	0.239
	8	0.444	0.518
Transfer of Acetyl Groups into Mitochondria	0	1.88E-07	3.08E-06
	8	2.05E-05	0.00015
	12	0.0849	0.347
Trehalose Degradation	0	0.151	0.195
	8	0.0807	0.122
	12	0.222	0.567
Tryptophan Metabolism	0	0.00314	0.00962
	8	0.00335	0.0103
	12	0.395	0.682
Tyrosine Metabolism	0	0.164	0.207
	8	0.0891	0.13
	12	0.49	0.696
Ubiquinone Biosynthesis	0	0.366	0.427
Urea Cycle	0	4.09E-06	4.28E-05
	8	1.04E-07	1.46E-06

	12	0.0003	0.0147
Valine, Leucine and Isoleucine Degradation	0	0.00019	0.00106
	8	0.013	0.027
	12	0.395	0.682
Vitamin B6 Metabolism	0	0.0332	0.0602
	8	0.596	0.65
Vitamin K Metabolism	0	0.0537	0.0892
	8	0.469	0.535
Warburg Effect	0	1.84E-10	9.00E-09
	8	1.95E-11	1.91E-09
	12	0.00121	0.026

Table 8.6 Pathways enriched for differential abundant metabolites in the BFCN differentiation (HILIC measurements, Over Representation Analysis)

8.3.5 Pathways enriched for differential abundant metabolites (mDA)

Pathway	**Day**	**Raw p**	**FDR**
Alanine Metabolism	0	0.262	0.951
	8	0.0376	0.263
Amino Sugar Metabolism	0	0.0179	0.251
	8	0.0208	0.17
Ammonia Recycling	0	0.0164	0.251
	8	0.0191	0.17
Androgen and Estrogen Metabolism	0	0.448	1
	8	0.466	1
Androstenedione Metabolism	0	0.35	0.967
	8	0.365	1
Arachidonic Acid Metabolism	8	0.738	1
Arginine and Proline Metabolism	0	0.238	0.897
	8	0.0139	0.151
Aspartate Metabolism	0	0.021	0.255
	8	0.000287	0.0141
Beta-Alanine Metabolism	0	0.118	0.64
	8	0.0225	0.17
Betaine Metabolism	0	0.0503	0.411
Cardiolipin Biosynthesis	0	0.0146	0.251
	8	0.187	0.705
Catecholamine Biosynthesis	0	0.301	0.951
Citric Acid Cycle	0	0.106	0.612
	8	0.116	0.6
Cysteine Metabolism	8	0.389	1
De Novo Triacylglycerol Biosynthesis	0	0.148	0.726
	8	0.156	0.636
Estrone Metabolism	0	0.35	0.967

	8	0.365	1
Folate Metabolism	8	0.423	1
Fructose and Mannose Degradation	8	0.456	1
Galactose Metabolism	0	0.497	1
	8	0.516	1
Gluconeogenesis	8	0.487	1
Glucose-Alanine Cycle	0	0.207	0.829
	8	0.0225	0.17
Glutamate Metabolism	0	0.211	0.829
	8	0.0106	0.148
Glutathione Metabolism	0	0.313	0.96
	8	0.0555	0.34
Glycerol Phosphate Shuttle	0	0.178	0.793
	8	0.187	0.705
Glycerolipid Metabolism	0	0.362	0.967
	8	0.0759	0.438
Glycine and Serine Metabolism	0	0.0166	0.251
	8	0.00334	0.0654
Histidine Metabolism	0	0.541	1
	8	0.561	1
Homocysteine Degradation	8	0.156	0.636
Lactose Synthesis	0	0.301	0.951
	8	0.315	1
Lysine Degradation	8	0.435	1
Malate-Aspartate Shuttle	8	0.0134	0.151
Methionine Metabolism	0	0.173	0.793
	8	0.561	1
Methylhistidine Metabolism	0	0.0686	0.517
Mitochondrial Electron Transport Chain	0	0.0418	0.41
	8	0.0462	0.302
Nicotinate and Nicotinamide Metabolism	0	0.487	1
	8	0.148	0.636
Pantothenate and CoA Biosynthesis	0	0.0503	0.411
Phenylacetate Metabolism	0	0.148	0.726
	8	0.156	0.636
Phenylalanine and Tyrosine Metabolism	0	0.0842	0.549
	8	0.0926	0.504
Phosphatidylcholine Biosynthesis	0	0.0234	0.255
Phosphatidylethanolamine Biosynthesis	0	0.0174	0.251
Phospholipid Biosynthesis	0	0.0896	0.549
	8	0.423	1
Porphyrin Metabolism	0	0.515	1
	8	0.534	1

Propanoate Metabolism	0	0.532	1
	8	0.552	1
Purine Metabolism	0	0.378	0.975
	8	0.00899	0.147
Pyrimidine Metabolism	0	0.0166	0.251
	8	0.00334	0.0654
Pyruvate Metabolism	0	0.582	1
	8	0.222	0.808
Selenoamino Acid Metabolism	0	0.395	0.994
	8	0.412	1
Sphingolipid Metabolism	0	0.515	1
	8	0.534	1
Starch and Sucrose Metabolism	0	0.428	1
	8	0.445	1
Threonine and 2-Oxobutanoate Degradation	0	0.301	0.951
Thyroid hormone synthesis	0	0.207	0.829
Transfer of Acetyl Groups into Mitochondria	0	0.326	0.967
	8	0.341	1
Tryptophan Metabolism	0	0.285	0.951
	8	0.307	1
Tyrosine Metabolism	0	0.365	0.967
	8	0.144	0.636
Urea Cycle	0	0.0125	0.251
	8	0.000113	0.011
Valine, Leucine and Isoleucine Degradation	0	0.666	1
	8	0.307	1
Warburg Effect	0	0.0768	0.537
	8	0.00309	0.0654

Table 8.7 Pathways enriched for differential abundant metabolites in the mDA differentiation (HILIC measurements, Over Representation Analysis)

8.4 Supplementary information regarding the sc-RNAseq experiments

8.4.1 Plots regarding quality control of the sc-RNAseq data set

Figure 8.2 Quality control plots of the sc-RNAseq data containing the raw measurements, the centred measurements, and the scaled measurements. The plots depict the quality control for each sample. "Count" refers to the sequencing

count, how many genes were captured per cell. “Feature” refers to the sequencing depth, a value for the abundance of each individual transcript.

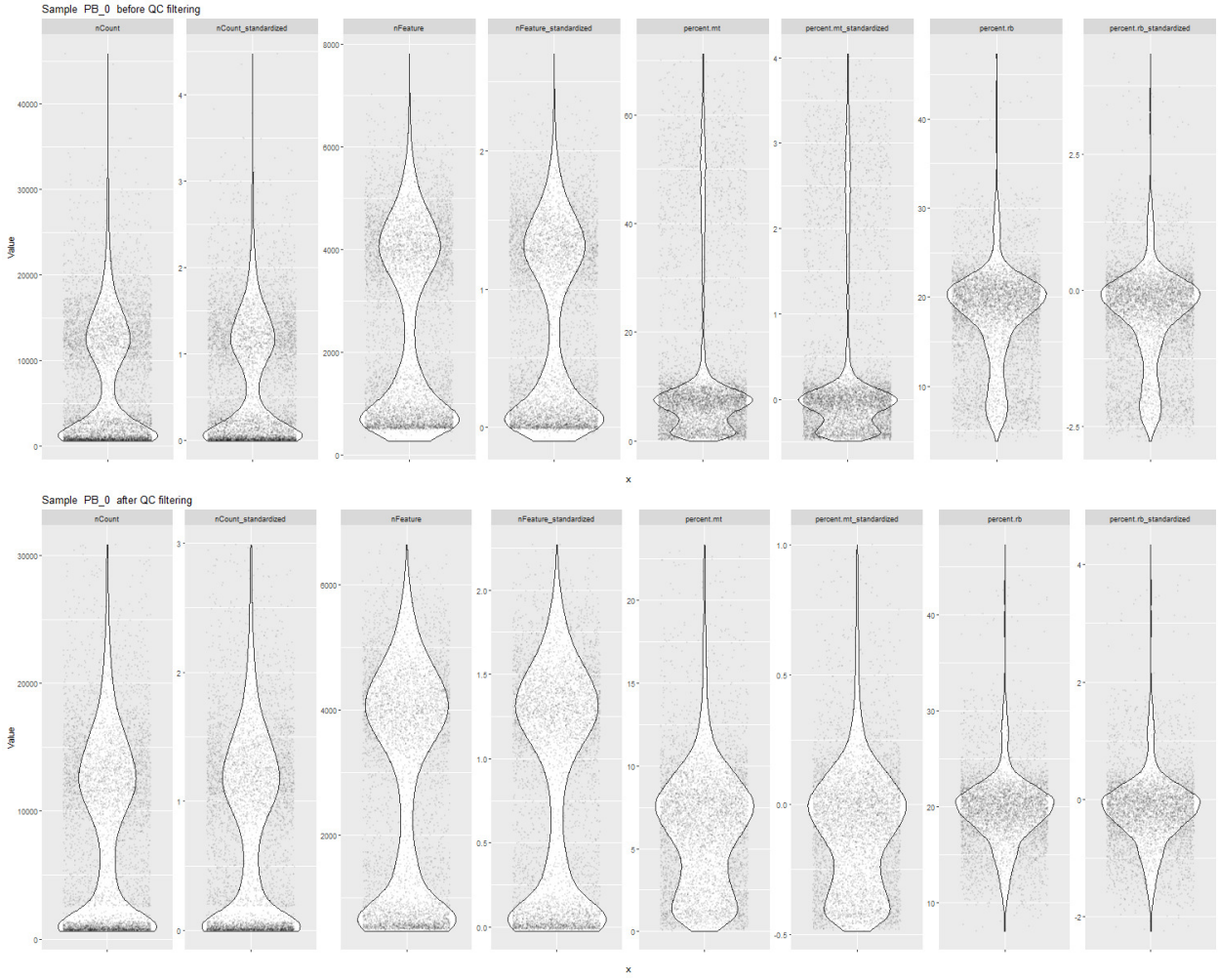

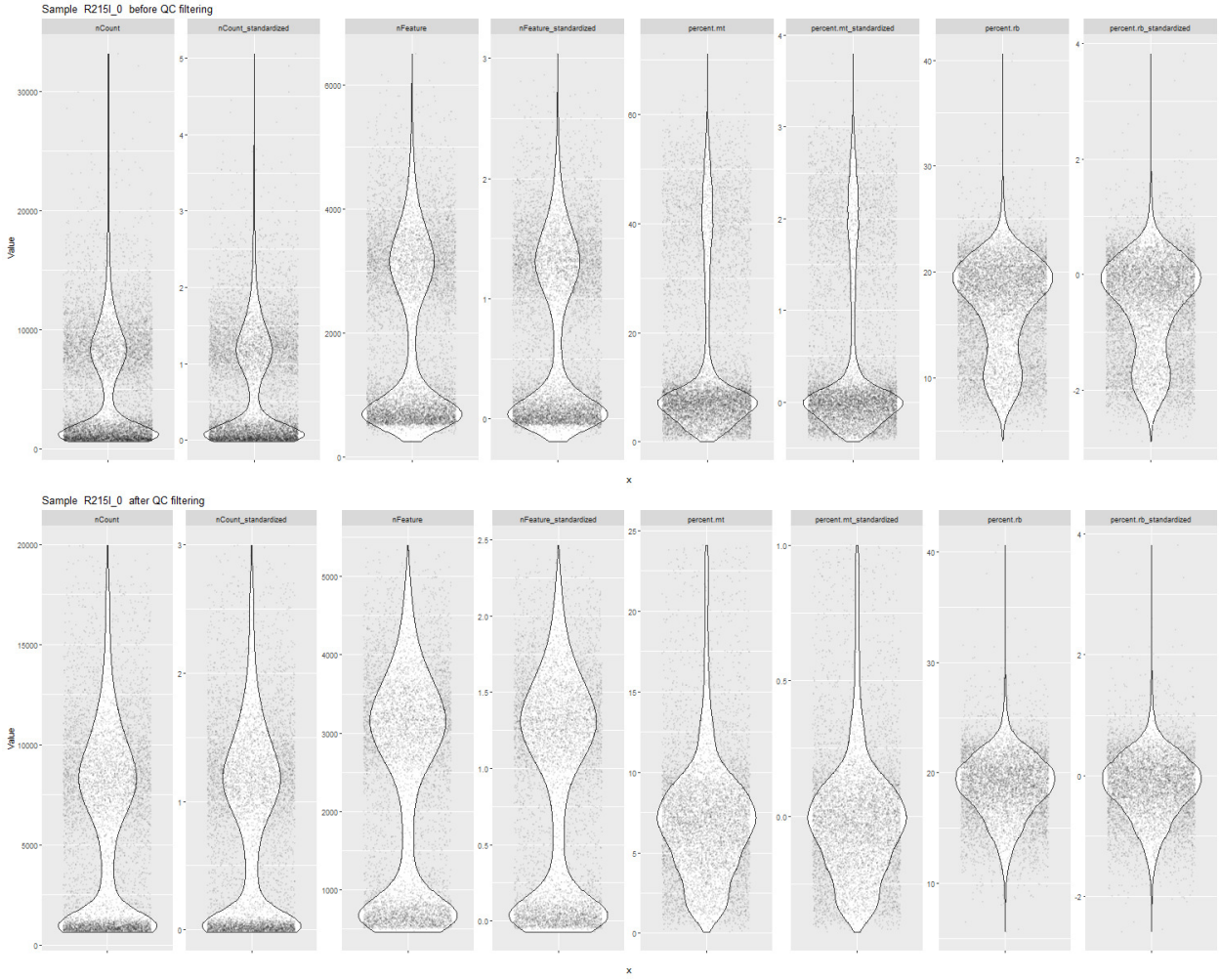
Sample R215l_0 before QC filtering
nCount
nCount_standardized
nFeature
nFeature_standardized
percent.mt
percent.mt_standardized
percent.rb
percent.rb_standardized
Value
x
Sample R215l_0 after QC filtering
nCount
nCount_standardized
nFeature
nFeature_standardized
percent.mt
percent.mt_standardized
percent.rb
percent.rb_standardized
Value
x

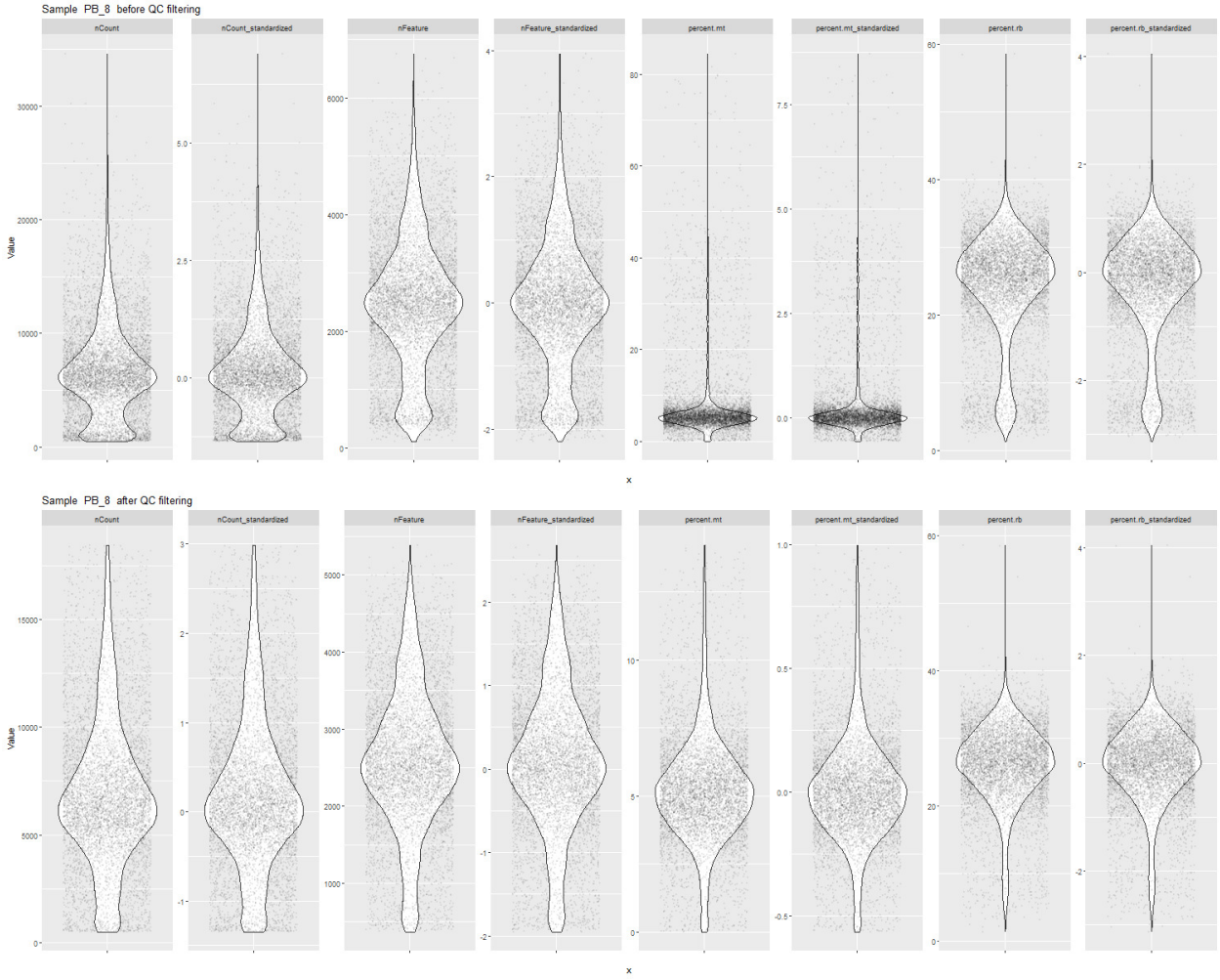
Sample PB_8 before QC filtering
nCount
nCount_standardized
nFeature
nFeature_standardized
percent.mt
percent.mt_standardized
percent.rb
percent.rb_standardized
Value
x
Sample PB_8 after QC filtering
nCount
nCount_standardized
nFeature
nFeature_standardized
percent.mt
percent.mt_standardized
percent.rb
percent.rb_standardized
Value
x

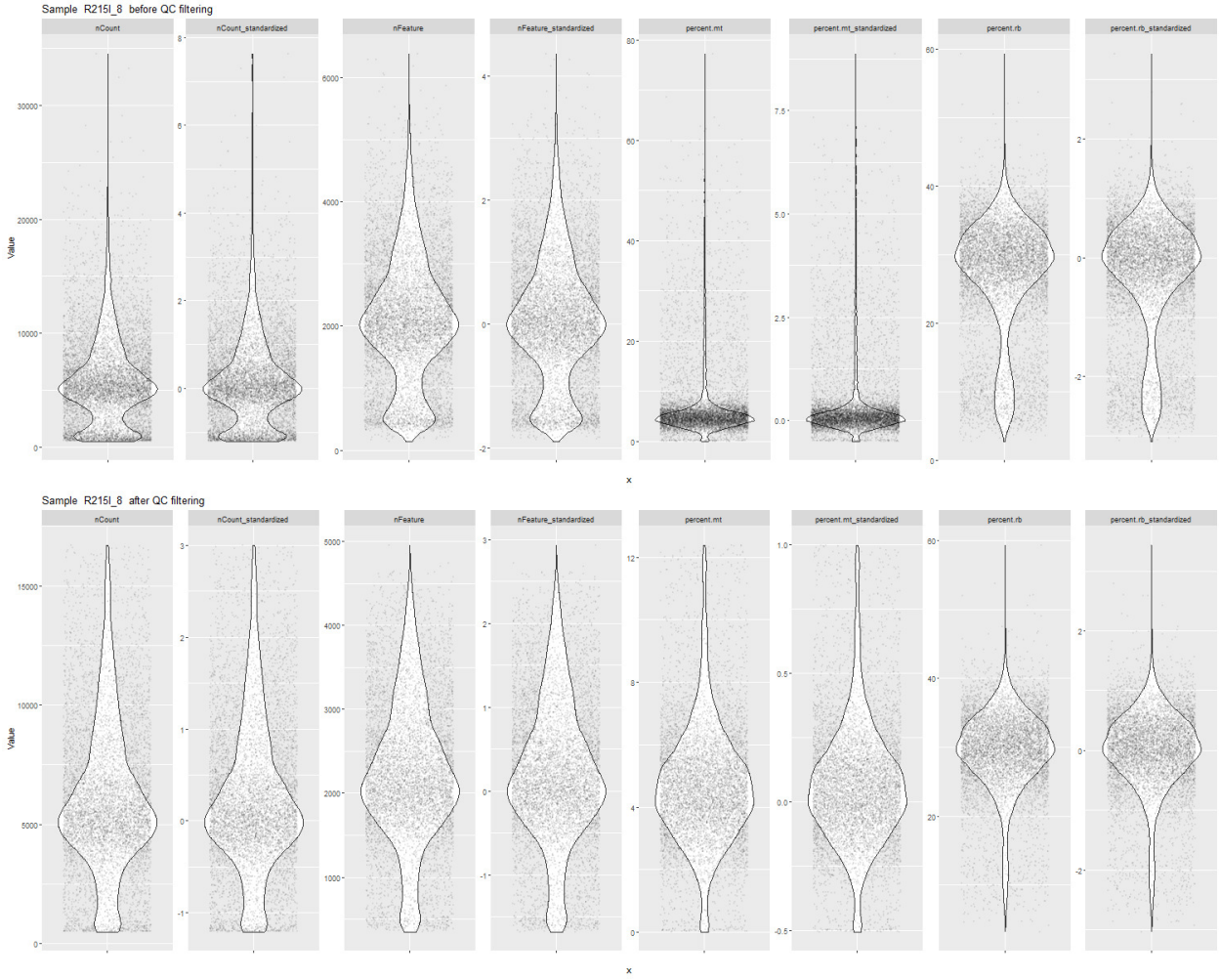
Sample R215l_8 before QC filtering
nCount
nCount_standardized
nFeature
nFeature_standardized
percent.mt
percent.mt_standardized
percent.rb
percent.rb_standardized
Value
x
Sample R215l_8 after QC filtering
nCount
nCount_standardized
nFeature
nFeature_standardized
percent.mt
percent.mt_standardized
percent.rb
percent.rb_standardized
Value
x


Sample PB_12 before QC filtering
nCount
nCount_standardized
nFeature
nFeature_standardized
percent.mt
percent.mt_standardized
percent.rb
percent.rb_standardized
Value
x
Sample PB_12 after QC filtering
nCount
nCount_standardized
nFeature
nFeature_standardized
percent.mt
percent.mt_standardized
percent.rb
percent.rb_standardized
Value
x

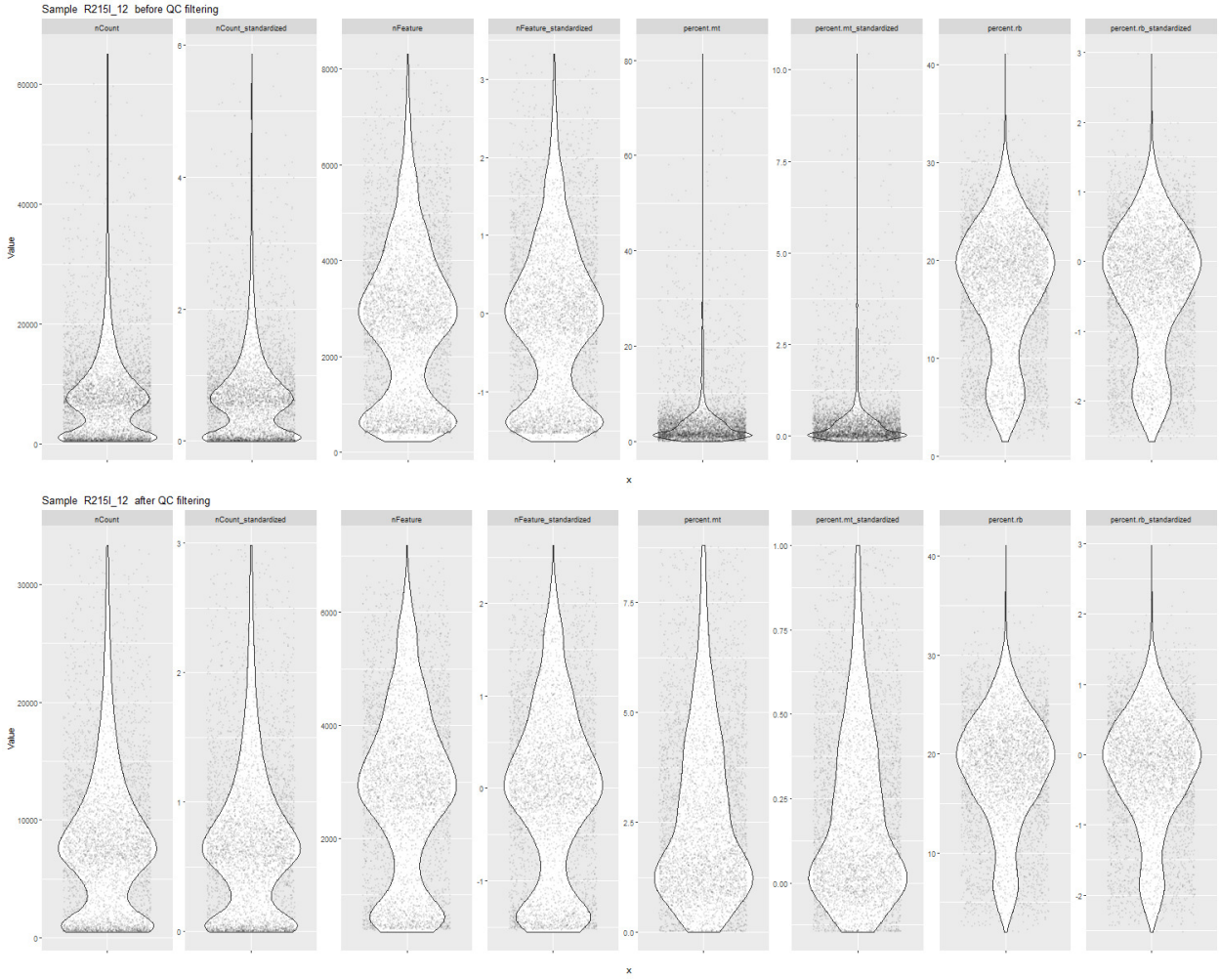
Sample R215l_12 before QC filtering
nCount
nCount_standardized
nFeature
nFeature_standardized
percent.mt
percent.mt_standardized
percent.rb
percent.rb_standardized
Value
x
Sample R215l_12 after QC filtering
nCount
nCount_standardized
nFeature
nFeature_standardized
percent.mt
percent.mt_standardized
percent.rb
percent.rb_standardized
Value
x

8.4.2 Normalisation and batch correction plots

Figure 8.3 The normalization and batch correction plots. Each line represents one Day of Differentiation. Canonical log normalization of the transcript concentration was performed with Seurat (NormalizeData). Batch correction was performed to correct for the small differences present in sequencing depth amongst all datasets.

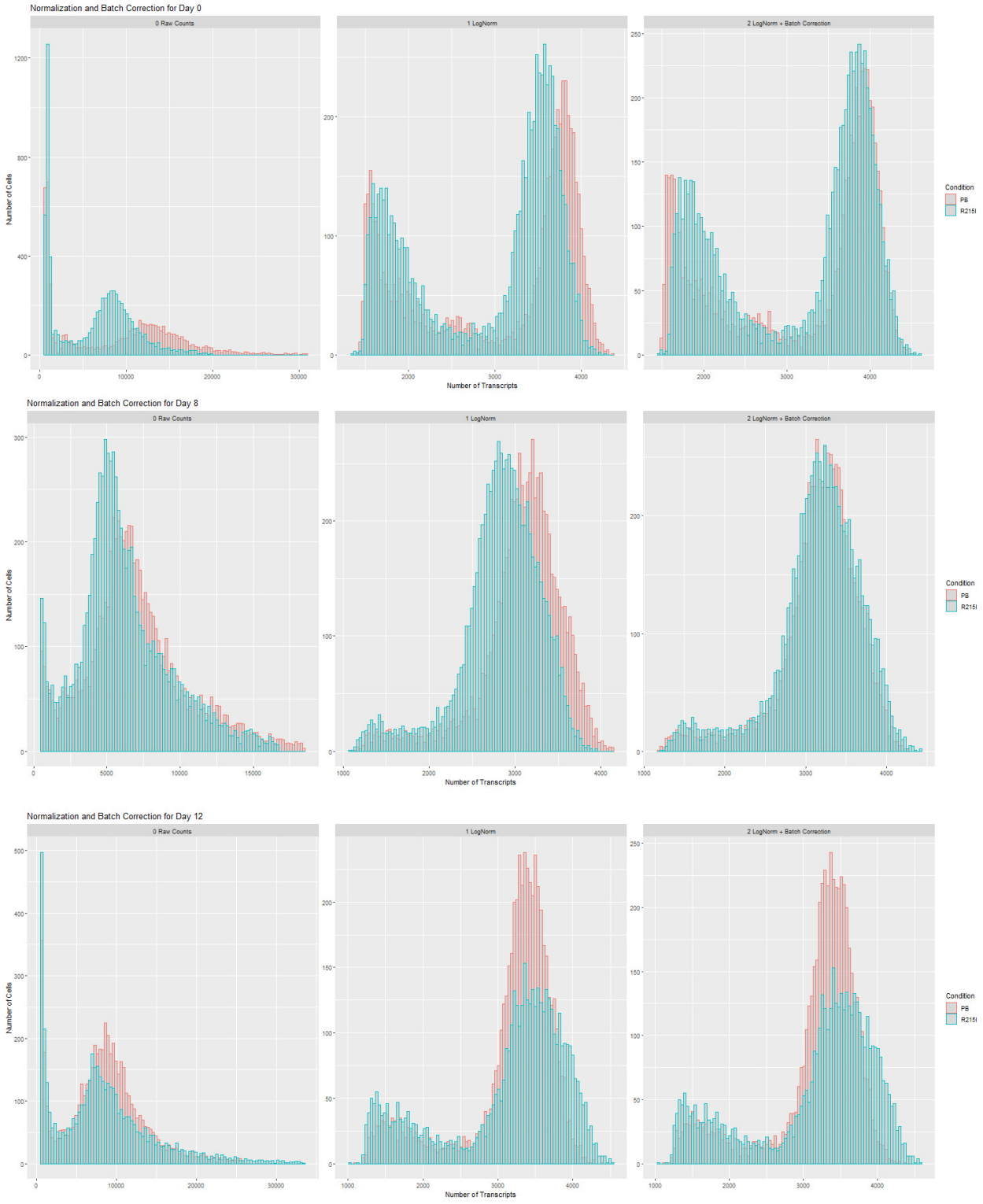

8.4.3 Differential expressed genes detected with sc-RNAseq of early timepoints of BFCN differentiation

	DEGs overexpressed in R215I	DEGs overexpressed in control
Day 0	AC011447.3 BEX2 BEX3 EIF1AX EIF2S3 FIRRE GPC4 MORF4L2 POLA1 PRDX4 RBBP7 SMARCA1 SMS STAG2 TCEAL8 TCEAL9 USP9X WFDC2 ZNF90	LNCPRESS1 MT2A XIST
Day 8	AL683813.1 AMOT ANP32B AP1S2 AUXG01000058.1 BEX3 C6orf141 CAPN6 CASK CCDC144NL-AS1 CD99 CRABP1 CRABP2 DLK1 EIF1AX EIF2S3 FGF8 FRZB FZD5 GPC3 H1F0 HSPA5 HTR2C IGFBP3 KDM6A	ANKRD33B ARL4A ARX CDK6 CKB ELAVL4 EPHA7 FOXB1 HES4 HYMAI ID4 IGDCC3 JADE1 JAG1 OTX1 PEG10 PLAGL1 POU3F2 PRTG PTPN13 PTX3 PURPL SHH SMIM14 SPON1

	KIZ L1TD1 LINC00632 LINC01833 LMAN1 MAF MEST MGST1 MORF4L2 NNAT PERP PHF6 PRDX4 RAX RBBP7 S1PR3 SAT1 SEMA6A SFRP1 SHISA2 SIX3 SIX6 SMOC1 SMS SNAPC1 SOX3 SREK1IP1 STAG2 TBL1X TCEAL8 TCEAL9 TCF7L2 TMSB4X USP9X ZDHHC9 ZNF90	TAGLN3 TPBG TSC22D1 TSIX TUBB3 WLS XIST ZFHX4 ZNF503

Day 12	ABCA1	ANKRD11
	AC011447.3	ARG2
	AFF2	ARMCX3
	AKAP12	ATF5
	ANKRD1	BCAT1
	ANXA2	CADM2
	AP1S2	CALR
	ARHGAP29	CANX
	AUXG01000058.1	CBX4
	B2M	CD47
	BEX3	CDK2AP2
	BMP7	CDK6
	CALD1	CEBPB
	CAMK2D	CEBPG
	CAPN6	CHAC1
	CAV1	CISD2
	CAV2	COPE
	CCDC144NL-AS1	CRELD2
	CCDC160	DDIT3
	CCND1	DNAJB11
	CD99	DNAJB9
	CDH11	DNAJC10
	CDKN1C	DNAJC3
	CELF2	EIF4EBP1
	COL11A1	ELAVL3
	COL1A1	ERP29
	COL2A1	FABP7
	COL4A1	FKBP11
	COL4A2	FKBP1A
	COL4A5	FOXB1
	COL4A6	GADD45A
	COL5A2	GARS
	COL8A1	GAS5
	COTL1	GFPT1
	CPE	GFRA1
	CRABP1	GHITM
	CRABP2	GOT1
	CSRP2	HAX1
	CXXC4	HERPUD1
	DAAM1	HHIP
	DIAPH2	HM13
	DLK1	HSP90B1
	DSEL	HSPA13
	DTX4	HSPA5
	ELOVL6	HSPA8
	EPB41L2	HSPA9
	F2R	HYOU1
	FABP5	IARS
	FAT1	KDELR2
	FGF8	KIF5C
	FZD2	LHX5-AS1

	FZD5	LINC00662
	GPC4	LMAN1
	HES1	LONP1
	HES5	MANF
	HTR2C	MAP6
	ID3	MCFD2
	IFITM2	MTHFD2
	IGF1R	MT-ND3
	IGFBP3	MYDGF
	IGFBP5	NANS
	KCNK12	NARS
	KDM6A	NBR2
	LAMB1	NEFM
	LAMC1	NFE2L1
	LIMCH1	NHLH1
	LIMS1	NIBAN1
	LINC00472	NRP2
	LINC01833	NUCB2
	LPP	ONECUT2
	LTBP1	OSTC
	MACF1	P4HB
	MAF	PDIA3
	MBIP	PDIA4
	MEST	PDIA6
	MGST1	PEG10
	MID1	PGM3
	MYH9	PHGDH
	NCALD	PLAGL1
	NEK6	PLPP5
	NELL2	PPIB
	NEXN	PRTG
	NKX2-1	PSAT1
	NKX2-2	PSPH
	NLGN4X	PYCR1
	NNAT	RCN1
	PARD3B	RPN1
	PDGFB	RPN2
	PDLIM5	SARS
	PHACTR2	SDF2L1
	PHF6	SEC11C
	PHIP	SEC24D
	PI15	SEC61A1
	PMP22	SEC61B
	POU3F1	SEC61G
	PREX2	SEC63
	PTCH1	SEL1L
	PTN	SELENOK
	PTPRZ1	SELENOS
	QKI	SERP1
	RDX	SESN2
	RNF145	SHMT2

	RTN4 S100A11 S100A6 S1PR3 SALL2 SAT1 SCD5 SEMA5A SEMA6A SFRP1 SFRP2 SFTA3 SHISA9 SHTN1 SIX3 SIX6 SLC2A1 SLC2A3 SMARCA1 SMS SORBS2 SOX11 SOX5 SOX9 SPARC SPRED1 SREK1IP1 ST5 STAG2 STK26 SVIL TAGLN TBL1X TCEAL9 TCF4 TCF7L2 TFDP2 TMEM132B TMEM38B TMSB10 TMSB4X TPM1 TRIB2 TTYH1 TUBA1A UBE2H UBL3 UPP1 USP9X VCAN VCL	SLC1A5 SLC33A1 SLC35B1 SLC39A14 SLC3A2 SLC5A6 SLC7A1 SLC7A11 SLC7A3 SLIT2 SNHG1 SNHG6 SNHG7 SNHG8 SPCS2 SPCS3 SRM SRP19 SSR1 SSR2 SSR3 SSR4 STMN2 STT3A SYT4 TAC1 THBS1 TMED10 TMED2 TMED7 TMED9 TMEM41B TNFRSF10B TPBG TRAM1 TRIB3 TSC22D1 TSIX TSPYL2 TXNDC5 UCHL1 UNC5B VEGFA WARS WLS XBP1 XIST XPOT YBX3 ZFAS1

	WFDC2 ZFP36L1 ZMYND8 ZNF462	

Table 8.8 DEGs between R215I and isogenic ctr. This tables list all DEG found in the differentiation of BFCN progenitors.

8.4.4 Violine plot of iPSC markers and characterisation of Cluster 7

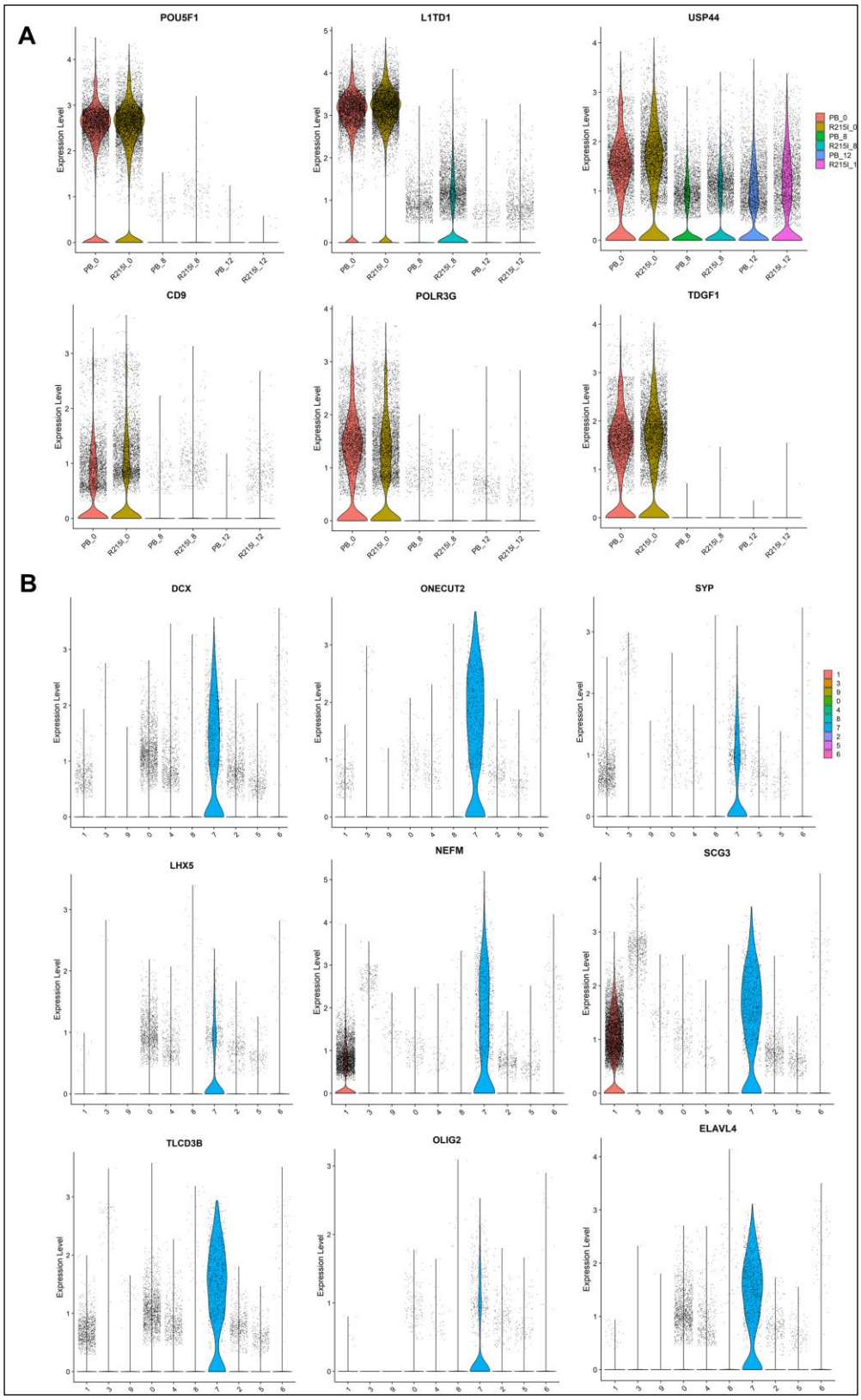

Figure 8.4 Violine plot of iPSC markers and characterisation of Cluster 7. ***(A)*** *Violone plots show expression of iPSC marker genes at Day 0. The panel supports Figure 4.10, as not all plots could be shown there due to space restrictions* ***(B)*** *Violine plots for characteristic genes of cluster 7. The panel supports Figure 4.11, as not all plots could be shown there due to space restrictions. R215I is the mutant cell line, PB is the ctr.*